COMPLEXITY OF RUPTURE PROPAGATION IN LARGE EARTHQUAKES IN RELATION TO TECTONIC ENVIRONMENT

Thesis by

Gordon Selbie Stewart

In Partial Fulfillment of the Requirements

for the Degree of

Doctor of Philsophy

California Institute of Technology

Pasadena, California

1982

(Submitted August 28, 1981)

To my parents:

They made it all possible

ACKNOWLEDGEMENTS

I would like to thank, most sincerely, the faculty, students and staff of the Seismological Laboratory who nurtured me during the preparation of this thesis and helped in the development of many of the ideas presented in it.

Hiroo Kanamori, my thesis advisor, has given much support and encouragement and has been a continual source of inspiration throughout this work. For this generosity I am most grateful. I have also benefitted from discussions with, and encouragement from, Don Helmberger, my academic advisor. "Thanks Don".

I want to also express my gratitude to the many people who have been involved directly, or contributed indirectly, in the research presented here. In this regard, I would like to thank Rhett Butler, John Ebel, Eric Chael, Steve Cohn, Jeff Given, Steve Hartzell, Don Helmberger, Hiroo Kanamori, Charles Langston, Karen McNally and James Pechmann.

I thank Liz Wieschollek for her efficient typing of the thesis and Lazlo Lenches for his superb work in drafting many of the figures, as well as his efforts in coordinating their final preparation.

This research was supported in part by the National Science Foundation under grant numbers EAR76-14262, EAR77-13641, EAR78-11973 and EAR78-14786; by the United States Geological Survey under contract numbers 14-08-0001-15893, 14-08-0001-16776, 14-08-0001-17631, 14-08-0001-18371 and 14-08-0001-19265.

ABSTRACT

Complexity in the earthquake rupture process can result from many factors. This study investigates the origin of such complexity by examining several recent, large earthquakes in detail. In each case the local tectonic environment plays an important role in understanding the source of the complexity.

Several large shallow earthquakes ($M_s > 7.0$) along the Middle American Trench have similarities and differences between them that may lead to a better understanding of fracture and subduction processes. They are predominantly thrust events consistent with the known subduction of the Cocos plate beneath N. America. Two events occurring along this subduction zone close to triple junctions show considerable complexity. This may be attributable to a more heterogeneous stress environment in these regions and as such has implications for other subduction zone boundaries.

An event which looks complex but is actually rather simple is the 1978 Bermuda earthquake ($M_s \sim 6$). It is located predominantly in the mantle. Its mechanism is one of pure thrust faulting with a strike N 20°W and dip 42°NE. Its apparent complexity is caused by local crustal structure. This is an important event in terms of understanding and estimating seismic hazard on the eastern seaboard of N. America.

A study of several large strike-slip continental earthquakes identifies characteristics which are common to them and may be useful in determining what to expect from the next great earthquake on the San

Andreas fault. The events are the 1976 Guatemala earthquake on the Motagua fault and two events on the Anatolian fault in Turkey (the 1967, Mudurnu Valley and 1976, E. Turkey events). An attempt to model the complex P-waveforms of these events results in good synthetic fits for the Guatemala and Mudurnu Valley events. However, the E. Turkey event proves to be too complex as it may have associated thrust or normal faulting. Several individual sources occurring at intervals of between 5 and 20 seconds characterize the Guatemala and Mudurnu Valley events. The maximum size of an individual source appears to be bounded at about 5×10^{26} dyne-cm. A detailed source study including directivity is performed on the Guatemala event. The source time history of the Mudurnu Valley event illustrates its significance in modeling strong-ground motion in the near field. The complex source time series of the 1967 event produces amplitudes greater by a factor of 2.5 than a uniform model scaled to the same size for a station 20 km from the fault.

Three large and important earthquakes demonstrate an important type of complexity --- multiple-fault complexity. The first, the 1976 Philippine earthquake, an oblique thrust event, represents the first seismological evidence for a northeast dipping subduction zone beneath the island of Mindanao. A large event, following the mainshock by 12 hours, occurred outside the aftershock area and apparently resulted from motion on a subsidiary fault since the event had a strike-slip mechanism.

An aftershock of the great 1960 Chilean earthquake on June 6, 1960, proved to be an interesting discovery. It appears to be a large

strike-slip event at the main rupture's southern boundary. It most likely occurred on the landward extension of the Chile Rise transform fault, in the subducting plate. The results for this event suggest that a small event triggered a series of slow events; the duration of the whole sequence being longer than 1 hour. This is indeed a "slow earthquake".

Perhaps one of the most complex of events is the recent Tangshan, China event. It began as a large strike-slip event. Within several seconds of the mainshock it may have triggered thrust faulting to the south of the epicenter. There is no doubt, however, that it triggered a large oblique normal event to the northeast, 15 hours after the mainshock. This event certainly contributed to the great loss of life sustained as a result of the Tangshan earthquake sequence.

What has been learned from these studies has been applied to predict what one might expect from the next great earthquake on the San Andreas. The expectation from this study is that such an event would be a large complex event, not unlike, but perhaps larger than, the Guatemala or Mudurnu Valley events. That is to say, it will most likely consist of a series of individual events in sequence. It is also quite possible that the event could trigger associated faulting on neighboring fault systems such as those occurring in the Transverse Ranges. This has important bearing on the earthquake hazard estimation for the region.

TABLE OF CONTENTS

INTRODUCTION

In recent years our understanding of earthquakes has increased greatly. For a large part, progress has come through the analysis of seismograms recorded by the World-Wide Standardized Seismographic Network (WWSSN) which began operation in 1963. In particular, time-domain modeling techniques for both body waves and surface waves have played an important role in such progress and are now a significant part of any detailed earthquake study. These studies depend to a large degree on the calculation of synthetic seismograms and their comparison with observed data. The quality or "goodness of fit" of these synthetics gives an idea of how well one understands the earthquake process. The effects of source structure, propagation path, attenuation and the source geometry all play a part in the modeling procedure. In many of the first studies greatest progress was made in the modeling of "simple looking" body waveforms. By so doing, the theoretical concepts behind the modeling procedures could be tested and an understanding provided from which to progress to more complicated records.

The purpose of this thesis is to try to understand the mode of rupture of several recent earthquakes by investigating and seeking an explanation for the various degrees of complexity exhibited in the seismograms of these events. The selection of events is based mainly on their importance with respect to this question. A key factor in the analysis of any earthquake is the determination of its source mechanism. Both body wave and surface wave data are used to provide the best constraint possible to the focal mechanism, as a first step, so as to

avoid possible misinterpretations later in the analysis. When possible, the plate tectonic environment of the events is considered to provide a more complete picture of the relationship of the event to its surrounding environment.

To begin with, in Chapter 1, several relatively simple events are studied and an attempt made to understand the basis for their simplicity. In Chapter 1, Section 1.2, the recent Oaxaca, Mexico earthquake of November 29, 1978 is examined. It is important because of its location within a predetermined seismic gap. A detailed study of the event is made in this section. It appears, from modeling the long-period P-wave data, that it is a large, simple single event, perhaps the result of the breaking of a fault zone asperity.

The analysis of the Oaxaca earthquake is extended in Section 1.3 to include other $M \geq 7.0$ events along the Middle America Trench. The events adjacent to the Oaxaca event occurring on August 23, 1965 and August 2, 1968 appear to be very similar to it as does the Petatlán event of March 14, 1979. All these events are of predominantly thrust type, consistent with subduction to the northeast of the Cocos plate. Whereas the body waves of the 1965, 1968, 1978 and 1979 events along the trench indicate rather simple faulting processes, the 1970 and 1973 events, the eastern- and western-most, respectively, of the events studied here, show greater complexity in their body waves, perhaps representing a transition to regions of more complicated tectonics.

Whereas the P-waves of the 1965, 1968, 1978 and 1979 events studied in Section 1.2 and 1.3 "look simple", those from the Bermuda earthquake

of March 24, 1978 "look complex". In Section 1.4 the apparent complexity of this unusual oceanic intraplate event is studied. It appears that this complexity is due to the interaction of the seismic waves with the source structure, especially the water layer, rather than due to a complex source. The event, which lies just below the Moho, is the result of the application of present-day stress imposed on the region by the North American plate in the direction of its absolute motion.

Chapter 2 deals with the complexity of rupture propagation in large strike-slip earthquakes. Two major, global strike-slip fault regions are selected because of their recent activity with respect to large earthquakes. In Section 2.2 the Guatemala earthquake of February 4, 1976 on the Motagua fault is studied whereas in Section 2.3 two major events on the Anatolian fault in Turkey are investigated. These events all show extremely complicated WWSSN long-period P-waveforms. The body wave analysis suggests that the earthquakes consist of as many as ten independent and distinct events occurring at intervals between 5 and 20 seconds. Thus, for these cases, the rupture propagation is jagged and is perhaps a manifestation of a heterogeneous distribution of the mechanical properties along the fault which may be caused by either asperities, differences in strength, differences in pore pressure, differences in slip characteristics (stable sliding v's stick-slip) or combinations of these factors. These events are important because they occur in continental crustal environments not unlike that of the San Andreas fault and so an understanding of them may lead to a better

insight into what could be expected for the next major earthquake along other strike-slip systems such as the San Andreas fault.

Chapter 3 deals with multiple-fault complexity. Three events are discussed for which the principal aftershock in each case has a source mechanism completely different from that of the mainshock. They are the Mindanao, Philippine earthquake of August 16, 1976, the Chilean earthquake of May 22, 1960 and the Tangshan, China earthquake of July 27, 1976. Section 3.2 deals with the Philippine earthquake which occurred in the Moro Gulf, N. Celebes Sea, south of Mindanao. It had a shallow focus and caused a locally destructive tsunami. The source mechanism was one of predominant thrusting to the northeast, with subduction occurring beneath the island of Mindanao.

The largest aftershock (M_s = 6.8) occurred to the northwest of the main aftershock area, twelve hours following the mainshock and had a pure strike-slip mechanism. No bathymetric or fault-related features are known to correspond with the location of this event.

A similar relationship of mainshock thrusting triggering a large strike-slip event is discussed in Section 3.3. The May 22, 1960 Chilean earthquake, the largest recorded earthquake (M_w = 9.5) was followed by several large aftershocks. The one occurring on June 6, 1960 was especially anomalous, however. Although the surface wave magnitude was only 6.9, it excited anomalously long-period multiple surface waves with a seismic moment of 5.6×10^{27} dyne-cm. The event probably occurred on a transform fault, on the extension of the Chile Rise.

Even greater diversity in the nature of multiple faulting is to be

found in the example of the Tangshan, China earthquake. This event is discussed in Section 3.4. Strike-slip, thrust and normal faulting all appear to have been associated in a complex sequence of events. The mainshock (M_s = 7.7) occurred on a near-vertical right-lateral strike-slip fault. Two thrust events follow the strike-slip event by 11 and 19 seconds, respectively, and are located south of the initial event. The principal aftershock, which followed the main event by fifteen hours was a normal fault, double event. Triggering of lesser thrust and normal events by a large strike-slip event in the Tangshan sequence has important consequences in the assessment of earthquake hazard in other complex strike-slip systems like the San Andreas.

Chapter 4 summarizes the findings of the earlier chapters by considering what one might expect during the next great earthquake on the San Andreas fault. Although, by necessity, a speculative task, much insight can be gained from the studies of these other events, albeit they have occurred in different or similar environments around the world.

CHAPTER 1.

SIMPLE EARTHQUAKE SOURCES

1.1 Introduction.

Before examining several complex earthquakes in detail in Chapters 2 and 3, it is important first to look at and understand what is meant by the term "simple earthquake sources".

By a "simple earthquake source" I mean one which can be characterised and interpreted as consisting of a single event in the period range of the WWSSN long-period body waves. Such an event may have a time function of several seconds to tens of seconds duration with associated fault rupture on the scale of tens of kilometers. From the viewpoint of better understanding the relationship of an event to its tectonic environment it is these dimensions which are the most significant. By examining shorter period data, say as shown on the WWSSN short-period seismograms, an event viewed as simple in the long-period framework may no longer be such, but may become a complex sequence of events. Moving to shorter periods still, as with strong-motion records, the complexity would generally be greater. In the opposite sense, at very long periods, say on the order of several hundred seconds, corresponding to fault rupture of several hundred kilometers, most events appear simple.

One would expect that small to intermediate size events would have simple sources, e.g. the 1978 Thessaloniki, N. Greece earthquake

(Soufleris and Stewart, 1981), whereas large events would be complex, e.g. the 1964 Alaskan earthquake (Wyss and Brune, 1967). Although this is probably true, in general, there are several exceptions. In their studies of the 1971 San Fernando earthquake, Heaton (1981) and Langston (1978) found this small to intermediate size event to be quite complex. In Sections 1.2 and 1.3 of this chapter evidence for several large simple events will be presented. They are located along the Middle America Trench.

When viewed on the WWSSN long-period seismograms, some events may look quite complex although in fact they are actually very simple. Such a case is the 1978 Bermuda earthquake (m_b = 6.1) which is discussed in Section 1.4. As will be demonstrated, the apparent complexity displayed on the P-wave seismograms is actually due to a complicated source structure and not to the event itself.

In all sections, the tectonic implications of the results of the detailed analyses will be discussed.

1.2 The Oaxaca, Mexico Earthquake: A Large Simple Event.

ABSTRACT

The recent Oaxaca, Mexico earthquake November 29, 1978 (M_w = 7.6, M_s = 7.8, seismic moment, M_o = 3.2 x 10^{27} dyne-cm), is of special interest because of its location within a predetermined seismic gap. The event excited long-period (100-200 sec) multiple Rayleigh and Love waves which were well-recorded by the WWSSN. These data along with P-wave first-motion data and P-waveforms were used to constrain the source mechanism. The results indicate an oblique thrust mechanism consistent with subduction of the Cocos plate to the northeast beneath Mexico (dip = 14°, strike = N 90°W, rake = +54°); hence this event is indeed of the type anticipated by Ohtake et al. (1977a and 1977b). A local network of stations, installed in a joint University of Mexico-California Institute of Technology program, began operation 20 days prior to the mainshock [González (1979); McNally et al. (1980); Ponce et al. (1980)]. The 43 foreshocks of magnitude M ≥ 2.8 were recorded by the network in a period of 20 days prior to the mainshock. These events show an interesting spatial and temporal pattern, which culminates in the last 1.8 days of the sequence with an apparent migration of activity towards the epicenter of the impending earthquake. This pattern can be interpreted as a buildup of stress or migration of stress towards a fault zone asperity. With supplemental stations, the network continued operation until December 12, 1978 [Singh et al. (1980)] and provided good hypocentral control for the more than 169

aftershocks of magnitude M > 2.8. The area of the aftershock zone determined from these events is 5525 km^2 (85 km by 65 km). In spite of the large size of the event, P-waves for the Oaxaca event indicate an extremely simple source, at the period range of the WWSSN long-period seismographs. This simplicity suggests that the P-waves were generated by a limited portion of the rupture surface, perhaps by the breaking of a fault zone asperity. This result may be further supported by the discrepancy between the larger surface wave moment compared with that determined from body waves. Such simplicity also appears to be the case for the 1965 and 1968 Mexican earthquakes on the adjacent eastern and western ends of the Oaxaca aftershock zone, respectively [Chael et al. (1980)]. This type of body wave simplicity for a large subduction zone earthquake is an important characteristic of the mode of strain release along some subducting plate boundaries.

INTRODUCTION

The Oaxaca, Mexico earthquake of November 29, 1978 [origin time 19h 52m 45.5s U.T.: location 15°46'N, 96°48'W [González (1979); McNally et al. (1980); Ponce et al. (1980)]; depth 18 km; M_s = 7.8; M_w = 7.6 Kanamori (1978)] is one of several large earthquakes to have occurred along the Middle American Trench in recent years (Figure 1-1 and Table 1-1). The event is of special interest because of its location within a predetermined seismic gap [Kelleher et al. (1973); Kelleher et al. (1974); McCann et al. (1978); Ohtake et al. (1977a and 1977b)]. In fact, for a period of 20 days prior to the earthquake, a

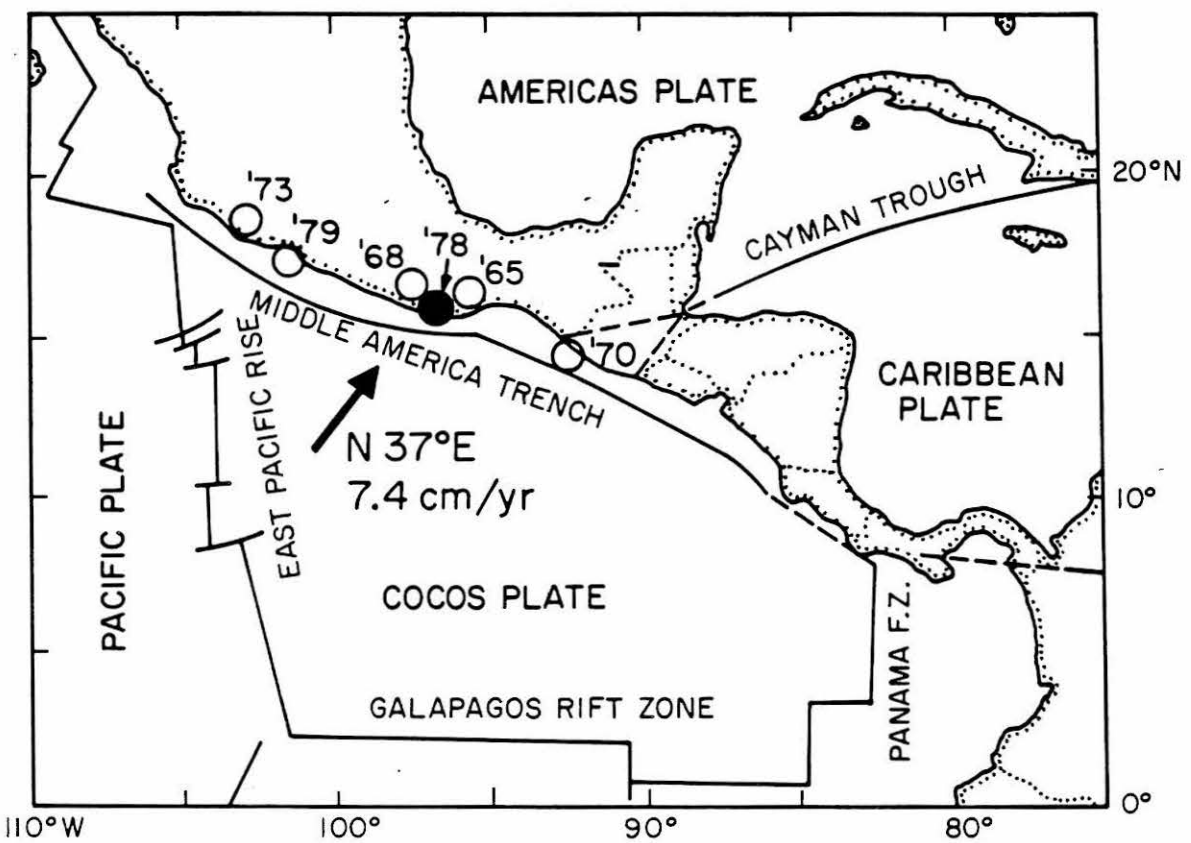

Figure 1-1. Map showing the relationship of the Cocos plate to the surrounding plates in the Central American region. Earthquakes of $M_s > 7.0$ along the northern Cocos plate boundary are plotted for the time period 1963-1979 (open circles) including the Oaxaca earthquake (solid circle). The large arrow represents the direction of motion of the Cocos plate with respect to the Americas plate at the location of the Oaxaca earthquake [calculated from Minster and Jordan (1978)]. This figure is modified from Molnar and Sykes (1969).

TABLE 1-1 Event Parameters

Date	Origin Time (U.T.)	Location		M_s
		^oN	^oW	
Aug. 23, 1965	19h 46m 01.8s	16.30	95.80	7.6
Aug. 2, 1968	14h 06m 43.9s	16.59	97.70	7.1
Apr. 29, 1970	14h 01m 32.8s	14.52	92.60	7.3
Jan. 30, 1973	21h 01m 12.5s	18.48	103.00	7.5
Nov. 29, 1978	19h 52m 45.5s	15.77	96.80	7.8
Mar. 14, 1979	11h 07m 11.2s	17.46	101.46	7.6

Event parameters are taken from McNally and Minster, 1981.

cooperative seismicity study between the Institute of Geophysics of the Universidad Nacional Autónoma de México (UNAM) and the Seismological Laboratory of the California Institute of Technology (CIT) was underway in the region of the identified gap. The mainshock body and surface wave data have been analyzed to constrain the source mechanism and to determine rupture characteristics including seismic moment and stress drop; additionally the results of foreshock and aftershock studies are reviewed in order to provide a more complete description of the rupture process [González (1979); McNally et al. (1980); Ponce et al. (1980)]. The Oaxaca earthquake is one of six events with $M_s > 7.0$ to have occurred along the northeast dipping, subducting boundary of the Cocos plate since the installation of the World-Wide Standardized Seismographic Network (WWSSN). It is concluded that the event represents oblique thrust faulting on a plane with strike N 90°W, dip 14°N and rake +54°. The resulting slip direction on the fault plane (N 37°E) agrees well with the predicted value for the direction of plate convergence at the Oaxaca epicenter obtained from Minster and Jordan (1978) viz. N 37°E and shown in Figure 1-1.

SURFACE WAVE ANALYSIS

As a first step in determining the mechanism of the Oaxaca earthquake, the P-wave first-motion data from all available WWSSN and Mexican stations were read. These data are shown in Figure 1-2. They were, however, only sufficient to constrain the steeply dipping,

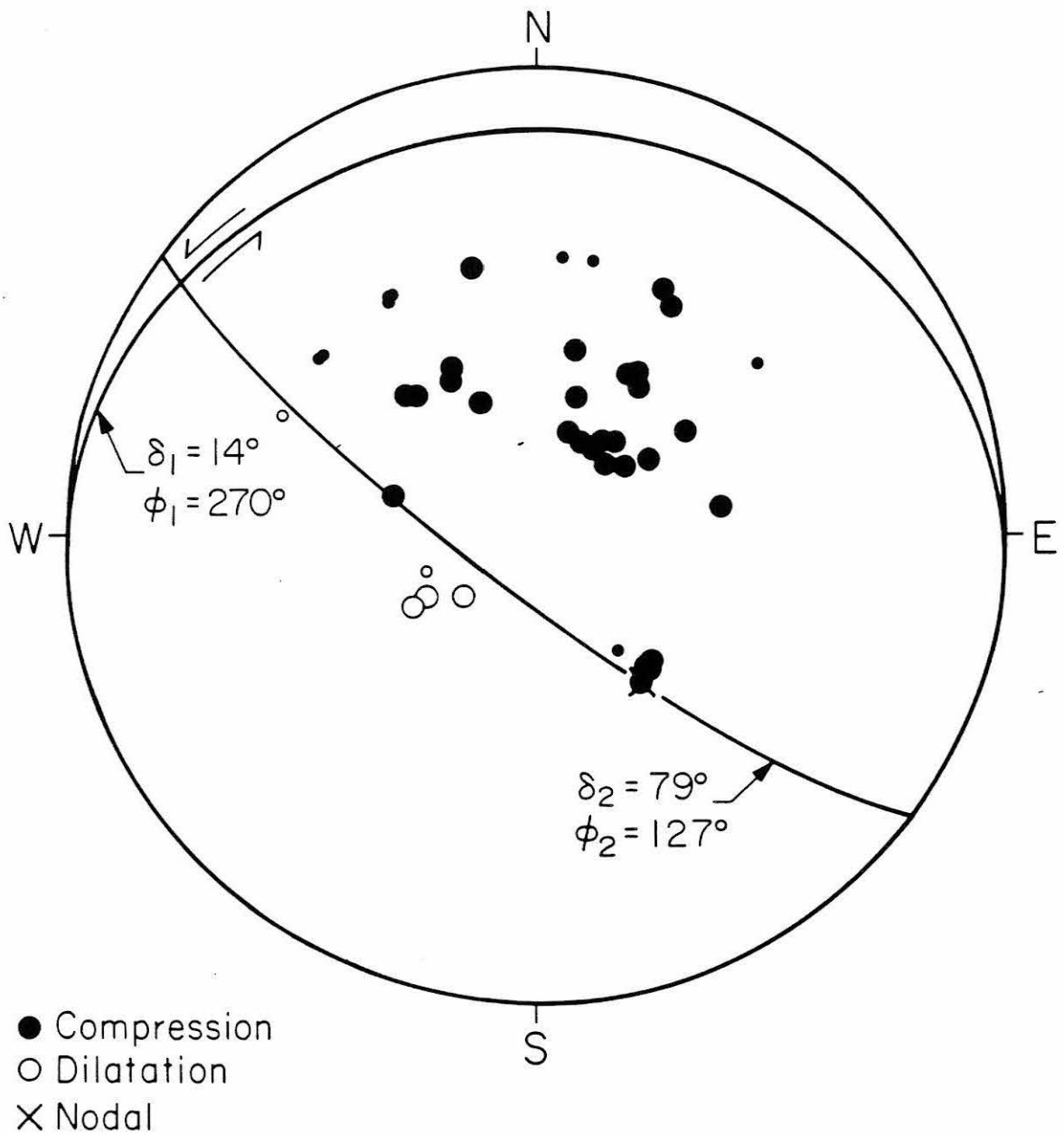

Figure 1-2. P-wave first-motion data for the Oaxaca earthquake of November 29, 1978 indicating shallow thrust faulting to the north. A small amount of left-lateral strike-slip motion is included. The fault plane is constrained by the P-wave data shown and the surface wave data. The smaller dots and circles represent less reliable readings. All data used in this plot were read from the WWSSN and Mexican seismograms, in this study. An equal-area projection on the lower focal hemisphere is shown.

presumed auxiliary plane. Of special significance in providing the constraint was the nodal character of the station Nañia, Peru (NNA). This is a common feature of dominantly shallow angle thrust events at subduction boundaries since few close-in azimuthally well-distributed P-wave first-motion data are usually available to constrain the shallow dipping plane [Abe (1972); Stewart and Cohn (1979)]. However, by using long-period surface waves it is usually possible to constrain both planes of the focal mechanism completely.

The surface waves used in the analysis are multiple R_3 (Rayleigh waves) and G_3 (Love waves) recorded by the World-Wide Standardized Seismographic Network (WWSSN) long-period seismographs and equalized to a propagation distance of $360^\circ + 90^\circ$. When these waves are unobtainable for a given azimuth they can be supplemented by using R_2, G_2 or R_4, G_4 waves which are propagated in either a forward or backward direction for comparison with R_3 or G_3. It should be noted, of course, that R_2, G_2, R_4, G_4 propagate in an azimuth 180° different from R_3 and G_3 waves, for a given station. The equalized data are shown in Figure 1-3. The details of the analysis are given in Kanamori (1970). Filtering of the data to remove short-period (less than 60s) surface waves which are severely affected by structural heterogeneities during propagation, as well as filtering to remove energy at periods greater than 300s was achieved using the method described in Kanamori and Stewart (1976). As seen in Figure 1-3 and 1-4, Rayleigh waves indicated a two-lobed radiation pattern, while the Love wave radiation pattern is four-lobed. Since, for example, the amplitude maxima for Rayleigh waves do not lie

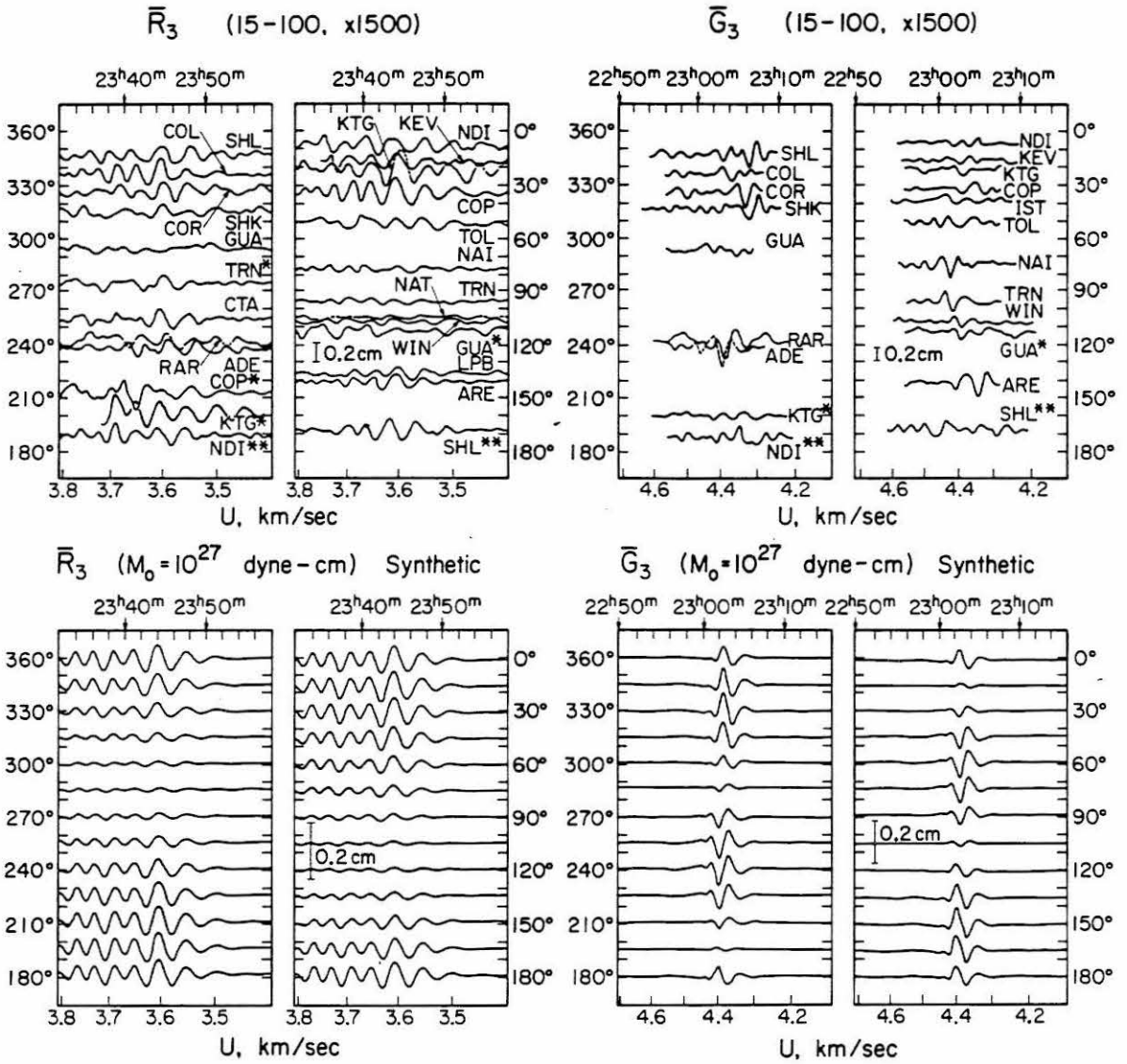

Figure 1-3. Azimuthal plots of equalized seismograms $\bar{R}_3$ and $\bar{G}_3$ and synthetic seismograms computed for the fault geometry shown in Figure 1-2 with a bilateral propagation (50-35 km), rupture velocity, v_r = 2.5 km/s and a rupture azimuth, ϕ_r = 270°. A seismic moment of 10^{27} dyne-cm was used in the synthesis. In the observed patterns one asterisk indicates that R_2 and G_2 were equalized to R_3 and G_3 distances. Two asterisks indicate that R_4 and G_4 were equalized to R_3 and G_3 distances. The amplitude scales are for the trace amplitudes on a WWSSN long-period instrument (15-100) with a magnification of 1500.

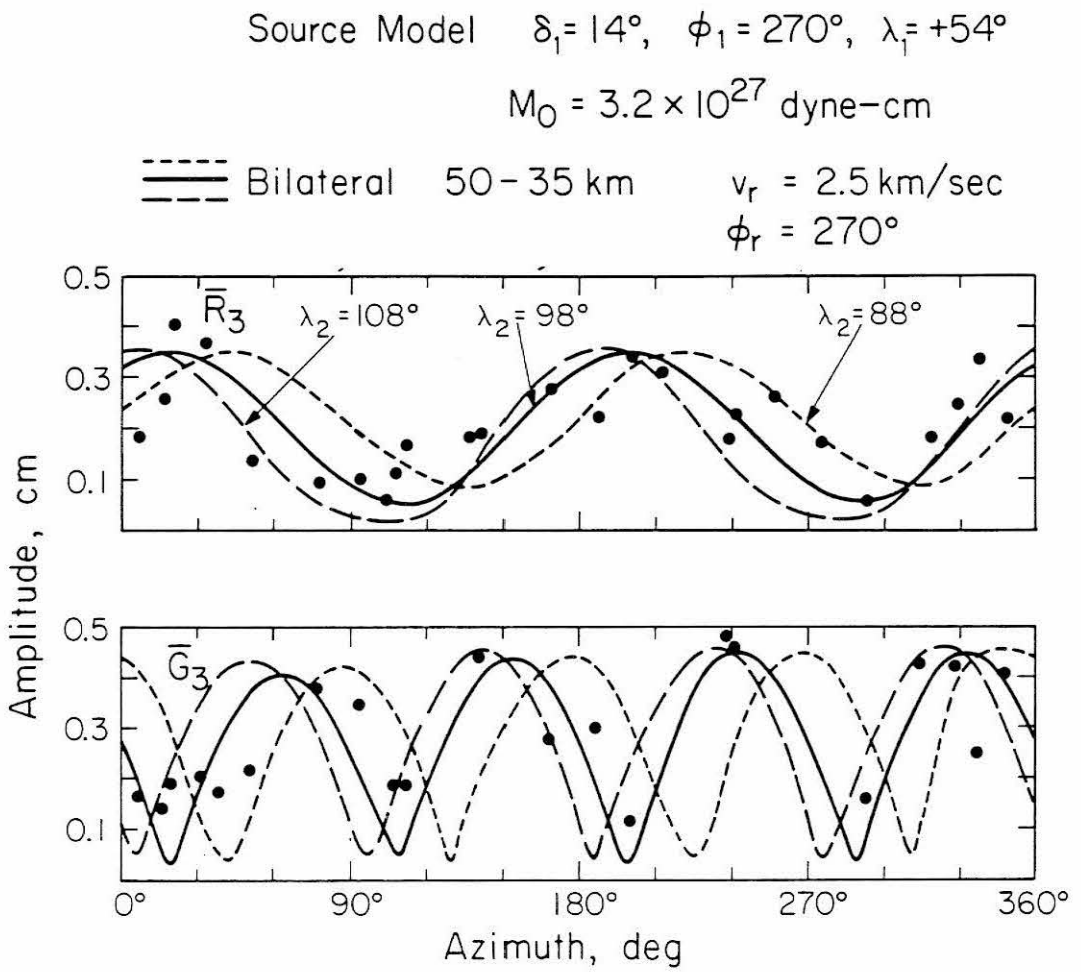

Figure 1-4. Equalized station peak-to-peak amplitudes for observed data ($\bar{R}_3$ and $\bar{G}_3$) plotted as a function of azimuth (solid circles). The solid curve represents the synthetic radiation pattern for the preferred source model ($\lambda_2 = 98^o$ on the auxiliary, constrained plane). The dashed curves are synthetic patterns for models with slip angles $\lambda_2 = \pm 10^o$ from the preferred model.

along the dip direction of the constrained plane, the mechanism cannot be one of pure thrust but must have some strike-slip component associated with it. A similar argument holds for Love waves. The relative maximum amplitude of Love to Rayleigh waves, 1.3 in this case, also changes as a function of the slip angle or rake. This fact is also used in the constraint of the mechanism.

In order to interpret the observed radiation pattern, shown in Figures 1-3 and 1-4, synthetic surface waves were computed for a finite source which ruptured bilaterally 50 km to the west northwest and 35 km to the east southeast from the hypocenter, as suggested by Figure 1-10. The method of synthesis, the gross earth structure and Q structure used in the modeling are described in Kanamori (1970) and Kanamori and Cipar (1974). The same filter which was used on the observed data in Figure 1-3 was applied to the synthetic records (60-300s) so that a direct comparison could be made. The analysis used a step response at 16 km depth which is similar to both the hypocentral depth of 18 km obtained in the P-wave modeling of the mainshock (discussed later), and the depth of 25 km obtained from a single close-in station. Since one fault plane was constrained (see Figure 1-2), it was kept fixed and the slip angle λ, varied until good agreement was obtained in the overall radiation pattern and maximum amplitude ratio for both Rayleigh and Love waves. The preferred solution is shown in Figures 1-2, 1-3, and 1-4. Note that the mechanism is not one of pure thrust but has a significant amount of strike-slip component (slip angle, $\lambda = +54^{o}$) associated with it. Since the fault dimensions in this case are relatively small,

~100 km, small changes in these dimensions, ~ tens of kilometers, or changes in the mode of propagation (unilateral instead of bilateral) as discussed later, make little significant difference to the overall radiation pattern or seismic moment, M_o. At any rate, such a difference could not be resolved from the observed data. In Figure 1-4 the maximum trace amplitudes of the observed Rayleigh and Love wave data for each station are plotted as solid circles, as a function of azimuth. The solid line represents the theoretical calculation and, as shown, the agreement between the observed and theoretical values is satisfactory. In applying the source finiteness a rupture velocity of v_r = 2.5 km/sec and rupture azimuth of $\phi_r = 270^o$ are assumed along with the source mechanism given in Figures 1-2 and 1-3. By matching the resulting amplitudes of the observed and synthetic data, a seismic moment, M_o of 3.2×10^{27} dyne-cm is obtained. This value is similar to that found by Masters et al. (1980) (2 to 3×10^{27}dyne-cm) from IDA data; however a direct comparison may not be meaningful since they use a different source mechanism in their determination. The above results can be interpreted in terms of the average dislocation on the fault, $\bar{D}$, and the average stress drop, $\Delta\sigma$. From Figure 1-10, a fault length, $L \simeq 85$ km and fault width $w \simeq 65$ km can be assumed. After correcting for the small dip angle, we have from Aki (1966) and Kanamori and Anderson (1975b), $\bar{D} = M_o/\mu Lw = 1.2$ m and $\Delta\sigma = 8\mu\bar{D}/3\pi w = 8$ bars where $\mu = 5 \times 10^{11}$ dyne/cm^2 is used.

BODY WAVE ANALYSIS

The available WWSSN records were examined carefully and those which had P-waveforms on-scale were selected for further analysis. Unfortunately, since most WWSSN stations operate at a magnification of 1500, many of the body wave traces are off-scale and so unusable. Of the station data available, it was possible to find three stations for which P-waveforms remained on-scale: Eskdalemuir, Scotland (ESK), Wellington, New Zealand (WEL) and Raratonga, Cook Islands (RAR). These were used together with the vertical component of the ultra long-period instrument at U.C. Berkeley, California (BKS) (T_p = 100, T_g = 300 and peaked at 90s) as shown in Figure 1-5. These waveforms recorded by stations within a distance range of 100° and of good azimuthal distribution, suggest a very simple source. To confirm this, synthetic P-waveforms were generated using the source mechanism in Figure 1-2, and a point source in a half-space structure of P-wave velocity, v_p = 6.1 km/s and S-wave velocity, v_s = 3.5 km/s. This model given by Meyer et al. (1980) was used since a more detailed crustal model was not available. Synthetic waveforms were then calculated using this model and a superposition of direct P and the surface reflected phases pP and sP as shown in Figure 1-5. The method used is described in Kanamori and Stewart (1976). In the modeling process, the depth, rise time and duration of the time function were varied to obtain optimal fits between the synthetic and observed body waves. The synthetic waveforms which were obtained for a depth of 18 km together with the broad time functions (4, 9, 15 sec), shown in Figure 1-5, are in excellent

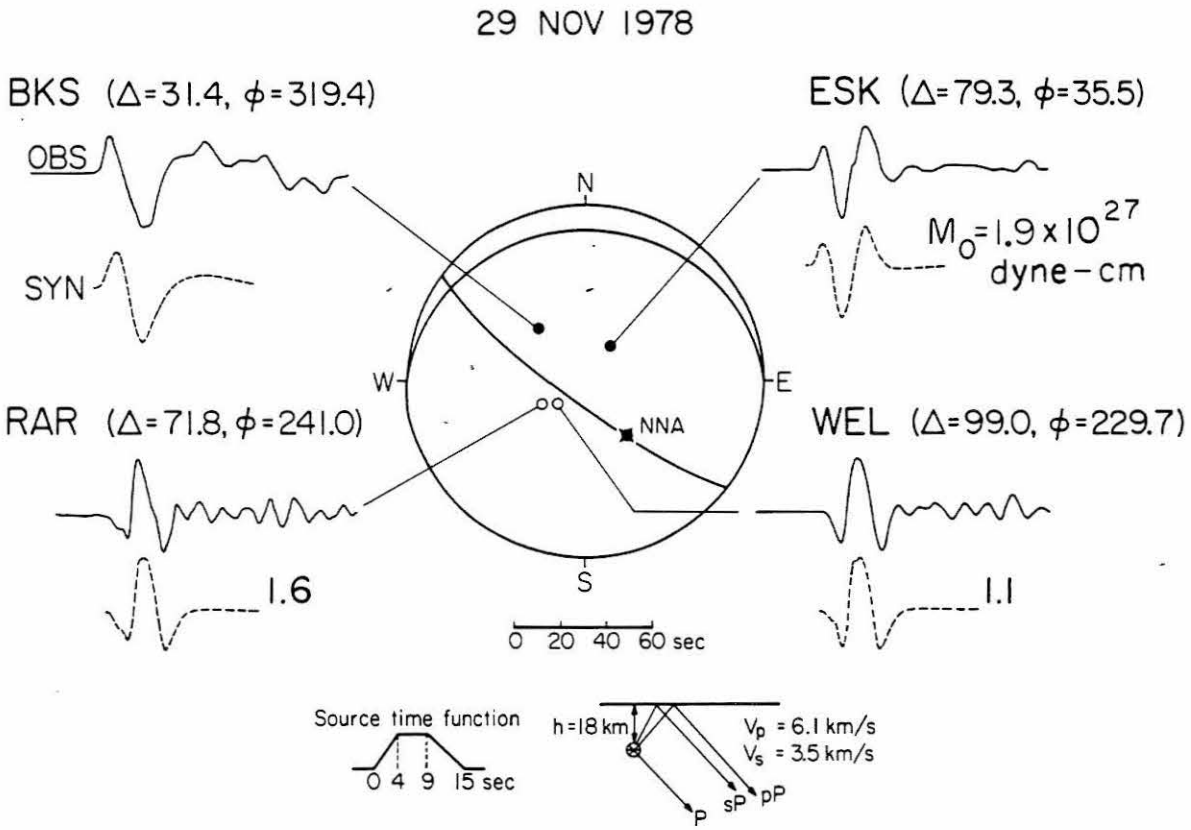

Figure 1-5. Observed and synthetic P-waves. The focal mechanism in the center of the figure is that determined from P-wave first-motions and surface wave data; only the nodal station NNA and those stations used for body wave modeling are shown. Observed P-waves are shown as solid lines, synthetics as broken lines. The synthetic waveforms were generated using the source geometry and time function shown. Records at ESK, WEL and RAR are from WWSSN 15-100 sec vertical component instruments; the BKS record is from an ultra long-period 100-300 sec vertical component instrument.

agreement with the observed data for all four stations. Comparing the observed and synthetic P-wave amplitudes, a body-wave moment of 1.6 to 1.9 x 10^{27} dyne-cm was obtained; somewhat smaller than that for surface waves. Note that the value for WEL is not considered reliable due to the station being beyond 90°. Reichle et al. (1980), however, found a value of 3.0 x 10^{27} dyne-cm for SRO body wave data, and Ward (1980) found values as high as 2.8 ± 0.3 x 10^{27} dyne-cm also for SRO body wave data.

A rough estimate of the rupture duration, τ, can be obtained from the source time function through the relation:

$$\tau = \tfrac{1}{2}\delta t_1 + \delta t_2 + \tfrac{1}{2}\delta t_3$$

(Helmberger and Johnson, 1977) where δt_1, δt_2, and δt_3 are the rise, top, and fall times, respectively. For this time function, δt_1 = 4 sec, δt_2 = 9 - 4 = 5 sec, δt_3 = 15 - 9 = 6 sec: these yield a rupture duration of 10 sec. Combining this with a rupture velocity of 2.5 km/sec gives a maximum rupture area of 1960 km^2 (the area of a circle with a radius of 25 km). This is significantly smaller than the 5525 km^2 area indicated by the aftershock distribution (Figure 1-10) which suggests that the observed P-waves were generated by only a limited portion of the rupture surface; strain in the remaining area may have been relieved more slowly (aseismically) as far as body wave radiation is concerned). This may be the reason for the difference between the surface and body wave moments. This large simple event may,

therefore, result from the initiation of fault rupture by the breaking of a single asperity on the fault surface.

To examine this point further, the first eight minutes of record from the Eskdalemuir (ESK) long-period vertical component instrument have been plotted for the six largest events ($M_s > 7.0$) since 1963, along the northern Cocos plate boundary with Central America. The records are shown in Figure 1-6. The station ESK represents a WWSSN station in a northeasterly azimuth with respect to the various epicenters, at a distance of approximately 80^o. Since all the events then are at similar distances and azimuths to ESK, differences between them should reflect differences in the local source processes, rather than the effects of structure along the propagation path or at the station. Also, one would not expect minor changes in the source mechanisms of the events to significantly affect the signal at the ESK station because of its particular location on the focal sphere. Consequently, any significant changes between events would rather reflect, for example, differences in depth, time function, degree of complexity, local structure, or major differences in focal mechanism. From Figure 1-6, the surprising fact is that four of the six events viz. 1965, 1968, 1978 and 1979 show remarkable similarity, while the other two, 1970 and 1973, are different and look more complex. In particular, it should be noted that the events which occurred adjacent to the Oaxaca gap, on the western side in 1968 and on the eastern side in 1965, look identical to the 1978 Oaxaca event itself, although different in amplitude. A more detailed examination of the other events

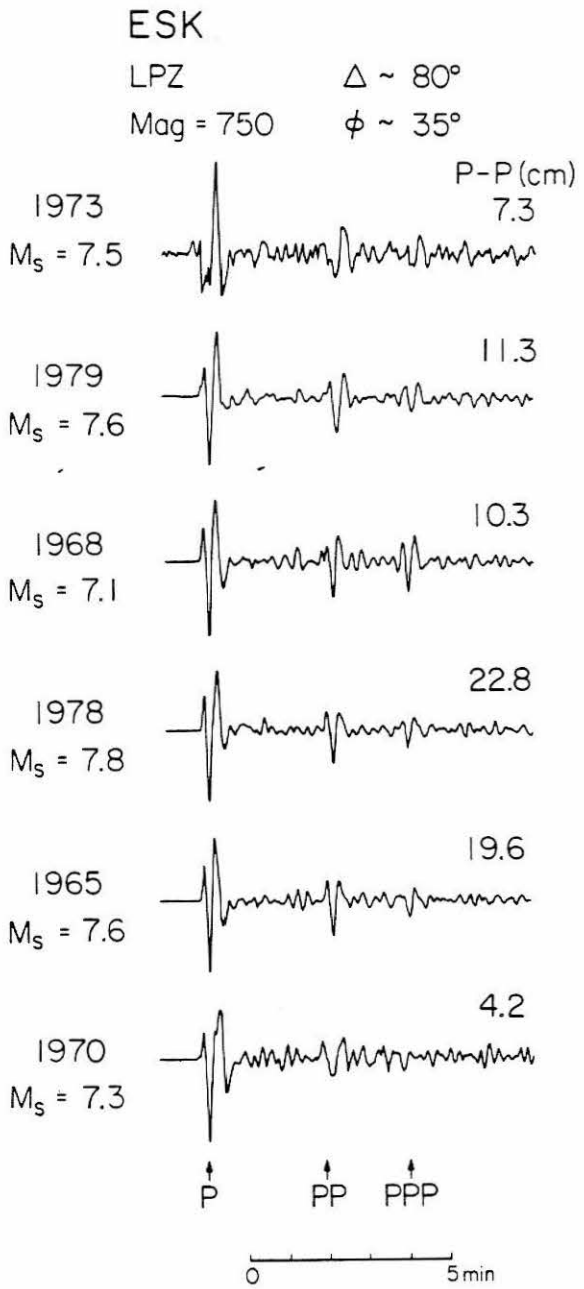

Figure 1-6. Vertical long-period WWSSN seismograms of P, PP and PPP-waves recorded at Eskdalemuir, Scotland (ESK) are shown for the events plotted in Figure 1-1. Note the simplicity of the 1978 Oaxaca event and its similarity to the 1965, 1968 and 1979 events. Peak-to-peak amplitudes for each waveform are also given. The 1978 event has the largest amplitude.

is presented in Section 1.3. Body wave simplicity of this nature has been observed for other subduction zone earthquakes of comparable seismic moment, notably in the Solomon Islands [Lay and Kanamori (1980)] and so represents an important characteristic of the mode of strain release along some subduction plate margins.

FORESHOCK AND AFTERSHOCK STUDIES

As a result of the work done by Ohtake et al. (1977a and 1977b) in identifying a seismic gap in Oaxaca, Mexico, the Institute of Geophysics of the Universidad Nacional Autónoma de México (UNAM) and the Seismological Laboratory of the California Institute of Technology (CIT) established a cooperative study to monitor the seismicity in the region of the Oaxaca gap. This study began on November 8, 1978. Six temporary seismographic stations were set up in and around the Oaxaca gap using smoked paper portable instruments from UNAM. The records were changed on a 24 to 48 hour basis and in the 20 days of recording up to the mainshock a total of 43 foreshocks of $M \geq 2.8$ were recorded.

The resulting locations, shown in Figure 1-7, are based on an assumed flat-layered crustal velocity model. Apart from the fact that most of them lie to the north of the mainshock epicenter, no obvious structure in the distribution of events can be noted. A north-south cross-section plot of these events shows no remarkable features either, which may be a result of the poorly constrained depths of the foreshocks. If, however, the 43 foreshocks are plotted in four time windows as shown in Figures 1-8a, b, c, and d, a pattern begins to

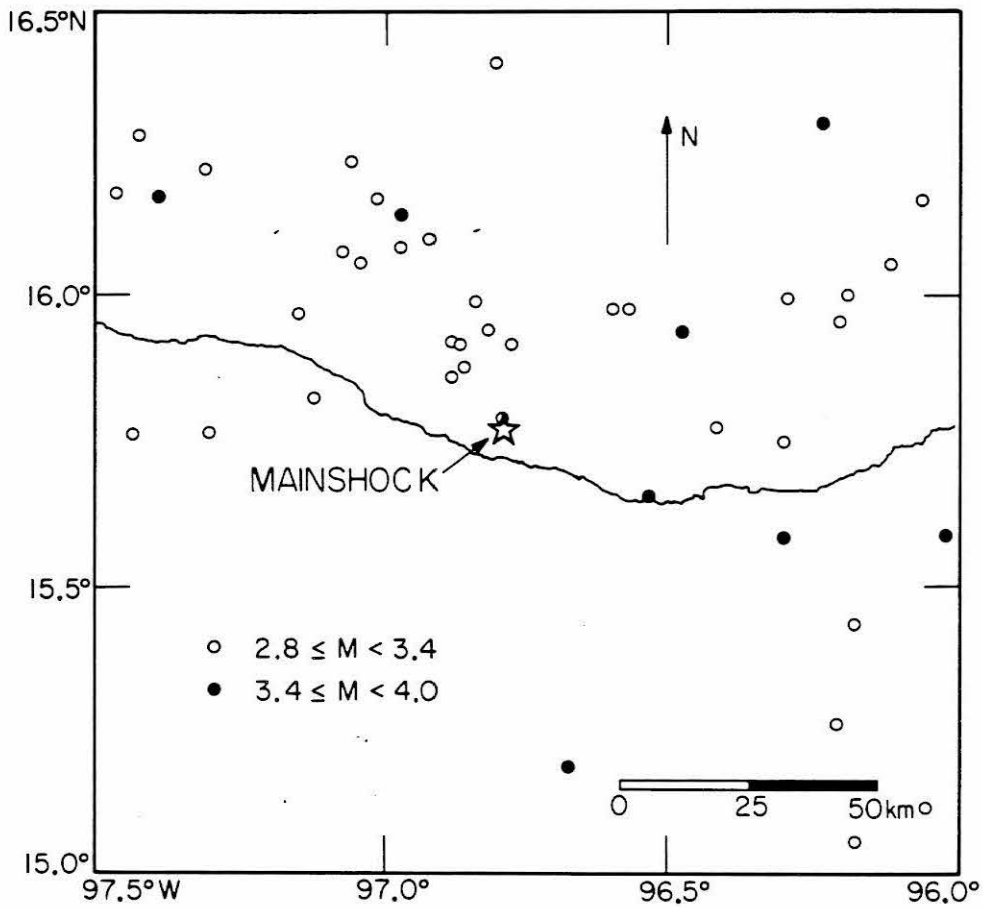

Figure 1-7. Foreshocks to the Oaxaca earthquake for the time period November 10, 1978 up to the mainshock (large star).

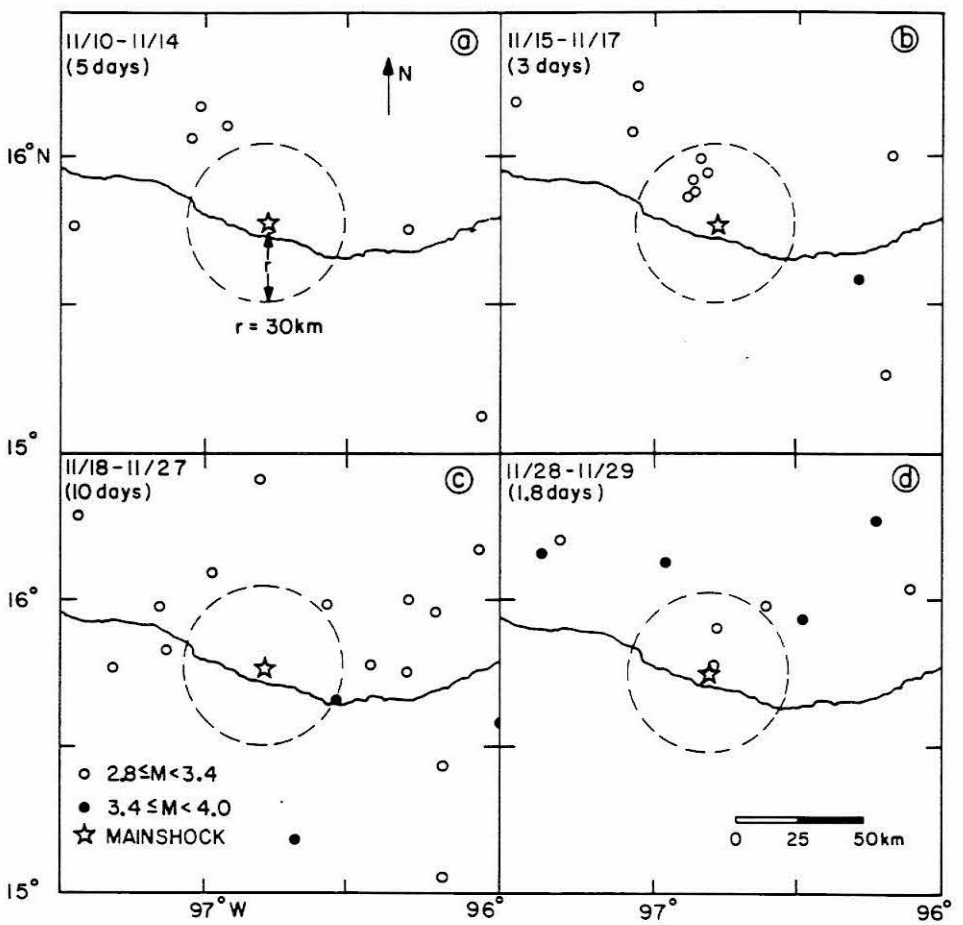

Figure 1-8a,b,c,d. Foreshocks to the Oaxaca earthquake shown in Figure 1-7 ($M \geq 2.8$) replotted for the time windows shown.

emerge. In the initial 5-day time window, from Nov. 10 to Nov. 14, Figure 1-8a, all of the events recorded lie outside a circle of radius 30 km centered on the epicenter of the impending earthquake (the star in Figures 1-8a through 1-8d). The subsequent 3 days of activity, Nov. 15 to Nov. 17, Figure 1-8b, include a clustering of epicenters to the northwest of the epicenter. The significance of this cluster is not clear at present; the clustering may reflect a buildup of stress close to the impending epicenter. However, for the following 10 days, Nov. 18 to Nov. 27, Figure 1-8c, the area inside of the circle is again quiet, while moderate activity occurs around it. In the last 1.8 days of the foreshock sequence the seismic activity occurs mainly to the north. During this time window, which is the shortest, the largest of the foreshocks occurs viz. $M \geq 3.4$. In addition, there appears to be an apparent migration of activity towards the impending epicenter. To investigate this further the foreshock activity in this interval was examined more closely; six additional events of $M < 2.8$ were located and added to those already plotted in Figure 1-8d. The resulting pattern is shown in Figure 1-9. The initial event of the sequence, shown in Figure 1-9 is labelled "1". After this event a pattern appears to form in which several events, illustrated by the curved lines, apparently migrate towards the impending mainshock. The sequence can be followed in curves a through d. This apparent migration pattern may be interpreted as a buildup of stress towards a "soon to break" asperity or fault "hang up." This point then becomes the hypocenter of the mainshock, as the rising stress level reaches the critical stress level

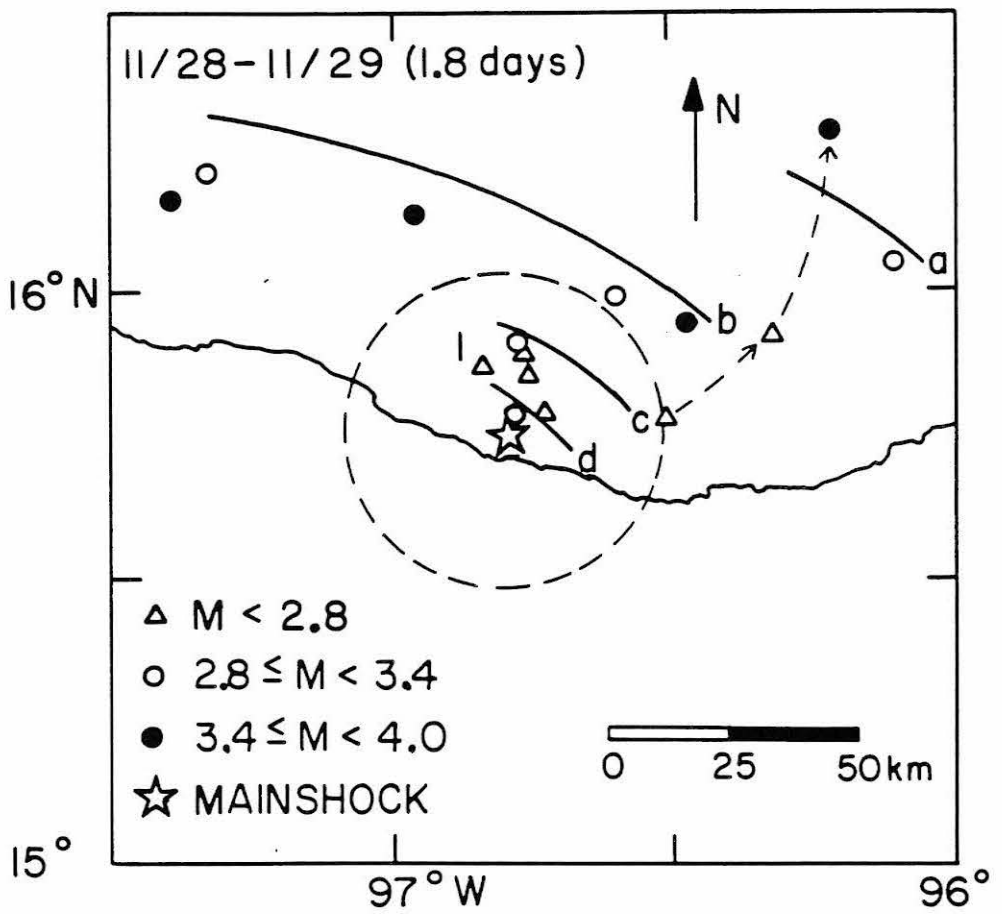

Figure 1-9. Foreshocks of all magnitudes occurring in the 1.8 day period prior to the Oaxaca mainshock. The "1" represents the initial foreshock in this time period with several events subsequently migrating from a through d at the mainshock epicenter and then outwards following the dashed line.

for failure. Just prior to the mainshock three events occur in sequence moving away from the source region as indicated by the dashed curved line and arrows. At this point their significance to the overall pattern is not understood but because they are few in number, their presence only minimally disrupts the pattern shown by curves a through d.

Following the Oaxaca mainshock of November 29, 1978 additional portable seismographs were sent to the field area both from UNAM and from CIT. A denser network of stations was thus established to monitor aftershock activity [Singh et al. (1980)]. More than 169 aftershocks were recorded and located using this network, in the period up through December 12, 1978. The epicenters of the aftershocks are plotted in Figure 1-10. The shaded area in Figure 1-10 gives an estimate of the fault plane area. Its dimensions are approximately L = 85 km and w = 65 km, with the rupture occurring in an asymmetric bilateral mode. In Figure 1-11 the same events are plotted in the north-south cross-section AB shown in Figure 1-10. The fault plane taken from Figure 1-2, dipping 14^{o} to the north is also plotted in Figure 1-11 and appears to be a reasonable fit to the data. Note that many of the larger events ($M > 4.0$) plot close to the plane. Many of the aftershocks may not lie on the fault plane, however, but may be distributed in the crust above or below it as a result of local stress redistribution following the mainshock.

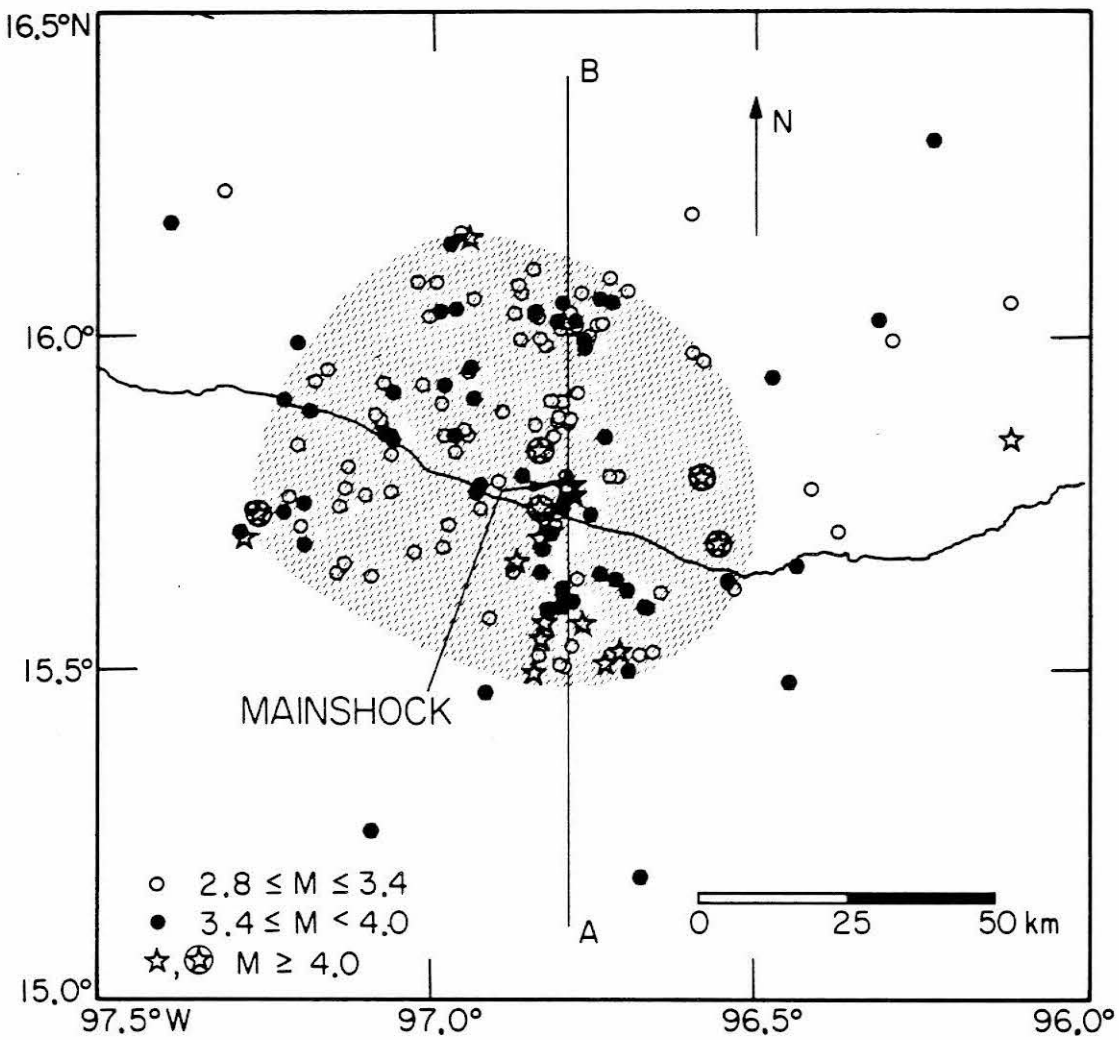

Figure 1-10. Aftershocks of the Oaxaca earthquake for the time period from the mainshock (large star) to the end of December 1978. Events shown are for magnitudes $M \geq 2.8$. The circled stars represent larger aftershocks $M \geq 4.0$ occurring prior to the installation of the local aftershock network. They are located relative to the mainshock by a master event technique [Singh et al., (1980)].

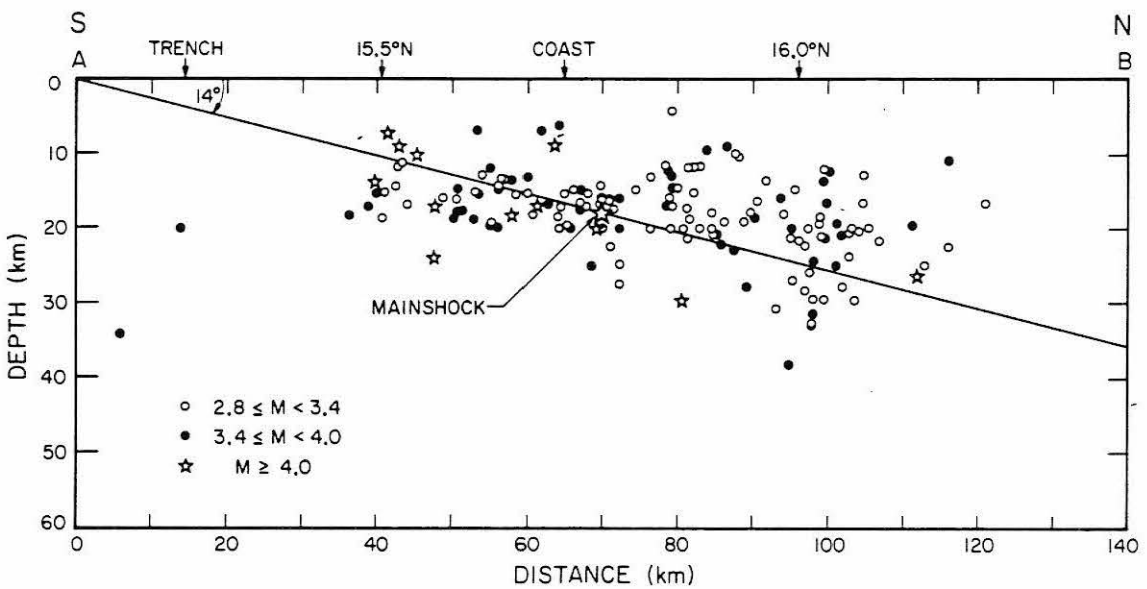

Figure 1-11. A north-south cross-section A-B through the aftershock zone. See Figure 1-10 for location. The fault plane obtained from the source mechanism study (Figure 1-2) is also drawn dipping to the north at 14°.

CONCLUSIONS

The Oaxaca earthquake appears to be a large simple event. With the availability of a varied high quality data set from both local and WWSSN stations, it has been possible to examine several characteristics of the event. The source mechanism of the November 29, 1978 Oaxaca, Mexico earthquake is one of oblique thrust, with the fault plane dipping to the north (strike N 90°W, dip 14° and rake +54°, see Figure 1-2). The seismic moment, $M_o = 3.2 \times 10^{27}$ dyne-cm, is calculated from WWSSN long-period multiple surface-wave data. The event is remarkable because of its simplicity in the period range of the WWSSN long-period seismographs. Synthetic modeling of a set of four well-recorded P-waves confirms the above mechanism, as well as establishes a depth of 18 km for the mainshock hypocenter. This depth is in good agreement with that determined for the mainshock from the local network data. Foreshock data analyzed in this study indicate a migration pattern towards the epicenter of the impending earthquake for the time period 1.8 days prior to the mainshock. This pattern suggests a buildup of stress at a fault zone asperity just prior to failure. Aftershock epicenters delineate an aftershock zone of area 5525 km^2 (85 km by 65 km). These data, together with synthetic modeling of the WWSSN long-period P-waves, suggest that the P-waves were generated from an area smaller than the total aftershock area. A discrepancy in the body wave and surface wave moments for the Oaxaca event may also be the result of this. Reichle et al. (1980) did not find such a moment discrepancy in their study. They did, however, support the conclusion of the initial rupture taking

place over a small area (asperity in the definition used here) and spreading into a larger area. They determined the source radius of the initial rupture to be about 10 km, with an implied stress drop of over a kilobar, in contrast to a stress drop of 10 bars determined from long-period surface wave data and the total aftershock area. Such detailed analyses will be discussed in Section 1.3 for other events along the Middle America Trench. They are also being carried out for other subduction zones. Lay and Kanamori (1980), for example, found similar results for doublet events in the Solomon Islands, lending support to the asperity model of rupture propagation for at least some subduction zone boundaries.

1.3 Middle American Trench Events of $M_s > 7.0$: Simple Subduction Events.

ABSTRACT

Several large shallow earthquakes ($M_s > 7.0$) have occurred along the Middle American Trench since the installation of the WWSSN network. Included are the 1965, 1968, and 1978 Oaxaca events, the 1970 Chiapas event, the 1973 Colima event and the 1979 Petatlán event. These earthquakes have been studied in an attempt to identify similarities and differences between them that may lead to a better understanding of fracture and subduction processes. The events have seismic moments ranging from 1.0×10^{27} dyne-cm for the 1968 event to 3.2×10^{27} dyne-cm for the 1978 event. All events are of predominantly thrust type, consistent with subduction to the northeast of the Cocos plate. Body waves for the 1965, 1968, 1978 and 1979 events along the trench indicate rather simple faulting processes. These events all had focal depths of 15 to 20 km and stress drops on the order of 10 bars. Similarities which Ohtake et al. (1977a and 1977b) identified in the precursory seismicity of events along the Middle American Trench thus appear to continue through the mainshock sequences. The 1970 and 1973 events, the eastern- and western-most, respectively, of the events studied here, are located close to triple junctions for the Cocos-N. America-Caribbean plates (1970) and the Cocos-N. America-Rivera plates (1973). They show greater complexity in their body waves, perhaps representing a transition to regions of more complicated tectonics.

INTRODUCTION

Synthetic modeling of body wave and surface wave seismograms has led, in recent years, to a better understanding of the source processes of many earthquakes. This has resulted in more detailed knowledge of the tectonic environments in which these events occurred.

Studies based on synthetic modeling can be made for most events, regardless of the focal mechanism or rupture complexity. For example, Soufleris and Stewart (1981) analysed the P- and S-waves of the 1978 Thessaloniki earthquake sequence in N. Greece, an area of predominantly normal faulting. Rial (1978) modeled the P, SH and Love waves of the 1967 Caracas, Venezuela earthquake in order to gain a better understanding of this complex strike-slip event. Lay and Kanamori (1980) studied the body and surface waves of several large thrust events in the Solomon Islands, providing insight into the tectonics of a rather complicated region. These studies demonstrate the flexibility of synthetic modeling methods for studying earthquakes on a world-wide basis. In differing environments such detailed studies can elucidate the tectonic relationships which may otherwise go unnoticed because of the inaccessibility of the primary faulting.

In this study, six shallow $M_s > 7.0$ events that have occurred along the subduction zone in Central America since the installation of the WWSSN network in 1963 are analysed. They are shown in Figure 1-12 and listed in Table 1-2. Note that they all occur in the northern section of the Middle America Trench, along the southern coast of Mexico.

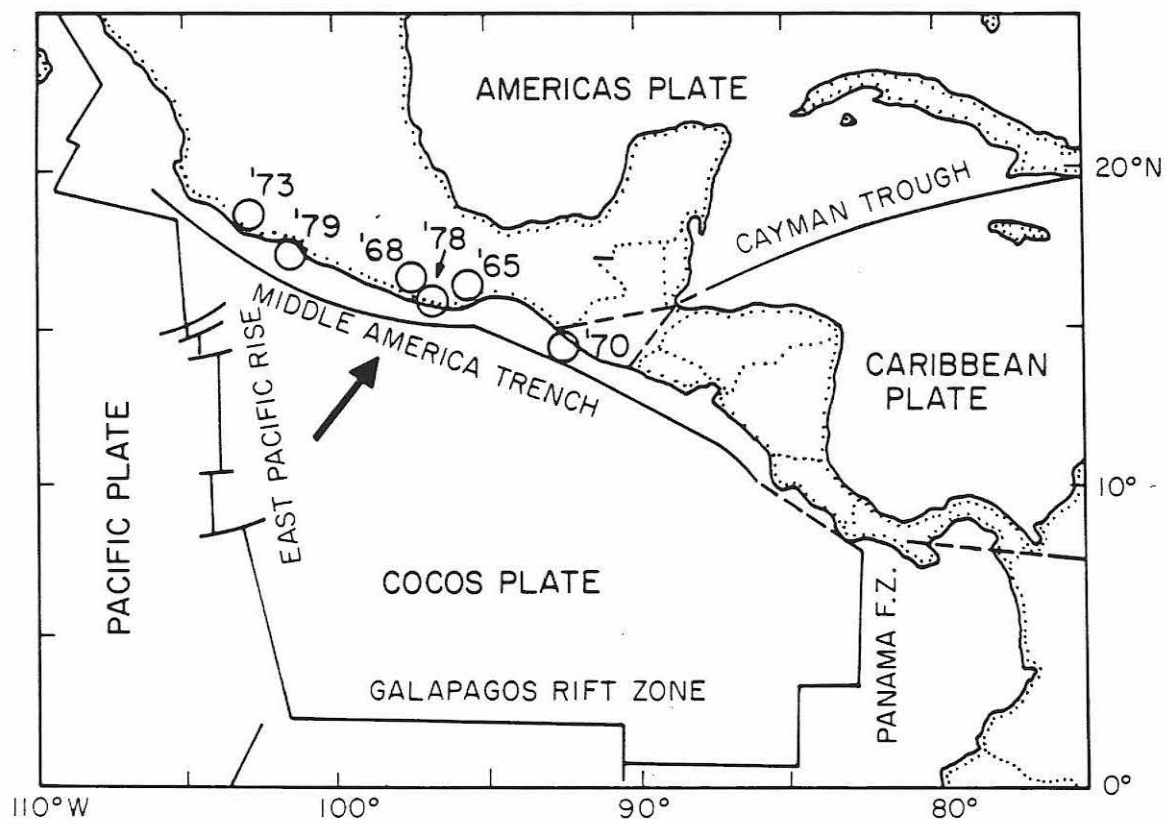

Figure 1-12. Map showing the relationship of the Cocos plate to the surrounding plates in the Central American region. Earthquakes of $M_s > 7.0$ along the northern Cocos plate boundary are plotted for the time period 1963-1979 (open circles). The large arrow represents the direction of motion of the Cocos plate with respect to the North American plate. This figure is modified from Molnar and Sykes (1969).

TABLE 1-2 Event Parameters

Date	Origin Time (U.T.)*	Location* °N	Location* °W	Depth (km)	L (km)	w (km)	A (km^2)	M_o (x 10^{27} dyne-cm) P-waves	M_o (x 10^{27} dyne-cm) Rayleigh waves	$\bar{D}$ (m)`	$\overline{\Delta\sigma}$ (bars)	M_s^*	M_w^o	Slip Direction +
Aug 23, 1965	19h 46m 01.8s	16.30	95.80	16	105	47	4940	1.9	1.7	0.7	6	7.6	7.5	N35°E
Aug 2, 1968	14h 06m 43.9s	16.59	97.70	16	84	50	4200	0.8	1.0	0.5	4	7.1	7.3	31°
Apr 29, 1970	14h 01m 32.8s	14.52	92.60	25	130	96	12480	0.5	1.2	0.2	1	7.3	7.4	26°
Jan 30, 1973	21h 01m 12.5s	18.48	103.00	-	90	63	5670	-	3.0	1.1	7	7.5	7.6	32°
Nov 29, 1978	19h 52m 45.5s	15.77	96.80	18	85	67	5690	1.9	3.2	1.2	8	7.8	7.6	37°
Mar 14, 1979	11h 07m 11.2s	17.46	101.46	20	70	57	3990	1.0	2.7	1.4	10	7.6	7.6	26°

* Taken from McNally and Minster, 1981.

o Calculated from Kanamori, 1978.

\+ Motion of Cocos plate relative to continent.

Other event parameters were determined in this study.

Dimensions of aftershock areas are for the projection onto the fault plane with the dip as given by focal mechanisms in Figure 1-13.

This section was motivated by a study of the 1978 Oaxaca event by Stewart et al. (1981). That study revealed the rupture time history of the large 1978 event to have been remarkably simple. As a result it was considered important to investigate the other $M_s > 7.0$ events in the region and compare them with the 1978 Oaxaca earthquake. In this regard, the events on either side of the 1978 event - the 1968 event to the west and the 1965 event to the east - are especially significant.

It was fortunate to have P-waves on-scale for many of the WWSSN seismograms. This is rather unusual since many of the subduction zone events around the world are large enough to cause P-waves at most WWSSN stations to go off-scale. The typical subduction events in Central America have smaller rupture areas and are generally smaller in magnitude compared with those in other regions (Kelleher et al., 1973).

The six events are studied using various methods to constrain as completely as possible the various source parameters. In particular, synthetic modeling of P-waves and Rayleigh waves was performed. The P-wave analysis determined the depth, rupture time history, and degree of complexity of the events, while the Rayleigh wave analysis constrained the seismic moment and mechanism of each event.

The six events appear remarkably similar; most exhibit simple, smoothly propagating ruptures. The two events with the greatest complexity lie near the eastern and western ends of the Cocos-N. America plate boundary.

TECTONIC SETTING

The principal tectonic activity (Figure 1-12) in southern Mexico and Central America is the subduction of the Cocos plate along the Middle American Trench, beneath the North American and Caribbean plates (Molnar and Sykes, 1969; Dean and Drake, 1978). The descending slab dips more steeply under the Caribbean plate; south of Guatemala one sees a rapid progression from shallow to intermediate depth seismicity landward of the trench (Molnar and Sykes, 1969). In this region, a prominent chain of Quaternary volcanoes parallels the trench (Stoiber and Carr, 1973 and Figure 1-24). The Cayman Trough - Motagua Fault transform system divides the Caribbean and North American plates. The Guatemala earthquake of February 4, 1976 (M_s = 7.5) resulted from left-lateral strike-slip motion on the Motagua Fault (Kanamori and Stewart, 1978). To the northwest of this transform, the Cocos plate subducts at a relatively shallow angle ($\sim 10^o - 20^o$) beneath Mexico (Molnar and Sykes, 1969). Large earthquakes ($M_s > 7.0$) occur all along the Middle American Trench, though apparently they are more frequent along the Cocos-N. America plate portion (see Figure 5 of Kelleher et al., 1973). Some segments of the subduction zone in this region have apparently ruptured as large shocks two or more times this century. Source parameters of the six events selected for this study are compiled in Table 1-2 ; the epicenters are spaced along more than 1200 km of the trench. Ohtake et al. (1977a and 1977b) have reported on similarities in the foreshock patterns of events along the Middle American Trench, a

factor they used in their forecast of the 1978 Oaxaca earthquake.

SOURCE PARAMETER DETERMINATION

Surface Waves

P-wave first-motion data are dominated by compressional arrivals for North American and European stations (see Figure 1-13). Fortunately, for many of the events, there were enough dilatational readings from stations in the Pacific and South America to tightly constrain a steeply dipping nodal plane. In some cases, the observed nodal character of the P-wave at certain stations was used as an additional constraint, e.g. in the 1978 Oaxaca earthquake (Stewart et al., 1981). However, due to a lack of well-distributed, close-in stations, the shallow-dipping plane could not be constrained from first-motion data alone. To determine this plane, the radiation patterns of Rayleigh surface waves were examined.

Analysis of the surface waves followed the procedure given by Kanamori (1970). Typically, the R_3 arrivals on the WWSSN long-period vertical records were digitized and low-pass filtered (short-period cut-off at approximately 60 sec), then equalized to a uniform propagation distance of $360^\circ + 90^\circ$ (see Figure 1-14). Peak amplitudes of the resulting signals were then plotted as a function of azimuth from the event. For azimuthal ranges with poor station coverage, supplemental data from R_2 or R_4 arrivals were used; these arrivals propagated from the epicenter in the opposite direction to the R_3 arrivals. The resulting plots (see Figure 1-15) display the two-lobed

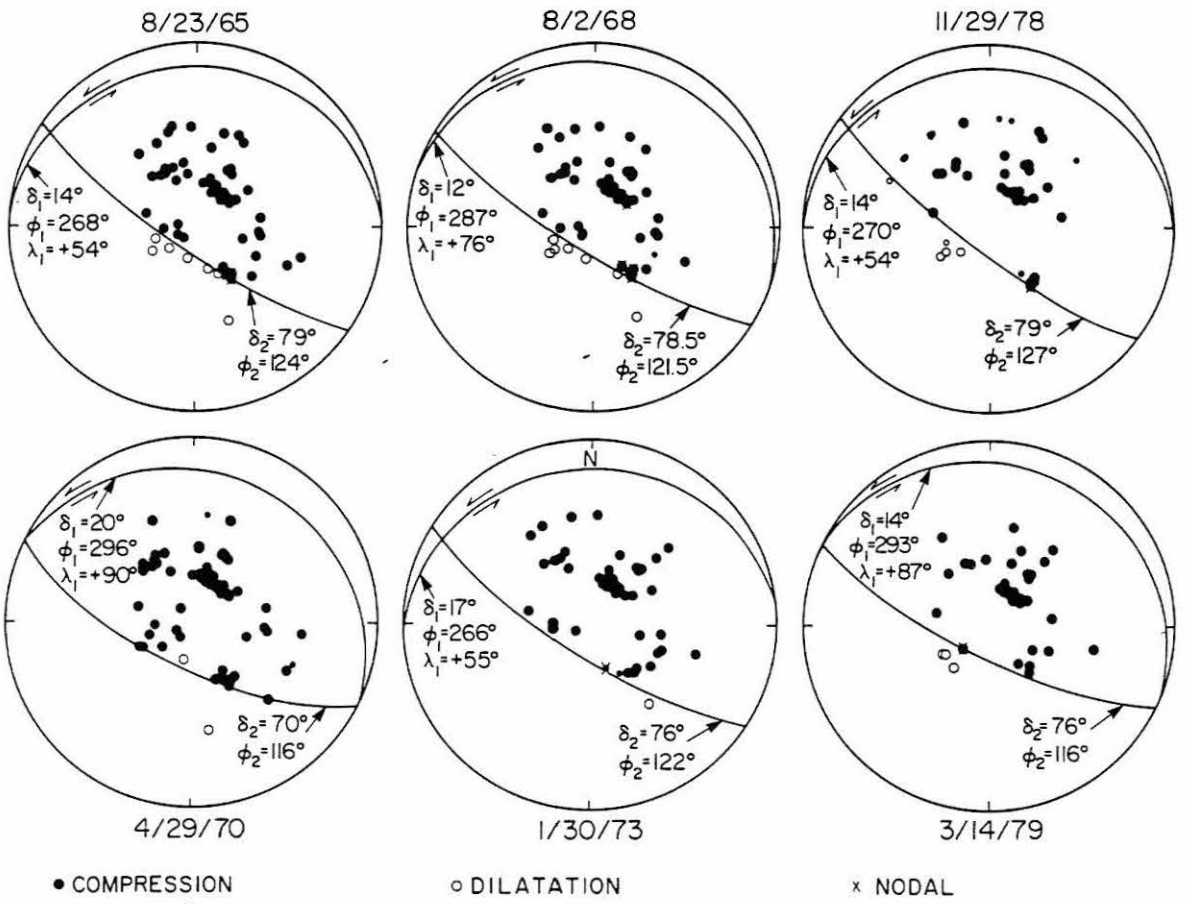

Figure 1-13. P-wave first-motion data for the six events of this study. All events indicate shallow thrust faulting to the north or northeast. Events 8/23/65, 8/2/68, 1/30/73, 11/29/78 and 3/14/79 have a small amount of left-lateral strike-slip motion associated with them. The fault planes are constrained by the P-wave first-motion data shown and the surface wave data. The smaller dots and circles represent less reliable readings. All data used in the plot were read from the WWSSN or Mexican seismograms, in this study. Equal-area projections of the lower focal hemisphere are shown.

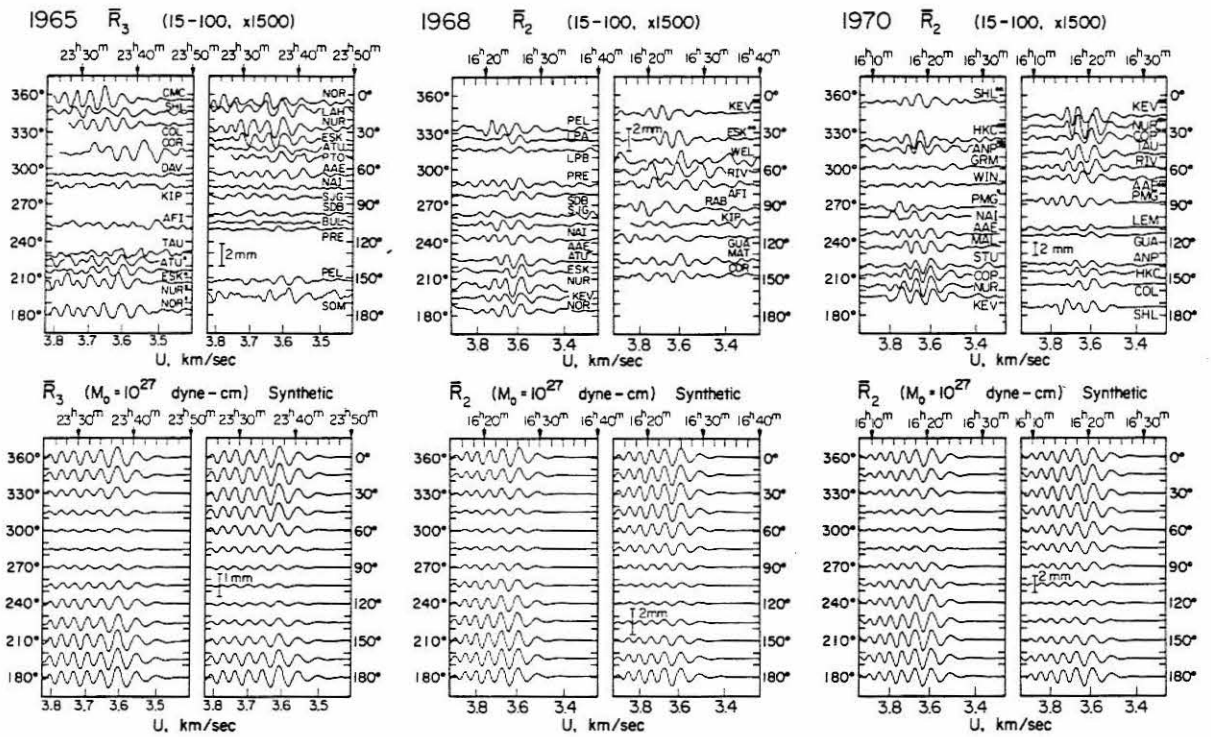

Figure 1-14. Azimuthal plots of equalized seismograms for $\bar{R}_2$ and $\bar{R}_3$ and synthetic seismograms computed for the fault geometries shown in Figure 1-13. A seismic moment of 10^{27} dyne-cm was used in the synthesis. In the observed patterns, one asterisk indicates that R_2 was equalized to R_3 distances for the 1965 event and R_1 was equalized to R_2 distances for the 1970 event. Two asterisks indicate that R_3 was equalized to R_2 distances for the 1968 and 1970 events. The amplitude scales are for trace amplitudes on a WWSSN long-period instrument (15-100) with a magnification of 1500.

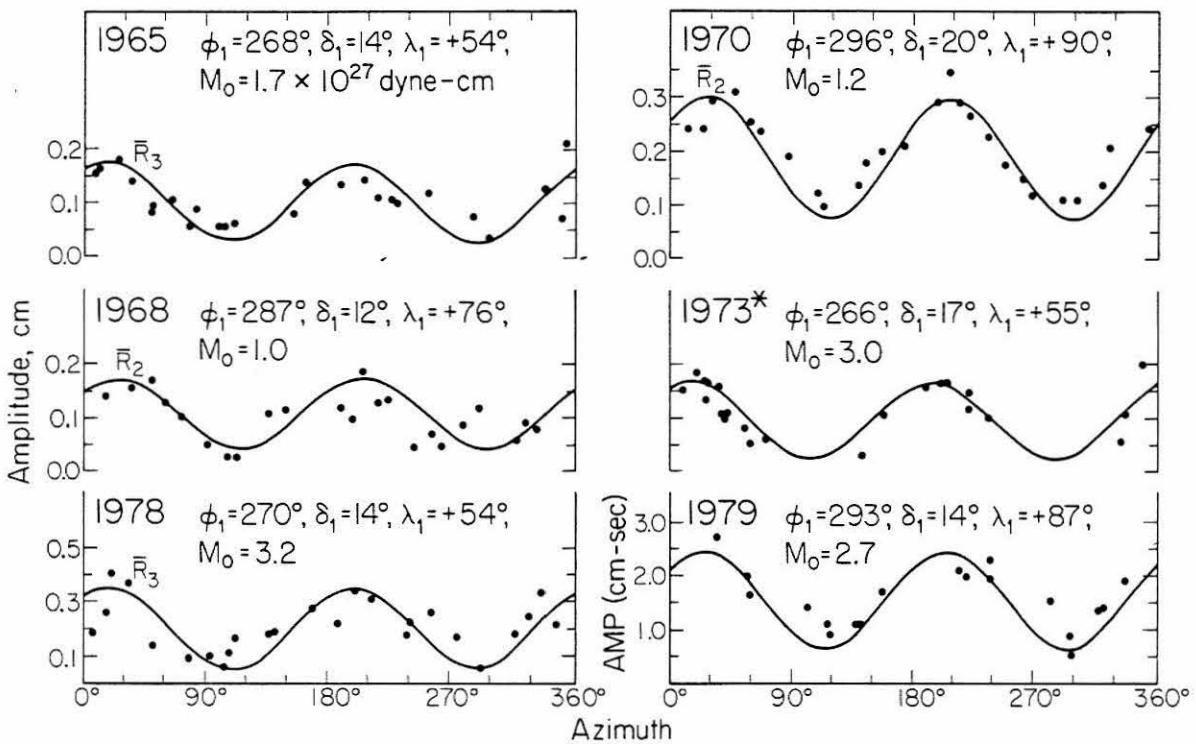

Figure 1-15. Equalized station peak-to-peak amplitudes for observed $\bar{R}_2$ and $\bar{R}_3$ data, plotted as a function of azimuth (solid circles). The solid curve in each case represents the synthetic radiation pattern for the given source model. For the 1973 event the data are spectral amplitudes at 200 seconds, obtained from Reyes et al. (1979). For 1979, R_2 and R_3 data are taken from the IDA network (spectral amplitudes at a period of 256 seconds). The 1973 and 1979 values are normalised at the source.

radiation pattern which is a characteristic of predominantly thrust events. In most cases, however, the amplitude maximum does not occur along the dip direction of the steep plane, indicating that the mechanism must have a component of strike-slip motion associated with it.

Synthetic radiation patterns were generated using the strike and dip of the steep plane, allowing only the slip angle (or rake, λ) on this plane to vary. A step-function source at a depth of 16 km was used, with bilateral rupture propagation. Since the fault dimensions (estimated from the aftershock areas) were small, relative to the wavelengths analysed, the results were not sensitive to the specifics of the rupture propagation (unilateral versus bilateral); i.e. these events exhibited no significant directivity. Figure 1-16 shows an example, for the 1965 event, of how the radiation pattern varied with changes in the slip angle, λ. This angle could typically be resolved to within 5° for a best fit to the data. With the slip angle on the steep plane determined, the strike, dip and slip angle of the shallow plane (presumably the fault plane for subduction of the Cocos plate to the northeast) could be calculated. These planes have been added in Figure 1-13, which shows the final solutions for all the focal mechanisms. Surface wave moments were obtained by scaling the amplitudes of the synthetic curves to match the data. The results are given in Table 1-2.

Note that R_2 arrivals were used for the 1968 and 1970 events, instead of R_3. For the 1973 event, the spectral amplitudes at a period

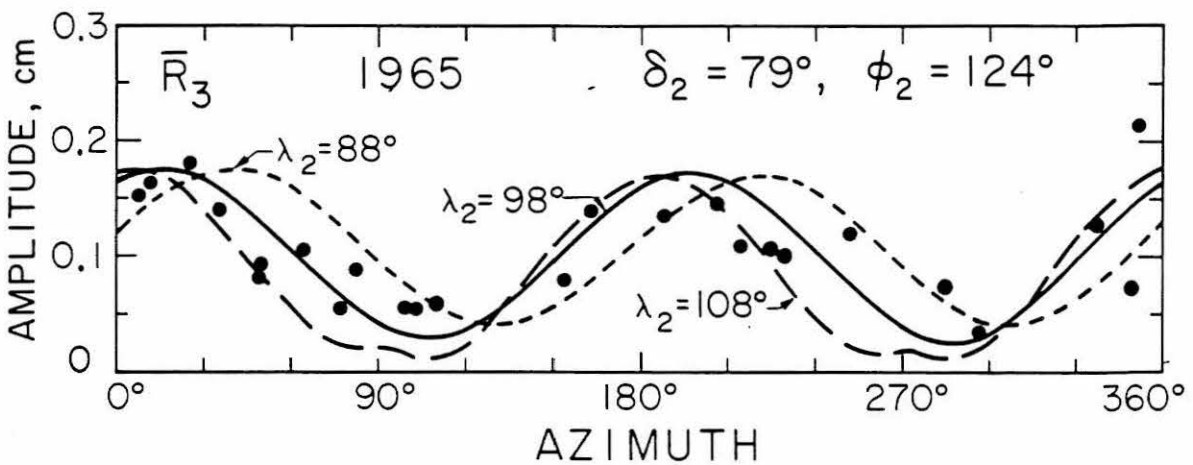

Figure 1-16. Equalized station peak-to-peak amplitudes for observed $\bar{R}_3$ data for the 1965 event, plotted as a function of azimuth (solid circles). Synthetic R_3 waves are calculated with dip (δ_2) and strike (ϕ_2) of the auxiliary plane fixed and varying the rake (λ_2) (dashed curves) until a suitable fit is obtained to the observed data (solid curve, $\lambda_2 = 98^\circ$). This approach is used to constrain the strike of the fault planes of all six events in Figure 1-13.

of 200 seconds have been used. They are taken from Reyes et al. (1979). Their moment value for this event is used, but a slightly different focal mechanism is determined which agrees with the larger set of first-motion readings of this study. The mechanism and moment of the 1979 Petatlán event were obtained from the International Deployment of Accelerographs (IDA) digital records using a moment tensor inversion routine developed by Kanamori and Given (1981).

Body Waves

Using the focal mechanisms determined by the above procedure, an attempt was made to model the P-waves. A suite of azimuthally well-distributed WWSSN stations at distances of 30° to 90°, with the P-waves on-scale, was selected for each event. Synthetics were generated using a point source in a half-space with v_p = 6.1 km/s and v_s = 3.5 km/s. These velocities were obtained from Meyer et al. (1980); a more detailed crustal model was not available. The synthetic waveforms include the direct P and surface reflected phases pP and sP. Basically, the Green's function responses of the three phases, for a properly oriented point double-couple at a given depth, are convolved with instrument, attenuation and source time function operators. The procedure has been described in greater detail by Kanamori and Stewart (1976). The parameters to be determined were the source depth and the dimensions of the time function trapezoid. Effects of variations in these parameters are shown in Figures 1-17 and 1-18. Increasing the depth, for example, acted to delay the strong down-swing at

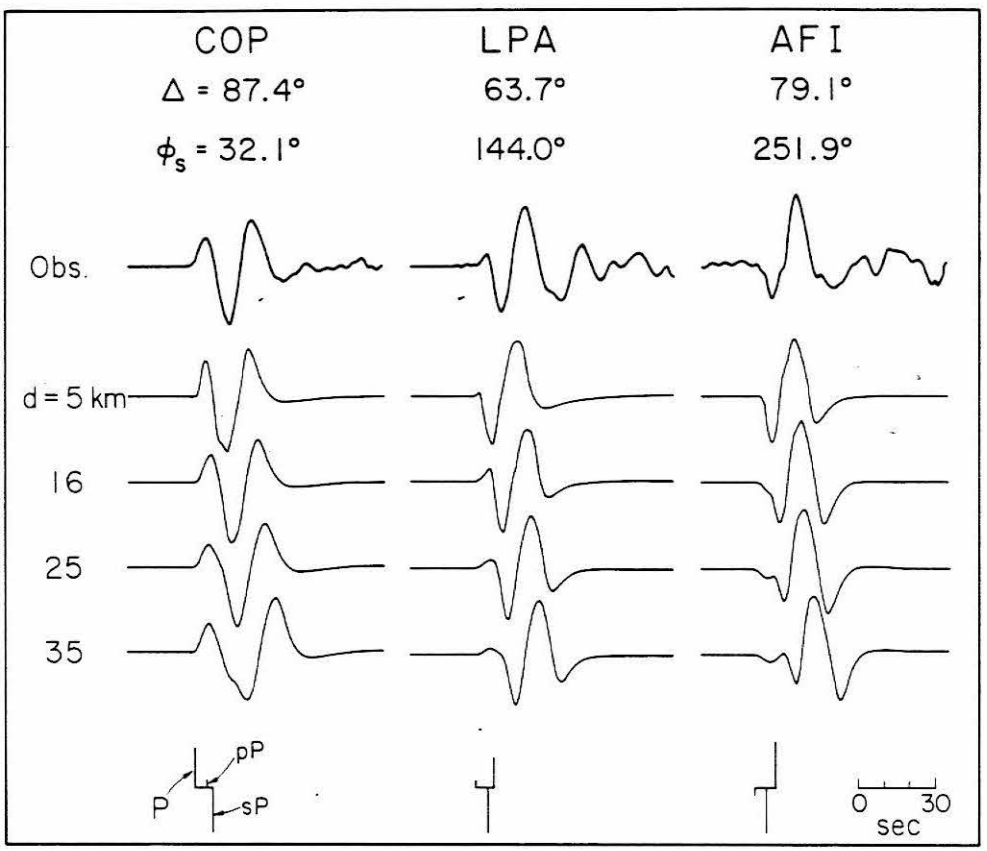

Figure 1-17. A comparison of observed P-waveforms at WWSSN stations COP, LPA, and AFI, for the 1968 event, with synthetic waveforms for various source depths. The relative amplitudes of pP and sP with respect to that of P is shown at the bottom of the figure, for the preferred depth of 16 km. Note the variation in polarity and relative amplitude of P, pP, and sP for each station. The duration of the time function used is 16 seconds. Note the depth sensitivity to the width of the first pulse.

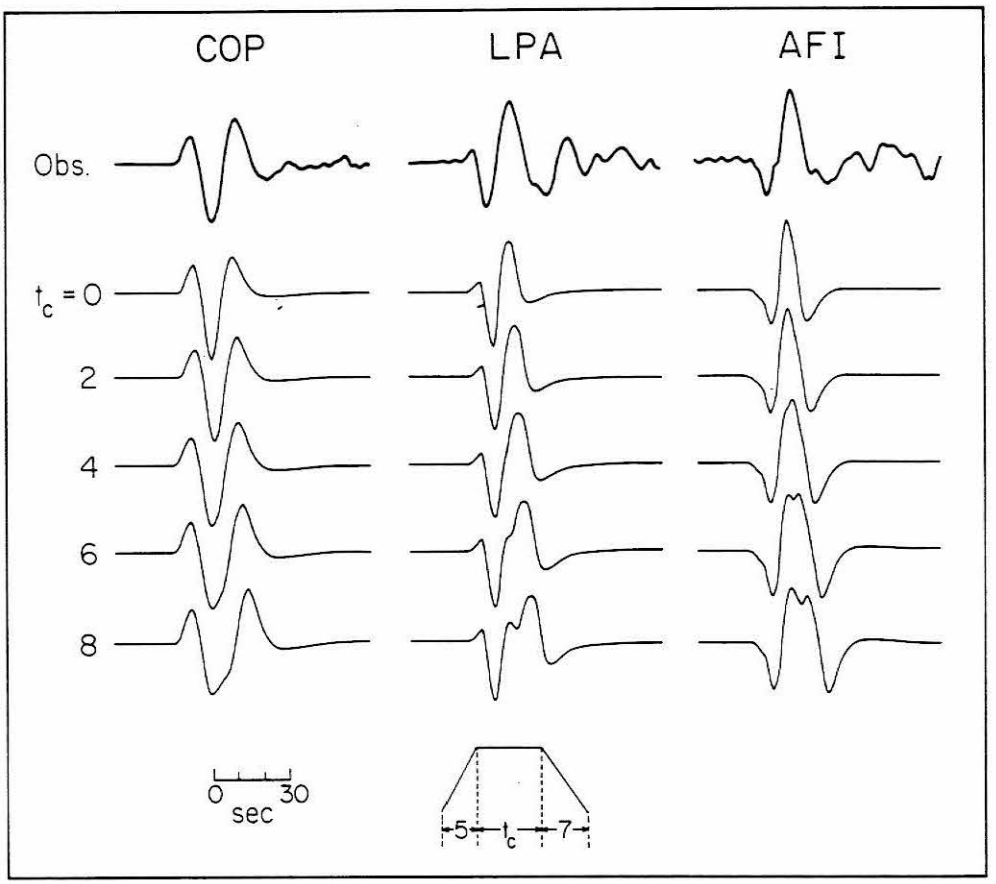

Figure 1-18. A comparison of observed P-waveforms at COP, LPA, and AFI, for the 1968 event, with synthetic waveforms for different durations of the time function. The source depth is 16 km. Notice how the width of the first pulse, which is sensitive to depth variations (see Figure 1-17), stays virtually unaffected by changes in t_c. The preferred time function is (5,4,7).

compressional stations, such as COP, caused by the reflected pP and sP phases. The source function rise time most strongly affected the rise time of the initial pulse, while the sum of the rise and top times affected the overall timing of the first three prominent peaks. The waveforms were not very sensitive to the decay times of the trapezoids. For a particular station, significant trade-offs between depth and time function features were certainly possible, but successfully fitting the complete set of records for an event greatly reduced the allowable ranges for each parameter. The depths could be resolved to ± 5 km; significant changes in the source velocity model may change the absolute depths somewhat, but the relative depths between the events will not change. The rise time and top time of the source function should be accurate to ± 1 second each, and again are most reliable in a relative sense between the events. Four of the six events viz. 1965, 1968, 1978 and 1979 were modeled very successfully using a single trapezoid as shown in Figures 1-19 and 1-20, Figure 5 in Stewart et al. (1981) and Figure 1-21. The 1970 event, with more complicated waveforms as shown in Figure 1-22, required two trapezoids. In this case, the first trapezoid was reasonably constrained using the above forward modeling procedure. A waveform inversion routine, developed by Burdick and Mellman (1976), was then employed to determine the features of the second source, including its relative amplitude and location as well as its shape. P-waves for the 1973 Colima event, shown in Figure 1-23, have not been modeled as yet due to their extremely complex nature. Estimates of the body wave moments were made by scaling the synthetic

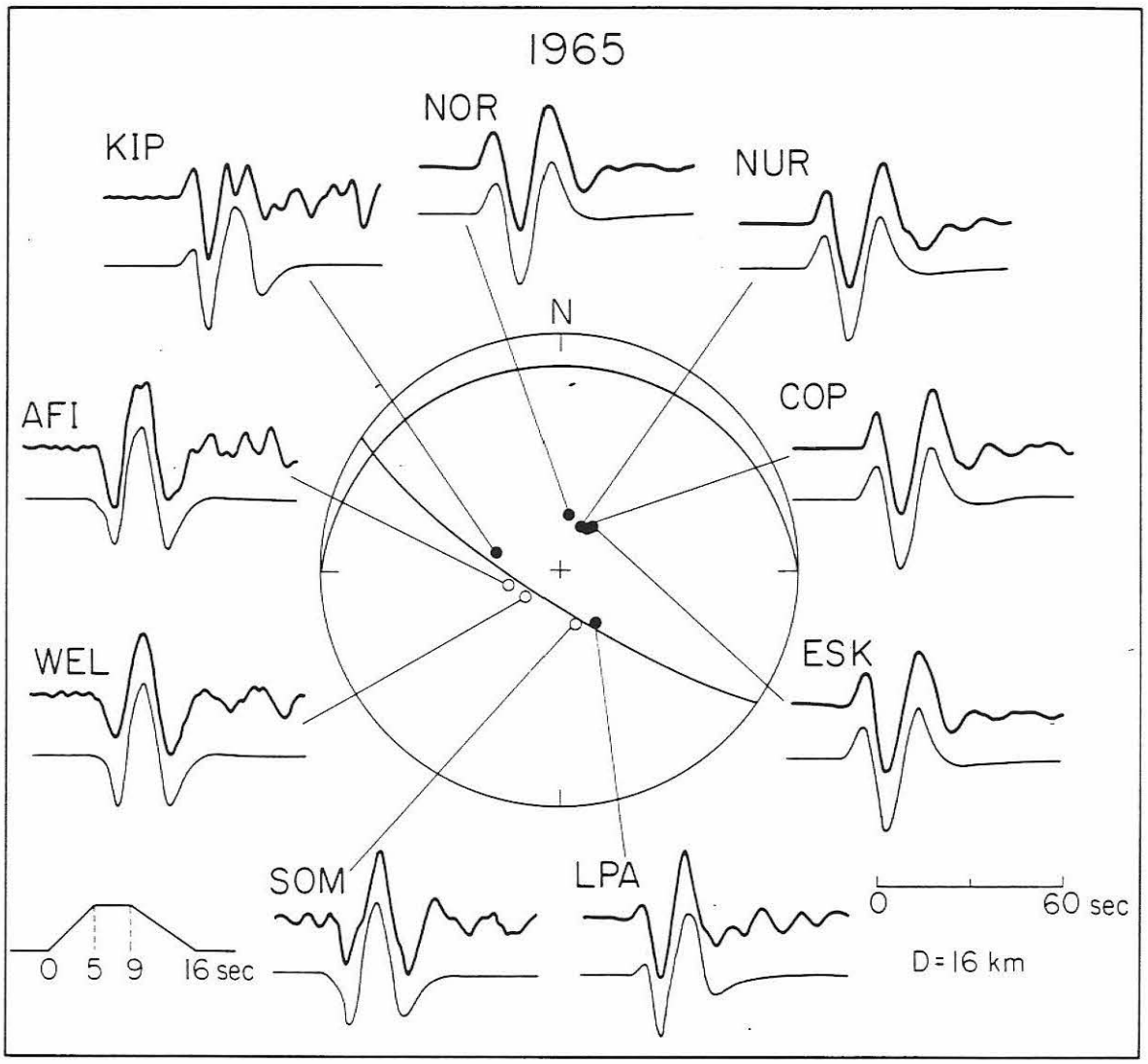

Figure 1-19. WWSSN observed and synthetic P-waves for the 1965 event. The focal mechanism in the center of the figure is that determined from P-wave first-motions and surface wave data (see Figures 1-13 and 1-15). Observed P-waves are shown as heavy curves (upper) with corresponding synthetic waveforms (below). The synthetic waveforms are generated using the source mechanism, time function, and depth shown.

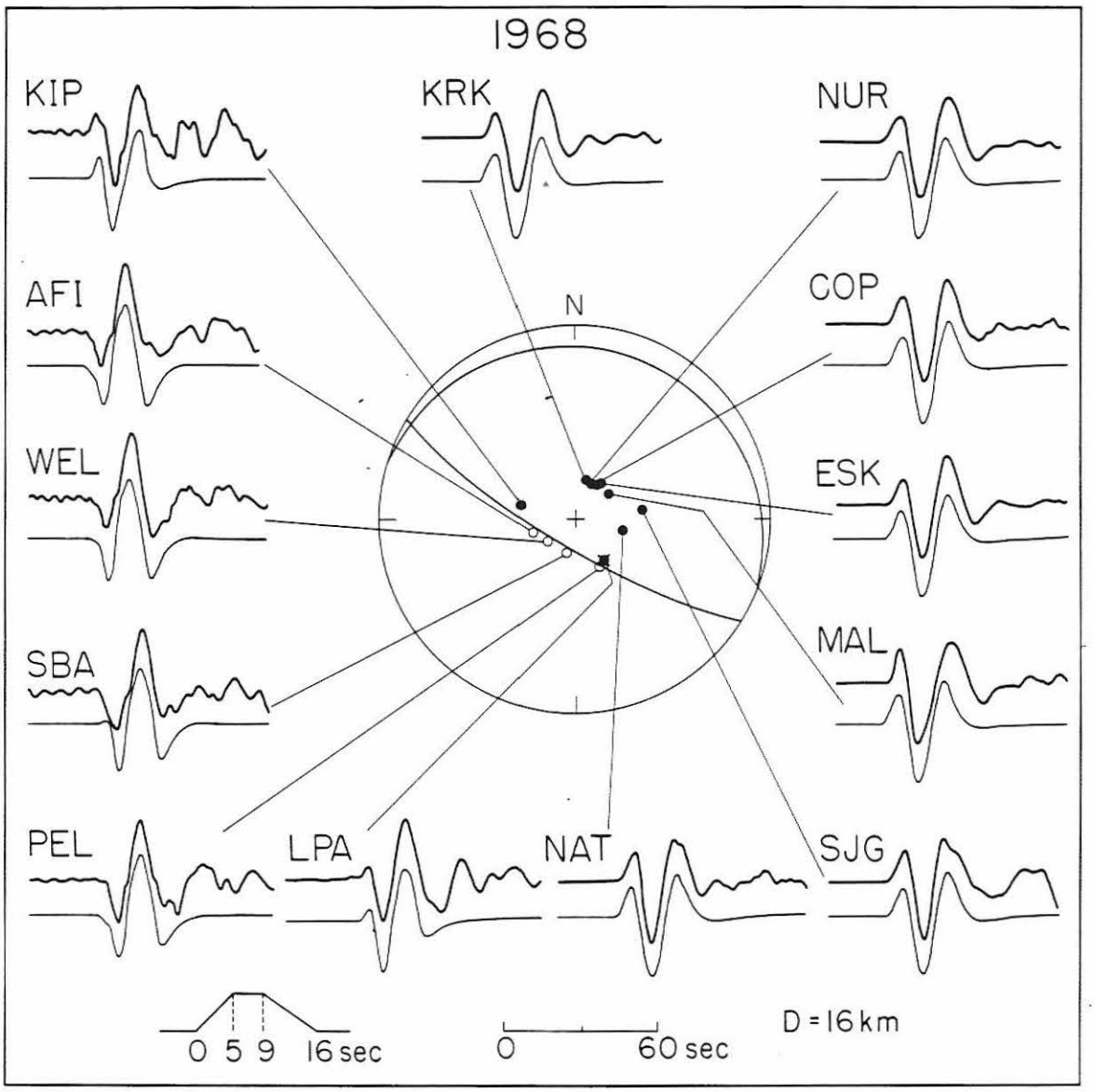

Figure 1-20. WWSSN observed and synthetic P-waves for the 1968 event. The focal mechanism in the center of the figure is that determined from P-wave first-motions and surface wave data (see Figures 1-13 and 1-15). Observed P-waves are shown as heavy curves (upper) with corresponding synthetic waveforms (below). The synthetic waveforms are generated using the source mechanism, time function, and depth shown.

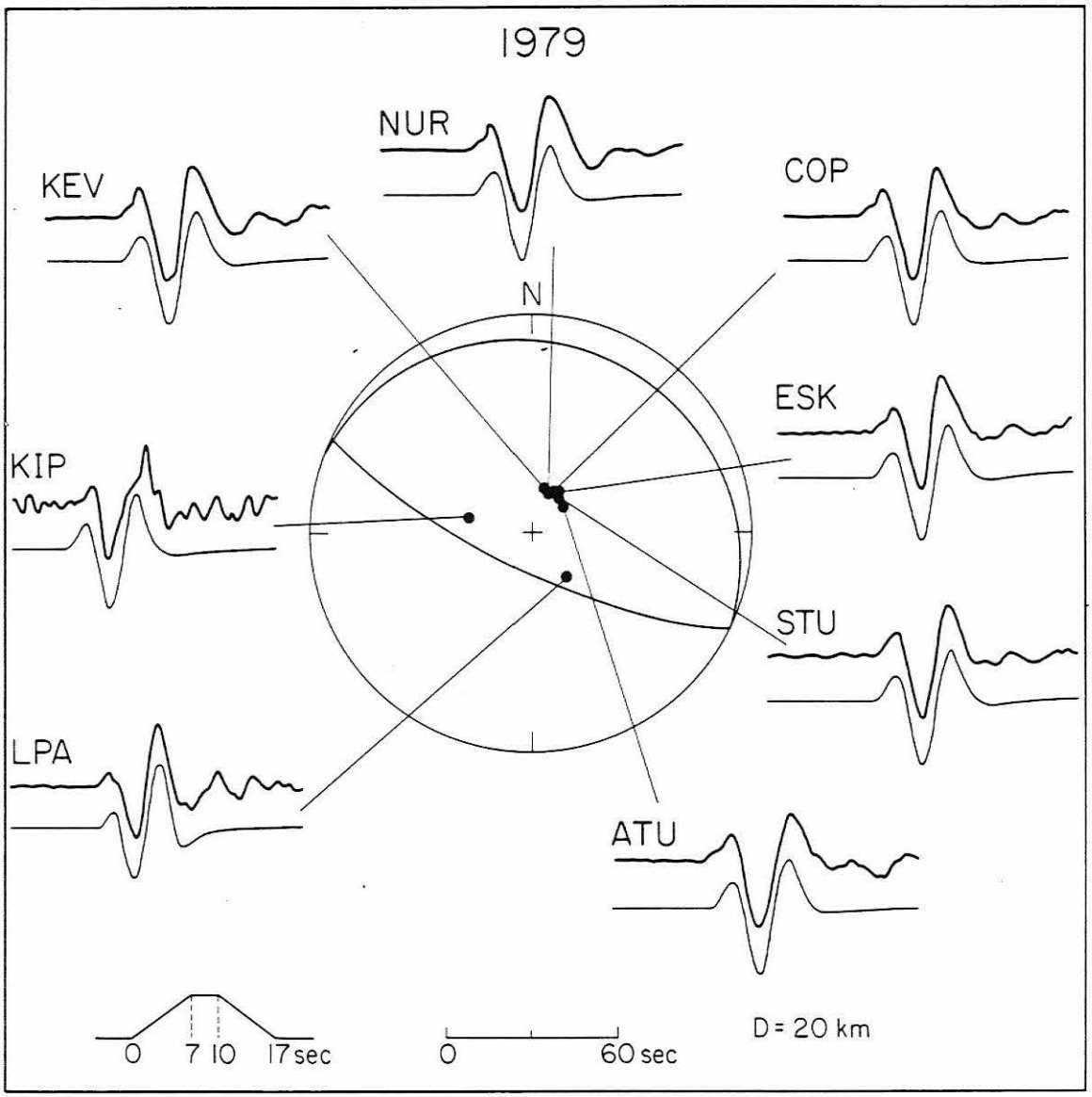

Figure 1-21. WWSSN observed and synthetic P-waves for the 1979 event. The focal mechanism in the center of the figure is that determined from P-wave first-motions and IDA surface wave data (see Figures 1-13 and 1-15). Observed P-waves are shown as heavy curves (upper) with corresponding synthetic waveforms (below). The synthetic waveforms were generated using the source mechanism, time function, and depth shown.

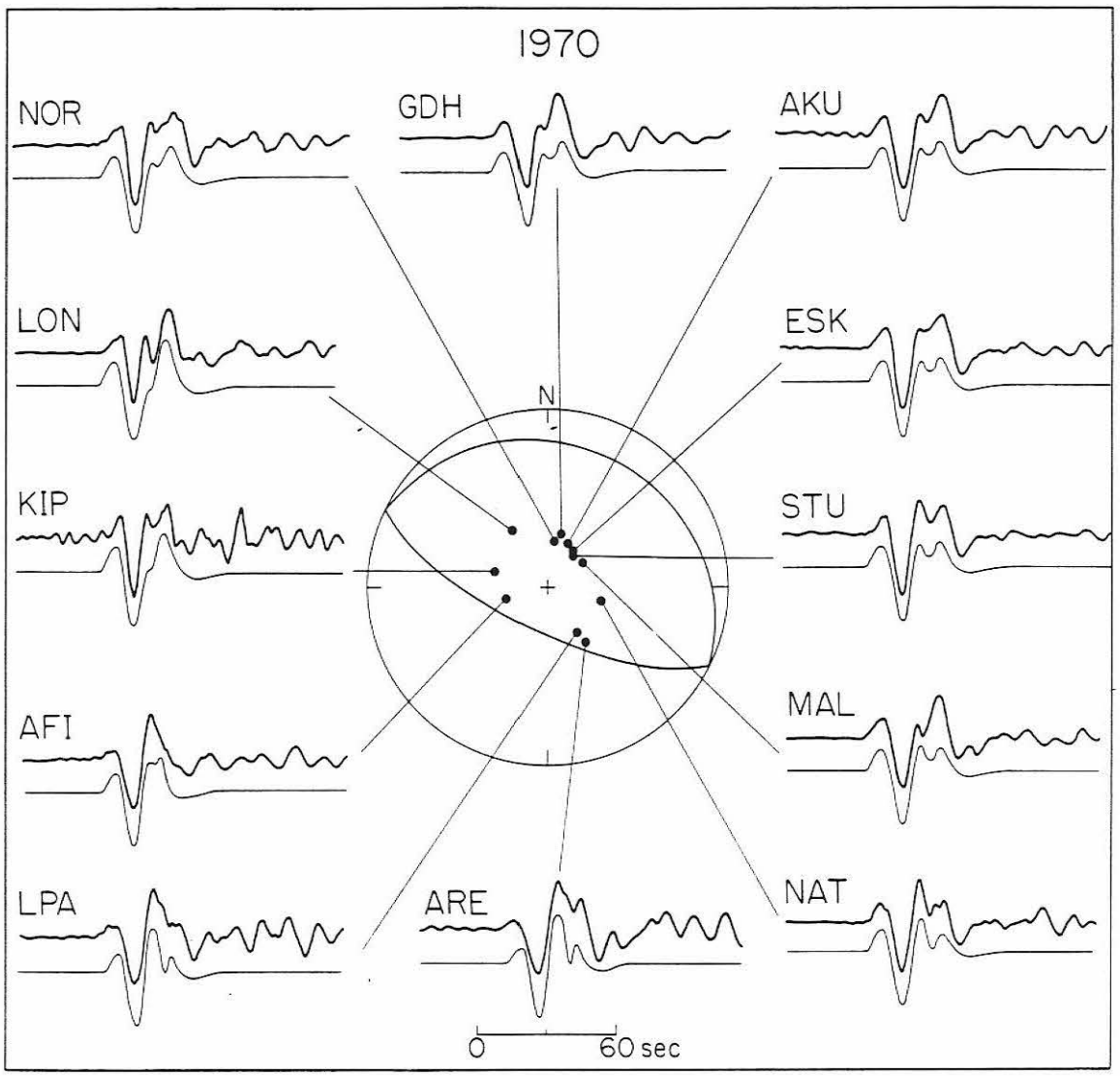

Figure 1-22. WWSSN observed and synthetic P-waves for the 1970 event. The focal mechanism in the center of the figure is that determined from P-wave first-motions and surface wave data (see Figures 1-13 and 1-15). Observed P-waves are shown as heavy curves (upper) with corresponding synthetic waveforms (below). The synthetic waveforms were generated using two events with the second located 38 km north, 4 km west with respect to the first. The depths are 23 km and 13 km and the time functions are (7,9,16) and (5,8,9) for the first and second events, respectively. The same source mechanism was used for both events.

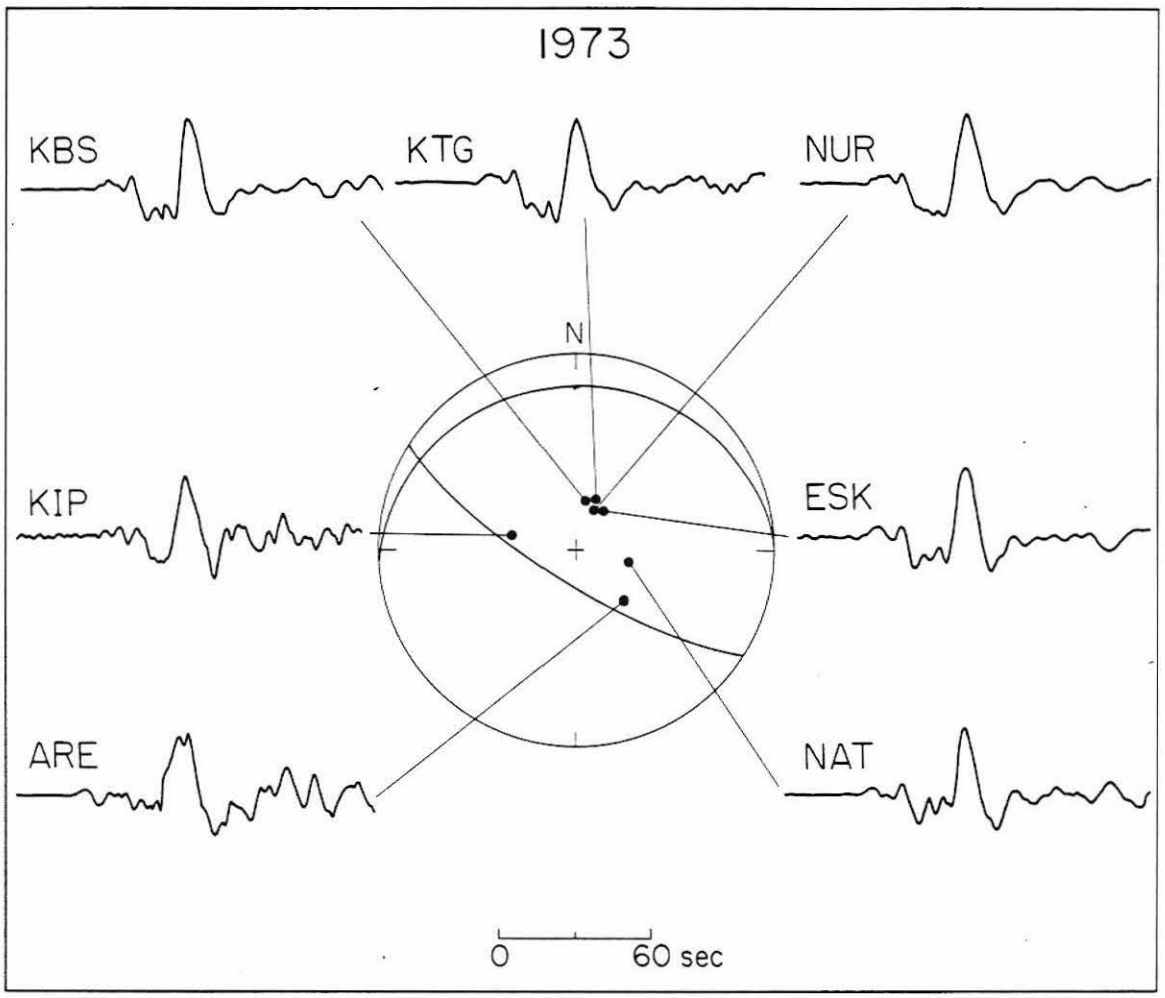

Figure 1-23. WWSSN observed P-waves for the 1973 event. The focal mechanism in the center of the figure is that determined from P-wave first-motions and surface wave data (see Figures 1-13 and 1-15). Only observed P-waves are shown, since due to the complexity of the waveforms no synthetic waveform analysis was attempted. Note, however, the similarities in the waveforms at azimuths around the source, suggesting complexity in the source itself. The waveforms are dominated by a large event preceded by several small events.

waveforms to the observed amplitudes at all stations, then averaging the values for each event. They are given in Table 1-2.

DISCUSSION OF EVENTS

Oaxaca Events

The three Oaxaca events viz. 1965, 1968 and 1978, look very much alike in most of the properties which have been examined (Figures 1-19 and 1-20 and Figure 5 in Stewart et al., 1981). The aftershock areas of these events (see Figure 1-24) show that they broke nearly adjacent segments of the trench. In the region of the 1965 and 1978 events the coastline and the bathymetric expression of the trench trend very nearly east-west. This trend is reflected in the focal mechanisms of these events (see Figure 1-13). Note, in particular, that the trench bathymetry changes to a more northwesterly strike moving westward to the region of the 1968 event from the 1965 and 1978 events. It is encouraging that the strike of the subducting plane of the 1968 event (see Figure 1-13) is found to be rotated in a similar fashion, matching this trend (see Figure 1-24). Instead of dipping along the direction of relative plate motion (the normal to the steep auxiliary plane), the shallow-dipping fault planes strike more nearly east-west. As a result, the Oaxaca quakes were all oblique thrust events with components of left-lateral motion. The P-waveforms from stations which recorded all three Oaxaca events (1965, 1968 and 1978) are virtually identical, after equalizing their peak-to-peak amplitudes (see Figure 1-25). Modeling of the P-waves yielded source depths of 16, 16 and 18 km, and time

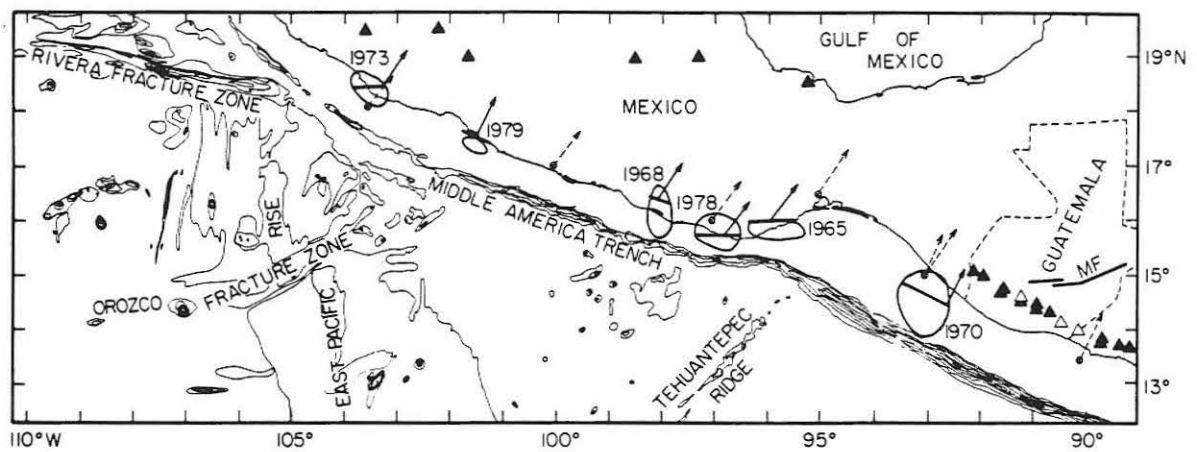

Figure 1-24. Map showing the tectonic environment of Central America. Aftershock areas are shown for each event. The bars associated with each area indicate the lateral extent of faulting and strike. The solid arrows show the slip direction from the epicenter. The dashed arrows indicate the calculated slip direction for the Cocos - N. America plate near the 1970 event and to the northwest, while near the 1970 event and to the southeast they represent the slip direction for the Cocos - Caribbean plate interaction. Both values are indicated near the 1970 event since there is some uncertainty as to the location of the triple junction. MF is the Motagua Fault in Guatemala. The solid triangles are active volcanoes, the open triangles are inactive volcanoes. The bathymetry for the Middle America Trench is indicated by contours of depth greater than 4000 m, while the bathymetry of the ridges and fracture zones is for depths shallower than 3300 m. The contour interval is 200 m. Note the proximities of the 1970 event to the N. America - Caribbean - Cocos plate triple junction and the 1973 event to the Rivera - N. America - Cocos triple junction.

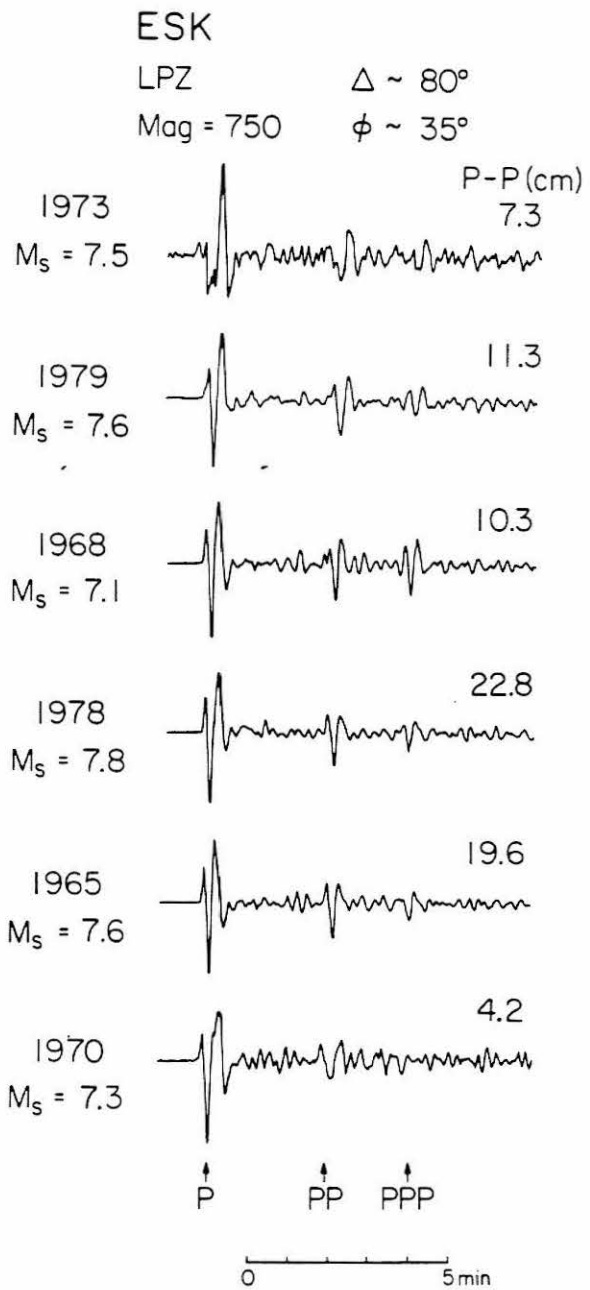

Figure 1-25. Vertical long-period WWSSN seismograms of P, PP, and PPP waves recorded at Eskdalemuir, Scotland (ESK) are shown for the events plotted in Figure 1-12. Note the simplicity and similarity of the 1965, 1968, 1978, and 1979 events compared with the 1970 and 1973 events which show a greater degree of complexity. Peak-to-peak amplitudes for each waveform are also given. The 1978 Oaxaca event has the largest amplitude.

functions of (5,9,16), (5,9,16) and (4,9,15) seconds respectively; in other words, there were no significantly resolvable differences in these properties. Based on their time functions, these earthquakes appear to have been generated by simple, smoothly propagating ruptures.

The greatest differences to be found among the Oaxaca events are in their body and surface wave moments (Table 1-2). Stations which recorded all three events consistently give P-wave amplitudes for the 1968 shock which are about half of the 1965 and 1978 values, and thus the body wave moments differ by a factor of two. The fact that their P-wave time functions are so similar suggests that the areas of rupture which contributed to the body wave radiation were roughly equal for the Oaxaca events; if this is true, the differences in body wave moments imply that the fault displacement contributing to the P-wave for the 1968 event was half that for the 1965 and 1978 quakes. The surface wave moments of the 1965 and 1968 events agree quite well with their respective body wave values. In contrast, surface waves of the 1978 event yielded a moment estimate substantially larger than that obtained from the body waves.

1979 Event

The 1979 Petatlán event, located 540 km northwest of the Oaxaca activity, showed some small differences from those events. The focal mechanism of the 1979 event indicates almost pure thrust motion on a fault plane dipping N 23°E. This is consistent with the local trend of the coastline and trench axis, which run more northwesterly here than

off Oaxaca (Figure 1-24). A source depth of 20 km, and a time function of (7,10,17) seconds was obtained. The longer rise time (7 sec vs. 5 sec) for this event, compared with the Oaxaca events, is reflected in the initial peak of the P-wave, noticeably broader for Petatlán than for the Oaxaca shocks (compare Figures 1-19 and 1-20 with Figure 1-21). On several of the records, a small shoulder is visible on the initial rise, indicating somewhat greater complexity in the source-time history. The Petatlán quake had a very definite discrepancy in its body and surface wave moments, with the surface wave value larger by almost a factor of three.

1970 Event

The epicenter of the 1970 Chiapas event, 470 km southeast of Oaxaca, falls very near the presumed location of the Cocos-N. America-Caribbean triple junction, along the westerly extension of the Motagua Fault in Guatemala (see Figure 1-24). Due to the uncertainty in position of this triple junction, it is not clear from the event location alone whether the N. American or the Caribbean plate is interacting with the Cocos plate. Because the Caribbean plate is moving eastward (Molnar and Sykes, 1969) relative to N. America, one would expect the slip vector of a Cocos-Caribbean event to be rotated somewhat towards the north with respect to a Cocos-N. America event. At this time, the fault planes of the 1970 event (see Figure 1-13) are not well enough constrained to favor either of the slip directions.

The P-waveforms of the 1970 shock show greater complexity than

those examined so far (Figure 1-22). There is an obvious glitch in the second upswing on all the compressional stations. This feature is interpreted to be the result of actual complexity in the rupture history. Were it due to a greater source depth, say, affecting the interference of the direct P with the reflected pP and sP phases, the glitch should occur at the same time at all stations. However, it appears consistently earlier at northern azimuths than those to the south. The event was modeled as a double source, using the same mechanism for both. The first event was placed at a depth of 23 km, and had a (7,9,16) second time function. The second event was located 38 km north of the first, began 12 seconds later, had half the moment of the first event and a time function of (5,8,9) seconds. The depth resolution for the second event was very poor. Combining the distance (38 km) and delay (12 seconds) gives a velocity of roughly 3 km/s, a reasonable rupture velocity. Thus it may be that the double event actually represents a sort of "re-energizing" of a single rupture, perhaps as it encountered a more highly stressed region (an asperity) on the fault.

Matching the synthetic and observed P-wave amplitudes gave a value of 0.5×10^{27} dyne-cm as the total moment of the double source; the surface wave moment of this earthquake was somewhat larger at 1.2×10^{27} dyne-cm.

1973 Event

The 1973 Colima event also occurred near a tectonically complicated

region. Just west of the 1973 epicenter, the Middle American Trench approaches the East Pacific Rise - Rivera Fracture Zone intersection. This is virtually a quadruple junction between the Pacific, Cocos, North American, and the small Rivera plates (Figure 1-24). The focal mechanism for the 1973 event resembles those of the Oaxaca events, with left-lateral oblique thrusting on a fault plane dipping to the north. P-waves for the 1973 event (Figure 1-23) display the greatest complexity of any of the events studied. Though a synthesis of these waveforms was not attempted, it appears safe to say that the rupture did not propagate in the smooth, simple fashion of the Oaxaca or Petatlán events. The P-wave amplitudes indicate a body wave moment between the values for the 1968 and 1970 events, or 0.5 to 1.0 x 10^{27} dyne-cm, which is one-sixth to one-third the surface wave moment of 3.0 x 10^{27} dyne-cm, given by Reyes et al. (1979).

Aftershock Areas and Stress Drops

Aftershock areas of the six earthquakes studied have been compiled from a variety of sources (1973 event [Reyes et al. (1979)]; 1979 event [Zuniga et al. (1980)]; 1970 event [Yamamoto, 1978]; 1965 and 1968 events [Tajima and McNally, 1981]; 1978 event [Stewart et al. (1981)]). The data sets for these area determinations were not uniform, so the relative accuracies of the results are somewhat uncertain. The results are shown in Figure 1-24. By projecting the aftershock areas onto the dipping fault planes, rupture areas in the range of 4-12.5 x 10^3 km^2 were obtained. The area values were combined with the surface wave

moments to yield estimates of the average displacements and stress drops for the events, through the relations given by Kanamori and Anderson (1975b):

$\bar{D} = M_o / \mu A$

$\Delta\sigma = 8\mu\bar{D}/3\pi w$ (thrust fault geometry)

where:

$\bar{D}$ = average displacement

M_o = seismic moment

μ = rigidity (5×10^{11} dyne/cm^2)

A = rupture area

$\Delta\sigma$ = average stress drop

w = fault width

The calculated stress drops vary from 1 to 10 bars (a narrow range considering the uncertainties involved), which puts them towards the low end of the range observed for other thrust events (Kanamori and Anderson, 1975b).

An estimate of the rupture duration, τ, can be obtained from :

$$\tau = \tfrac{1}{2}\delta t_1 + \delta t_2 + \tfrac{1}{2}\delta t_3$$

(Helmberger and Johnson, 1977), where δt_1, δt_2 and δt_3 are the rise, top and fall times, respectively, of the source time function. Using this relation, P-wave rupture durations of about 10 seconds were obtained for

the events that have been modeled. If a rupture velocity of 2.5 km/s is assumed, the 10 second duration suggests a maximum rupture area of about 2000 km^2 (the area of a circle with a 25 km radius); the observed aftershock areas are all significantly larger than this. This suggests that some motion occurred which did not contribute much to the observed P-waves. This additional, possibly slower, motion could also explain the discrepancies between the body wave and surface wave moments for some of the events.

Model

A model of the generating process of these earthquakes which satisfies the observations in a broadly qualitative sense begins with the assumption of a fairly simple stress distribution along the trench. The pattern is dominated by a few broad zones of stress concentration around large asperities, or locked segments of the fault. An earthquake occurs when the local stress reaches the breaking strength of an asperity. The central, highly stressed region fails vigorously but smoothly, generating the simple observed body waves. The rupture then progresses more gradually beyond the asperity, contributing additional energy to the long-period surface waves. The spacing and strength of the asperities are such that they fail as single events, without triggering adjacent ones. The stress distribution becomes more irregular as the trench approaches other plate boundaries, and thus events in such vicinities, such as the 1970 and 1973 events, rupture in a more complex fashion.

Since the long-period energy released by these Central American events is being examined, the arguments made here apply on the scale of a few seconds or tens of kilometers. A lack of detailed knowledge of the local crustal structure makes analysis of teleseismic records at shorter period difficult. Previous studies of mainly strike-slip events (Kanamori and Stewart, 1978; Rial, 1978; Stewart and Kanamori, 1978) have been reasonably successful in modeling teleseismic WWSSN long-period records and the interpretations for many of these events suggest a multiple event (or multiple asperity) rupture sequence.

The nature of the stress distribution could be expected to affect the local seismicity prior to a large event. Thus the consistent patterns in foreshock activity observed by Ohtake et al. (1977a and 1977b) for the Oaxaca 1965 and 1968 earthquakes may be intimately related to the dramatic similarity which has been demonstrated between the subsequent events. If this is true, the seismicity patterns characteristic of impending earthquakes in other tectonic regimes may be drastically different.

DISCUSSION OF TECTONICS

It is important to consider what can be learned from the above results in terms of the tectonic environment of Central America. As discussed earlier, the six events studied here are located along the northern section of the Cocos plate (see Figure 1-12). In the north the seismic activity suggests a more shallow mode of subduction than to the south for the Cocos plate (Molnar and Sykes, 1969). This is confirmed

by the distribution of Quaternary volcanoes in the region (Stoiber and Carr, 1973). In Figure 1-24 these volcanoes are shown located at various distances from the trench in the north, while to the south they lie in a distinct zone close to it. The shallower dipping subduction zone in the north allows a greater area of contact between the subducting oceanic crust and the continental crust and consequently may result in larger seismic events here than along the southern plate boundary.

A factor that is thought by some (Vogt et al., 1976) to influence the occurrence and mode of failure of subduction zone events is offshore bathymetry. A particularly good example is the Tehuantepec Ridge shown in Figure 1-24. The Tehuantepec Ridge strikes northeast and would intersect the coastline just to the east of the 1965 Oaxaca event. Throughout historic times this area has been a seismic gap for large events (McNally and Minster, 1981). The evidence presented here shows no indication of any anomalous features which could be attributed to the 1965 event, the event closest to the Tehuantepec Ridge.

From the detailed studies presented earlier it is possible to determine slip vectors for all six events. They are shown as the solid arrows in Figure 1-24. However, as can be seen in Figure 1-13, the reliability is variable and depends on the degree of constraint of the steep dipping auxiliary plane. For the 1965, 1968 and 1978 events this constraint is good and consequently reliable slip vectors have been determined. They agree very well with the theoretical slip vectors calculated from Minster and Jordan (1978) for the Cocos-N. American

plate interaction (shown in Figure 1-24 as dashed arrows). For the other events, however, this plane is not as well constrained. Perhaps the most poorly constrained is unfortunately the 1970 event. Its location is close to the triple junction for the Cocos, N. America and Caribbean plates. It was hoped to be able to constrain the location of this triple junction by comparing the slip vector of the 1970 event with the theoretical value. However, due to the poorly constrained auxiliary, steep dipping plane (see Figure 1-13) this is not possible at this time and since it is not a major aim of this study it will be investigated in more detail at a later time.

CONCLUSIONS

Analysis of the body and surface waves of six large ($M_s > 7.0$) earthquakes along the Middle America Trench has revealed a remarkable degree of similarity among these events. These earthquakes had very similar focal mechanisms, source depths, rupture dimensions and stress drops. Body waves of four of the six events indicated surprisingly simple, smoothly propagating ruptures. Interestingly, the two events with more complicated body waves (1970 and 1973) were located in the vicinity of suspected triple junctions. Aftershock areas for the events were generally two to three times larger than the maximum P-wave rupture areas inferred from durations of the source time function. The most conspicuous differences among these six events appeared in their body wave and surface wave moments.

1.4 Simple Source - Complicated Source Structure Interactions: The Bermuda Earthquake of 1978.

ABSTRACT

The Bermuda earthquake (M ~ 6) occurred near the westerly extension of the Kane Fracture Zone roughly 370 km southwest of the island of Bermuda. It is one of the largest oceanic intraplate earthquakes to occur off the eastern coast of North America. Because of its size and location, it has provided an excellent set of WWSSN body waves. They can be used to infer its depth and faulting parameters by waveform modeling techniques. The results indicate a north-northwest striking thrust mechanism (strike = N 20^{o}W, dip = 42^{o}NE, rake = 90^{o}) with the hypocenter located at a depth of 11 km, which for an oceanic crust places it predominantly in the mantle. The event had a seismic moment of 3.4×10^{25} dyne-cm and its time history was modeled with a symmetric trapezoidal time function 3 seconds in duration. The north-northwest strike of the event is in good agreement with the bathymetry of the area, the epicenter being close to the southwestern edge of the Bermuda Rise. The strike of the event is also close to that of the inferred extensions of the present ridge fracture zones in the region. The presence of such fracture zones is indicative of local weak zones in the lithosphere. The Bermuda earthquake most likely is associated with one of these zones of weakness and is the result of the application of present day stress imposed on the region by the North American plate in the direction of its absolute motion. This is an important event in

terms of understanding and estimating seismic hazard on the eastern seaboard of North America.

INTRODUCTION

The Bermuda earthquake of March 24, 1978 (origin time 00h 42m 37.7s U.T.; location 29.9° N, 67.3°W; depth = 11 km [this study]; m_b = 6.1, M_s = 5.8) is one of the largest eastern North American plate events to occur since the installation of the World-Wide Standardized Seismographic Network (WWSSN) in 1963. Because of the size and location of this event (Figure 1-26) it was well-recorded by the WWSSN and in particular it provided a high quality body wave data set, suitable not only for the analysis of the source properties of the event itself but also for the study of the upper mantle structure beneath eastern North America (Stewart and Helmberger, 1979; Given et al., 1981). This paper deals with a detailed analysis of the body waves from the event and the constraint that these data place on the various source parameters of the Bermuda earthquake. The event is located within the oceanic plate off the coast of eastern North America, 370 km southwest of Bermuda. As such, it is the largest event to have occurred there since seismographic recording began. It was widely felt along the southeast coast of the United States. Because of the paucity of well-recorded earthquakes from that area, it is an important event to study since it may help elucidate the tectonic origin of intraplate events, especially within the environment of eastern North America.

Results from the analysis of P-wave and SH-wave first-motions and

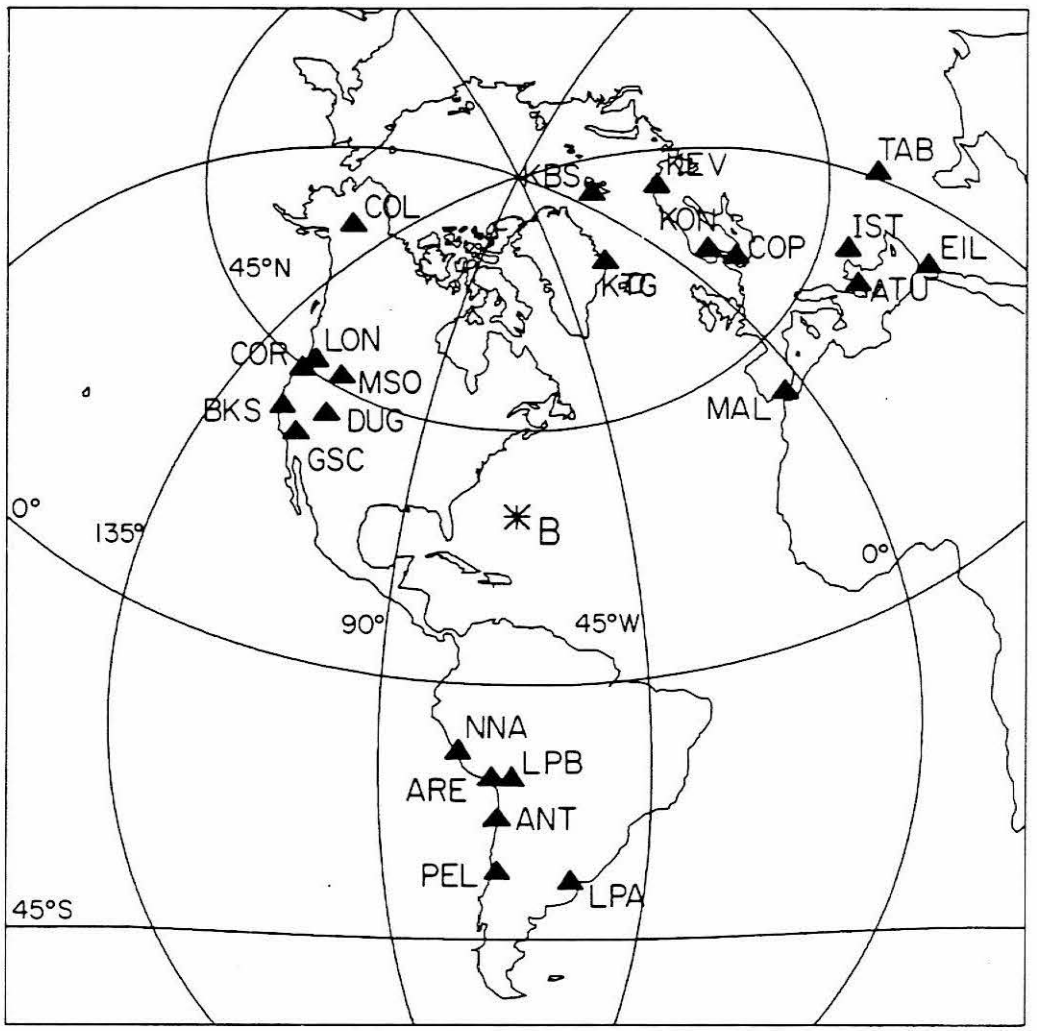

Figure 1-26. Map showing locations of 23 WWSSN stations used in the P-wave modeling of the Bermuda earthquake. Note the good azimuthal coverage of stations around the epicenter (B). An azimuthal equidistant projection is shown. See Table 1-3 for distances and azimuths.

waveforms in this study indicate that the event had a pure thrust mechanism with planes of approximately 45^{o} dip, striking in a north-northwest direction. It was located at a depth of 11 km, predominantly below the Mohorovicic discontinuity, a somewhat unusual result which was required by the high quality data set. The earthquake occurred close to zones of weakness of ancient fracture zones in the proximity of a major zone of plate motion disruption at magnetic anomaly M11 (~125 m.y.b.p.), the time when the South Atlantic began opening. This resulted in local changes in spreading direction and plate velocity in this region. The Bermuda earthquake occurred as a result of the application of present day stress imposed on the region by the North American plate in the direction of its absolute motion.

BODY WAVE ANALYSIS

In order to constrain the source parameters such as focal mechanism, size, depth and time function for the Bermuda earthquake, a complete study of the body waves from the event was made. The data, which were taken primarily from WWSSN and Canadian long-period seismograms, consist of P-wave first-motions, SH polarities and P- and S-waveforms. P-wave first-motion data, which were read in this study, are plotted in Figures 1-27a and 1-27b. Initially, a hypocenter which was located in the crust with a source velocity of 6.3 km/s, as shown in Figure 1-28, (star) was assumed. This resulted in the focal mechanism plot shown in Figure 1-27a. The long dashed planes show a solution similar to that published by Nishenko et al. (1978). The short dashed

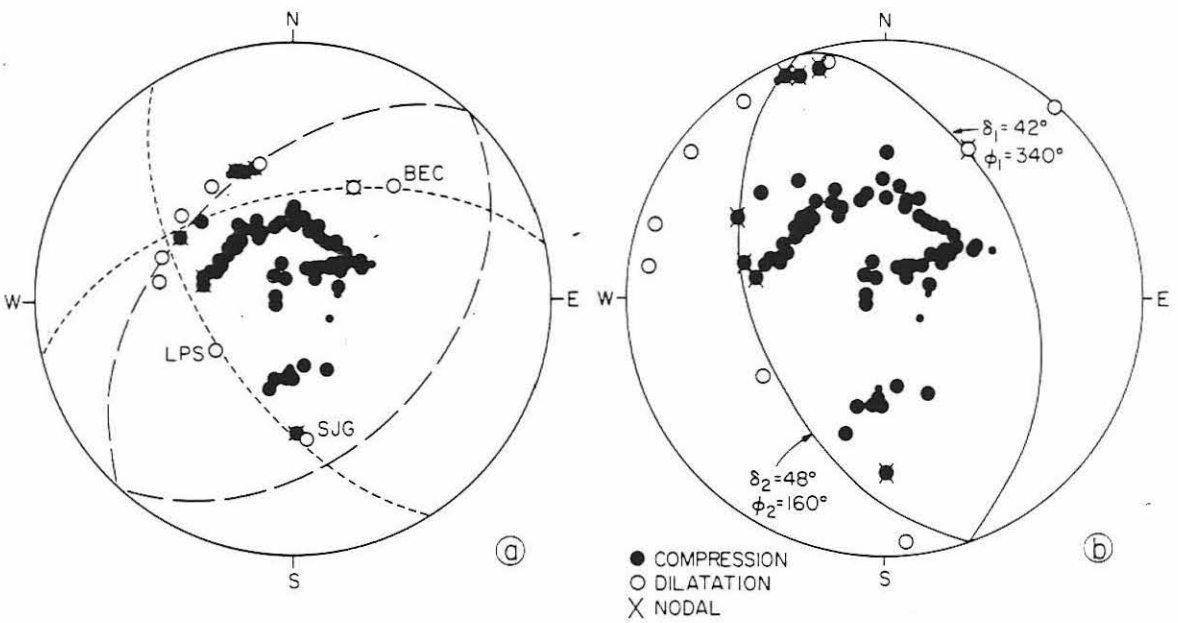

Figure 1-27. (a) The P-wave first-motion data for the Bermuda earthquake of March 24, 1978 with the hypocenter located in the crust (see Figure 1-28 [star]). Note that the first-motion data plot closer to the center of the focal sphere compared with the data for a source in the mantle (b). In this case, two orthogonal focal planes cannot be fit to the data without violating several very good P-wave readings. The pure thrust mechanism shown (long dashed planes) is similar to that obtained by Nishenko et al. (1978). Another possible solution is indicated by the short dashed planes. An equal-area projection of the lower focal hemisphere is shown. (b) The P-wave first-motion data for the Bermuda earthquake of March 24, 1978 with the hypocenter located in the mantle (see Figure 1-28 [asterisk]). The mechanism indicates approximately 45° pure thrust faulting on a plane striking N 20°W. The actual fault plane and auxiliary plane cannot be distinguished. Data used in this plot were read mainly from WWSSN seismograms in this study. An equal-area projection of the lower focal hemisphere is shown.

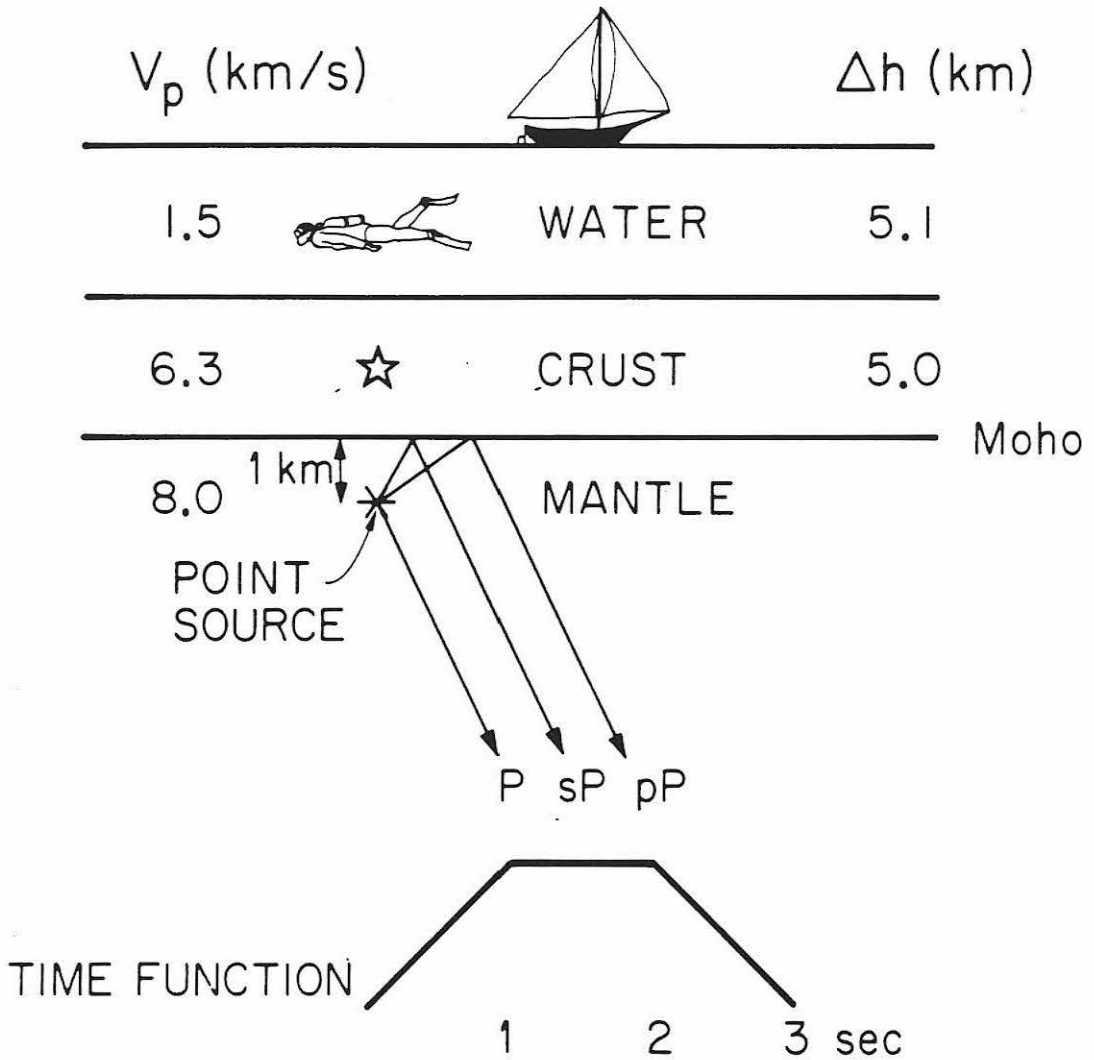

Figure 1-28. Velocity structure used in this study (modified from Officer et al. [1952] and Ewing et al. [1954]). The star indicates a crustal hypocenter while the asterisk indicates a hypocenter located 1 km beneath the Mohorovicic discontinuity, the preferred location. The time function used in the modeling of the source is also shown.

fault planes show another possible solution. However, both mechanisms are inconsistent with several good quality first-motion data and no solution is possible without contradiction of at least some of these data points. If instead, the hypocenter is located in the mantle, where the source velocity is 8.0 km/s, as shown in Figure 1-28 (asterisk), the station positions are shifted outward on the focal sphere and the result is given in Figure 1-27b. Now it is possible to draw fault planes that can separate well the compressional and dilatational fields. In particular, stations LPS, SJG and BEC, some or all of which previously were inconsistent, now plot in the appropriate dilatational areas. To verify this solution, obtain a depth and time function for the event and study the degree of complexity of the source, synthetic seismograms were calculated and compared with the observed data. Neither of the P-wave solutions shown in Figure 1-27a, with the source located in the crust, could explain the P and SH waveforms shown in Figures 1-29 and 1-32.

P-WAVE ANALYSIS

An initial look at the observed P-wave seismograms, shown in Figure 1-29, indicates a complex sequence of arrivals at most stations. It was not known at first, what this complexity was due to. At the beginning of the trace the pulse looks relatively simple and of larger amplitude than the later arrivals. Since the source is located beneath the ocean, the later arrivals could be due to water reverberations, which have been observed previously on vertical long-period seismograms for sources below a water layer (Ward, 1979). Another possibility is

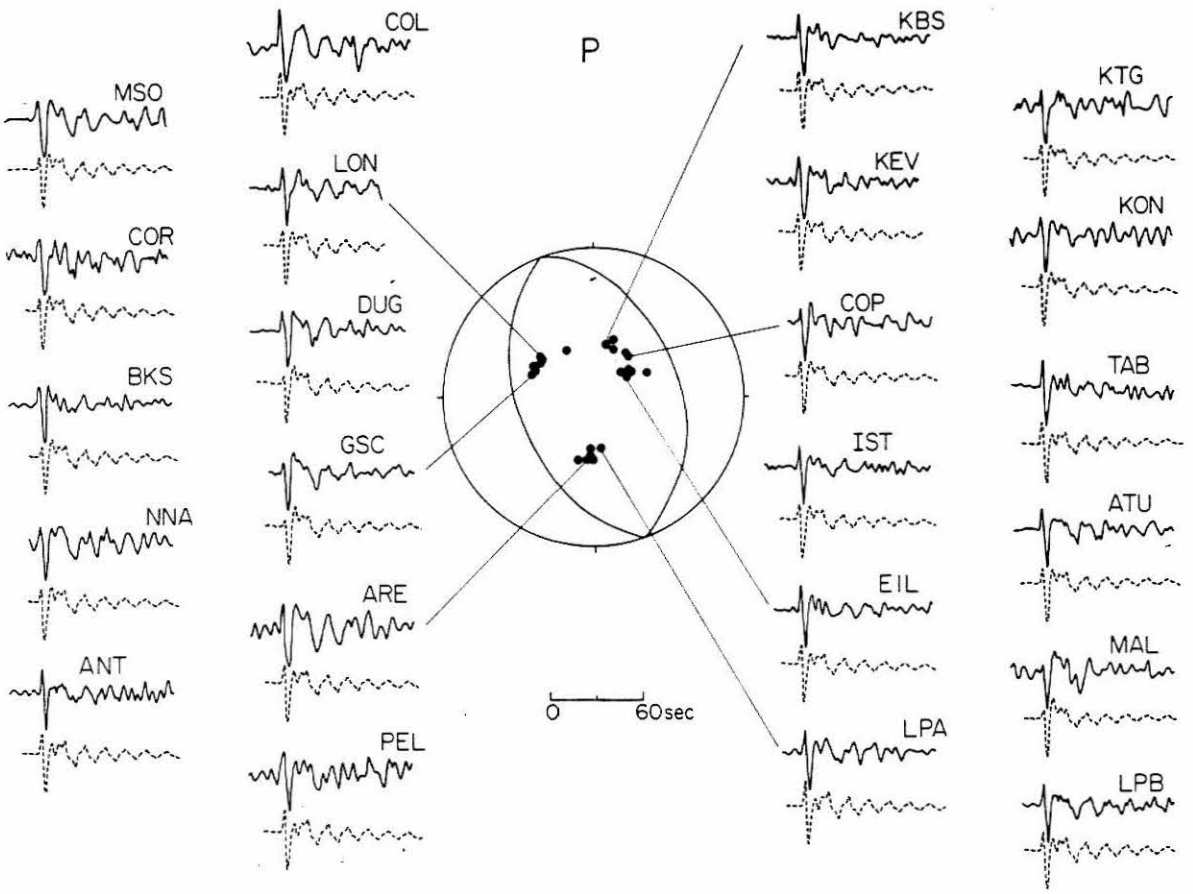

Figure 1-29. Observed (upper) and synthetic (lower) P-wave traces from the vertical long-period WWSSN seismograms for stations shown in Figure 1-26 and listed in Table 1-3. Note an initial simple event followed by more complicated water reverberations. The fault plane solution from Figure 1-27b is shown in the center, along with the locations of the P-wave stations on the focal sphere (solid circles).

that the complicated waveforms might be due to complexity in the source dislocation process itself, for example as in Butler et al. (1978), Kanamori and Stewart (1978), Rial (1978) and Stewart and Kanamori (1978). To examine this question further, synthetic P-wave seismograms were calculated for a point source beneath a layered crust and the results compared with the observed data. If satisfactory fits could be found using a single point source then the source could be regarded as simple and the complexity of the waveforms would be due to interactions with the source crustal structure, rather than to the source itself.

A particular advantage in this study is the epicentral location of the Bermuda earthquake. As shown in Figure 1-26 and in Table 1-3, the event is centered in an area that provides an excellent azimuthal coverage of WWSSN stations in appropriate distance ranges for the study of P-waveforms, i.e., 30^{o} to 90^{o}. The observed P-waveforms from vertical long-period instruments are shown in Figure 1-29 along with the station positions on the focal sphere. At first glance, data in different azimuths look similar, i.e., one large initial pulse followed by later arrivals. However, on closer examination some differences exist. For example, stations KBS, TAB, EIL, LPB, ANT and COL have large initial upswings compared with the second upswings. For stations such as KON, COP, NNA, BKS and MSO the second upswing is comparable to or slightly greater than the amplitude of the first upswing, while for stations MAL and GSC the initial upswing is low in amplitude compared with the second and might be regarded as almost nodal in character.

TABLE 1-3 Station Parameters

STATION	Δ (deg)	ϕ_{ES}	ϕ_{SE}	C or D	M_o^+	Waves Used
WWSSN						
AAE	99.21	74.1	302.3	C		P
AAM	18.07	317.6	127.9	C		P
ALQ	33.29	289.0	87.5	C		P
ANT	53.37	183.6	3.4	C	2.55	P, PW, S, SW
AQU	64.11	54.4	287.7	C		P
ARE	46.26	185.6	5.0	C		P, PW, S, SW
ATL	14.93	288.0	99.0	D		P
ATU	73.05	55.7	294.8	C		P, PW
BDF	49.00	154.9	337.5	C		P
BEC	3.34	41.6	222.9	D		P
BKS	45.74	295.2	83.0	C	5.79	P, PW, S, SW
BLA	13.14	307.1	119.9	D		P
BOG	25.94	195.6	13.5	C		P
CAR	19.30	178.9	359.0	C**		P
COL	59.35	330.7	84.5	C	2.45	P, PW, S
COP	60.24	39.9	280.2	C	4.54	P, PW, S
COR	46.06	304.6	88.8	C	3.44	P, PW, S, SW
CTA	148.16	280.0	65.5	C		PKP
DAG	52.05	12.6	235.6	C		P, S, SW
DAL	25.31	284.3	88.7	C**		P
DAV	141.20	339.3	18.0	C		PKP
DUG	38.29	298.1	91.0	C		P, PW
EIL	85.25	58.7	301.6	C		P, PW
EPT	33.59	283.3	82.7	C		P
ESK	51.41	41.1	268.0			S
FVM	20.78	299.0	106.0	C		P
GDH	40.19	7.6	198.7	C		P, S
GRM	108.67	118.1	293.9	C*		PKP
GSC	41.71	290.8	83.0	C	4.15	P, PW
GUA	126.82	319.6	35.3	C		PKP
IST	75.38	51.0	296.9	C	3.99	P, PW, S
JCT	28.05	279.4	82.8	C**		P
KBS	58.81	12.8	265.8	C	3.74	P, PW, S, SW
KEV	63.76	22.8	285.1	C	2.90	P, PW, S
KJF	65.63	28.6	288.3	C		P
KOD	127.64	45.8	320.8	C		P
KON	58.20	35.6	275.6	C	3.56	P, PW, S, SW
KTG	47.72	18.9	236.6	C	2.77	P, PW, S
LON	45.03	307.7	92.0	C		P, PW
LPA	65.06	171.5	351.0	C	4.25	P, PW, S, SW
LPB	46.16	181.1	1.0	C	4.01	P, PW, S, SW
LPS	25.45	237.1	48.8	D		P
LUB	29.55	286.1	87.6	C		P
MAL	52.18	64.9	281.9	C	2.98	P, PW, S

MSO	39.65	308.5	98.4	C	2.77	P, PW,S
NAI	102.85	84.0	300.2	C*		PKP
NDI	112.61	33.6	326.9	C*		PKP
NNA	42.64	193.9	12.3	C	2.04	P, PW, S, SW
NUR	65.40	33.0	287.3	C		P
OGD	12.63	333.9	149.6	C**		P
PDA	35.24	65.9	269.8	C*		P
PEL	62.77	183.2	3.3	C*	2.97	P, PW
PTO	48.26	59.9	276.1	C		P
QUE	106.06	40.2	319.7	C		PKP
RIV	147.23	253.0	86.2	C		PKP
SCP	13.87	324.5	138.4	D		P
SHA	18.02	277.7	87.2	D		P
SHI	97.58	49.7	310.5	C		P
SHK	113.21	342.1	18.8	C		PKP
SHL	121.35	22.1	338.8	C		P
SJG	11.78	174.6	355.1	D		P
STU	59.66	48.2	281.8	C		P, S
TAB	88.30	46.3	307.3	C	2.98	P, PW, S
TOL	51.87	60.9	279.7	C		P
TUC	37.12	285.1	81.9	C		P
WES	12.87	346.5	164.1	D		P

$\overline{M_o^+} = 3.4$

CANADIAN

ALE	52.74	0.8	85.3	C		P
EDM	40.65	318.3	106.3	C		P
FCC	34.18	335.3	135.9	C		P
FFC	35.09	325.0	120.7	C		P, S
FRB	33.87	359.0	178.1	C		P
FSJ	47.22	318.1	97.4	C		P
LHC	24.98	323.8	129.7	C		P
INK	53.08	328.9	96.4	C		P
MBC	52.46	346.2	120.3	C**		P
MNT	16.34	344.1	160.2	C**		P
OTT	16.82	339.1	154.0	C**		P
PHC	48.88	312.9	91.4	C		P
PNT	43.74	311.5	96.4	C		P
RES	46.95	350.3	146.6	C		P
SCH	24.91	0.7	181.1	C		P
SES	34.48	314.7	105.4	C		P
STJ	20.92	28.5	217.7	D**		P
VIC	46.18	310.1	92.5	C		P
YKC	44.50	330.9	114.6	C		P

IDA

CAN	149.19	250.9				R1, R2
CMO	59.32	330.7				R1
GAR	100.80	32.2				R1

NNA	42.64	193.9	R1, R2
PFO	41.66	288.3	R2, R3
RAR	102.40	252.8	R1
SUR	103.97	119.2	R1, R2

ϕ_{ES} is the azimuth of the station from the epicenter.

ϕ_{SE} is the azimuth of the epicenter from the station.

\+ the units of M_o are x 10^{25} dyne-cm.

* poor reading.

** nodal reading.

P P-wave first motion used.

PKP PKP-wave first-motion used.

S S-wave polarity used.

PW P-waveform used.

SW S-waveform used.

R1, R2, R3 multiple Rayleigh wave used.

Although these variations are subtle for some stations, there do appear to be overall differences in the initial P-wave shape. An attempt to match these was made by generating synthetic waveforms. No crustal structure information was obtainable for the epicentral region of the Bermuda event. However, in the vicinity of Bermuda itself and to the northwest and southeast of the island, several refraction studies have been made. They are presented in Officer et al. (1952) and Ewing et al. (1954) and the resulting crustal structure is shown in Figure 1-28 in a modified form. This structure was considered to be appropriate for the crust beneath the Bermuda epicenter. A 1.2 km thick sedimentary layer of velocity 2 km/s was omitted from the top of the crust since such a layer made only negligible differences to the synthetic waveforms and would not be resolvable in the observed data. Omitting this layer also simplifies the presentation. Using the crustal structure shown in Figure 1-28 and a point source in the mantle, P-wave synthetic seismograms were generated using the method described by Langston and Helmberger (1975) and Langston (1976). Rays P, pP and sP are shown in Figure 1-28 leaving the source region. Here, pP and sP are reflections from the base of the crust. However, to explain the initial pulse on the P-wave seismograms, additional rays have to be included. They result from the energy transmitted into the crust and water layers by upgoing P and S wave radiation, the source conversions of P to S and S to P at the various interfaces and eventually transmitted to the mantle, and multiple reflections of P, S and combinations of these within and between the crust and water layers. In all, for an adequate

modeling of the initial pulses shown in Figure 1-29, 22 rays were used. Their description is given in Figure 1-30a. As a check and for the final modeling shown in Figure 1-29, the modification of the Thomsen-Haskell layered matrix method by Harkrider (1964), Douglas et al. (1974) and Langston (1976) was employed. This allowed us to model easily the P wavetrain for the first 1.5 minutes of record. The later energy comes from P-wave reflections within the water layer and because of the high reflection coefficient at the water-crust interface, the amplitude decay of this reverberation is slow. From an amplitude comparison of observed with synthetic P-waveforms an averaged seismic moment of $M_o = 3.4 \times 10^{25}$ dyne-cm was obtained. Individual values for some of the stations are given in Table 1-3. The depth and time functions were varied in the above P-wave analysis and in the later SH-wave analysis. The best fits obtained, consistent with both P and S wave data are for a point source located 1 km beneath the Mohorovicic discontinuity, with a three second duration time function, as shown in Figure 1-28. In the P-wave modeling a t^* value of 1.0 was used.

S-WAVE ANALYSIS

Many of the WWSSN stations were favorably located with respect to P-wave radiation from the Bermuda source as discussed in the previous section on the P-wave analysis. The same fortunate circumstance applied to the distribution of WWSSN and Canadian stations for the S-waves. The stations grouped in three dominant areas of the world, i.e. North America, South America and Europe. This can be seen in Figure 1-31, in

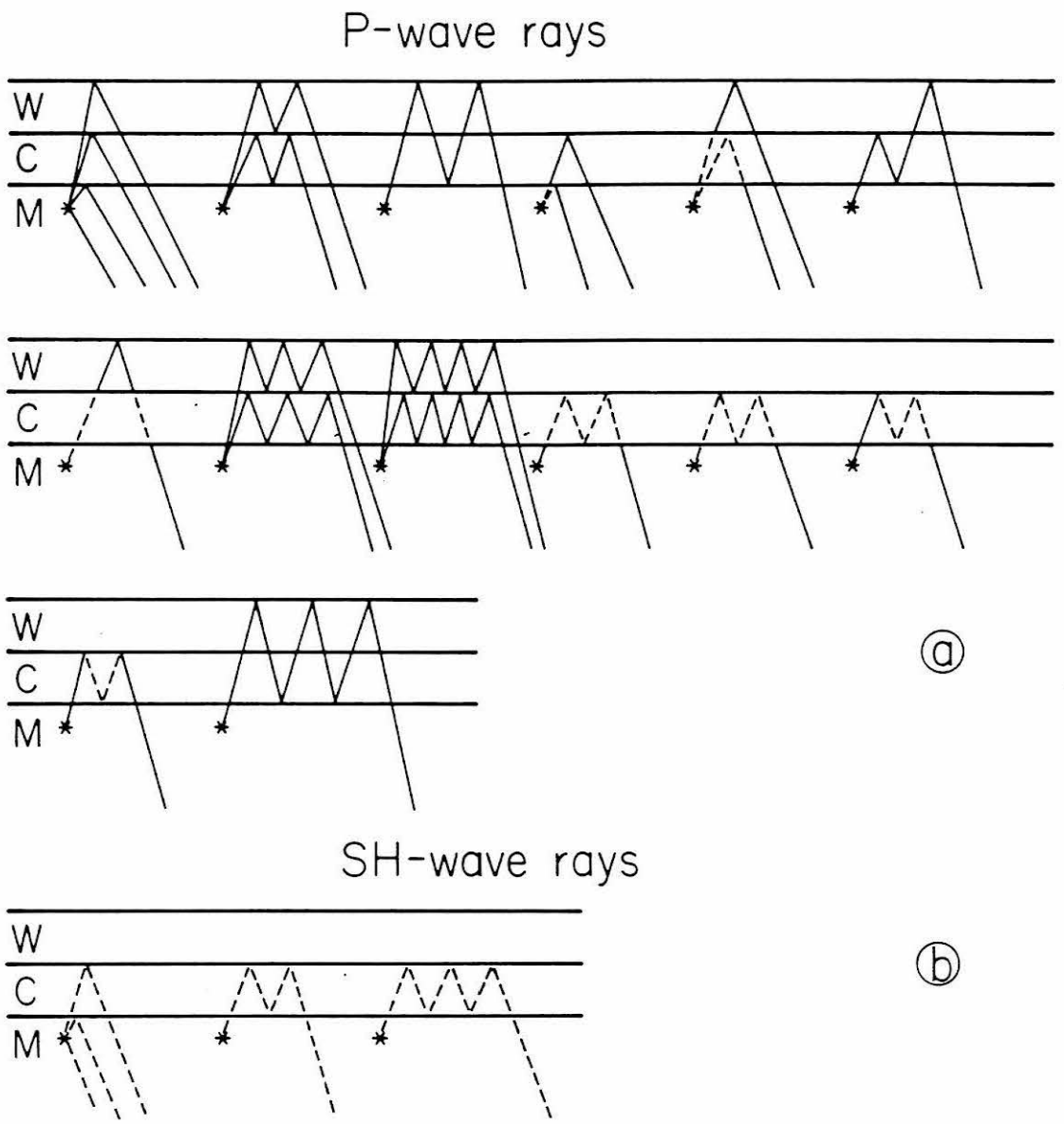

Figure 1-30. (a) Schematic figure showing the 22 rays used in the modeling of the P-wave synthetics for the Bermuda earthquake. Solid lines represent P-waves, dashed lines represent SV-waves. Note that the rays shown include direct reflections, P to S and S to P conversions and multiple reflections at the various boundaries. (W - water; C - crust; M - mantle). (b) Schematic figure showing the 5 rays used in the modeling of the SH-wave synthetics for the Bermuda earthquake. Dashed lines represent SH-waves.

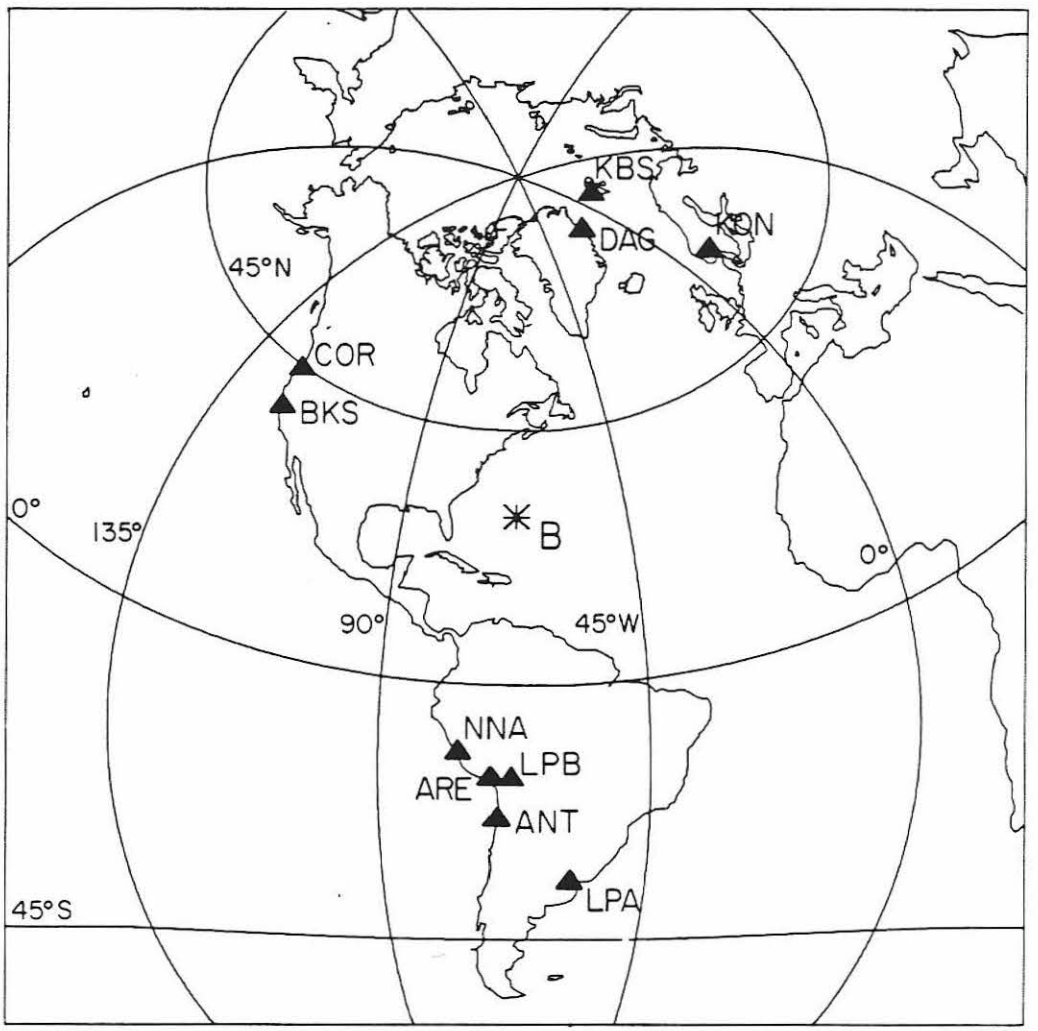

Figure 1-31. Map showing locations of 10 WWSSN stations used in the S-wave modeling of the Bermuda earthquake. Note the good azimuthal coverage of stations around the epicenter (B). An azimuthal equidistant projection is shown. See Table 1-3 for distances and azimuths.

Table 1-3 and is shown by the solid circles in Figure 1-32. Also from Figure 1-31 and Table 1-3 it can be noted that most of these stations are close to being naturally rotated into pure SH and SV radiation with respect to the S-waves from the Bermuda event. For stations in North America and Europe, SH waves are well-recorded on the north-south components, SV waves on the east-west components, while in South America SH waves record well on the east-west components, SV on the north-south components. This fortunate occurrence allowed easy identification of the waveforms and polarities of SH and SV waves to be made. These polarities were read from as many of the WWSSN and Canadian stations as possible. All SV waves showed negative polarity or motion towards the source. The SH wave polarities are plotted in Figure 1-32. Here positive polarity corresponds to clockwise motion. Representative S-wave seismograms from different azimuths from the earthquake source were rotated, as necessary, and the resulting SH-waves plotted in Figure 1-32. The solid lines on the focal sphere represent nodes in the SH-wave radiation which are consistent with the P-wave focal mechanism shown in Figure 1-27b. Note that the polarity of the observed records changes with azimuth in moving from one quadrant to the next. Again, as for the P-waves, there are differences in the waveforms. The SH waveforms for stations DAG and KBS show almost symmetric waveforms as far as the first (positive) and second (negative) pulses are concerned. On the other hand, the data from stations LPA, LPB, ARE and BKS show an asymmetric waveform having a narrower first pulse and broader second pulse. Presumably, these features should be reproduced synthetically if

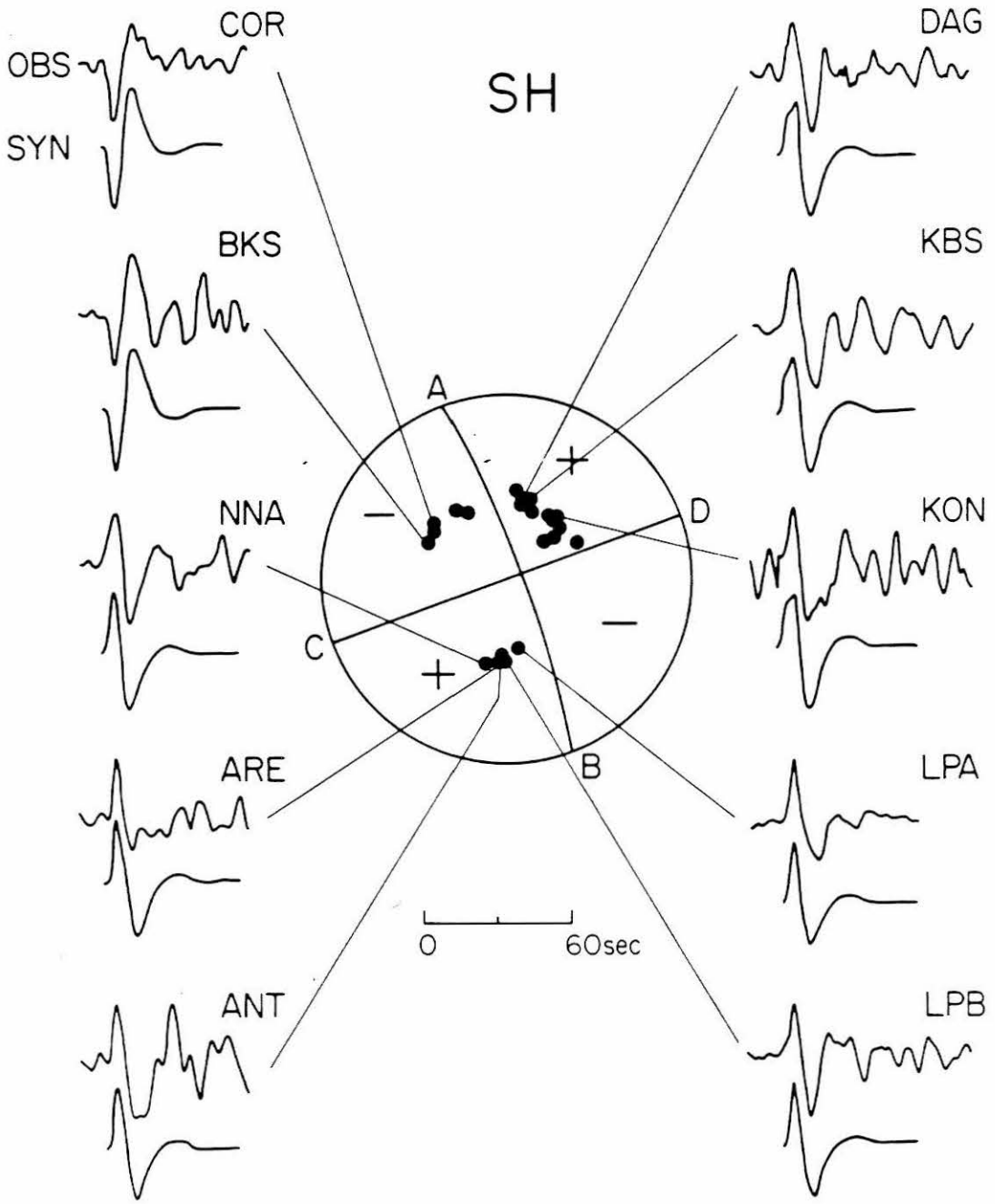

Figure 1-32. Observed and synthetic SH-wave traces, computer rotated from the horizontal long-period WWSSN seismograms for the stations shown in Figure 1-31. The SH-wave focal mechanism solution is shown in the center along with the locations of the S-wave stations on the focal sphere (solid circles). The stations shown in the figure are plotted along with stations for which the polarities of SH-waves were determined. The positive and negative quadrants represent clockwise and counterclockwise directions of first-motion respectively, for SH-waves.

the proper choice of source parameters can be found. With a point source located in the mantle as shown in Figure 1-28, synthetic SH-waveforms were generated and matched to the data. In this case, only 5 rays proved to be significant and they are sketched in Figure 1-30b. At first, the mechanism shown in Figure 1-27b was tried, with a dip of 45^{o} ascribed to both planes. The depth and time functions were varied as in the P-wave analysis with a t^{*} value of 4.0 being used for the S-wave modeling. The best result produced waveforms with polarities which agreed with the observed data. However, both the first and second pulses were symmetric and the narrow first pulse, broad second pulse feature was not observed. This effect could be explained by changing the dips of the northeast and southwest dipping planes to 42^{o} and 48^{o} respectively, as shown in Figure 1-27b. The SH-wave synthetics for this model are shown in Figure 1-32. For stations to the southwest of nodal line AB of Figure 1-32, direct S becomes less nodal and sS more nodal than for the 45^{o} case. Stations to the northeast of line AB have the opposite effect, with a less dramatic effect on the resulting waveforms. The nodal line CD remains the same with the change in dip angle of the fault planes away from 45^{o}. Thus, modeling of a set of SH polarities and waveforms for the Bermuda earthquake gives results consistent with those obtained from P-wave first-motions and P-waveform modeling. The source mechanism indicated in Figure 1-27b and velocity model shown in Figure 1-28 with the hypocenter 1 km below the Mohorovicic discontinuity are preferred over that with either of the mechanisms indicated in Figure 1-27a and a crustal source. SV polarities and waveforms obtained

from the WWSSN and Canadian stations are all identical and so provide no additional constraint other than being consistent with this mechanism.

The P-wave coda discussed earlier could be explained successfully by simply adding in the contributions of the many rays partially trapped in the water layer. However, the SH-wave coda appears much more complicated and difficult to explain. Complicated S-wavetrains have been observed for other non-strike-slip events, see Langston (1978) and Langston and Butler (1976). On the other hand, the SH-wavetrains observed for pure strike-slip events at the appropriate SH-loop maxima are remarkably simple as in the work by Helmberger and Engen (1974). These observations suggest that the above complications occur in the presence of strong SV motions in the source region at ray parameters not far removed from those appropriate for SH and may in fact be SV-to-SH conversions caused by non-planar structure; see, for instance, Langston (1978).

SURFACE WAVE ANALYSIS

As a check on the focal mechanism solution from the body wave analysis and in order to estimate a long-period surface wave moment, the Rayleigh waves excited by the Bermuda earthquake were analyzed. The records used in the analysis were produced by the International Deployment of Accelerographs (IDA) world-wide network of digitally recording gravimeters discussed by Agnew et al. (1976). The data used consisted of R_1, Rayleigh waves from six IDA stations (CAN, Canberra, Australia; CMO, College, Alaska; GAR, Garm, USSR; NNA, Naña, Peru;

RAR, Raratonga, Cook Islands and SUR, Sutherland, South Africa), R_2 waves from four stations (CAN, NNA, PFO [Pinon Flats, California, USA] and SUR) and R_3 waves from PFO. The method of analysis, described by Kanamori and Given (1981), uses these wave amplitudes at a period of 165 seconds. The amplitudes are corrected for distance assuming the spherically symmetric earth model and attenuation described in Kanamori and Given (1981). The resulting station relative amplitudes are plotted in Figure 1-33 as a function of azimuth around the source. Synthetic radiation patterns were then determined for each of the focal mechanisms shown in Figures 1-27a and 1-27b and are also plotted in Figure 1-33. The dashed curves, which are the radiation patterns for the mechanisms in Figure 1-27a, do not fit the observed data as well as the solid curve which is the pattern for the preferred mechanism for the Bermuda earthquake (Figure 1-27b). By matching the observed data to the synthetic calculations, a long-period surface wave moment of 3.1×10^{25} dyne-cm was obtained. This is in good agreement with the value of 3.4×10^{25} dyne-cm determined from the P-wave data.

DISCUSSION

The island of Bermuda is a topographic peak on the elevated Bermuda Rise or Pedestal and is shown on bathymetric maps by Chase (1975) and Shuran (1971). The 1978 event occurred off the southwest point of the Bermuda Rise at its junction with the Hatteras Abyssal Plain, near the 5,000 m bathymetric contour. It is interesting to note that the strike obtained for the Bermuda event mechanism is in reasonable agreement with

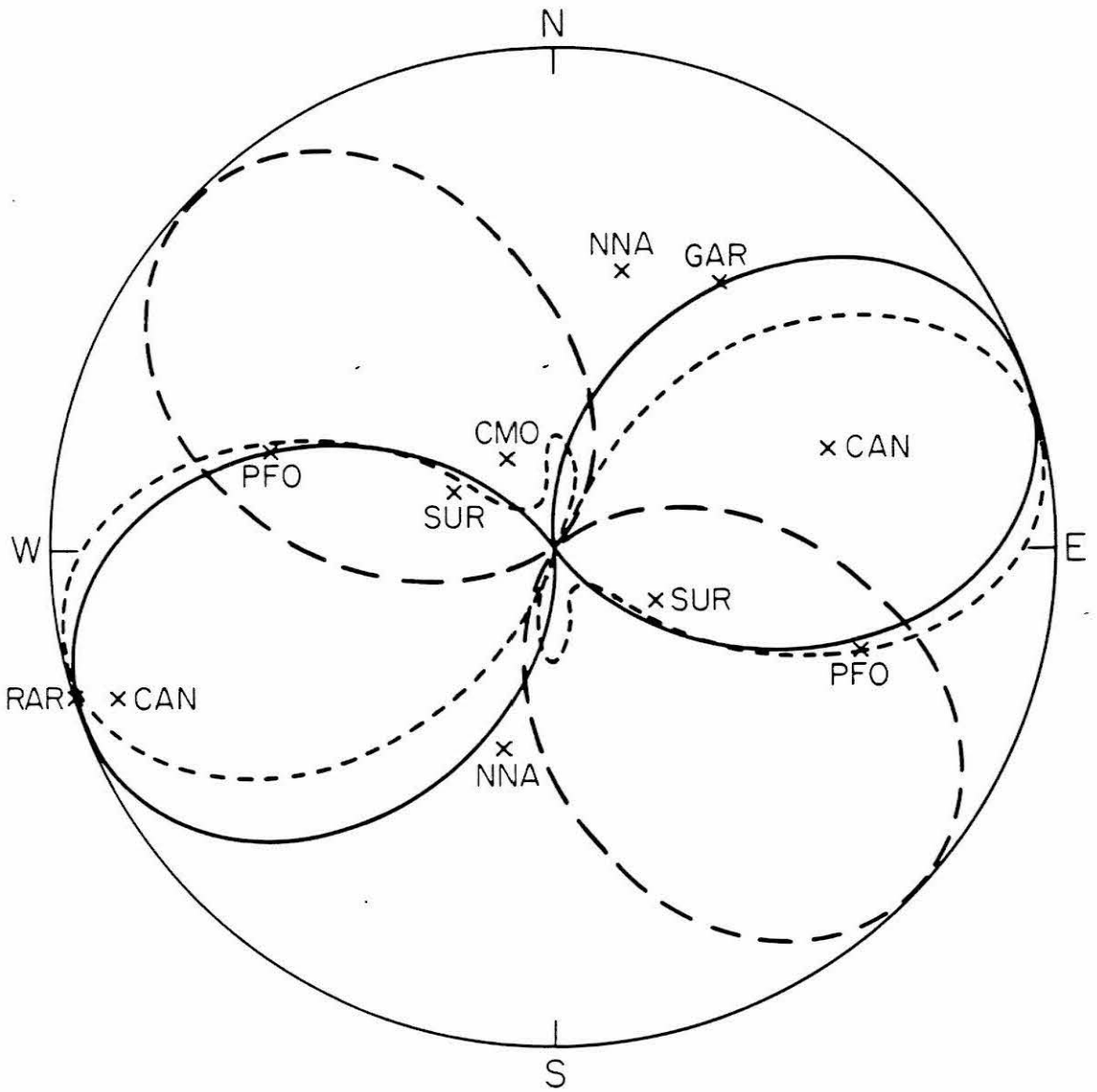

Figure 1-33. Amplitudes as a function of azimuth for R_1, R_2 and R_3 surface waves at 165 sec period for IDA stations (crosses) which recorded the Bermuda event. The solid curve represents the synthetic radiation pattern for the preferred mechanism (Figure 1-27b). The dashed curves are for the solutions shown in Figure 1-27a and do not fit the data as well.

the strike of the steep slope between the Bermuda Rise and the Hatteras Abyssal Plain, namely north-northwest. The extent of rupture from 11 km towards the surface is unknown. However, the body wave modeling implies it is not significant.

The oceanic crust in this region is relatively old, the epicenter occurring in Mesozoic crust of Lower Cretaceous age, approximately 125 m.y. old (Heezen and Fornari (1975)). From Heezen and Fornari (1975) and Schouten and Klitgord (1981) the magnetic lineations are seen to trend in a northeast or north-northeast direction (Figure 1-34) and so are quite different in strike from the mechanism of the Bermuda earthquake, suggesting that the event is not associated with these. As seen in Figure 1-34, the epicenter lies just to the southeast of anomaly M11. From this figure, it can be seen that the now presumed inactive faults, which are the western extensions of the active transform fault system between the ridge crests of the Mid-Atlantic Ridge system, also change strike across this part of the western Atlantic. Between magnetic anomalies M18 and M11 the strike is west-northwest, while to the southeast of M11 the strike is more northwesterly. In the epicentral region of the Bermuda event, near the western extension of the Kane Fracture Zone, the strike of these features is approximately northwest (Figure 1-34), in reasonable agreement with the mechanism determined in this study.

The class of earthquakes which are referred to as intraplate events have received much attention recently due to the hazard they pose by way of damage and loss of life in areas which are poorly prepared for their

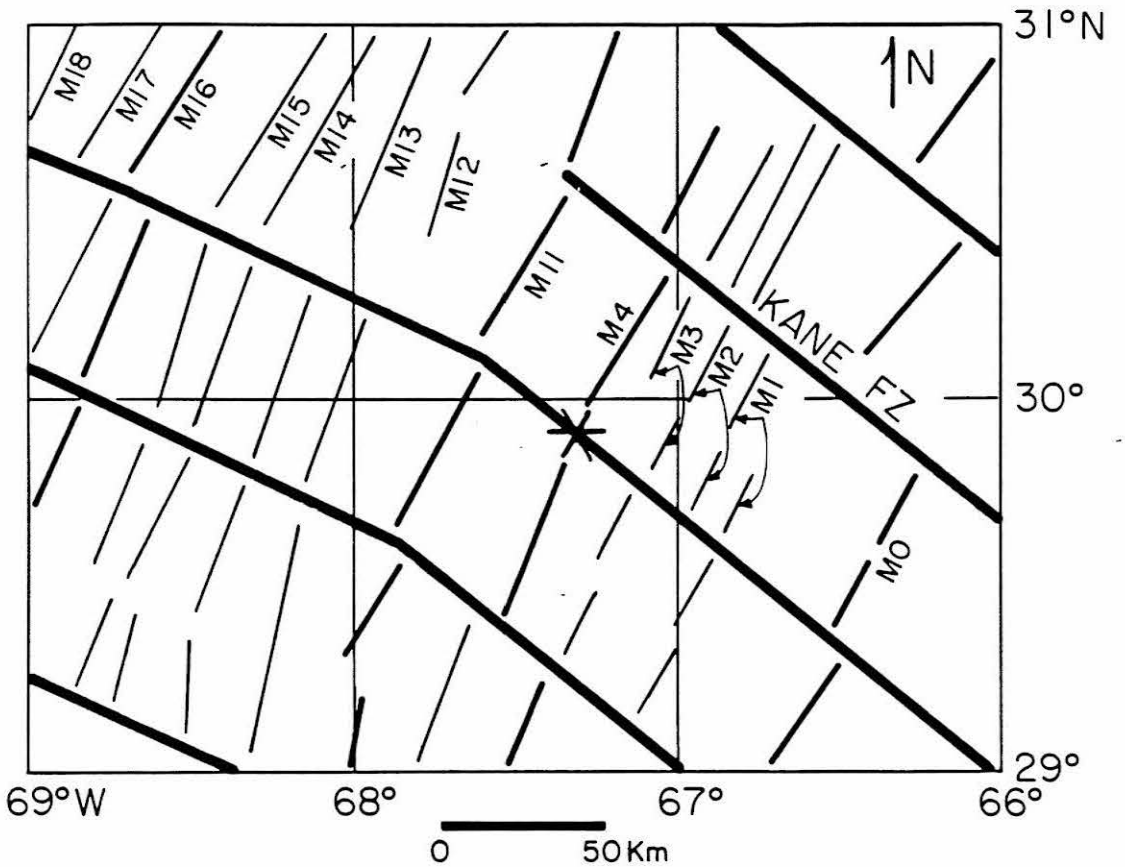

Figure 1-34. Map, modified from Schouten and Klitgord (1981) indicating the locations of magnetic anomalies and inferred fracture zones in the western Atlantic in the vicinity of the Bermuda earthquake (asterisk).

occurrence. Perhaps the most dramatic example of the 1976 Tangshan, China earthquake in which over 650,000 people lost their lives, illustrates this point well. It was estimated by Butler et al. (1978) to be one of the largest continental intraplate events to have occurred recently. Although China and Asia as a whole host many of the large continental intraplate events, other continental environments have not been devoid of such. In particular, within eastern North America, many events have occurred in the time period 1900-1977 as shown in Figure 1-35a. Several of these have been of magnitude $M \geq 5.0$ (Figure 1-35b). Two, in particular, were events of magnitude $M \geq 7$, viz. the 1925 La Malbaie, Canada event (7.0) and the 1929 Newfoundland Banks earthquake (7.2) (Stewart, 1979). Also, prior to 1900, several significant events occurred in eastern North America. Notable among them are the 1811-12 New Madrid events in southeastern Missouri and the 1886 Charleston, S. Carolina earthquake. Intraplate activity, however, occurs not only within continental plates but within oceanic plates as well, the Hawaiian earthquake of November 29, 1975 being one of the largest examples. The focus of this study, the Bermuda earthquake, is another significant oceanic intraplate event.

The Bermuda earthquake is the largest seismically recorded event to occur in the oceanic plate off the eastern coast of North America. As shown in Figures 1-35a and 1-35b one other large event, the 1929 Newfoundland Banks earthquake (NFB) is located offshore in the region of the continental shelf (Stewart, 1979). From studying Figure 1-35a one might consider the Bermuda event to be located in a region of relative

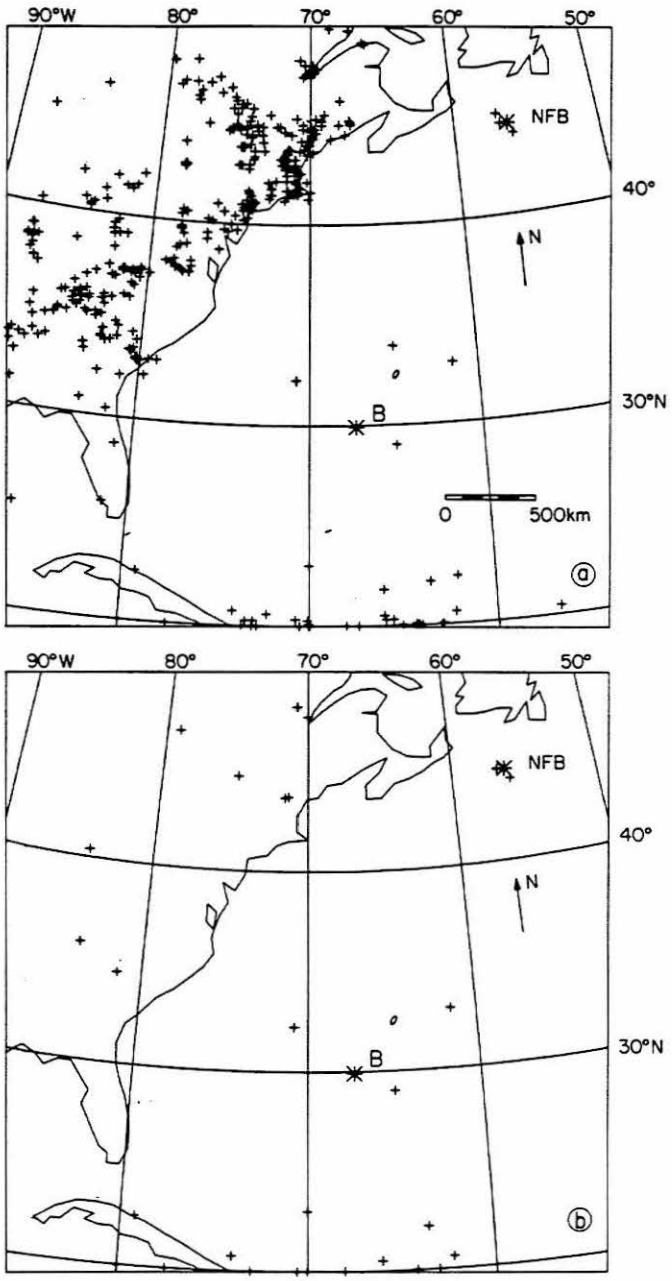

Figure 1-35. (a) Map showing epicenters of all events in the time period 1900-1977 for eastern North America and the western Atlantic Ocean. Note that the two largest events in the offshore area are the Newfoundland Banks earthquake of November 18, 1929, M = 7.2 (NFB) (Stewart, 1979) and the Bermuda earthquake (B). Note the relatively low level of seismic activity in the offshore area compared with the activity in eastern North America. (b) Map showing epicenters of $M \geq 5.0$ events in the time period 1900-1977 for eastern North America and the western Atlantic Ocean. The seismicity in the offshore region is of comparable amount to the activity in eastern North America. Seismicity is taken from the USGS/NOAA world-wide catalogue.

seismic quiescence compared with the rest of eastern North America. However, since events of all magnitudes in the time period 1900-1977 have been shown in this plot, it is reasonable to assume that more events are located onshore due to the presence of a large number of seismographic stations in this region and hence better recording capability for smaller events compared with events offshore. To test this, events of magnitude $M > 5.0$ have been plotted for the same region. Magnitude of 5.0 probably represents the detection threshold for events in the offshore area. The result, shown in Figure 1-35b, indicates that the seismicity in the western Atlantic appears to be at a level similar to that in eastern North America.

The intraplate events discussed above appear to be present within all plates. Recently, Sykes (1978) reviewed intraplate seismicity and suggests its origin may be related to the reactivation of pre-existing zones of weakness. In particular, Fletcher et al. (1978) suggest that the Newfoundland Fracture Zone, the New England Seamount Chain and the Blake Fracture Zone perhaps control the location of eastern North American seismicity (Figure 1-36). Assuming their hypothesis is correct, and in the absence of any recent large seismic event, perhaps the Bermuda event can be considered as an analog for earthquake hazards prediction for the eastern seaboard. That is, the suggested style of faulting is relatively deep and of a thrusting nature. The consequence of these features on strong motion estimation is substantial.

Estimating earthquake hazards is a relatively difficult task because of the large number of unknowns involved. Fortunately, a

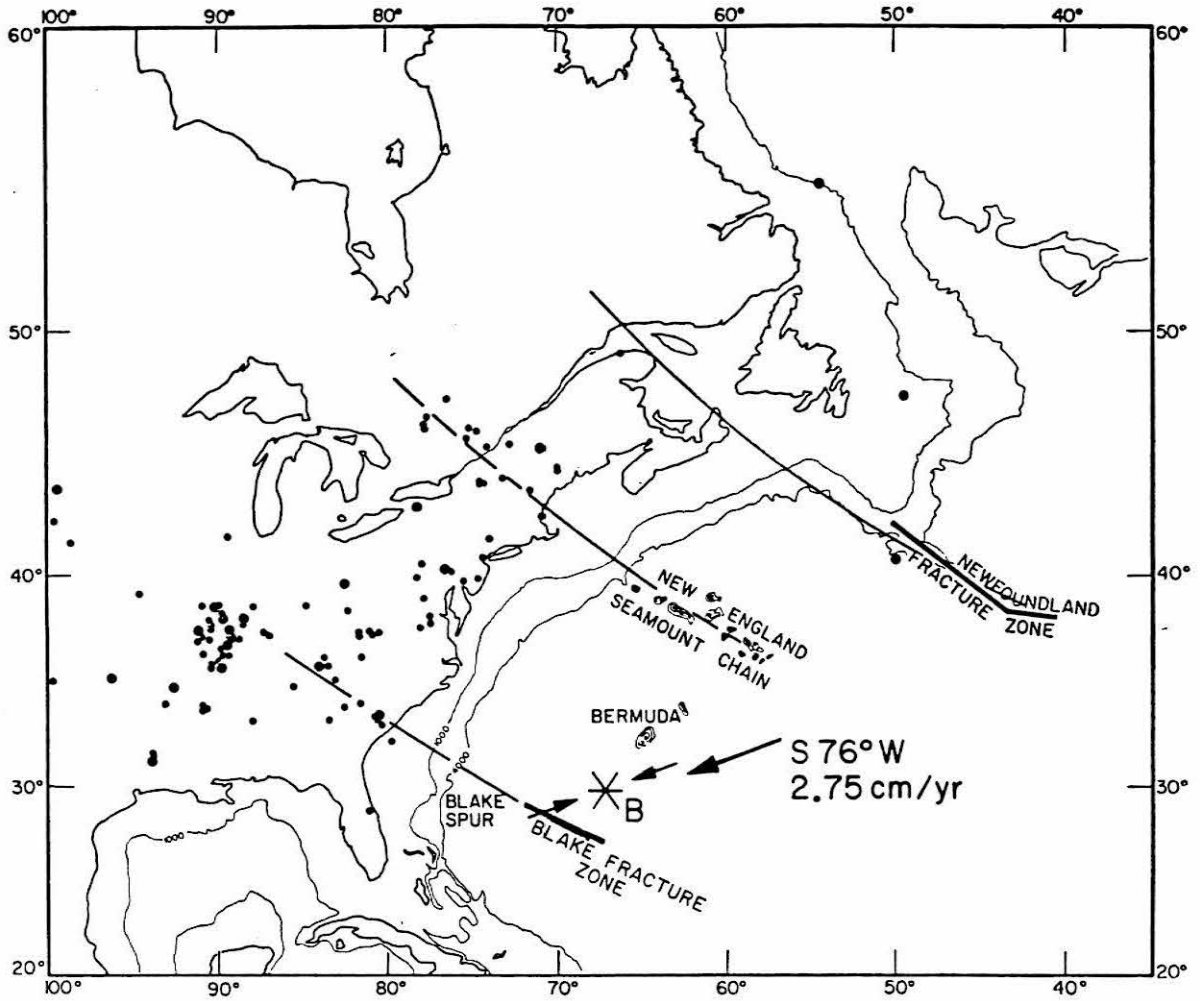

Figure 1-36. The location of the Bermuda earthquake of March 24, 1978 (B) is shown along with the direction of maximum compression associated with it, determined in this study (small arrows). The large arrow indicates the direction of absolute plate motion of the North American plate at the epicenter of the Bermuda earthquake, calculated from Minster and Jordan (1978). This figure is modified from Sykes (1978).

substantial number of strong motion recordings have been obtained from recent events on the west coast which can be used to great advantage. For example, the San Fernando experience can be contrasted with what happened during the Santa Barbara event; both had thrust mechanisms with the latter being a deeper event. A relatively large amount of energy release occurred near the surface in the San Fernando situation as reported on by Heaton and Helmberger (1979) and as a consequence the microzonation techniques were not very successful, for example see Hudson (1972). Microzonation techniques assume that the seismic waves are traveling vertically near the surface, which is probably not the case in this situation. On the other hand, the strong motions produced by the Santa Barbara earthquake show a considerable degree of variability which can be explained by near-surface geology as discussed by Wallace and Helmberger (1981). Thus, microzonation methods can be expected to be far more effective in situations involving deep sources. There are many other effects involving attenuation, the relationship of intensity maps to mechanisms, etc., which are influenced by the style of faulting and are better discussed elsewhere. In short, a detailed analysis of the larger historic events in this region should be conducted to test the above assertion on the style of faulting.

CONCLUSIONS

As the largest event to occur recently, close to the eastern seaboard of North America, the Bermuda earthquake was worthy of study in an attempt to elucidate its tectonic origin.

From studying a well-recorded body-wave data set, the source mechanism for the Bermuda earthquake is constrained to be a north-northwest striking pure thrust mechanism (strike = N 20°W, dip = 42°NE, rake = 90°) with the hypocenter located at a depth of 11 km, predominantly in the mantle. The event had a seismic moment of 3.4×10^{25} dyne-cm determined from P-wave data, while a value of 3.1×10^{25} dyne-cm was determined from long-period Rayleigh wave data recorded by the IDA network. The north-northwest strike of the event is in good agreement with the bathymetry of the area, the epicenter being close to the southwestern edge of the Bermuda Rise. The strike of the Bermuda source mechanism (north-northwest) is close to the northwesterly strike of the presumed inactive fracture zones in the western Atlantic, suggesting that one of these zones acted as a nucleus for the event. The results from this study indicate that the direction of maximum compression for the Bermuda earthquake source is oriented in an east-northeast, west-southwest direction (small arrows in Figure 1-36). This direction is in remarkably good agreement with the direction of absolute motion of the North American plate (S 76°W) at the epicenter of the Bermuda event calculated from Minster and Jordan (1978).

CHAPTER 2.

COMPLEXITY OF RUPTURE PROPAGATION IN LARGE STRIKE-SLIP EARTHQUAKES

2.1 Introduction.

Although it is important to understand the source rupture process in simple events (the subject of Chapter 1), a greater challenge lies in attempting to understand the rupture process when more than one source is involved. As discussed in Chapter 1, the main aim in this study is to understand complexity viewed in the period range of the WWSSN long-period seismograms, viz., the range of tectonic interest.

Previous studies have attempted to unravel such complexity. Take, for example, the 1971 San Fernando earthquake. Langston (1978) and Heaton (1981) have both attempted to understand the details of this small to intermediate size earthquake. Both found it to be quite complex and have proposed rupture on two faults of different orientation to explain the observed seismological data. Undoubtedly, with the number of unconstrained parameters for this event, it is almost certainly possible to find additional models that are just as compatible with the observed data.

Unless one can constrain the depths and mechanisms of the multiple sources well, the unknown parameters are too numerous for a predominantly thrust or normal fault source sequence to be well-constrained.

On the other hand, some simplifying assumptions can be introduced in dealing with the complexity associated with rupture propagation in large strike-slip earthquakes. In these events the depth of faulting is usually restricted to the upper 20 km. Since rupture takes place along the strike of such faults, one can assume that such rupture consists of several point sources, located at say 10 km depth, distributed along the fault at varying intervals.

Because of the geometry of strike-slip faults (ribbon-like), it is possible to assume that each source has an almost identical mechanism since the change in the strike direction for such faults is usually not very significant ($< 20^{o}$ to 30^{o}). Other variables to be concerned about are the source time function and finiteness over the total rupture plane. These are important and may have to be included if the rupture requires them.

In this chapter an attempt is made to model several large strike-slip earthquakes. In Section 2.2 the Guatemala earthquake is studied, with particular emphasis being placed on a detailed examination of its rupture sequence. Its tectonic implications are also examined. Turkish events occurring along the Anatolian fault are studied in Section 2.3. One event (Mudurnu Valley) could be explained in a fashion similar to the Guatemala event. However, the other (E. Turkey) appeared to be even more complex. The implications of these results for strong ground motion are also discussed.

2.2 Complexity of the Rupture Process along the Motagua Fault in the Guatemala Earthquake.

ABSTRACT

Detailed analyses of teleseismic surface waves and body waves from the Guatemala earthquake of February 4, 1976 show that: (1) Left-lateral displacement along a vertical fault with a strike varying from N 66°E to N 98°E is consistent with the teleseismic data. (2) The seismic moment was 2.6×10^{27} dyne-cm. The directivity of the surface-wave radiation indicates an asymmetric (1:2.3) bilateral faulting with a total length of 250 km. In modeling the displacement a rupture velocity of 3 km/sec was used and the fault curvature included. (3) If a fault width of 15 km is assumed, the average offset is estimated to be about 2 m. This value is about twice as large as the average surface offset. (4) Although the observed directivity suggests a uniform overall displacement along the fault, the body-wave analysis suggests that the earthquake consists of as many as ten independent events, each having a seismic moment of 1.3 to 5.3×10^{26} dyne-cm and a fault length of about 10 km. The spatial separation of these events varies from 14 to 40 km. This multiple shock sequence suggests that the rupture propagation is jagged and partially incoherent with an average velocity of 2 km/sec. (5) The average stress drop estimated from surface waves is about 30 bars, but the local stress drop for the individual events may be significantly higher than this. (6) The complex multiple event is a manifestation of heterogeneous distribution

of the mechanical properties along the fault which may be caused by either asperities, differences in strength, differences in pore pressure, differences in slip characteristics (stable sliding vs. stick slip) or combinations of these factors. (7) This complexity has important bearing on the state of stress along transform faults and is important in assessing the effect of large earthquakes along other transform faults like the San Andreas.

INTRODUCTION

The Guatemala earthquake of February 4, 1976 ($09^h\ 01^m\ 42.2^s$ U.T.; 15.2^oN, 89.25^oW; $M_s = 7.5$; $m_b = 5.8$) is not only one of the most disastrous earthquakes in recent history but also unique in various aspects. According to the preliminary reports of the U.S. Geological Survey (1976) and Plafker (1976), this earthquake is one of the largest events of transform fault mechanism, characterized by a very long fault with a relatively shallow depth. The surface breaks associated with this earthquake have been mapped in detail by Plafker et al. (1976), and the distribution of aftershocks has been studied by Person et al. (1976), Langer et al. (1976) and Matumoto and Latham (1976). Teleseismic data are very complete and have been used to study the fault mechanism of this earthquake (Dewey and Julian, 1976). This completeness of various kinds of data warrants a further seismological investigation into the details of the faulting mechanism of this important event. This section is primarily concerned with: (1) A comparison of the surface offset with the displacement determined from

seismological data. (2) The variation of the displacement along the fault. (3) The complexity of the rupture propagation along the fault. These features will provide a key to the understanding of the nature of plate motion along transform faults, as well as the mechanical properties of earthquake faulting. The results will be useful for predicting the nature of faulting in other major transform fault earthquakes, such as the 1906 San Francisco and the 1857 Fort Tejon type earthquakes along the San Andreas fault. This will be discussed further in Chapter 4.

In this study, long-period surface waves were used to constrain the overall source parameters such as the seismic moment and the directivity and body waves were used to study the details of the faulting. The far-field body waves recorded on the WWSSN (World-Wide Standardized Seismographic Network) long-period seismograms are very complex, indicating that the Guatemala earthquake is a multiple event. It is widely known that most large earthquakes are multiple shocks. Imamura (see Imamura, 1937, p. 267), made a detailed analysis of seismograms of the 1923 Kanto earthquakes to determine the location and the size of the individual events of the multiple shock sequence. Wyss and Brune (1967) analyzed a large number of seismograms of the 1964 Alaskan earthquake and located six individual events. From the time intervals between these events, they obtained an average rupture velocity of 3.5 km/sec. Other studies pertinent to multiple shocks include Miyamura et al. (1964) and Trifunac and Brune (1970). These studies clarified the details of complex rupture propagation associated with very large

earthquakes. In the present study the observed P-waveforms were matched with synthetic waveforms to investigate the details of the rupture propagation associated with the Guatemala earthquake.

BASIC SEISMOLOGICAL DATA

The P-wave first-motion data are shown in Figure 2-1 and are listed in Table 2-1. All of the data points were read from the WWSSN records in this study. The result is consistent with that given by Dewey and Julian (1976). The dip angles and the strike directions are shown in the figure. The strike of the northeast trending nodal plane and the sense of displacement along it agree with those of the Motagua fault at the earthquake epicenter.

The distribution of aftershocks shown in Figure 2-1 is taken from Langer et al. (1976). The horizontal and vertical extent of the aftershock zone and the location of the mainshock with respect to the aftershock zone were used to partially constrain the geometry of the fault plane.

Figure 2-2 shows surface waves G_3 (Love waves) and R_3 (Rayleigh waves) which were recorded by the WWSSN long-period seismographs and equalized to a propagation distance of $360^\circ + 90^\circ$. The method of equalization is that described by Kanamori (1970). Short-period surface waves have been removed by using a filter described in Kanamori and Stewart (1976) with a short-period cut-off at 40 sec. Both Love and Rayleigh waves indicate a four-lobed radiation pattern which is

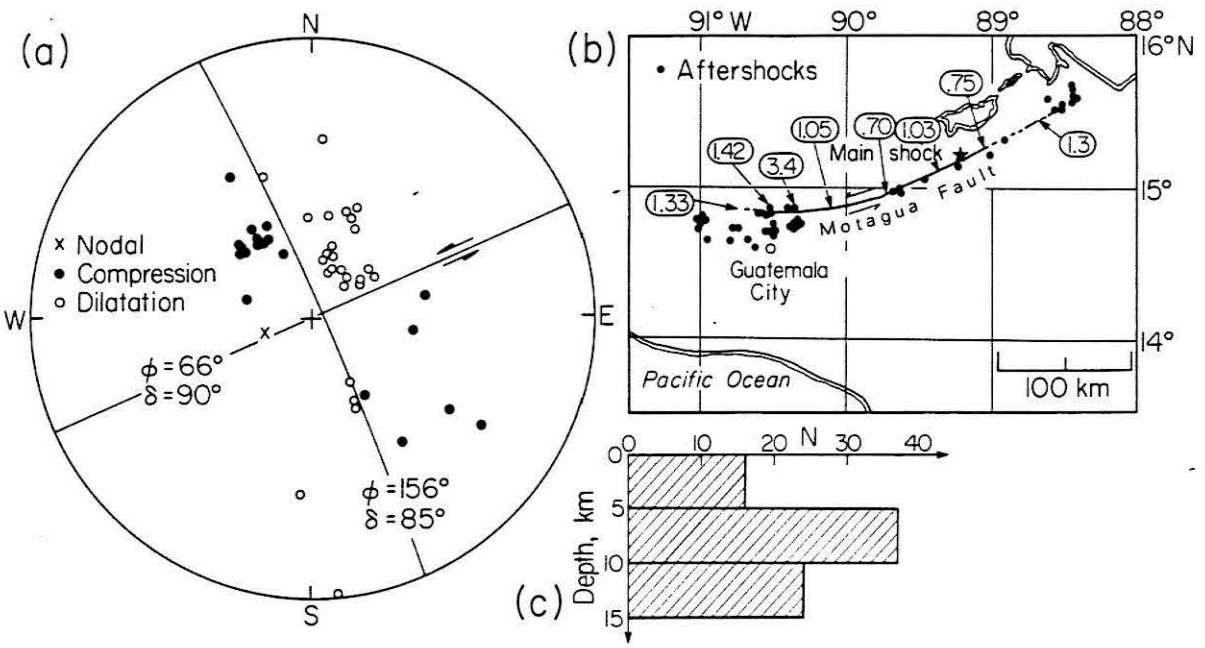

Figure 2-1. (a) The P-wave first-motion data for the Guatemala earthquake, indicating left-lateral strike-slip motion on the preferred fault striking N 66°E. A stereographic projection of the lower focal hemisphere is shown. (b) A map of the mainshock and aftershock locations. The observed displacements along the Motagua fault are plotted inside the circles (values are in meters) (after Langer et al., 1976 and Plafker, 1976). (c) A plot of the number of aftershocks as a function of depth (after Langer et al., 1976).

Table 2-1 Station Parameters

STATION	Δ (deg)	ϕ_{ES}	ϕ_{SE}	C or D	Waves Used
AAE	123.12	68.3	294.8	-	R3, G3, G4
AAM	27.36	9.0	-	D	P
ADE	132.85	236.3	-		R3
AFI	86.60	254.7	73.5	nodal	P, G2, G3, G4
ALQ	24.95	324.8	-	C	P
ANP	129.84	322.9	40.0	-	R4, G4
ANT	42.88	154.2	-	D	P
ATU	97.90	47.3	296.2	-	R3, G3
BAG	136.90	315.7	44.6	-	R2, R3, G2, G3
BEC	28.09	48.3	-	D	P
BDF	51.11	125.2	-	C	P, R3
BHP	11.36	122.4	-	C	P
BKS	36.81	314.0	-	C	P
BLA	23.22	18.1	-	D	P
BOG	18.30	123.8	-	C	P
BUL	120.89	104.5	276.1	-	R3, G3
CHG	145.20	346.3	-	D	PKP, R3
COL	63.16	335.9	112.7	C	P, R3, R4, G3, G4
COP	83.97	33.9	288.1	D	P, nP, R3, R4, G3, G4
COR	41.02	322.4	-	C	P
CTA	127.10	256.2	85.7	C	PKP, R3, G3, G4
DAG	70.80	13.3	254.4	D	P, G3, G4
DAL	18.79	340.0	-	D	P
DAV	138.96	300.3	57.1	-	R3, G3
DUG	32.23	325.0	-	C	P
FVM	22.60	357.6	-	D	P
GDH	58.41	14.1	-	D	P
GEO	25.86	22.2	-	D	P
GIE	15.93	183.8	-	D	P
GOL	28.13	333.0	-	C	P
GRM	119.70	119.8	-	-	R3
GSC	31.74	314.0	-	C	P
GUA	119.26	295.3	63.7	-	R3, R4, G3, G4
HLW	107.28	51.6	-	C	PKP
IST	100.04	42.6	-	D	P
JCT	17.97	329.2	-	C	P
KBS	77.26	11.2	-	D	P
KEV	84.45	18.3	299.6	D	P, nP, R3, R4, G3, G4
KIP	65.12	286.8	82.6	C	P, R2, R3, G3
KJF	87.49	22.98	-	D	P, nP
KON	81.39	30.5	-	D	P
KTG	68.16	19.6	-	D	P, nP
LON	41.46	326.0	-	C	P
LPA	58.09	149.8	-	D	P
LPB	37.87	145.7	325.4	C	P, nP, R3, G3
LPS	0.98	174.9	-	D	P

LUB	21.51	10.1	-	C	P
MAL	76.97	55.2	-	D	P
MAT	111.74	320.3	50.0	D	PKP, G3
MNT	32.89	20.4	-	C	P
MSO	37.59	332.0	-	C	P
MUN	151.46	229.9	-	D	PKP, R3
NNA	29.74	154.9	-	D	P
NUR	88.06	26.9	298.0	D	P, nP, R3, R4, G3, G4
OTT	32.12	18.1	-	D	P
PAS	32.13	311.0	-	C	P, R2
PDA	60.01	55.1	-	D	P
PMG	124.72	269.0	78.0	-	R3, R4, G3
POO	142.52	27.0	-	D	PKP
PTO	73.15	51.1	-	D	P
QUE	129.32	26.9	-	D	PKP
QUI	18.68	144.4	-	C	P
RIV	122.8	239.5	93.2	C	PKP, R3, G3
SEO	117.38	328.1	-	C	PKP
SHA	15.38	3.6	-	D	P
SHK	116.44	322.0	46.1	D	PKP, R3, G3
SHL	139.40	358.4	1.7	D	PKP, R3, G3
SJG	22.30	79.5	-	C	P
SNG	155.65	335.6	-	D	PKP, R3
STU	84.18	41.1	-	D	P, nP
TAB	112.55	36.7	-	D	PKP
TOL	76.75	52.0	278.9	D	P, R3, G3, G4
TRN	27.51	96.2	282.6	C	P, R3, R4, G3, G4
TUC	25.91	314.7	-	C	P
WES	31.11	26.2	-	D	P

Δ is the epicentral distance

ϕ_{ES} is the azimuth of the station from the epicenter.

ϕ_{SE} is the azimuth of the epicenter from the station.

C or D denote compression or dilatation of the P-wave first-motion.

P P-wave first-motion used.

nP denotes that station was used in the multiple event analysis.

PKP PKP-wave first-motion used.

R2, R3, R4 multiple Rayleigh wave used.

G2, G3, G4 multiple Love wave used.

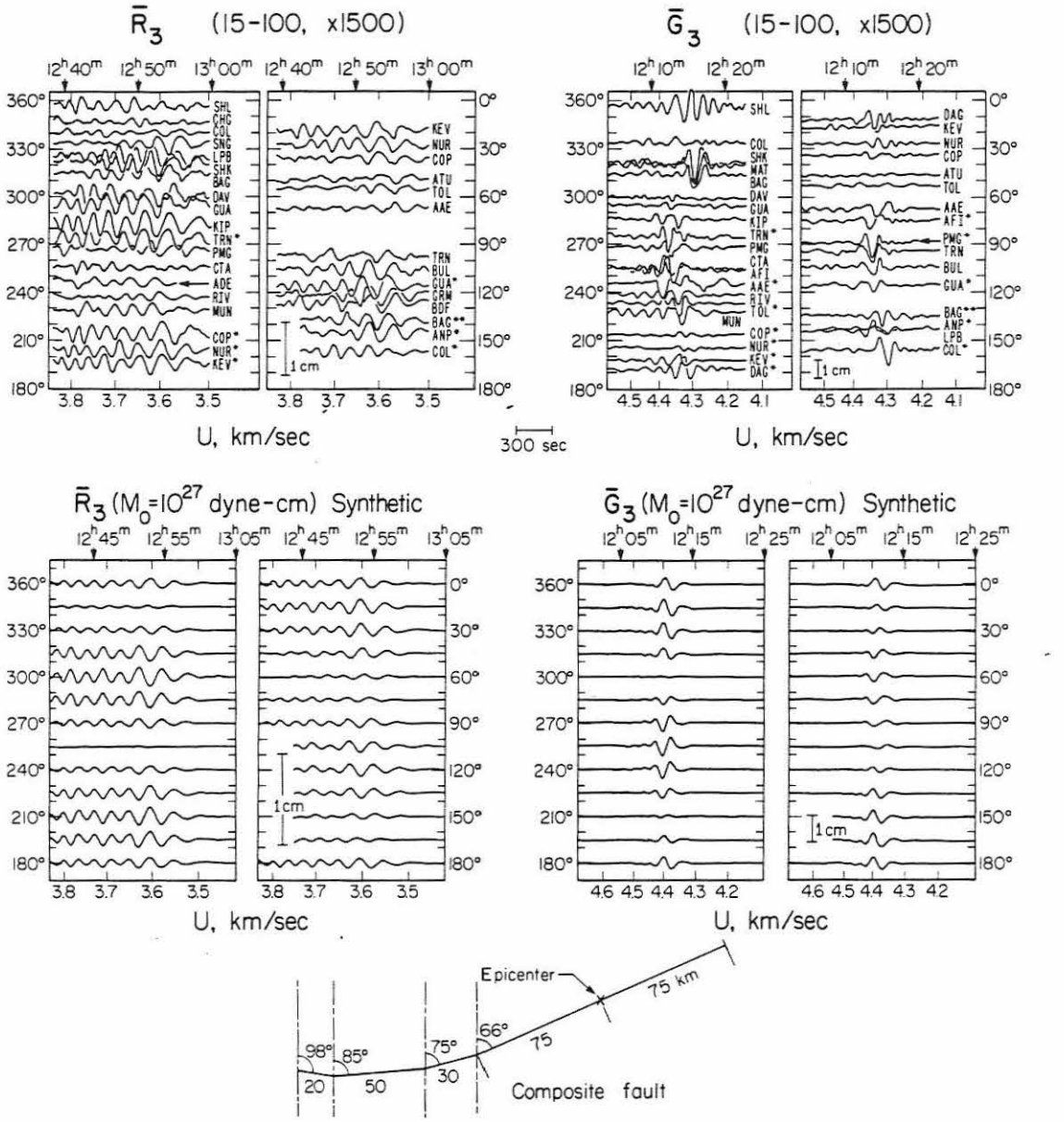

Figure 2-2 Azimuthal plots of equalized seismograms for $\bar{R}_3$ and $\bar{G}_3$ and synthetic seismograms computed for the composite fault geometry shown. A seismic moment of 10^{27} dyne-cm was used in the synthesis. In the observed patterns one asterisk indicates that R_4 and G_4 data were equalized to R_3 and G_3 distances. Two asterisks indicate that R_2 or G_2 were equalized to R_3 or G_3 distances. The amplitude scale is for the trace amplitude on the WWSSN long-period instrument (15-100) with a magnification of 1500.

consistent with the fault geometry determined by the P-wave data shown in Figure 2-1. The theoretical radiation patterns of Love and Rayleigh waves for a shallow strike-slip fault are shown in Kanamori and Stewart (1976). These are the fundamental seismological data sets to be used in the following analysis.

SURFACE WAVE ANALYSIS

Since short-period ($T \leq 40$ sec) surface waves are severely affected during propagation by structural heterogeneities, only long-period signals were used in the present analysis to determine the seismic moment M_o.

Since the overall radiation pattern is consistent with the geometry determined from P-waves, synthetic surface waves were computed first for a point double-couple source corresponding to the P-wave mechanism. This is shown in Figure 2-2. The point source had the same epicenter as the mainshock and a depth of 16 km. The method of synthesis, the velocity and the Q structure are described by Kanamori (1970) and Kanamori and Cipar (1974). The same filter as was used for the observed records was applied to the synthetic records so that they could be compared directly. The maximum trace amplitudes of the observed and synthetic records are compared in Figure 2-3 as a function of azimuth. Although the overall agreement is satisfactory, the observed amplitudes are clearly too small in the azimuthal range of 0^o to 90^o, indicating a rupture propagation toward the west. This direction of propagation is consistent with the location of the mainshock relative to the aftershock

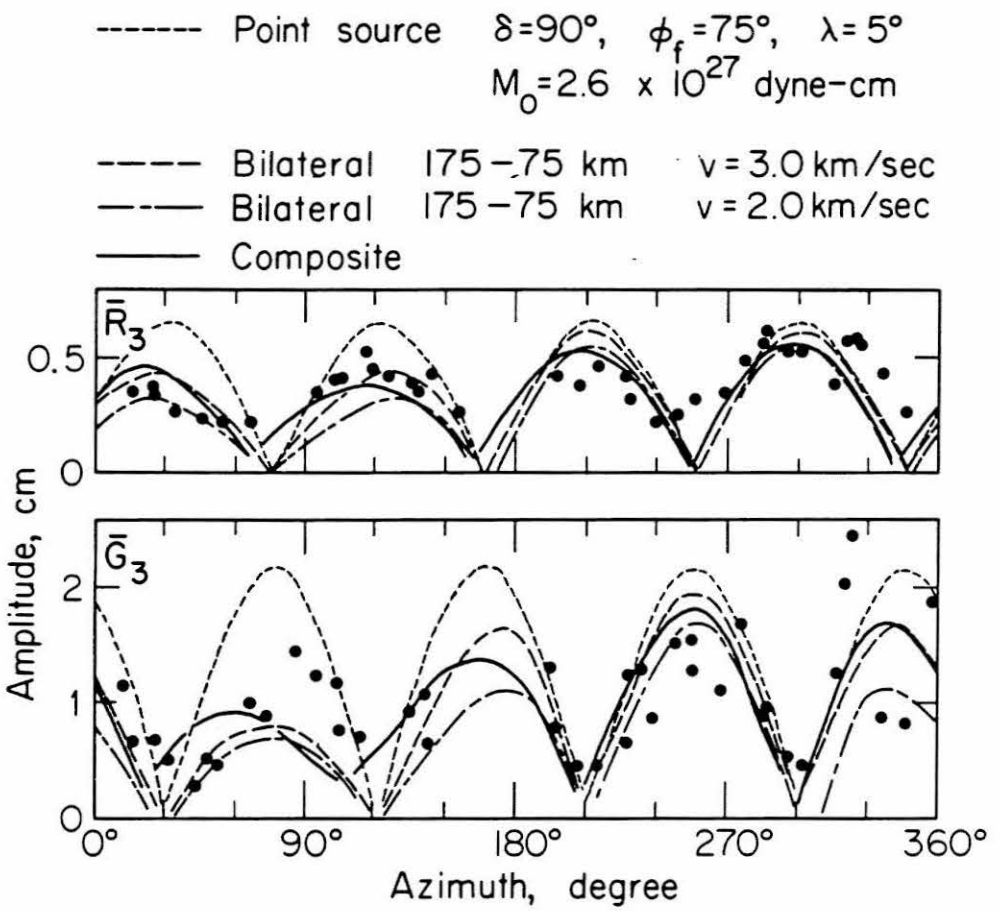

Figure 2-3. Equalized station peak-to-peak amplitudes for observed $\bar{R}_3$ and $\bar{G}_3$ data plotted as a function of azimuth (solid circles). Curves represent the various fault models used in this study.

zone. A seismic moment of 2×10^{27} dyne-cm gives a reasonably good fit. The preliminary analysis made by Dewey and Julian (1976) using a point source and estimated spectral amplitudes of Love waves at 100 sec period gave a value, 2.6×10^{27} dyne-cm, which is in reasonably good agreement with this value, despite their simplified method.

The slight asymmetry of the observed radiation pattern can be explained in terms of the directivity (Ben-Menahem, 1961). To a first approximation, the fault geometry shown in Figure 2-1 can be modeled by an asymmetric bilateral fault with $\delta = 90^{\circ}$, $\phi = 75^{\circ}$ and $\lambda = 5^{\circ}$ extending over a distance of 250 km, the eastern and the western branches being 75 and 175 km long respectively (δ = dip angle; ϕ = the average strike of the Motagua fault measured clockwise from north; λ = slip angle). Sign conventions are given in Kanamori and Stewart (1976a). The synthetic seismograms for this geometry with a rupture velocity of 3 km/sec were computed and the amplitude variation shown in Figure 2-3. The fit in the eastern azimuths is significantly improved. A rupture velocity of 2 km/sec was tried; as shown in Figure 2-3, the asymmetry of the radiation pattern of the synthetic seismogram becomes too large to match the data. However, in view of the scatter of the data, a rupture velocity of 2.5 km/sec is still acceptable. In order to investigate further details of the rupture propagation the directivity functions were computed for a suite of models and compared with those for several stations. For Love waves, three stations AFI, AAE and CTA were chosen because they are nearly in the direction of the fault strike ($\phi_f = 66^{\circ}$) and are most sensitive to the directivity of the source. Since these

stations are nearly in the same azimuth ($\Theta = 8.7^{\circ}$ for AFI, $\Theta = 2.7^{\circ}$ for AAE and $\Theta = 10.2^{\circ}$ for CTA where Θ is the angle between the fault strike and the great circle passing through the epicenter and the station), the directivity function was computed for $\Theta = 10^{\circ}$. The results are shown in Figure 2-4. Although the scatter is considerable, it is evident that the combinations (150, 50, 2.5) and (175, 75, 3.0) give a satisfactory fit to the data where the first, second and third numbers in parentheses denote the fault lengths of the western and eastern segments and the rupture velocity, respectively. When a rupture velocity of 2 km/sec is used the fit becomes worse than for these two cases. For Rayleigh waves, stations BUL and KIP were chosen. These stations are in the direction of the maximum of the radiation pattern yet they have $\Theta = 38.5^{\circ}$ and 40.8° respectively and are still sensitive to the source directivity. The directivity functions were computed for $\Theta = 41^{\circ}$ and compared with the data in Figure 2-4. Again the combination (175, 75, 3.0) gave a satisfactory fit. A rupture velocity of 2 km/sec did not give a good fit. It is important to note that the dislocation was assumed to be uniform along the fault strike in these models. The fact that these models can explain the observed asymmetric radiation pattern (Figure 2-3) and the directivities (Figure 2-4) indicates that the fault displacement, averaged over the length of the fault is relatively uniform, although small scale irregularities are very likely to exist.

As shown in Figure 2-1, the Motagua fault is not straight but is slightly convex toward the south. For completeness sake, synthetic seismograms were computed for the geometry shown at the bottom of

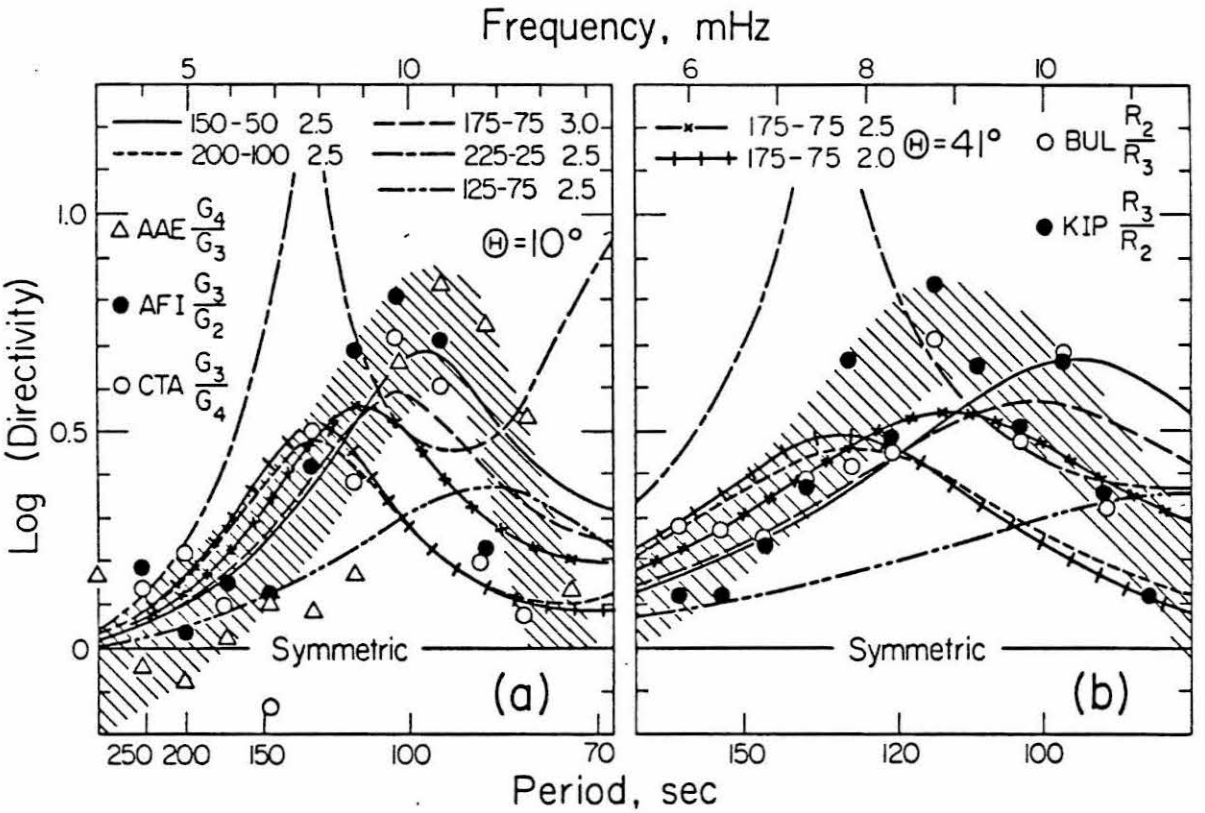

Figure 2-4. Observed and computed directivity for (a) Love waves and (b) Rayleigh waves. The preferred model for both data sets is the 175-75-3.0 combination. Θ is the angle between the fault strike and the rupture direction. Hatchings indicate the range of the observed data.

Figure 2-2. In this calculation, the fault was broken up into four segments, synthetic seismograms were computed for each segment by the standard method, and then the results for each segment were added with delays appropriate for a rupture velocity of 3 km/sec. The results are shown in Figure 2-2 and the azimuthal variation of the amplitude is compared with the observed one in Figure 2-3. The difference between the straight and curved fault models is very small, and is probably unresolvable by the present data. However, it is important that a realistic fault geometry can explain the overall radiation patterns of surface waves and the amplitude ratio of Rayleigh to Love waves very well. By matching the amplitude a seismic moment of 2.6×10^{27} dyne-cm was obtained from both Love and Rayleigh waves.

In order to supplement the WWSSN data, a seismogram from an ultra long-period instrument at the Seismological Laboratory, Caltech was used. This instrument (PAS, No. 33) has a peak response at 150 sec and is adequate for recording very long-period surface waves. Figure 2-5 shows the observed and synthetic R_2 wave at Pasadena. No filtering has been applied. The synthetic seismogram was computed for the fault geometry shown at the bottom of Figure 2-2. The agreement of the waveforms is very good. A seismic moment of 2.3×10^{27} dyne-cm was found which is in good agreement with that obtained from the WWSSN data. This agreement suggests that the source spectrum is flat at periods of 100 to 300 sec. In the later discussion, the moment of 2.6×10^{27} dyne-cm obtained from the WWSSN data will be used.

The results obtained above can be interpreted in terms of the

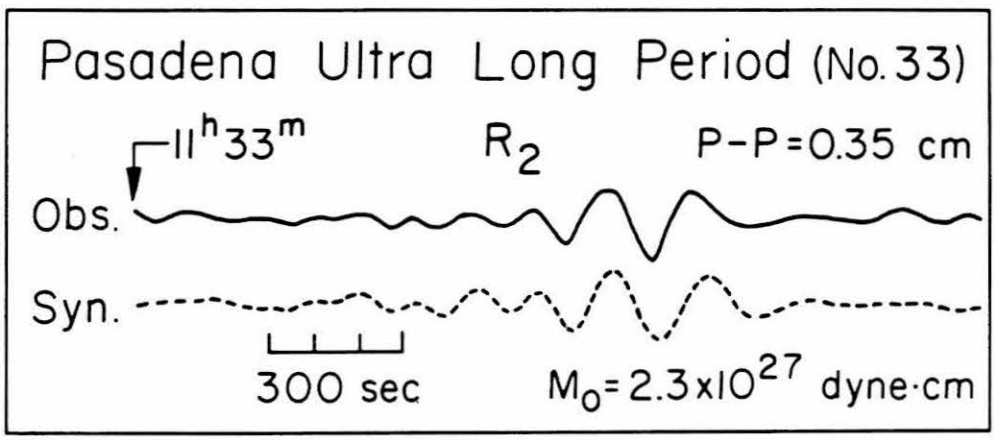

Figure 2-5. Observed and synthetic Rayleigh waves (R_2) at Pasadena (ultra long-period instrument, No. 33). Note the agreement of the phase.

average dislocation (displacement discontinuity) $\bar{D}$ and the stress drop $\Delta\sigma$. The vertical extent w of the fault cannot be directly determined from the present data, but the distribution of the aftershocks indicates that $w \simeq 15$ km (Figure 2-1). By using the fault length L = 250 km suggested by the extent of the surface break, the asymmetry and the directivity, we have $\bar{D} = M_o/\mu Lw = 2m$ and $\Delta\sigma = 2\mu\bar{D}/\pi w = 30$ bars where $\mu = 3.5 \times 10^{11}$ dyne/cm^2 is used.

Since the wavelength of the surface waves used in the present analysis is longer than about 300 km, these waves are not significantly affected by structural heterogeneity along the propagation path, and give a reliable gross average of $\bar{D}$ and $\Delta\sigma$ over the entire length of the fault. Although a depth of 16 km was used in the above analysis, the amplitude of these long-period surface waves is not sensitive to a change in the source depth from 0 to 16 km, in particular, for a vertical strike-slip mechanism.

BODY WAVE ANALYSIS

Although the surface wave analyses described above provide reliable gross fault parameters, they are inadequate to resolve the details of the rupture process. On the other hand, seismic body waves represent the short-period end of the source spectrum and provide important information regarding the details of the rupture process. Unfortunately, for the Guatemala earthquake, both P- and S-waves were off-scale at most stations. P-waves were on-scale at some stations near a node of the radiation pattern, but use of these stations for waveform

analyses is not desirable. Figure 2-6 shows waveforms of P-waves at seven stations which are considerably removed from the radiation nodes. Except LPB, all stations lie in a narrow azimuthal range from 19.6° to 41.1°. Thus this data set is somewhat limited in terms of azimuthal coverage, but it is evident that the waveforms at these stations exhibit a very remarkable complexity. Since the distances to these stations are larger than 68° (except LPB), this complexity is unlikely to be due to later phases. At these distances, the only later phase that arrives within two minutes after the onset of the P-wave is the PcP phase, but, for a vertical strike-slip fault, PcP is always nearly nodal. Thus, most of the complexities are considered to be due to the source. From these figures, it appears that the radiation from the source lasted about two minutes. Since the distance to LPB is only 38° and the PP phase arrives about 1 minute after P, only the first minute of that record is shown.

Although the azimuthal coverage of the data is somewhat limited, these records contain extremely important information regarding the rupture process. In the following, an attempt is made to interpret these complex records in terms of multiple events. Inspection of these records suggests that at least seven major pulses are distinguishable during the two-minute time interval. Each pulse corresponds to an individual event of the multiple-shock sequence. Since such a sequence involves a very large number of parameters, e.g., source geometry of each event, spatial and temporal separation of the multiple events, the strength (the seismic moment), the fault length and the rise time of

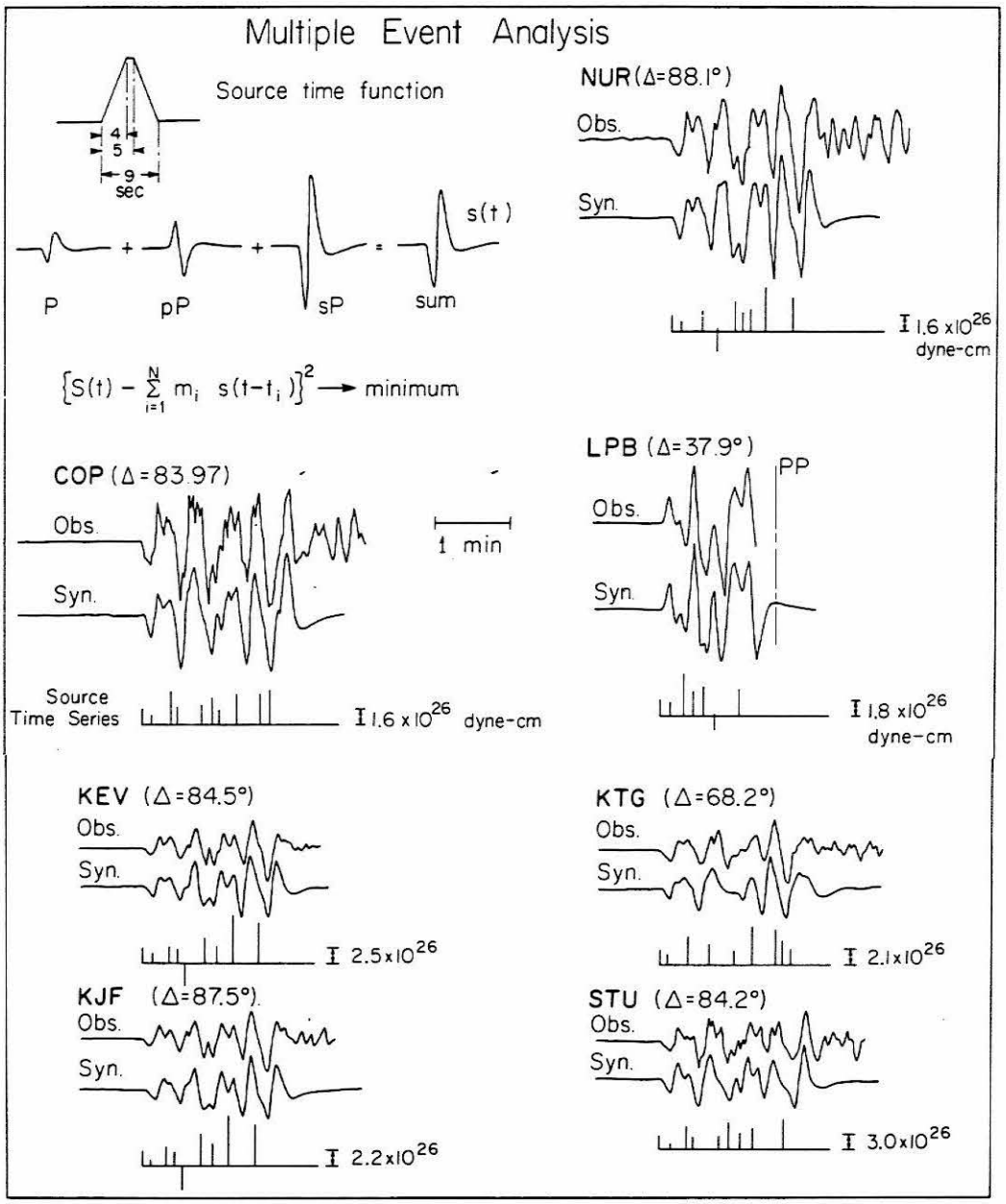

Figure 2-6. Observed and synthetic P-waves for individual WWSSN stations obtained from the multiple-shock analysis. For each station the source time series is obtained using the mechanism given in Figure 2-1a and the source time function shown here. The surface reflections pP and sP are included in the source time function. The resulting series is given for each station along with the moment for the first event. The height of the vertical bar is proportional to the moment of the individual event. Δ is the epicentral distance.

each event, etc., it is extremely difficult to determine all of these parameters. Hence, the following procedure was used.

The station NUR was taken first and a match to the first part of the P-wave record attempted with a synthetic waveform computed for a point source whose time function is adjusted so that it matches the overall waveform of the first pulse of the P-wave record. A symmetric trapezoidal source time function with a rise time (and fall-off time) of 4 sec and a total width of 9 sec was chosen (Figure 2-6). Although the details of this time function are not resolvable by our data, it can explain the first part of the seismogram satisfactorily. The point source was placed at a depth of 5 km in a homogeneous half space. In the synthesis the surface reflections pP and sP were included (Figure 2-6). This type of modeling has been successfully applied to the determination of source parameters of relatively simple events (Langston, 1976). The seismic moment of this first event was estimated to be 1.6×10^{26} dyne-cm. Then the synthetic trace was subtracted from the observed one, and the procedure repeated for the second event. Although the time function and the mechanism of the second event may be different from those of the first event, it is extremely difficult to resolve such details from the available data. It is assumed, therefore, that the time function and the mechanism of the second event are identical to those of the first event. In view of the results of the surface wave analyses which indicate a relatively uniform left-lateral slip over the entire length of the fault, the assumption of the identical mechanism is probably justified even though the fault trace

has some degree of curvature. Since the rise time and the pulse width are determined by the initial tectonic stress, stress drop and the dimension of the individual event, they are likely to vary considerably from event to event.

The above procedure was repeated for the later events until the two-minute record of the P-wave was satisfactorily matched. The later events were placed at the same location as the first event. This first approximation to the time sequence of the events was then adjusted to better fit the observations by the method of least squares. Let S(t) and s(t) be the observed P-wave and the synthetic wavelet for the individual event ("sum" shown in Figure 2-6) respectively. A minimization of the function:

$$\left[S(t) - \sum_{i=1}^{N} m_i s(t-t_i) \right]^2$$

was sought, where m_i and t_i are the moment and the onset time, respectively, of the ith event and N is the total number of events. The result of this inversion is shown in Figure 2-6. The source time sequences (e.g. plot of m_i as a function of t_i) are shown under the individual synthetic records. It is encouraging that a very good match between the observed and synthetic records is obtained by a superposition of events having positive m_i's. Only one of the nine events was of reversed polarity. This result suggests that the

assumption of identical mechanism is reasonable.

The above method was applied to other signals shown in Figure 2-6, and the resulting synthetic records and the source time sequences are shown. In all cases, a very good agreement is obtained with positive m_i's for most events. If all of the multiple events had the same mechanism and occurred at the same location, the source time sequence should be identical for all the stations. Actually, as shown in Figure 2-6, the derived source time sequences are similar from station to station, although there are some differences. These irregularities are due to the following causes. First, the various events probably were distributed along the fault, so that the difference between the arrival times of the signals varies from station to station, depending on the azimuth and, to a lesser extent, the distance. Second, noise in the records can cause errors in the measured arrival times of the events. Third, a slight change in the mechanism also results in errors. For a vertical strike-slip event, all teleseismic P rays leave the source in a nearly nodal direction, so that a slight change in the mechanism can cause a significant change in the waveform thereby affecting the determination of the arrival times. In view of these complex effects, some ranges of arrival times in identifying the individual events must be allowed. Figure 2-7 compares the time sequences for the seven stations. Allowing for ranges of arrival times as shown by hatched belts, events 1, 2, 3, 6, 7, 8 and 9 can probably be identified as marked on the figure. It may be noted that the 8th and 9th events are 2 to 2.5 times larger than the first event. A quiet

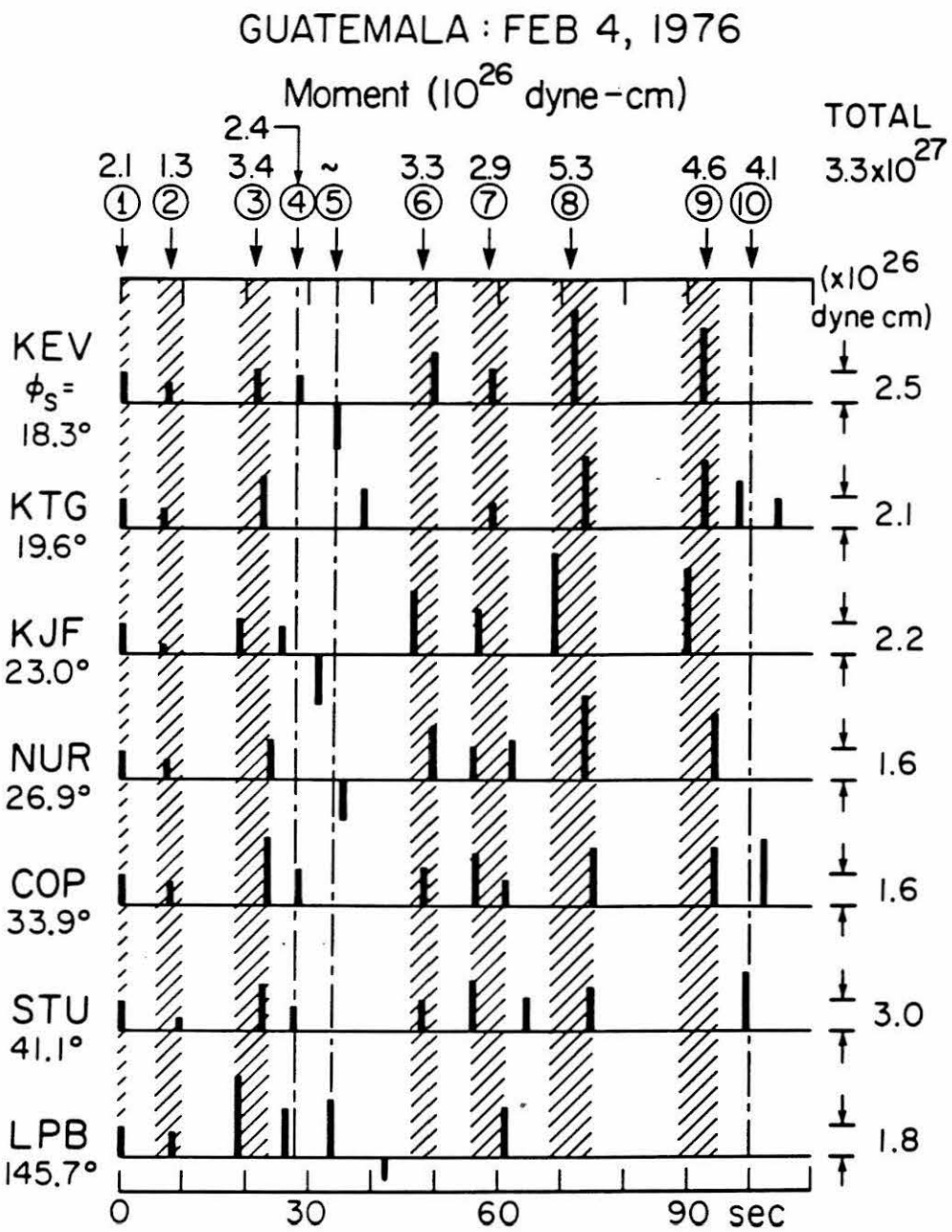

Figure 2-7. A comparison of the source time sequences for the seven stations used in this study. The hatched zones denote ranges of arrival times. ϕ_s is the station azimuth. The values given at the top are the seismic moments of the individual events of the multiple-shock sequence.

interval of about 10 sec between the 2nd and 3rd events and a 15 sec interval between the 8th and 9th events are common to all the stations. Some complication is observed around the 4th and 5th events where some stations indicate a negative pulse. The cause of this complication is unclear but one possibility is that the arrivals from the eastern and the western branches of the fault interact with each other resulting in complex waveforms. The average moment of each event is shown at the top of Figure 2-7. The sum of the moments is 3.3×10^{27} dyne-cm which is slightly larger than that obtained from surface waves. However, in view of the various errors involved in the body-wave analysis, this difference is insignificant.

It is interesting to note that Plafker (1976) found very large surface breaks, with a maximum of 3.4 m, near the western end of the fault, about 150 km to the west of the epicenter (Figure 2-1). The large events, 8 and 9, probably correspond to these large displacements. Kikuchi and Kanamori (1981), in a recent study, confirmed the location of these events at the western end of the fault. Assuming that the 8th event was 150 km to the west of the initial epicenter, the time separation of about 72 sec between the first and the 8th events (see Figure 2-7) suggests an average rupture velocity of about 2 km/sec, which is somewhat smaller than that obtained from the surface wave directivity, viz. 3 km/sec. As shown in Figure 2-3 a smooth rupture propagation with a rupture velocity of 2 km/sec results in a stronger asymmetry than the observed data indicate. However, if the rupture propagation is jagged and partially incoherent as demonstrated by the

P-wave analysis, the effect of rupture propagation would become less pronounced than that for smooth propagation (Haskell, 1966). Thus, the value of 3 km/sec obtained from the surface wave analysis under the assumption of smooth propagation should not be given too much signficance. The result obtained from the P-wave analysis is preferred: the rupture propagation is jagged with an average velocity of 2 km/sec.

The results of the body-wave analysis can be summarized as follows: The entire rupture sequence can be represented by the sequential occurrence of approximately ten distinct events, the seismic moments of which varied by a factor of about four, and with time separations varying from 7 to 20 sec. Since the average rupture velocity is about 2 km/sec, this variation of time separation corresponds roughly to a spatial separation of 14 to 40 km. The trapezoidal time function used to model the point sources has an effective pulse-width of about 5 sec, which corresponds to a source dimension of about 10 km. However, as mentioned before, the details of the time function cannot be resolved so that this dimension should be considered a very crude measure of the size of the individual events. It is probable that the source dimensions also varied considerably from event to event.

This complex multiple event may be envisaged in terms of the heterogeneous mechanical properties along the fault plane. This heterogeneity may be caused either by asperities, differences in strength, differences in pore pressure, differences in slip characteristics (stable sliding vs. stick slip) or combinations of these factors.

CONCLUSIONS AND DISCUSSION

The seismic moment of the 1976 Guatemala earthquake is estimated from long-period surface waves to be 2.6×10^{27} dyne-cm, which suggests an average displacement of 2 m and a stress drop of 30 bars if the vertical width of the fault is taken as 15 km on the basis of the aftershock distribution. It is possible that the actual fault plane extends deeper than the aftershock zone, but it is unlikely that a fault plane that is completely incapable of generating aftershocks can generate 100 to 200 sec surface waves very efficiently. On this basis, the above estimate of 2 m of displacement is considered to represent the actual average over the depth range of 15 km. On the other hand, Plafker et al. (1976) and Plafker (1976) reported that the average surface displacement measured immediately after the earthquake is about 1 m with a maximum value of 3.4 m at one locality. This value is about half the average displacement derived from surface waves. It is possible that the surface layers are partially decoupled from the layers at depth so that the surface displacement represents a fraction of the fault displacement at depth. In this case, post-seismic creep along the fault over a prolonged period of time might be expected. In fact, Lisowski and Thatcher (1981) discuss a 15-station geodetic control network across the Motagua fault which was reoccupied in 1978 to determine co-seismic fault slip assuming a simple dislocation model. The model was split into three sections with depth. For the upper surface layer an inversion of the data predicted 1 m of average

left-lateral slip, (the same as the average slip observed by Plafker et al. (1976) and Plafker (1976)) increasing to 2 m in the 5 to 15 km deep section (the same as that determined here). Slip was unconstrained at greater depths. The seismic moment that Lisowski and Thatcher (1981) calculated for the 0 to 15 km displacements over the 250 km long fault was 2.2×10^{27} dyne-cm in good agreement with the value found here. Of interest, in this regard, is the fact that Bucknam et al. (1976) and Plafker (personal communication, 1977) found a significant increase in the surface offset (as much as 37% of the initial break) during the period from February to October, 1976. Although the total displacement is still smaller than the seismic displacement, the creep is still continuing so that it is possible that the surface break will eventually catch up with the displacement at depth. Scholz et al. (1969) suggest that, for the 1966 Parkfield earthquake, near-surface afterslip above 4 km depth can explain the discrepancy between surface slip observed immediately after the earthquake and seismic estimates of the average co-seismic slip.

On the other hand, the possibility that the fault plane responsible for surface wave radiation is significantly larger than that inferred from the aftershock zone cannot be completely excluded. If this is the case then both the average displacement and stress drop would have values lower than those estimated for the vertical width of 15 km discussed earlier.

The asymmetry of the radiation pattern (Figures 2-2 and 2-3) and the directivity (Figure 2-4) suggest that the displacement is relatively

uniform along the entire length of the fault, although short-range irregularities are possible. A rupture velocity of 3 km/sec is suggested if the displacement is assumed to be uniform.

Teleseismic P-waves exhibit a complexity suggesting that this earthquake consists of about 10 distinct events. The duration of the sequence, about two minutes, probably corresponds to the time for the entire fault to break. Analysis of the P-waveforms suggests that the fault broke in a relatively coherent manner over distances of only 10 km or so. The spatial separation of the individual events is 14 to 40 km, suggesting that either stress, frictional characteristics, or sliding characteristics on the fault plane vary with comparable spatial scale along the fault plane. This result is in striking contrast with that obtained for large earthquakes along the Gibbs fracture zone (transform fault) of the Mid-Atlantic ridge. Kanamori and Stewart (1976) found that the rupture propagation in these earthquakes is relatively coherent over much longer distances, 40 km or so. This difference probably reflects the difference in the age of the faults and the structure between the two transform faults, and provides an important piece of information regarding the mechanical properties of various types of plate boundary. Although the average stress drop was relatively low, about 30 bars, the local stress drop for the individual events may have been significantly higher than this, perhaps by a factor of two or three. Burdick and Mellman (1976) reported a relatively high stress drop of 96 bars, over a circular rupture zone of radius 8 km for the 1968 Borrego Mountain earthquake, California.

The complexity of the rupture process as revealed by the present analysis has a very important effect on the strong ground motion which results from earthquakes of this type. Haskell (1966) and Aki (1967) showed that irregular fault motion significantly enhances the high-frequency end of the seismic spectrum (more details are given in Section 2.3).

The rate of the instantaneous plate motion of the Caribbean plate with respect to the North American plate in Guatemala is estimated to be about 2 cm/yr (Molnar and Sykes, 1969; Jordan, 1975; Minster and Jordan, 1978; Minster and Jordan, 1980). However, more recently this value has been questioned by Sykes and McCann (1981) and Sykes (personal communication, 1981) who suggest 3.7 cm/yr as a more appropriate value. Historical records suggest that the repeat time of major earthquakes on the central and western Motagua fault is about 200 years (Spence and Person, 1976). These results suggest a co-seismic displacement of about 4 m (2 cm/yr) or more likely 7.4 m (3.7cm/yr) if the strain is released totally in earthquakes. The discrepancy between these values and the average displacement, 2 m, in the 1976 Guatemala earthquake obtained by the present study indicates the following possibilities: 1) half (or 3/4 for 3.7 cm/yr) the displacement on the Motagua fault takes place in creep; 2) the repeat time fluctuates considerably; 3) the rate of plate motion has changed; 4) part of the plate motion is taken up by displacements along other faults; possibly the Polochic or Jocotán faults; 5) the estimate of the rate of plate motion is in error.

2.3 Large Strike-slip Events on the Anatolian Fault, Turkey.

ABSTRACT

Complexity of rupture propagation has important bearing on the state of stress along the earthquake fault plane and on the prediction of strong ground motion in the near-field. By studying far-field body waveforms recorded by WWSSN long-period seismograms it has been possible to investigate the degree of complexity of several Turkish earthquakes. The results, which are obtained by matching synthetic P-waveforms to observed data indicate that the July 22, 1967 Mudurnu Valley earthquake (M_s = 7.1) is a complex event which can be explained by the superposition of elementary sources with variable amplitudes and source time sequence history. In this regard it is very similar to the February 4, 1976 Guatemala earthquake (M_s = 7.5). A comparison of these two events indicates that their source time series ranges from 5 to approximately 20 seconds and regardless of the total moment of the earthquake the moment of the individual events is bounded at around 5×10^{26} dyne-cm. The November 24, 1976 E. Turkey earthquake (M_s = 7.3) has a complexity which, on the other hand, cannot be explained by such a simple model -- in this respect it may be more similar to the Tangshan, China earthquake and as such, may involve significant thrust or other complications to its faulting mechanism than the strike-slip mechanism of the P-wave first-motion data. The source time history for the 1967 Mudurnu Valley event is used to illustrate its significance in modeling strong ground motion in the near field. The complex source time series

of the 1967 event predicts greater amplitudes (2.5 larger) in strong ground motion than a uniform model scaled to the same size for a station 20 km from the fault. Such complexity is clearly important in understanding what strong ground motion to expect in the near-field of these and other continental strike-slip faults such as the San Andreas.

INTRODUCTION

The tectonics of Turkey are dominated by an east-west trending fault, the Anatolian fault (Figure 2-8). It extends from western Turkey, south of the Sea of Marmara across the country to the east to its junction with the E. Anatolian fault. It is presumed to extend further eastwards towards Van Gölü (Lake Van). A segment of the fault is also presumed to lie to the northeast of lake as shown in Figure 2-8. The exact location is best determined in the central part of the country (N. Anatolian fault) while its position both to the west and east is less certain. Ambraseys (1970) has described its surface expression in detail.

Throughout historic times the Anatolian fault has been the site of many large and destructive earthquakes. Such events have been partially-documented by Ambraseys (1971) from his investigations of Turkish historic records. Some events date back as far as 10 AD.

Because of this extensive historic record and the occurrence of many large events this century, the Anatolian fault is an ideal locality for investigating earthquake prediction (Allen, 1981) and attempting to understand the rupture process in large strike-slip events.

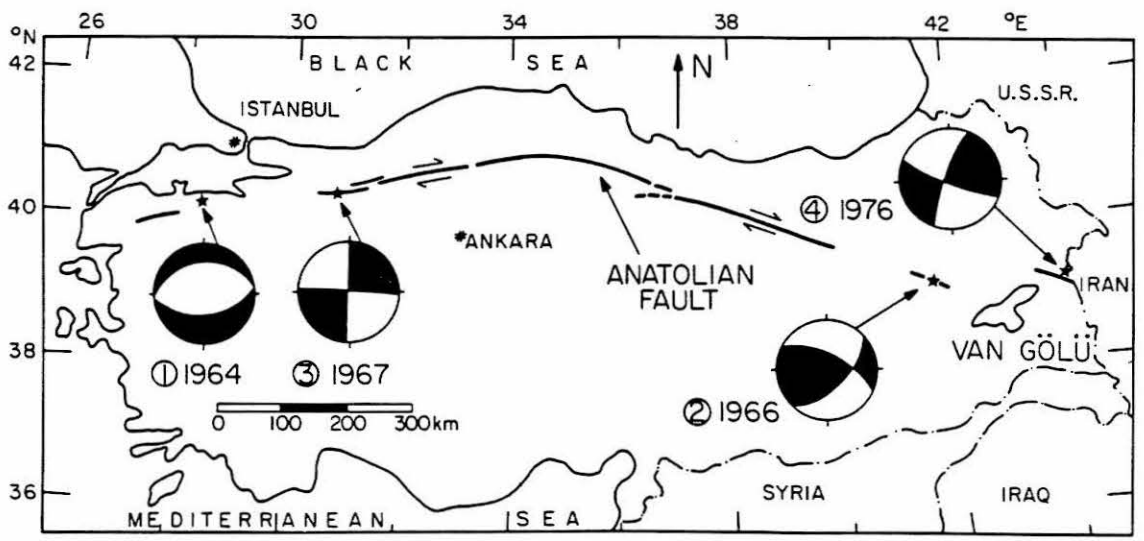

Figure 2-8. Map of Turkey and neighboring regions showing the epicenters of the earthquakes discussed in this paper, together with their respective focal mechanisms determined in this study (see Figure 2-9 for details). Equal-area projections of the lower focal hemispheres are shown. Black areas are compressional, white areas are dilatational. See Table 2-2 for detailed event parameters.

Additionally, being in a continental crustal environment, it is important to study large earthquakes occurring along the Anatolian fault as analogues for a great earthquake on the San Andreas fault in California (see Chapter 4).

Since the installation of the WWSSN network in 1963 several important events have occurred in Turkey. Especially significant are the 1967 Mudurnu Valley and 1976 E. Turkey events. Both were well-recorded by the WWSSN network as well as many other smaller events.

In this study four events occurring since 1963 are investigated. They are shown in Figure 2-8 along with their corresponding focal mechanisms, the details of which are shown in Figure 2-9. Event parameters are given in Table 2-2. The events in 1964 (M_s = 6.5) and 1966 (M_s = 6.8) are smaller than, and are used for comparison with, the events of major interest here -- the 1967 (M_s = 7.1) and 1976 (M_s = 7.3) quakes.

BODY WAVE ANALYSIS

1964 and 1966 Events

To demonstrate that the complexity exhibited by the 1967 and 1976 events is indeed real and not due to propagation or near-receiver effects, a smaller event near each of the complex events was selected for comparison. The October 6, 1964 and August 19, 1966 events were chosen as being suitable events close to the 1967 and 1976 events respectively. Their locations are shown in Figure 2-8 with the details of their focal mechanisms illustrated in Figure 2-9. The 1964 event is

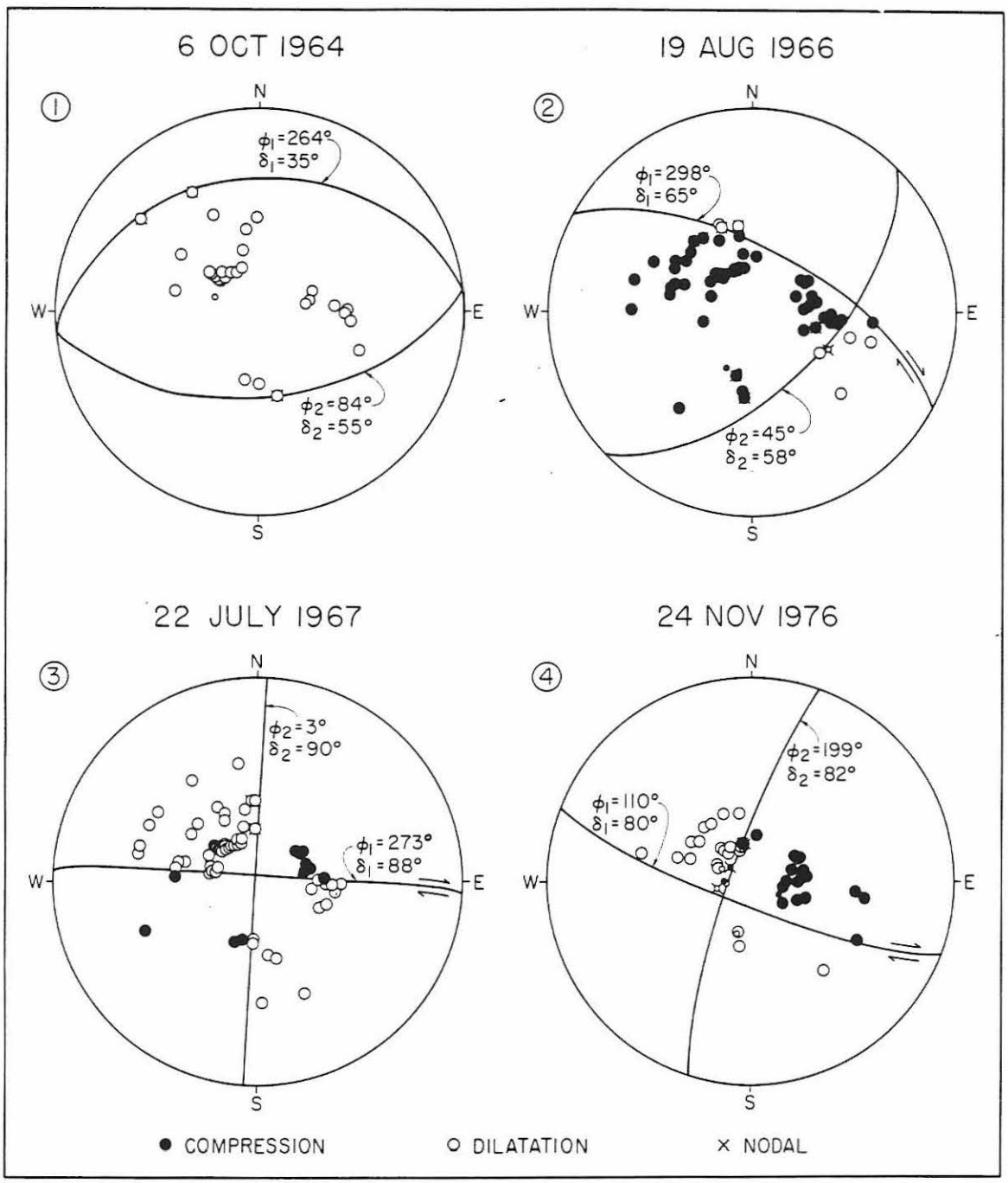

Figure 2-9. P-wave first-motion data and focal mechanisms for the events shown in Figure 2-8 and listed in Table 2-2. Events 2, 3 and 4 are well-constrained by the first-motion data. The sense of faulting is indicated on the presumed fault planes.

TABLE 2-2 Event Parameters

Date	Origin Time (U.T.)	Location		M_S^*
		^oN	^oE	
Turkey				
Oct. 6, 1964	14h 31m 23.0s	40.30	28.23	6.5
Aug. 19, 1966	12h 22m 10.5s	39.17	41.56	6.8
July 22, 1967	16h 56m 58.0s	40.67	30.69	7.1
Nov. 24, 1976	12h 22m 16.0s	39.05	44.04	7.3
Tangshan				
July 27, 1976	19h 42m 54.0s	39.56	117.87	7.7
		^oN	^oW	
Guatemala				
Feb. 4, 1976	09h 01m 43.9s	15.28	89.19	7.5

* M_S values are determined by the National Earthquake Information Service (NEIS) of the U.S. Geological Survey.

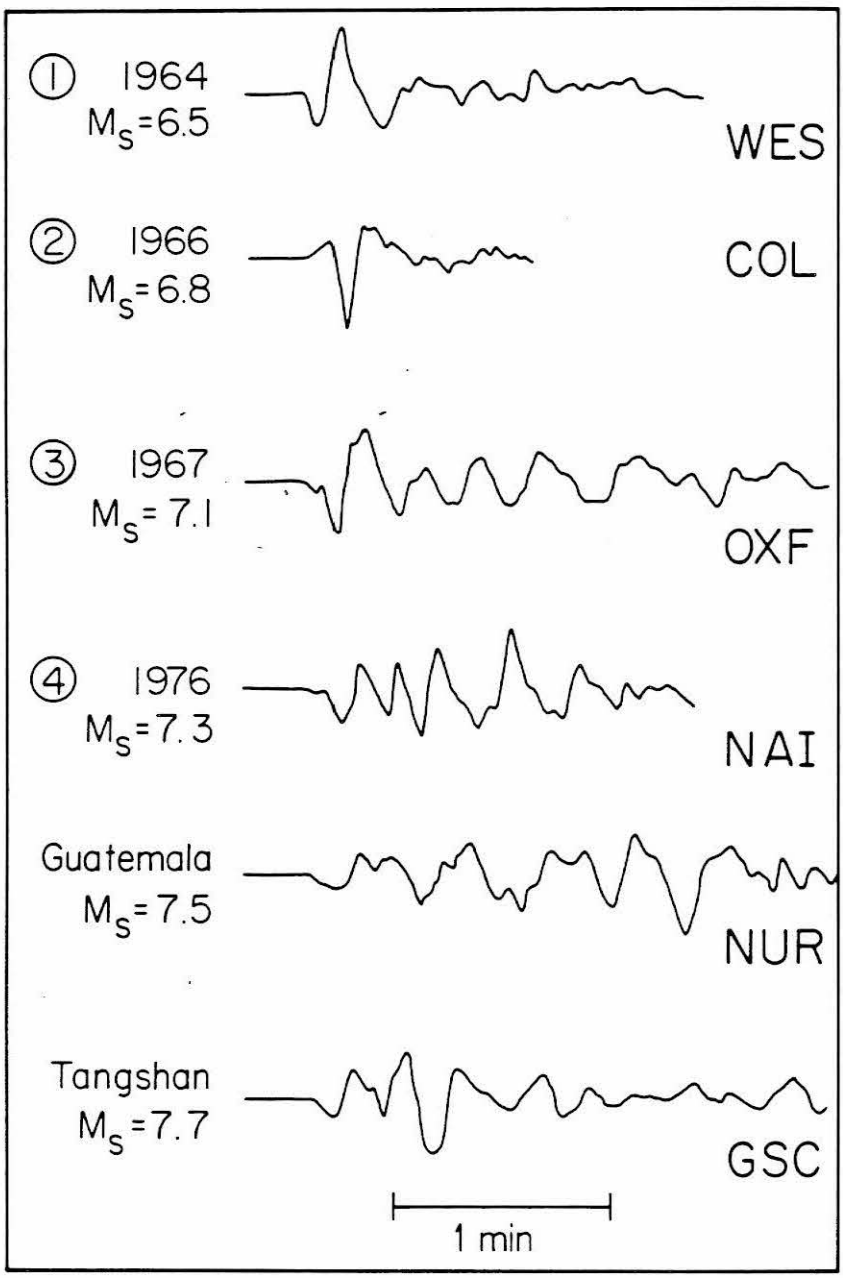

Figure 2-10. WWSSN vertical long-period seismograms showing representative waveforms for the four Turkish earthquakes studied in this paper, as well as for the February 4, 1976 Guatemala and July 27, 1976 Tangshan earthquakes. Note the simple waveforms of events 1 and 2 compared with the varied complexity of the others.

a predominantly normal fault event. The fault planes, however, are not well-constrained. McKenzie (1978) gives a similar solution for this event. The solution obtained for the 1966 event agrees well with that proposed by McKenzie (1969) but disagrees with the almost pure strike-slip solution obtained by Nowroozi (1972). Further details of the faulting and damage effects of the 1966 event can be found in Ambraseys and Zátopek (1968) and Wallace (1968).

The relative simplicity of the 1964 and 1966 events compared with the complex 1967 and 1976 events can be seen in Figure 2-10. This figure shows representative P-wave seismograms for all the Turkish events studied here as well as for the February 4, 1976 Guatemala earthquake studied in detail by Kanamori and Stewart (1978) and in Section 2.2 and the July 27, 1976 Tangshan, China earthquake studied by Butler et al. (1978). The event parameters are given in Table 2-2. Clearly compared with the others, the 1964 and 1966 events are simple and most probably consist of a single source.

As regards the complex events, each exhibits some characteristic differences. The 1976 event, for example, has a higher frequency content than the 1967 event. Also the largest trace amplitudes occur towards the end of the trace. Clearly for the 1967 event the largest pulse is at the start. The characteristic period of the Guatemala trace appears to be longer than any of the others, as is its total duration. As with the 1976 event, the larger amplitudes are to be found towards the later part of the record. The Tangshan event appears to be much shorter in duration with most of the energy arriving in the first minute

of record.

Examining only one seismogram for a particular earthquake may result in an incorrect interpretation for the event. To avoid this and to gain a better overall view of the characteristics of the source, seismograms were selected for examination from as many azimuths and suitable distances ($\Delta = 30^{o}$ to 90^{o}) as possible. This procedure was adopted for all of the events discussed here. The simplicity suggested by the WES P-waveform for the 1964 event seems to be representative of the waveforms at many other azimuths as indicated in Figure 2-11. The only station that shows any complexity is Ponta Delgada, Azores (PDA) and this is probably due to its noisy island location. The P-wave seismograms for the 1966, the other simple event are shown in Figure 2-12. The record at College, Alaska (COL) and the waveforms on the left-hand side of the figure are simple, for the most part, although not as simple as those of the 1964 event. On the right-hand side of the figure the waveforms appear somewhat more complex. However, this is probably due to their being located close to a double node so that the background noise is amplified relative to the low signal for these stations. The principal differences between these two events is most likely the result of their different mechanisms. Pure 45^{o} thrust or normal events give rise to symmetric radiation patterns with regard to P-wave excitation as a function of azimuth in the far-field. The 1966 event is clearly more complex than this. However, both events show simple enough waveforms to be used for comparison purposes. Thus the greater complexity demonstrated by the 1967 and 1976 events is due to a

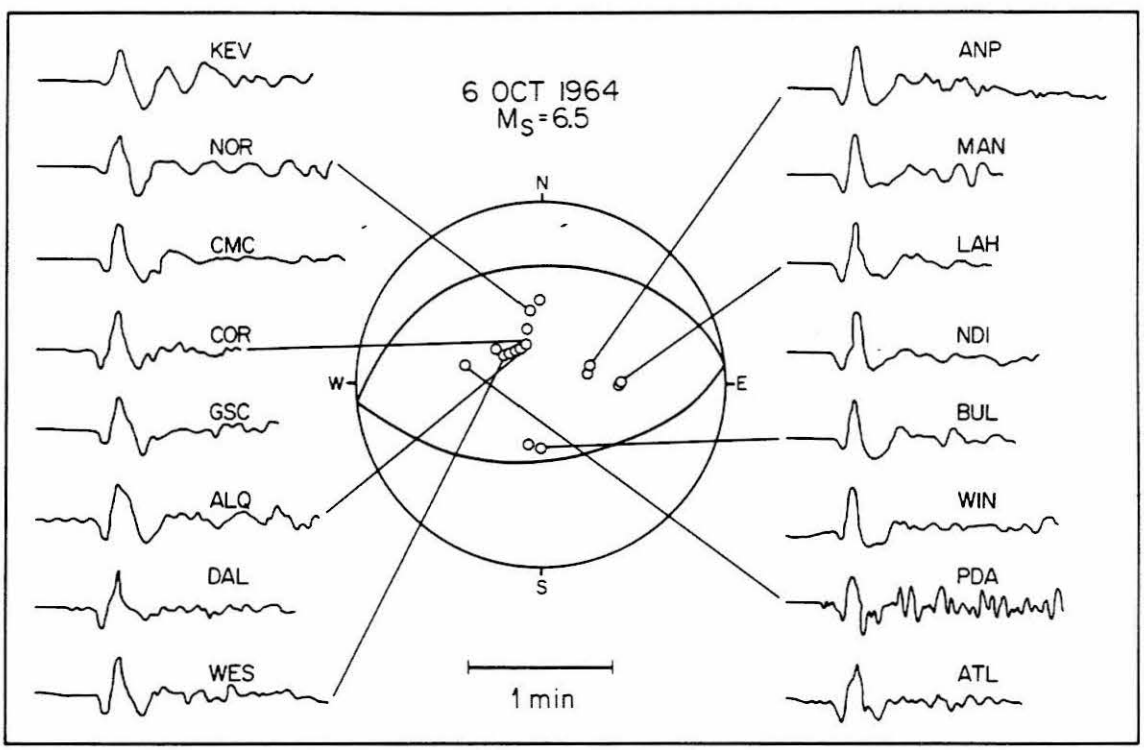

Figure 2-11. Vertical long-period seismograms for various WWSSN stations in the distance range 30° to 90° as a function of azimuth around the epicenter of the 1964 event. Note the fairly simple P-waveform at most stations. All stations are plotted with the same vertical scale. The open circles indicate the locations on the focal sphere of the stations shown. As seen in Figure 2-9 and here, the fault planes shown indicate one possible faulting mechanism and are not well-constrained.

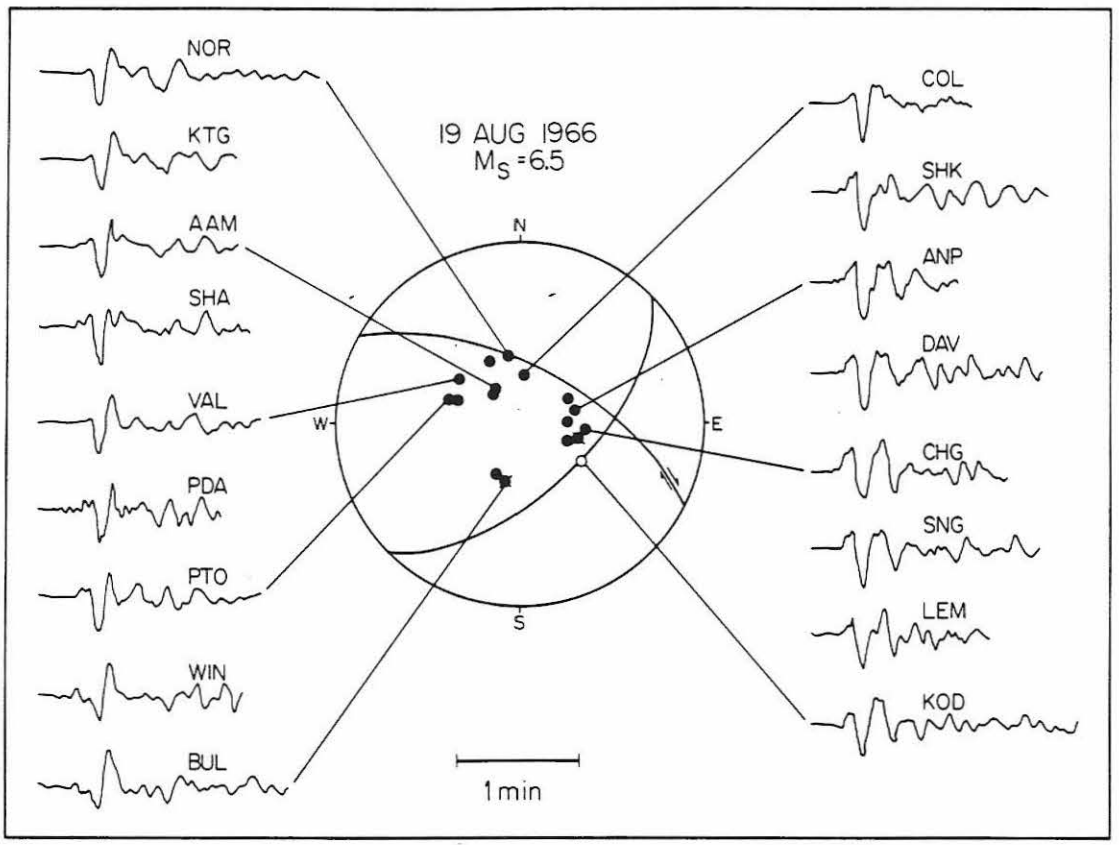

Figure 2-12. Vertical long-period seismograms for various WWSSN stations in the distance range 30^{o} to 90^{o} as a function of azimuth around the epicenter of the 1966 event. Note the fairly simple P-waveform at most stations. All stations are plotted with the same vertical scale. The stations to the east are close to a double node and so are of small amplitude. The apparently more complex looking waveforms are due to an amplification of the noise relative to the signal for these azimuths. The open and closed circles indicate the locations on the focal sphere of the stations shown. The fault planes are constrained by the data shown in Figure 2-9.

source effect and not to a propagation or near-receiver effect.

1967 event

The Mudurnu Valley earthquake of July 22, 1967 (M_s = 7.1) occurred along the N. Anatolian fault. Ambraseys and Zátopek (1969) reported the effects of damage and faulting caused by the earthquake. Their study indicated right-lateral faulting over a distance of 80 km. Although significant, this value is smaller than several other large events in the region. For example, the December 26, 1939 event (M_s = 8.0) had a 350 km rupture length associated with it, while the events of November 26, 1943 (M_s = 7.6) and February 1, 1944 (M_s = 7.6) had 270 km and 190 km respectively. In all cases, the displacement was predominantly right-lateral.

Nevertheless, the 1967 event represents the largest earthquake along the N. Anatolian fault to be recorded by the WWSSN since its operation began in 1963. Consequently, an analysis of such data would contribute to a better understanding of the mechanism of rupture along this important tectonic boundary. Such an analysis would help to predict the character of future activity in this region as well as in other regions of major continental strike-slip faults such as the San Andreas.

The P-wave first-motion study of the 1967 event indicates an almost pure strike-slip solution (Figure 2-9), with right-lateral motion along the east-west fault plane. Since the P-wave coda indicated a complex wavetrain (Figure 2-10), the technique devised by Kanamori and Stewart

(1978), in their study of the Guatemala earthquake, was applied in the hope of better understanding the nature of the complexity. Normally for such a large event one would expect the P-waves recorded on the WWSSN to be off-scale. However, due to the orientation of the P-wave radiation pattern from a vertical strike-slip fault the energy in the far-field is small enough to allow for P-waves to be well-recorded on many of the WWSSN seismograms. The poor azimuthal control found in the Guatemala study is not a problem here. Ten good quality records were used with good azimuthal coverage (Figure 2-13).

After some preliminary analysis a time function of 10 seconds duration was selected for use in the modeling process. A P-wave synthetic s(t) was calculated for each of the ten stations assuming the mechanism shown in Figure 2-9 and a depth of 7 km. As shown in Figure 2-13 the synthetic consisted of the sum of direct P and the surface reflections pP and sP. The synthetic pulse was added in a time series changing only the amplitude and time interval between pulses until the whole P-wave record was modeled for each station. The best fit to the observed record was found by a non-linear least-squares fit. The results for all the stations modeled are shown in Figure 2-13. The source time series below each observed and synthetic indicates the number, amplitude and time spacing of the sources used to obtain the above synthetic record. The fits obtained are good considering the simplified method used and that the same depth, mechanism and time function is used for each of the sources. The most notable differences between the observed and synthetic records occurs during the initial

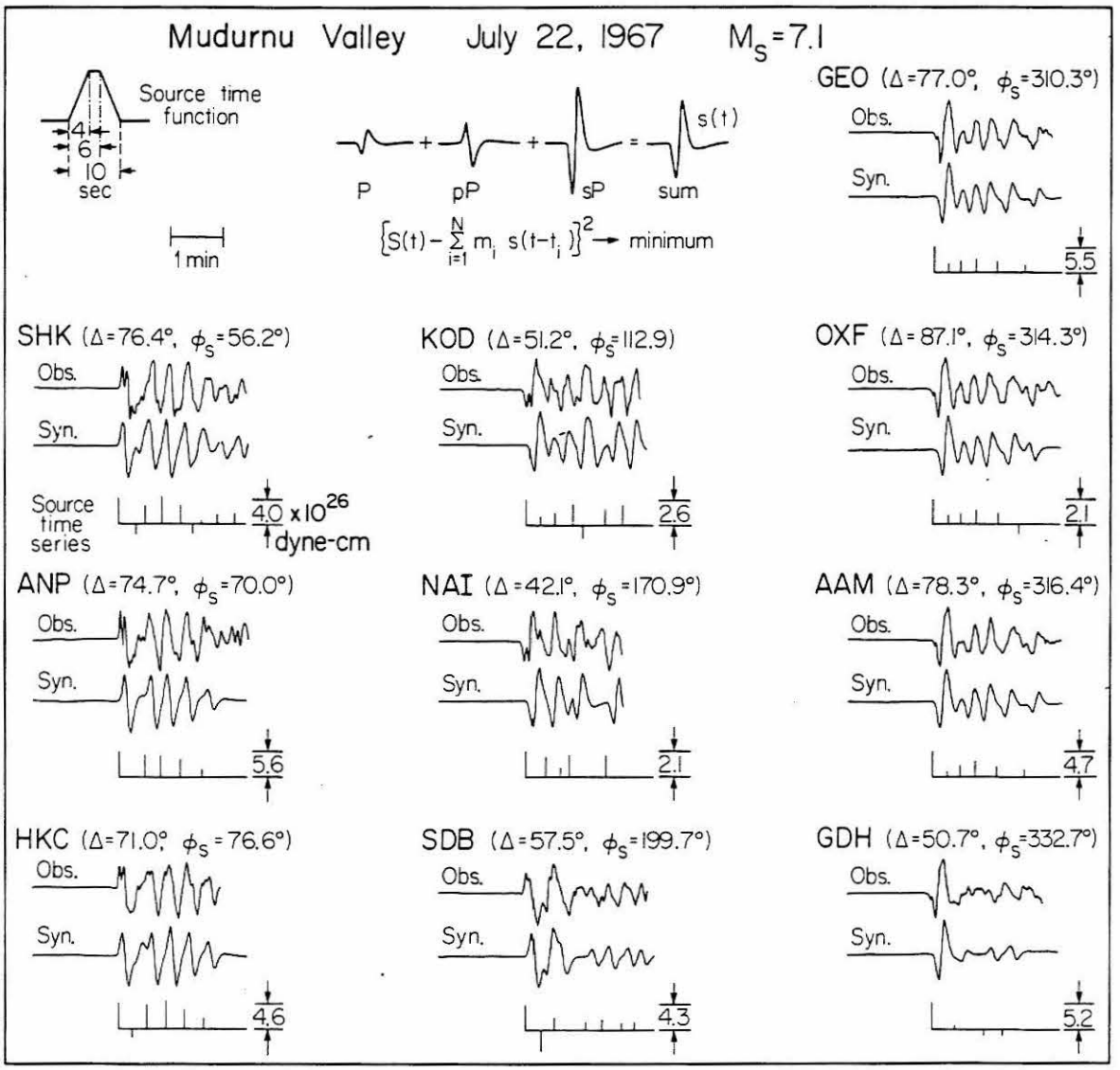

Figure 2-13. Observed and synthetic P-waveforms for individual WWSSN stations obtained from the multiple-shock analysis. For each station the source time series is obtained by using the mechanism shown in Figure 2-9 (number 3) and the source time function shown here. The surface reflections pP and sP are included in the source time function. The resulting series is given for each station along with the moment for the first event. The height of the vertical bar is proportional to the moment of the individual event; Δ is the epicentral distance and ϕ_s the station azimuth.

cycle. The higher frequency nature of the first pulse compared with the others obviously requires a shorter-duration time function for its exact modeling. Such a time function would be inappropriate for the modeling of the later arrivals, however. To simplify the procedure the time function of 10 seconds duration was kept throughout. The resulting source time series obtained for each station are replotted in Figure 2-14. Note that although there are differences from station to station the overall agreement is good. The shaded sections represent the range of times in which individual sources occur. The data indicate seven sources occurring in the first two minutes of record.

The largest source in each case is the first event. On the right-hand side of the figure the moment of this event is given together with the total moment of all sources. The average of the total moment is 1.5×10^{27} dyne-cm. This value is approximately twice that reported by Hanks & Wyss (1972). However, they used only part of the record in their analysis of body-wave spectra.

1976 event

The November 24, 1976 E. Turkey earthquake (M_S = 7.3) occurred along a section of fault northeast of Van Gölü (Lake Van). The event parameters are given in Table 2-2. As shown in Figure 2-8 the epicenter of the 1976 event lies close to the border of Turkey with Iran. Toksöz et al., 1977 reported that this was the only large earthquake to occur during the last century in this area according to a review they made of seismicity catalogues and the recollections of villagers. At the

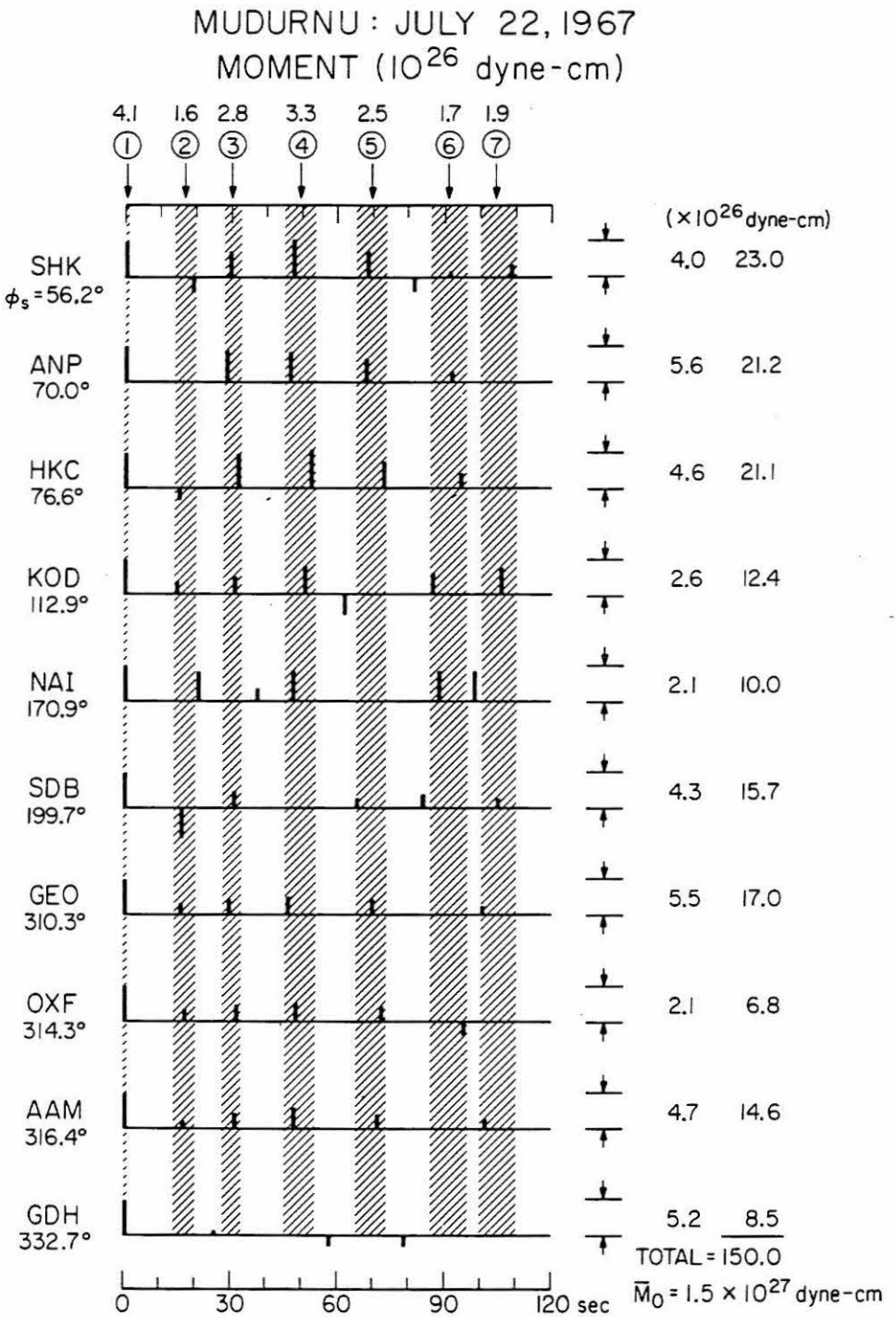

Figure 2-14. A comparison of the source time sequence for the ten stations used in this study. The hatched zones denote ranges of arrival times; ϕ_s is the station azimuth. The values at the top are the seismic moments of the individual events from the multiple-shock sequence. The values at the extreme right are the sum of the moments of the individual events for each station. The overall average is given below.

event's epicenter the fault strikes east-southeast. The association between this portion of the fault and the extension of the N. Anatolian fault is not clear although it is presumed that the two are part of the same tectonic province.

Evidence from field studies (Toksöz et al. 1977) indicated 55 km of right-lateral strike-slip rupture associated with the 1976 event. The average observed displacement reported was 2.5 m. The observed field evidence of right-lateral strike-slip motion is confirmed by the P-wave first-motion plots shown in Figures 2-8 and 2-9 and Toksöz et al. (1977).

As indicated in Figure 2-15, P-wave seismograms show a complex wavetrain. Compared with the other events shown in Figure 2-10, the 1976 event has a high frequency content overall, with most of the energy arriving in about 1.5 minutes. As with the Guatemala event the higher amplitude energy arrives later in the sequence. This is to be contrasted with the 1967 event where the largest energy arrives in the first pulse.

Following the procedure discussed earlier for the Guatemala (Section 2.2) and Mudurnu Valley events, an attempt was made to model the complex sequence of arrivals of the 1976 event. Again, due to its location, a good azimuthal station coverage was obtained. The eight WWSSN stations selected for study are shown in Figure 2-15. In this case, a shorter time function was selected (4.5 seconds duration). The resulting best-fitting synthetics are shown below the observed data. Also shown are the corresponding source time series.

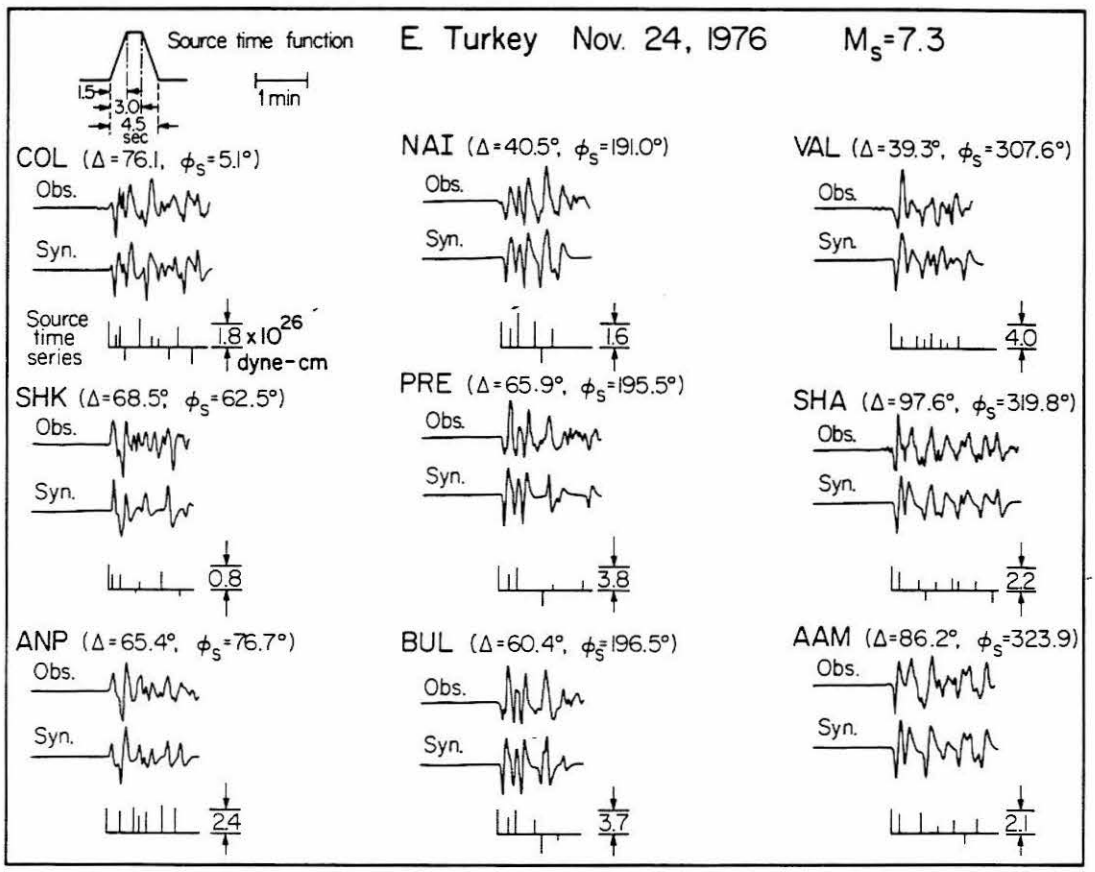

Figure 2-15. Observed and synthetic P-waveforms for individual WWSSN stations obtained from the multiple-shock analysis. For each station the source time series is obtained by using the mechanism shown in Figure 2-9 (number 4) and the source time function shown here. The surface reflections pP and sP are included in the source time function. The resulting series is given for each station along with the moment for the first event. The height of the vertical bar is proportional to the moment of the individual event; Δ is the epicentral distance and ϕ_s the station azimuth.

The impression on visually comparing the observed and synthetic data is that the fits are poor, at least not as good as those found for the Guatemala and Mudurnu Valley events. This becomes clearer when the source time series are replotted vertically as in Figure 2-16. The variability in amplitude and time separation from event to event is considerable. Events 1 and possibly 2 show consistency from station to station. For all of the others, however, the variability is unacceptable. Several different time functions and depths were tried but what is shown represents the best fits that could be obtained.

From this analysis one can conclude that not all large strike-slip events can be fit using this method. There are several reasons for this. In the modeling procedure, several assumptions were made about the individual sources. The depth was considered to be the same for all the events. Using the assumption of a shallow strike-slip source it seems unlikely that varying the depth from 0 to 20 km, for example, could result in enough variation in the synthetics to explain the observed waveforms. A variable time function for each source would similarly be unlikely to explain the complexity. The most likely explanation of poor fits is the assumptions regarding the source mechanisms of the individual sources. Since fault ruptures are rarely straight it is reasonable that the later events have a different mechanism from the mainshock; the assumption that was used in the modeling of the Guatemala, Mudurnu Valley and E. Turkey events was that the source mechanisms of the later events were identical to that of the mainshock. However, for this effect to be significant the mechanism

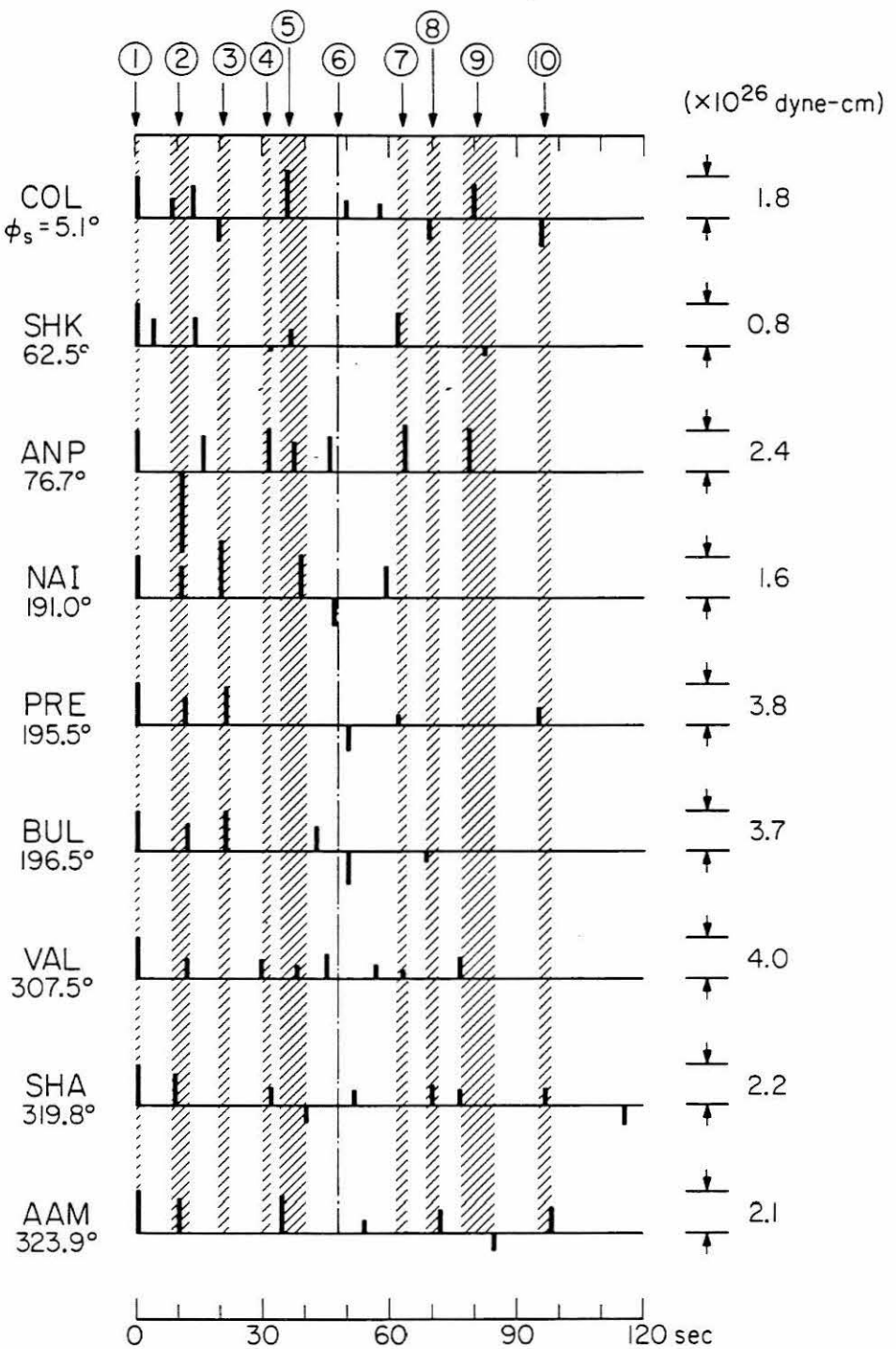

Figure 2-16. A comparison of the source time sequence for the nine stations used in this study. The hatched zones denote ranges of arrival times; ϕ_s is the station azimuth. The values at the right are the moments of the first event.

should be considerably different. It seems unlikely that rotating a fault plane by a few degrees to take account of the fault curvature would be sufficient. However, if some of the later sources had mechanisms very different from the strike-slip mechanism of the main event, then it would be very difficult to unravel the details. Perhaps a thrust or normal fault event on an associated fault structure may have been triggered by the main event. Toksöz et al. (1977) in their field study of the earthquake made no mention of any such associated faulting. However, because of the nature of the terrain and the winter conditions prevailing at the time of the earthquake, such an observation could easily have gone unnoticed. Furthermore, such an event may not have caused fault rupture at the surface.

Examples of such multiple fault complexity in different areas of the world will be discussed in Chapter 3.

DISCUSSION

In the above analysis an attempt has been made to understand the complexity of two Turkish earthquakes and compare the results with those obtained in the previous section for the Guatemala earthquake. From a study of both Turkish events a satisfactory interpretation was found only for the Mudurnu Valley, 1967 event. It was not possible to obtain a complete interpretation for the E. Turkey, 1976 event.

The amplitude values averaged over all the WWSSN stations used in each analysis are shown in Figure 2-17 for the Guatemalan and Mudurnu Valley events. The numerical values are shown at the top of Figures 2-7

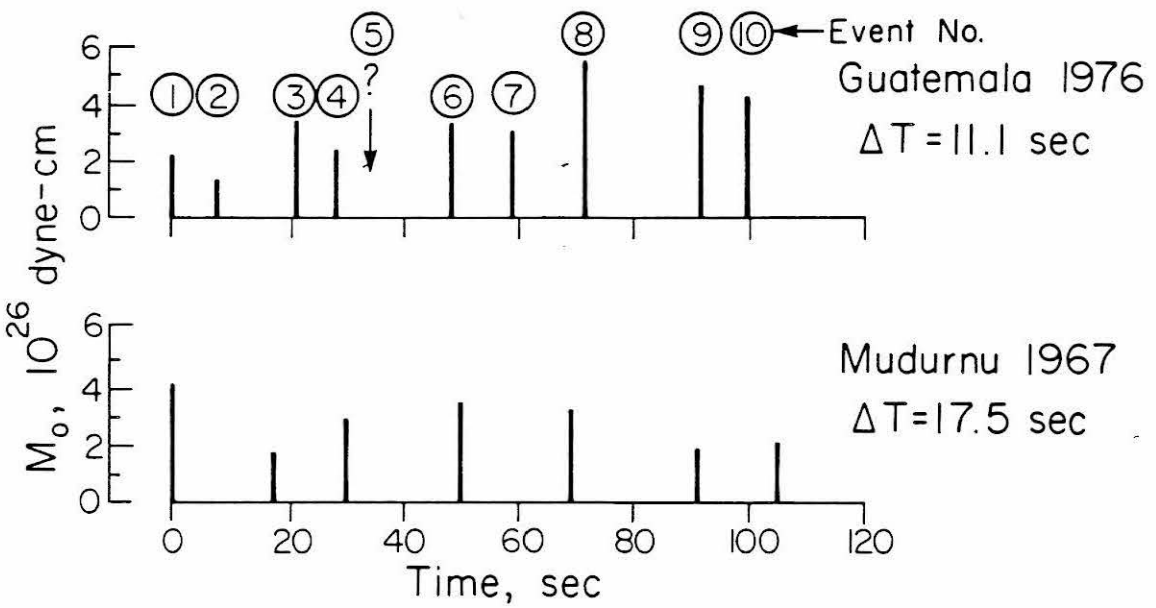

Figure 2-17. Overall comparison of source time series, averaged over all stations, for the Guatemala and Mudurnu Valley, Turkey earthquakes. Note that the maximum moment, for an individual event, for either earthquake is bounded around 5 x 10^{26} dyne-cm. The P-wave duration of both earthquakes is about the same (~ 2 minutes), however more individual events are required to explain the Guatemala earthquake. ΔT is the average time separation between each of the individual events.

and 2-14 respectively. Figure 2-17 summarizes the results of this study. The events differ by a factor of 2 in seismic moment. However, the maximum moment of an individual event is bounded at about 5×10^{26} dyne-cm, regardless. Each of these complex events can be expressed as a sequence of distinct events that occurred at 5 to approximately 20 seconds interval as shown in Figure 2-17. The average time separation is 11.1 and 17.5 seconds for the Guatemala and Mudurnu Valley events respectively.

In a recent study, Kikuchi and Kanamori (1981) re-examined the complex P-wave data for the Guatemala earthquake. They found essentially the same results as those reported here, using a single source time history to explain all the data.

Understanding such complexity is clearly important in predicting what strong ground motion to expect in the near-field of these and other continental strike-slip faults such as the San Andreas. This is shown in Figure 2-18. The upper figure (random model) schematically represents what occurred during the 1967 Mudurnu Valley earthquake. The fault is 80 km long and it is assumed here that the rupture took place from right to left in a unilateral sense. The individual sources are shown as solid circles along the fault. Each source is scaled according to the results shown in Figure 2-17. The sources are spaced equally along the fault and occur at the times indicated in Figure 2-17. The solid square represents a station 20 km from the point of initial rupture. The long-period ground motion resulting from the fault rupture is computed at this station. The observed ground motion from the 1968

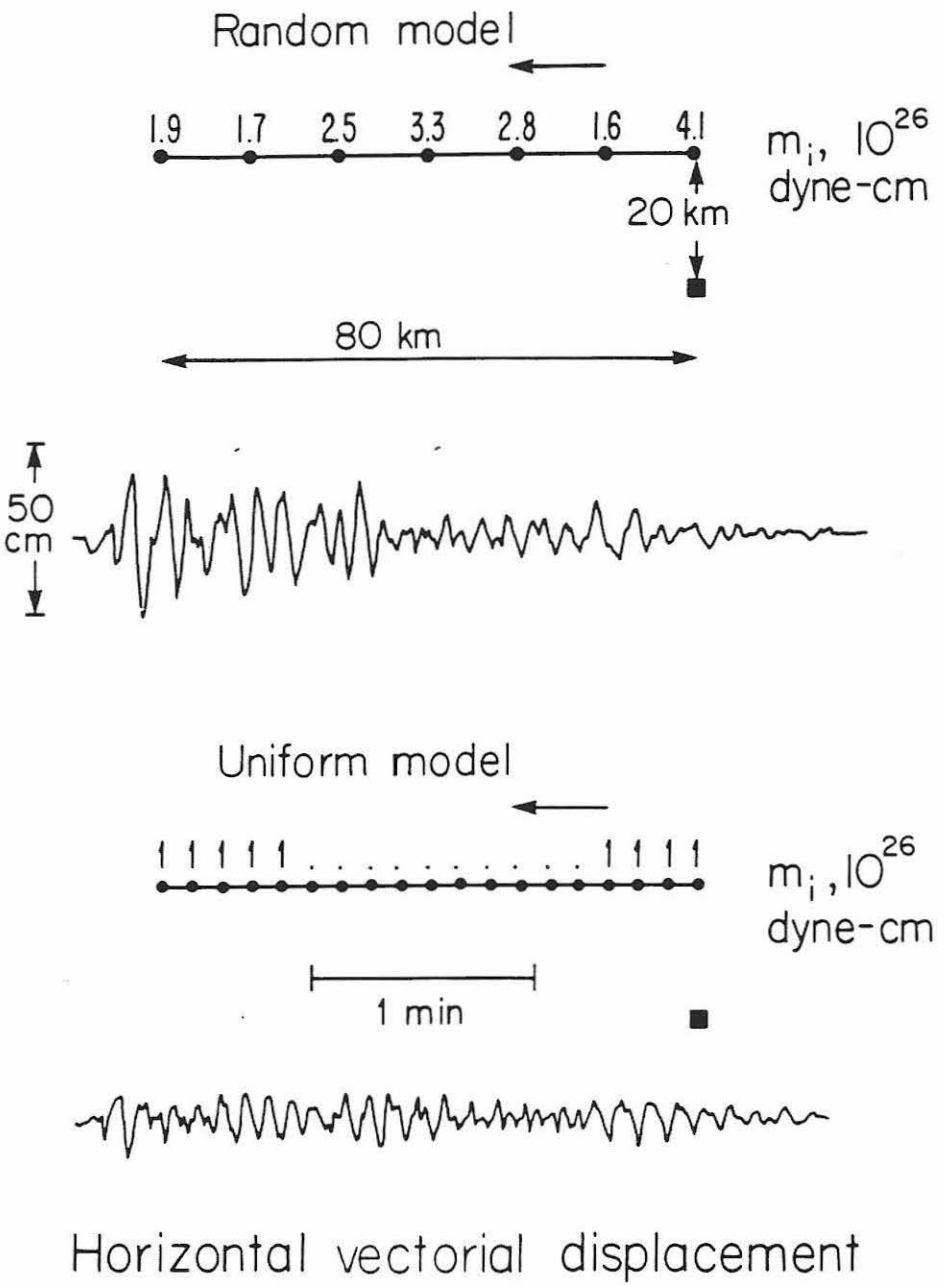

Figure 2-18. Displacements at 20 km from the fault (solid square), calculated for the random model (the specific example shown is for the Mudurnu Valley, Turkey event, shown in Figure 2-17, assuming a unilateral propagation of the source) and the uniform model. The total amount in each case is the same, only the distribution of the energy is different. Note that the random model leads to larger displacements than the uniform model.

Borrego Mountain earthquake is used as a Green's function for each point source. The ground displacement is computed for the station by a superposition of the sources, appropriately scaled and time delayed. This method is discussed in greater detail by Kanamori (1979). The resulting horizontal vectorial displacement is shown. The maximum amplitude computed for the random model is 40 cm. The calculation is repeated this time replacing the Mudurnu Valley source time series with a uniform model. The overall size (total moment) is kept the same but now the sources are of equal size and are spaced equally along the fault. They occur also at equal time intervals. The resulting displacement is plotted below. The resulting amplitude is decreased by more than one half that estimated for the random model.

Thus in estimating ground motion for a site near a fault, it is important to know whether the expected rupture will be uniform or occur as a series of random sources.

CONCLUSIONS

From an analysis of P-waveform data recorded by the WWSSN stations at teleseismic distances an attempt has been made to analyze two of the largest Turkish earthquakes recorded since the installation of the WWSSN network in 1963 -- the Mudurnu Valley, 1967 event and the E. Turkey, 1976 event. The complexity observed in the P-wave seismograms was shown to be the result of source effects since two smaller events close to these in 1964 and 1966 showed only simple waveforms in the far-field, ruling out the possibility of propagation or near-receiver effects.

The method of analysis followed that of Kanamori and Stewart (1978) for the Guatemala earthquake. The results for the 1967 event were quite successful in that the waveforms could be modeled as a series of individual sources of varying amplitude and time sequence history. Comparing the Guatemala and Mudurnu Valley data one can say that, based on these events, the source time series ranges from 5 to approximately 20 seconds and regardless of the total moment of the earthquake the moment of individual events is bounded at around 5×10^{26} dyne-cm.

On the other hand, the 1976 event analysis was not as successful. For this event it does not appear possible to model the event as a multiple source with each source having the same mechanism as that obtained from the P-wave first-motion data. A radical variation in the individual source mechanisms from that of the first event seems necessary, perhaps involving large components of thrust or normal faulting on associated neighbouring faults.

The multiple source character demonstrated by the Guatemala and Mudurnu Valley events has significance with regard to the prediction of strong ground motion. The strong ground motion was computed at a station 20 km from the Mudurnu Valley rupture zone assuming the model derived here. The resulting motion was 2.5 times greater than that obtained from a model of uniform displacement, all other parameters being kept the same.

An understanding of the mode of rupture in these events has important bearing with regard to other environments of continental strike-slip tectonics such as the San Andreas in California.

CHAPTER 3.

MULTIPLE FAULT COMPLEXITY

3.1 Introduction.

This chapter deals with complexity in the earthquake source process in a sense different from that discussed so far. In Chapter 1, the two most complex earthquakes discussed were the April 29, 1970 and the January 30, 1973 events. It was noted that these events occurred at the eastern and western ends of the Cocos-N. America plate boundary, near triple junctions. Although the exact nature of the complexity was not examined or modeled, especially for the 1973 event, the suggestion was made that it was related to the proximity of these events to their respective triple junctions. Because of the interaction of three plates in these localities, the stress distribution is considered to be heterogeneous. A large, or small event occurring along one boundary may cause sufficient stress readjustment to trigger an event (large or small) on an adjacent boundary or fault.

Indeed, during the aftershock sequences of many earthquakes several of the events probably do not occur exactly along the presumed planar boundary associated with the main event. They more likely occur in the regions adjacent to the fault plane. In the case of a large subduction zone event, these aftershocks may occur in the continental crust above or in the oceanic crust below the fault plane. Such variations can be

seen in either slight changes in the strike or the dip of the fault plane in focal mechanism studies. Such changes are usually not considered to be significant, however, and they are usually ascribed to local heterogeneities or to a non-planar fault.

On a larger scale, in some recent cases, earthquakes occurring along one particular boundary have clearly triggered a large earthquake or earthquakes on quite different boundaries or faults. The result is that these "large aftershocks", for lack of a better word, show significant variation compared with their respective mainshock focal mechanism solution. Such an example is suggested for the February 4, 1976, Guatemala earthquake, in which the mainshock (M_s = 7.5) was associated with N 66°E left-lateral strike-slip faulting on the Motagua fault (Kanamori and Stewart, 1978 and Chapter 2, Section 2.1), while the main aftershock (m_b = 5.8) may have occurred on the Mixco fault, a north-south trending normal fault (Person et al., 1976). In this case, a large strike-slip event triggered a significant, though smaller normal event. The different case of a large thrust event triggering a significant strike-slip event will be discussed in Section 3.2. Here the August 16, 1976 Philippine earthquake, a large oblique thrust event, triggered a strike-slip event (M_s = 6.8) twelve hours afterwards. In a similar fashion, the great Chilean earthquake (M_w = 9.5) of May 22, 1960 triggered a large strike-slip aftershock (M_w = 7.8) on June 6, 1960. This is the subject of discussion in Section 3.3.

As will be discussed, such "multiple-fault complexity" or "tectonic complexity" is seen as a feature of quite different tectonic

environments around the world. In addition to these cases, Dziewonski and Woodhouse (1981) and Dziewonski (personal communication, 1981) report similar findings for the St. Elias, Alaska earthquake of February 28, 1979. Here the details of the second event lie within the coda of the first. Through an inversion procedure they appear able to unravel this complexity into two events; the first event being due to the Pacific plate subducting beneath Alaska and the second due perhaps to associated tear faulting (strike-slip) along the northerly extension of the Fairweather fault at the eastern end of the aftershock zone.

Perhaps the most complex example of this type of deformation is to be found in the Tangshan, China earthquake sequence of July 27, 1976. Here the mainshock (M_s = 7.7), primarily a strike-slip event, had associated thrust faulting following 11 and 19 seconds afterwards, while the main aftershock (M_s = 7.2), occurring fifteen hours after the main event, represented an oblique normal fault motion on a plane, perpendicular to the mainshock rupture plane. This is discussed in Section 3.4.

Such complexity, although unusual, may be more common than is presently recognized.

3.2 The August 16, 1976, Mindanao, Philippine, Earthquake.

ABSTRACT

The Philippine earthquake of August 16, 1976, is one of the largest to have occurred world-wide in recent years (M_w = 8.1; M_s = 7.8; seismic moment, M_o = 1.9 x 10^{28} dyne-cm). It is, however, associated not with the Philippine Trench which is the dominant tectonic feature along the eastern Philippine Islands, but with a much less prominent trench system in the Moro Gulf, N. Celebes Sea, south of Mindanao. In this area most of the seismicity is at depths greater than 500 km, associated with the westward dipping Benioff zones of the Sangihe and Mindanao arc systems. This event, however, has a shallow focus and caused a locally destructive tsunami. The focal mechanism of the mainshock determined in this study from long-period surface and body waves indicates a predominantly thrust mechanism with strike N 33°W, dip 22° NE and rake +68°. A significant amount of directivity, which can be seen in the observed surface wave seismograms, is explained very well if the source rupture propagates 160 km unilaterally in an azimuth of 300° from the mainshock hypocenter, with rupture velocity 2.5 km/sec. The largest aftershock (M_s = 6.8) occurred outside the main aftershock area twelve hours following the mainshock and apparently resulted from motion on a subsidiary fault since the P-wave first-motion data indicate strike-slip motion for this event. Bathymetric data indicate the presence of a trench striking north-south in the region of the Moro Gulf, and seismic reflection profiling indicates disturbed sediments

east of the trench showing evidence for subduction. In addition, the geological structures mapped on the island of Mindanao are consistent with this mode of deformation. The only other known large earthquake in the region, on August 15, 1918 (M_s = 8.0), probably occurred along the same subduction zone, on an adjacent segment, to the south of the recent event. The August 16, 1976, Philippine earthquake thus represents the first clear seismic evidence for a northeast dipping subduction zone beneath Mindanao in the Moro Gulf, N. Celebes Sea.

INTRODUCTION

The Philippine earthquake of August 16, 1976 (origin time $16^h\ 11^m\ 07.3^s$ U.T.; location 6.26°N, 124.02°E; depth = 33 km ("normal"); m_b = 6.4 (U.S.G.S.); M_w = 8.1; M_s = 7.8 [this study]); is one of the largest earthquakes to have occurred world-wide in recent years. It occurred in the Moro Gulf, N. Celebes Sea, south of Mindanao, the largest island in the southern Philippine archipelago (Figures 3-1 and 3-8). The earthquake caused a locally destructive tsunami which was primarily responsible for the large loss of life (5,000 deaths), according to Wallace et al. (1977), who state that six out of every seven casualties resulted from the tsunami, while the damage and loss of life due to the effects of shaking were small.

Although the dominant tectonic feature of this region, the Philippine Trench, lies along the eastern Philippine Islands, this event was not associated with it, but with a less prominent though important bathymetric feature called the Cotabato Trench (Hamilton, 1974a;

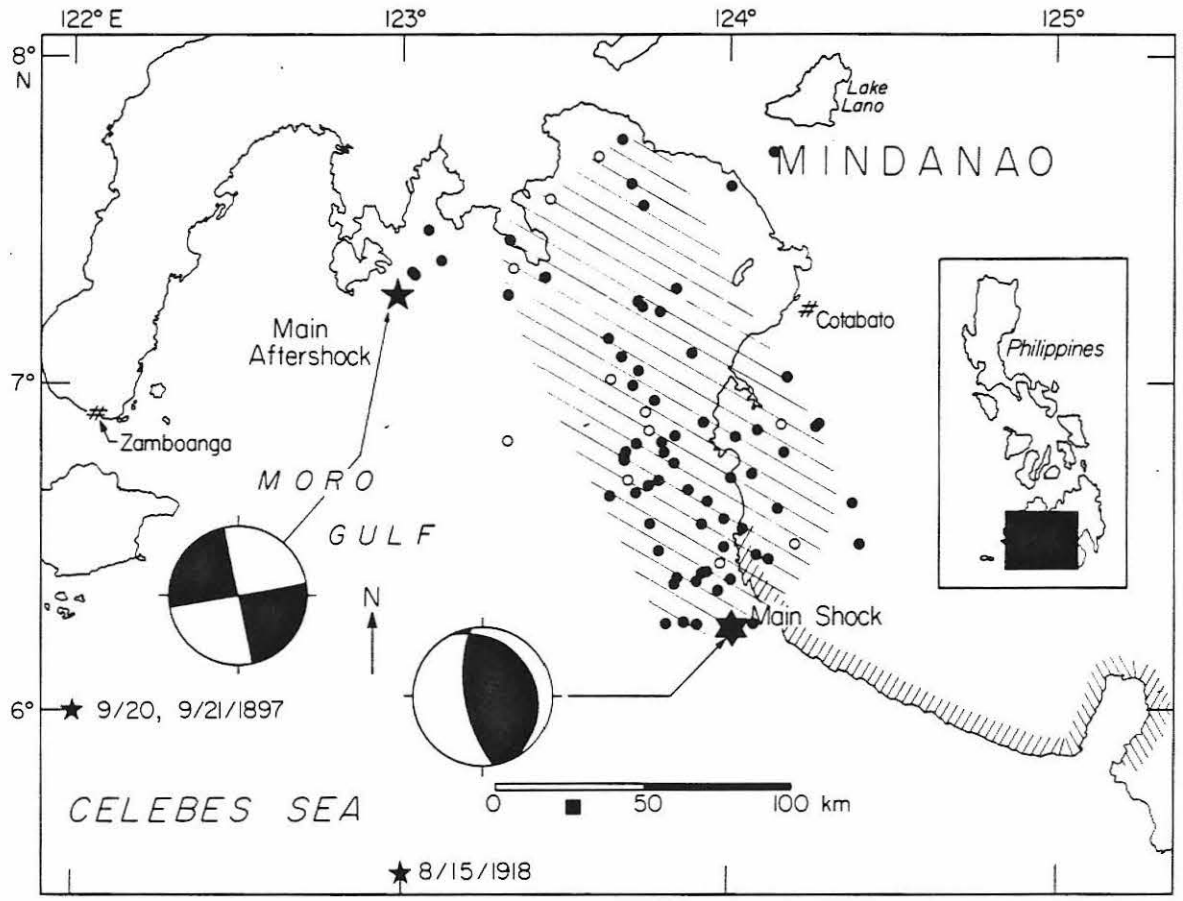

Figure 3-1. Map of southwest Mindanao, Philippines, showing the aftershock zone of the August 16, 1976 earthquake (hatched area). The open circles are aftershocks which occurred in the twelve hour period following the mainshock (before the main aftershock). The closed circles represent later aftershocks up to 1.5 months. All aftershocks have $m_b > 4.5$. The locations of the mainshock and main aftershock are shown together with their respective focal mechanisms (see Figures 3-2 and 3-3 for details). Locations of earlier earthquakes with $M_s > 8.0$ are shown (small stars). The solid square represents the relocation of the 1918 event (this study), indicating a shift to the east for the epicenter. The hatched zone represents the coastal zone along which tsunami damage from the 1918 event was the greatest (Masó, 1918).

Hamilton, 1974b; Hamilton, 1977) which strikes in a north-south direction in the N. Celebes Sea (Figure 3-8). Most of the background seismicity of the N. Celebes Sea occurs at depths in excess of 500 km, and is associated with the west-dipping Benioff zones of the Sangihe and Mindanao arc systems (Hamilton, 1974b; Cardwell and Isacks, 1978). Some shallow seismicity was evident, however, prior to the August 16, 1976 event. It is shown as a diffuse zone in this area by Hamilton (1974b) and Tarr (1974). Hypocentral locations of these early events do not define any fault plane or Benioff zone associated with the Cotabato Trench; however, the data are of poor quality. The relocated aftershock hypocenters, based on the presently available data, also fail to indicate a planar pattern. The previous major event in the region with $M_s \simeq 8.0$ occurred on August 15, 1918. A relocation of that earthquake for this study indicates that it probably was associated with a more southerly segment of the same subduction zone.

In this study, long-period surface waves were used to constrain the mechanism of the August 16, 1976, Philippine earthquake, as well as determining its seismic moment and source directivity. These data indicate that the earthquake has an oblique thrust mechanism with one shallow plane, the fault plane, dipping to the northeast beneath the island of Mindanao. Thus, the Philippine earthquake is the first seismic evidence for a northeast dipping subduction zone in the Moro Gulf.

SEISMOLOGICAL DATA

Relocation of the mainshock of the August 16, 1976, Philippine earthquake and relative locations of aftershocks with respect to the main event, were made in this study using P-wave first arrival time data taken from the Earthquake Data Reports (E.D.R.) of the U.S.G.S. All P-wave readings for stations in the distance range 0^{o} to 50^{o} with residuals less than 3.0 sec were used in the relative locations. The resulting epicenters are plotted in Figure 3-1. The majority of the aftershocks plotted lie to the northwest of the mainshock location, suggesting a unilateral propagation of the earthquake rupture, extending 160 km to the northwest. As will be shown later, this rupture propagation is consistent with the long-period surface wave data. It is also worth noting that the maximum tsunami damage occurred along the coastal area at the northwest end of the aftershock pattern (Wallace, personal communication, 1977), suggesting that the direction of source rupture propagation affected the propagation of the tsunami and its resulting effect along the coastline.

The P-wave first-motion data for the mainshock are shown in Figure 3-2. By use of these data alone, only one plane, that dipping to the west, is constrained. This is the typical situation for events which have a dominant thrust or normal component and for which few, close-in, azimuthally well-distributed P-wave first-motion data are available (Abe, 1972). However, long-period surface wave data can be used to provide a constraint to the other plane.

The surface waves G_3 (Love waves) and R_3 (Rayleigh waves) which

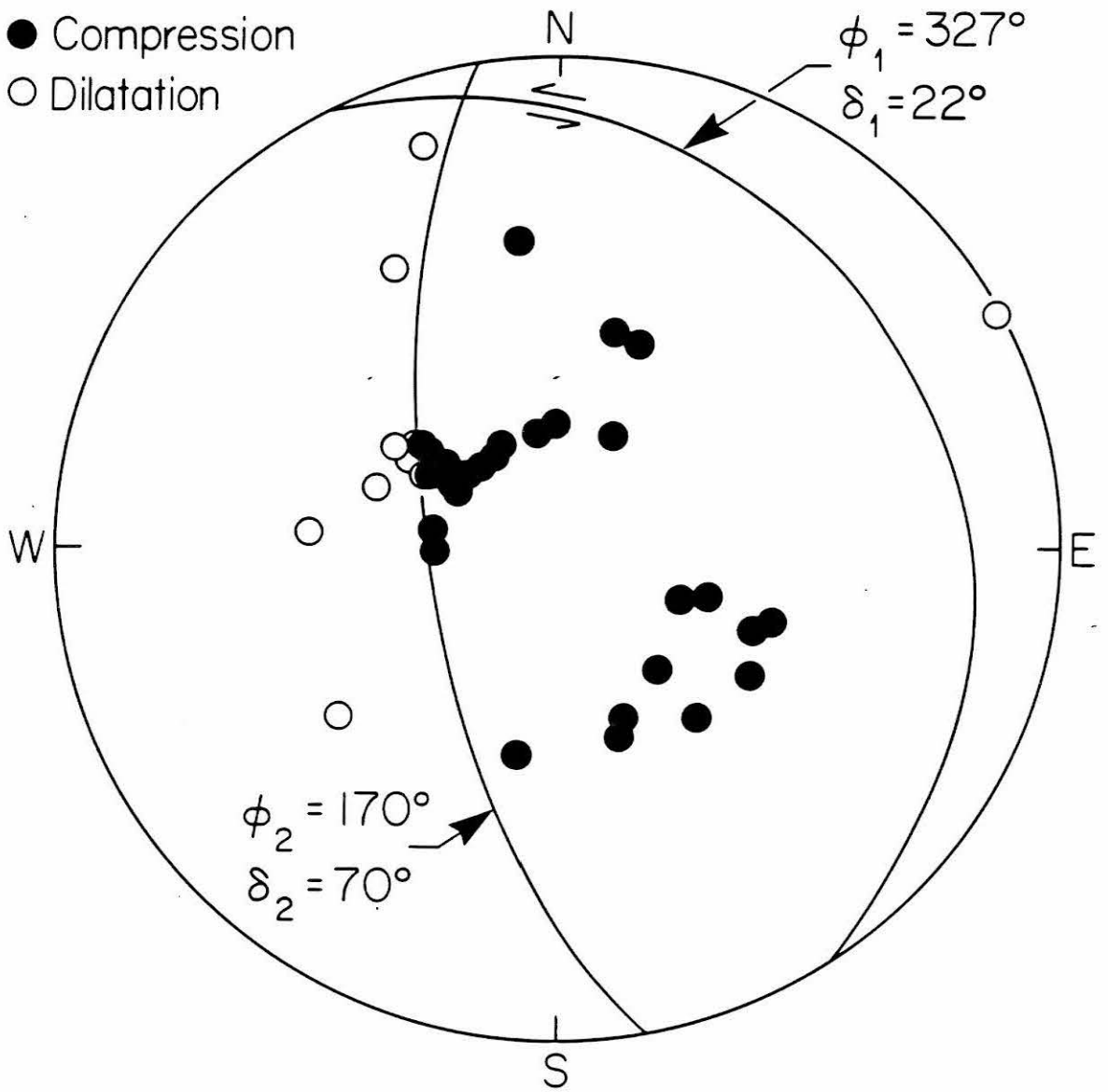

Figure 3-2. The P-wave first-motion data for the Philippine earthquake of August 16, 1976, indicating shallow thrust faulting to the northeast. A small amount of left-lateral strike-slip motion is included. The fault plane is constrained by the strike of the aftershock zone (see Figure 3-1) and the surface wave data. All data used in this plot were read from the WWSSN seismograms, in this study. An equal-area projection of the lower focal hemisphere is shown.

were recorded by the World-Wide Standardized Seismographic Network (WWSSN) long-period seismographs and equalized to a propagation distance of $360^{o} + 90^{o}$, are shown in Figure 3-5. The equalization method is discussed by Kanamori (1970). Using a filter described in Kanamori and Stewart (1976), short-period (less than 60 seconds) surface waves have been removed. The Rayleigh waves indicate a two-lobed radiation pattern, while the Love wave radiation pattern is four-lobed. These patterns are consistent with the mechanism shown in Figure 3-2. The theoretical radiation patterns of Love and Rayleigh waves for a shallow dipping thrust fault mechanism are shown in Kanamori (1970). These data will be discussed in detail in the section on surface wave analysis. Note that the solution shown in Figure 3-2 has a small amount of left-lateral strike-slip motion on the northeast dipping plane, so that the mechanism is described as oblique thrust. Agreement in the strike of this plane is provided by the strike of the aftershock zone (north-northwest trending). Aftershock hypocenters, although all less than 75 km in depth, are too diffuse to indicate support for either fault plane.

Twelve hours following the mainshock, a large earthquake occurred outside the main aftershock area [date August 17, 1976; origin time 04^{h} 19^{m} 27.3^{s} U.T.; location 7.2^{o}N, 122.9^{o}E; depth 22 km; $M_s = 6.8$; $m_b = 6.2$ (U.S.G.S.)]. Also of shallow focus, it is unusual in that the P-wave first-motion data, shown in Figure 3-3, indicate a pure strike-slip solution for this event. Its tectonic significance will be discussed later.

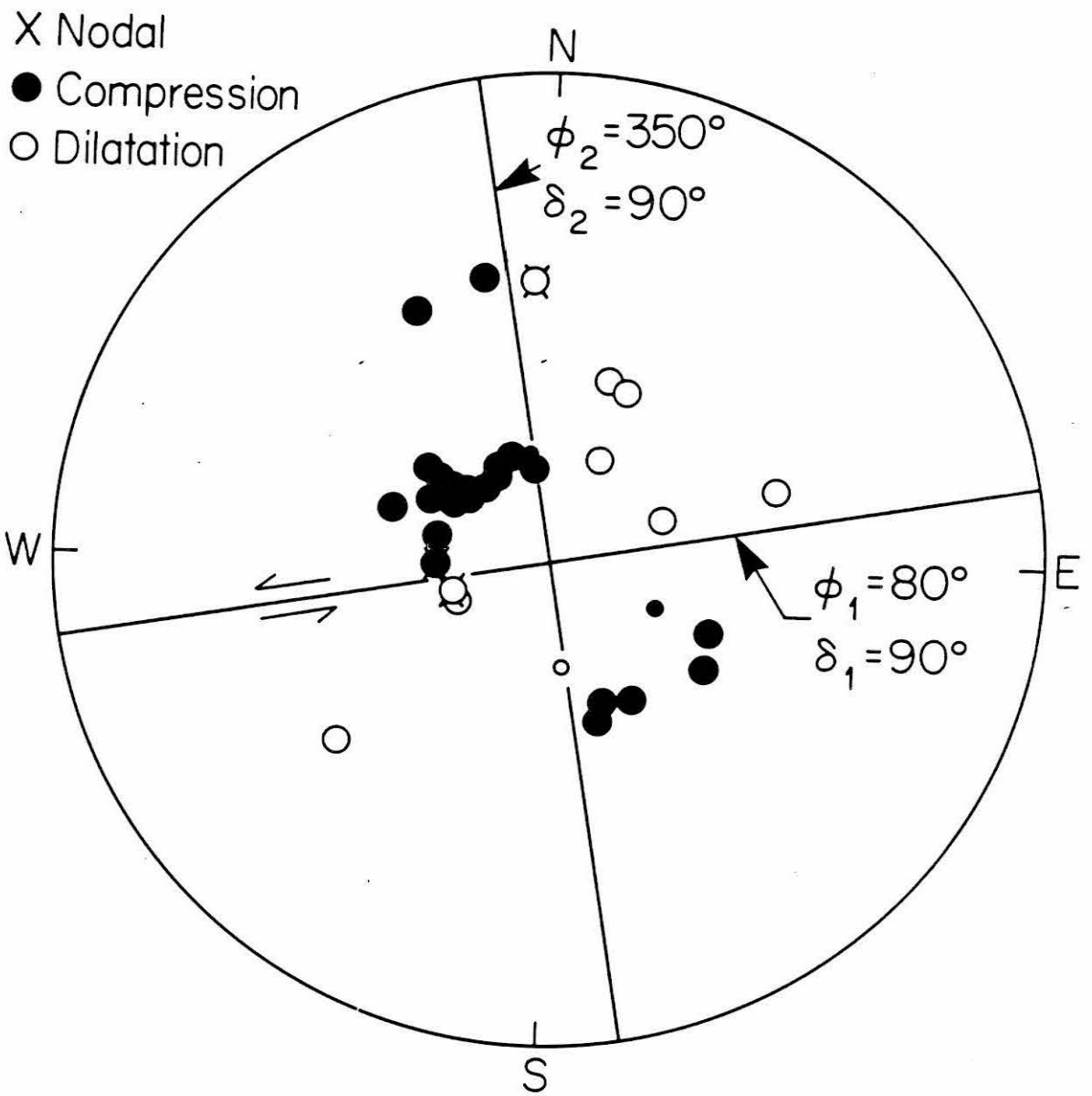

Figure 3-3. The P-wave first-motion data for the main aftershock (M_s = 6.8) of the August 16, 1976, Philippine earthquake, indicating left-lateral strike-slip motion on the preferred fault plane which strikes N 80°E. All data used in this plot were read from the WWSSN seismograms, in this study. The smaller open and closed circles represent less reliable readings.

SURFACE WAVE ANALYSIS

The WWSSN long-period seismograms for the August 16, 1976, Philippine earthquake show relatively large amplitude, multiple surface waves. These are seen clearly in Figure 3-4, where two such seismograms are illustrated. The upper record is a WWSSN long-period vertical seismogram for Bulawayo, Zimbabwe (BUL). This station, lying close to a maximum in the two-lobed radiation pattern indicated in Figure 3-5, shows clear multiple Rayleigh waves for R_3, R_5, and R_7. Earlier arrivals of R_1 and R_2 cannot be seen due to the large amplitude arrivals in this part of the seismogram. Rayleigh wave multiples R_4 and R_6 have very low amplitudes. The larger amplitudes of R_5 compared with R_4, and R_7 compared with R_6, suggest that significant directivity may be present in the rupture propagation. This suggestion is further enhanced by the observed Love waves appearing on the E-W component of the WWSSN station Godhaven, Greenland (GDH). This component is almost naturally rotated, with respect to the arrival of SH-wave radiation from the earthquake source (back azimuth, $\phi_{SE} = 2.5^{\circ}$), so it is ideal for observing Love waves. It also lies close in azimuth to a maximum in the Love wave four-lobed radiation pattern, shown in Figure 3-5, so large amplitude multiple Love waves are expected and are seen in the lower seismogram of Figure 3-4. Note that only the odd numbered Love wave multiples are clearly observed. Even numbered multiples show very small amplitudes, by comparison. This amplitude asymmetry is consistent with the directivity observed for Rayleigh waves.

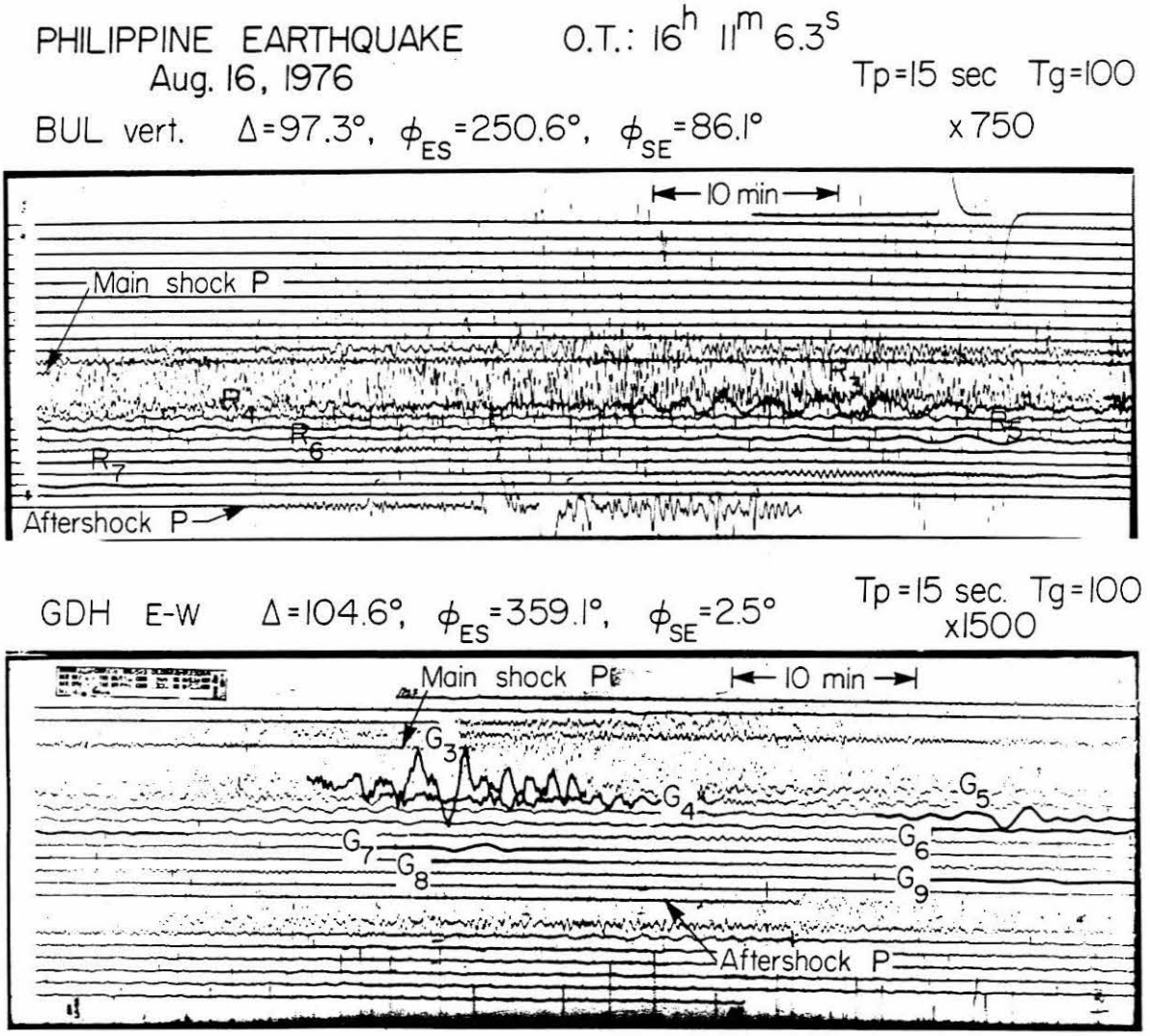

Figure 3-4. WWSSN long-period seismograms for the August 16, 1976, Philippine earthquake. The upper record is the vertical component from BULAWAYO, Zimbabwe (BUL). This station is in an azimuth of maximum radiation for Rayleigh waves. Note that only odd numbered Rayleigh wave multiples can be seen clearly. Even numbered multiples have very low amplitudes. Similarly for the lower trace, which is the E-W component from GODHAVEN, Greenland (GDH). This station is naturally rotated with respect to SH energy from the source region, and is close to a maximum in radiation for Love waves. Note that only odd numbered Love wave multiples can be seen clearly. These observations are consistent with the implied directivity to the northwest in the source rupture propagation.

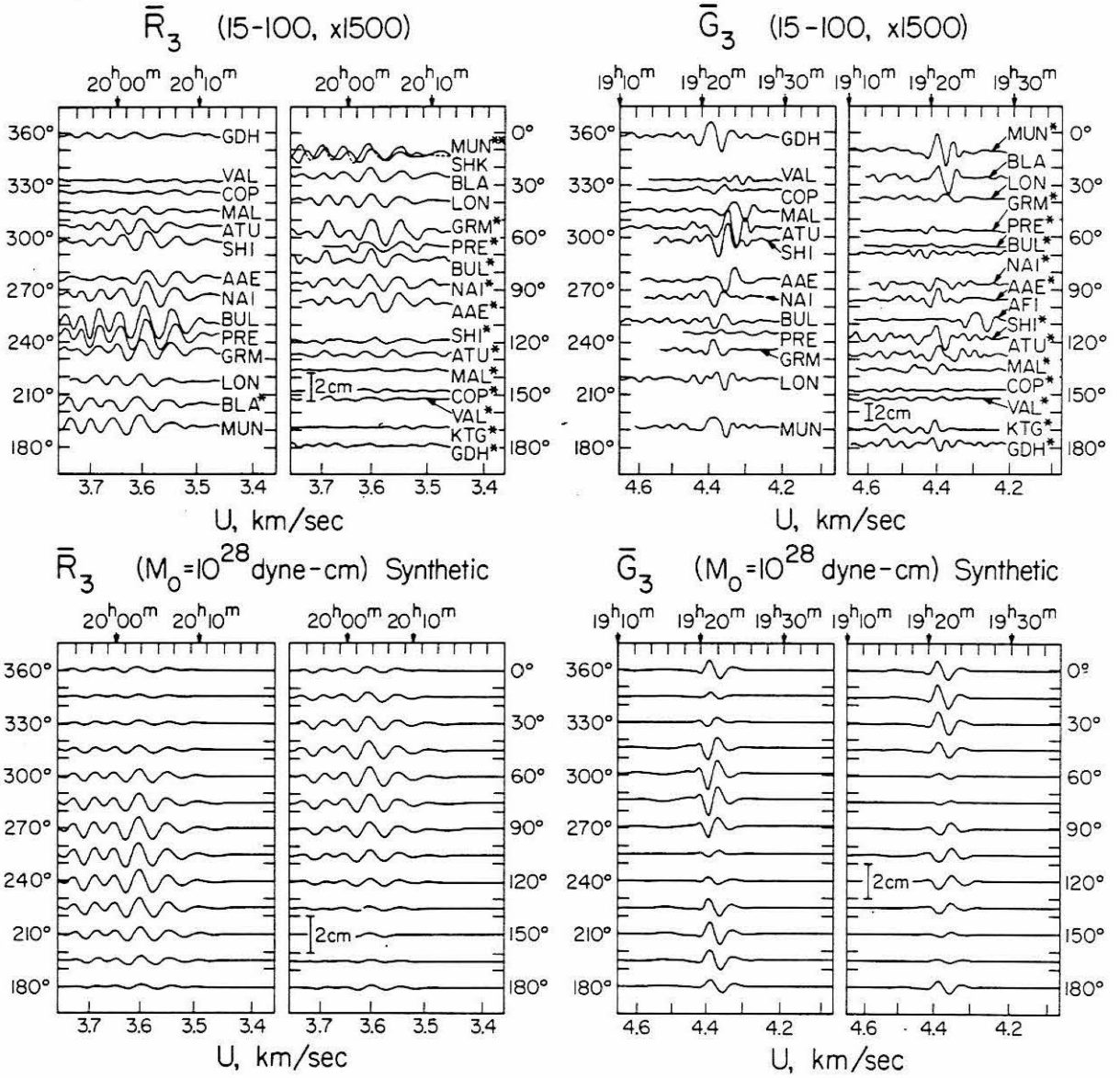

Figure 3-5. Azimuthal plots of equalized seismograms for $\bar{R}_3$ and $\bar{G}_3$ and synthetic seismograms computed for the fault geometry shown in Figure 3-2 with a unilateral propagation (160 - 0 km), rupture velocity, v_r = 2.5 km/sec and rupture azimuth, ϕ_r = 300°. A seismic moment of 10^{28} dyne-cm was used in the synthesis. In the observed patterns, one asterisk indicates that R_2 and G_2 were equalized to R_3 and G_3 distances. Two asterisks indicate that R_4 and G_4 were equalized to R_3 and G_3 distances. The amplitude scale is for the trace amplitude on a WWSSN long-period instrument (15-100) with magnification of 1500.

Since short-period ($T \lesssim 60$ sec) surface waves are severely affected by structural heterogeneities during propagation, only long-period signals are used in the present study to determine the overall seismic radiation pattern, the seismic moment M_o and the amount of directivity.

In order to match the overall radiation pattern shown in Figure 3-5, synthetic surface waves were first computed for a point double-couple source, located at a depth of 33 km. With the constrained west-dipping plane of the focal mechanism shown in Figure 3-2 remaining fixed, the slip angle, λ, was varied until good agreement in the overall radiation patterns for both Love and Rayleigh waves was found. The best fitting solution is that given in Figure 3-2. The method of synthesis, the velocity, and the Q structure are described by Kanamori (1970) and Kanamori and Cipar (1974). The same filter which was used on the observed data in Figure 3-5 was applied to the synthetic records so that a direct comparison could be made. In Figure 3-6, the maximum trace amplitudes of the observed Love and Rayleigh wave data are plotted as solid circles, as a function of azimuth. Although the overall agreement is satisfactory, the point source amplitudes are clearly too large in the azimuth range 0^o to 180^o for Rayleigh waves and 70^o to 240^o for Love waves. However, as discussed earlier, the aftershock zone extends to the northwest of the mainshock epicenter, a distance of 160 km, and so a point source modeling of the earthquake rupture appears inappropriate.

To obtain a better fit of the maximum trace amplitudes of Love and Rayleigh waves shown in Figure 3-6, the source finiteness was included in the modeling procedure. The asymmetry in amplitude of the observed

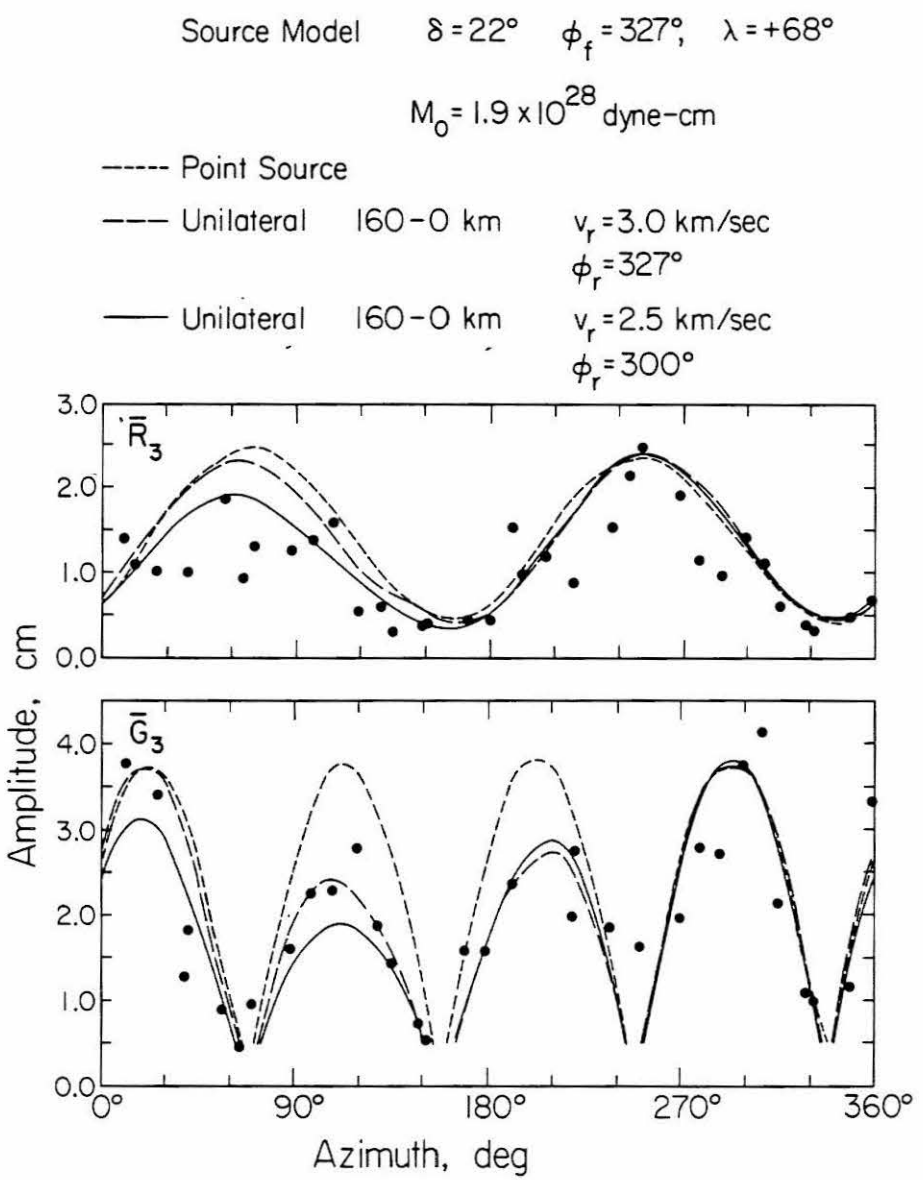

Figure 3-6. Equalized station peak-to-peak amplitudes for observed $\bar{R}_3$ and $\bar{G}_3$ data, plotted as a function of azimuth (solid circles). Curves represent the various fault models used in this study. The preferred model is that indicated by the solid line.

radiation pattern can then be explained by directivity (Ben-Menahem, 1961). In the first case, the fault geometry shown in Figure 3-2 was chosen, i.e., $\delta = 22^{o}$, $\phi_f = 327^{o}$ and $\lambda = +68^{o}$ (δ = dip angle; ϕ_f = strike of the fault measured clockwise from north; λ = slip angle; sign conventions are given in Kanamori and Stewart (1976) and included the source finiteness, with the rupture extending 160 km in an azimuth, $\phi_r = 327^{o}$, the same as the fault azimuth, with a rupture velocity, v_r = 3.0 km/sec. As seen in Figure 3-6, this model gave a much better fit to the observed data than the point source case. However, the synthetic amplitudes in the Rayleigh wave case were still too large in the azimuth range 30^{o} to 150^{o}. As a result, in the second case, using the same fault geometry, the rupture azimuth was reduced to $\phi_r = 300^{o}$ and the rupture velocity to $v_r = 2.5$ km/sec. This then reduced the Rayleigh wave amplitude in the azimuth range 30^{o} to 150^{o} to give a slightly better fit. In view of the quality of the observed data, it was not felt that further modeling would be appropriate. Thus these values represent the preferred mechanism. This result suggests the rupture propagated in an up-dip direction, a result that has been suggested for other large thrust events at subduction zone boundaries (Sykes, 1971; Kelleher et al., 1973; Kelleher et al., 1974). From a comparison of the maximum trace amplitudes of the observed and synthetic records for this final model (Figures 3-5 and 3-6), a seismic moment, M_o = 1.9×10^{28} dyne-cm is obtained from both Love and Rayleigh waves. It is important to note that this realistic fault geometry explains the overall radiation patterns of surface waves and the amplitude ratio of

Love to Rayleigh waves very well.

In order to supplement the WWSSN data, seismograms from the ultra long-period instruments at the Seismological Laboratory, California Institute of Technology and the Seismographic Station of the University of California at Berkeley were used. The Caltech instrument (PAS, No. 33) has a peak response at 150 sec and records very long-period surface waves well. The U.C. Berkeley instrument is peaked at 90 sec and also records very long-period surface waves well. Figure 3-7 shows the observed data for both instruments, filtered at a low-pass cut-off, T_o = 60 sec and a high-pass roll-off, T_∞ = 900 sec and also at T_o = 100 sec and T_∞ = 300 sec. Synthetic seismograms have been computed for the fault mechanism shown in Figure 3-2 with the source finiteness, discussed earlier, included (see final model in Figure 3-6). The same filter was applied to the synthetic records. The agreement of the waveforms is very good. A seismic moment, M_o = 1.4 x 10^{28} dyne-cm was found in all cases, which although a little smaller than the WWSSN data estimate, is still in agreement with it, considering all the uncertainties involved. In the later discussion, the moment of 1.9 x 10^{28} dyne-cm obtained from the WWSSN data will be used.

It is possible to interpret the above results in terms of the average dislocation of the fault, $\bar{D}$, and the average stress drop, $\Delta\sigma$. If a fault width, w ≃ 80 km is assumed from Figure 3-1, then by using a fault length, L = 160 km, also from Figure 3-1 and e.g., Aki (1966) and Kanamori and Anderson (1975b), we have $\bar{D} = M_o/\mu Lw$ = 3.0 m and $\Delta\sigma = 8\mu\bar{D}/3\pi w$ = 17 bars where μ = 5 x 10^{11} dyne/cm^2 is used.

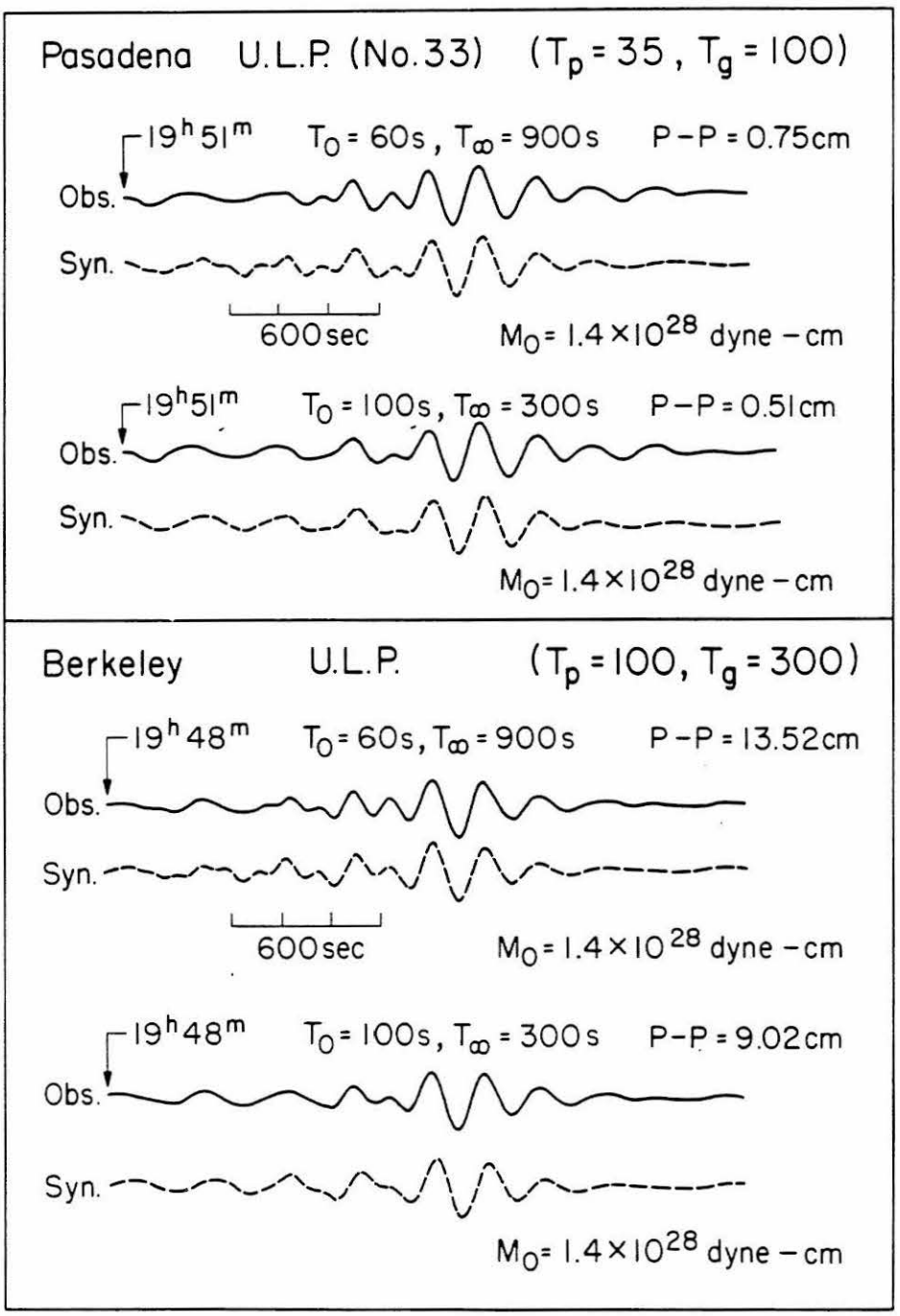

Figure 3-7. Observed and synthetic Rayleigh waves (R_3) at Pasadena and Berkeley (ultra long-period instruments). The records are filtered in two pass bands as shown (T_o is the short-period cut-off, T_∞ the long-period roll-off). Note the agreement of the phase.

TECTONIC SETTING

The Philippine earthquake of August 16, 1976, occurred in an area called the Moro Gulf in the N. Celebes Sea, south of the island of Mindanao. The major tectonic feature in the region, the Philippine Trench, lies approximately 400 km to the east of the mainshock epicenter (Figure 3-8). It is clear that this event is not directly associated with it. However, the influence of the westward dipping Benioff zones of the Sangihe and Mindanao arc systems (Hamilton, 1974b; Cardwell and Isacks, 1978) are seen as contributing to the seismicity of the region, albeit at depths in excess of 500 km. The shallow seismic events prior to the Philippine earthquake and the relocated aftershock hypocenters are diffuse and do not define any fault plane or Benioff zone. Thus this event offers the only seismic evidence for the existence of a subduction zone dipping to the northeast, beneath the island of Mindanao in the N. Celebes Sea. However, no evidence exists for this subduction zone extending deeper than the rupture indicated by the Philippine earthquake.

Several large earthquakes have occurred in this region in the past. Masó (1910) lists "violent and destructive earthquakes" in the time period 1599 to 1909 and Repetti (1946) catalogues earthquakes in the period 1589 to 1899 for the Philippines. However, since most of the locations they presented are based on felt reports or tsunami damage data, the association of such events with any tectonic feature must be considered tenuous. For example, two of the largest events in this area

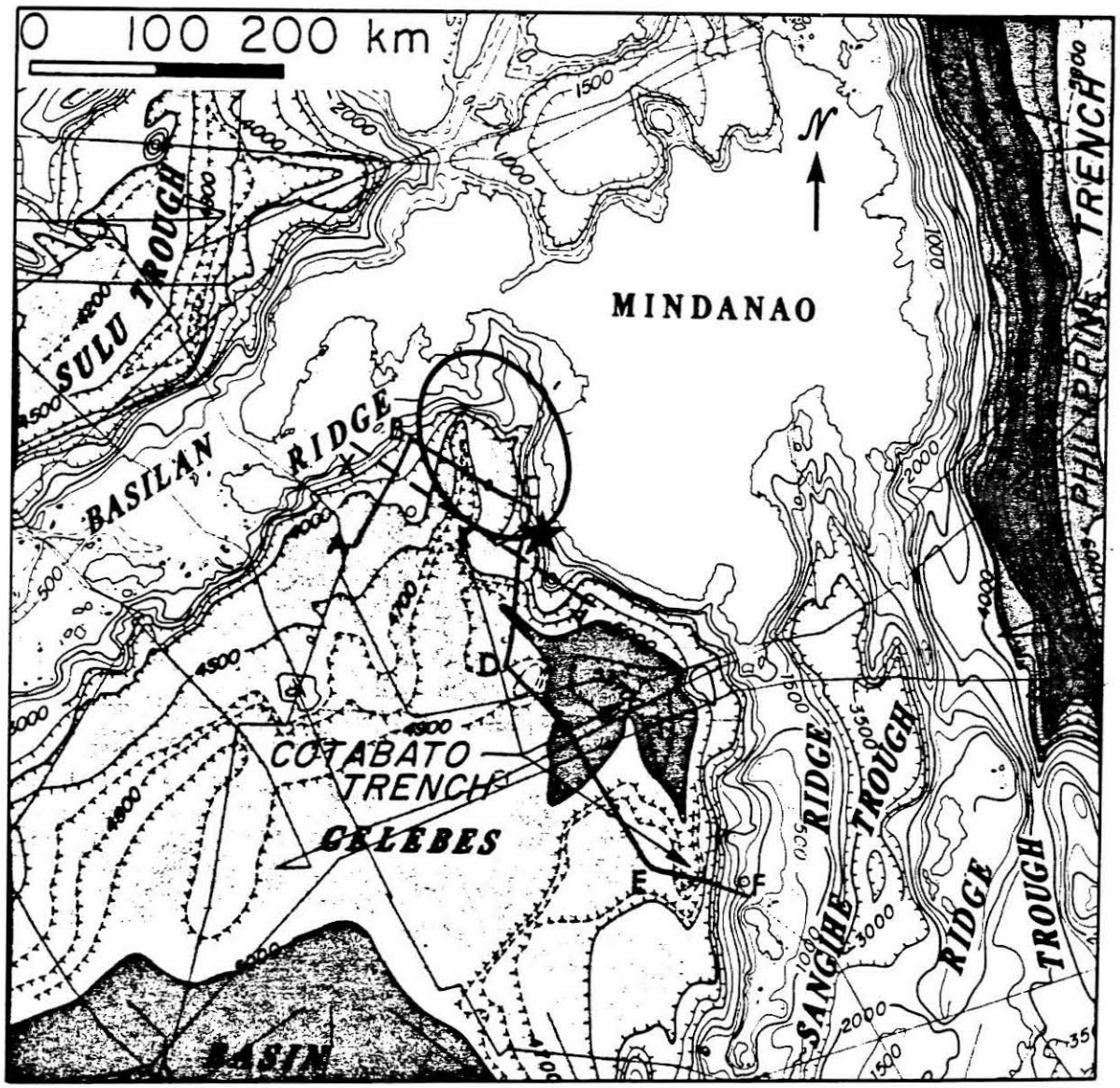

Figure 3-8. A bathymetric chart of the Moro Gulf, N. Celebes Sea region, southwest of Mindanao (after Mammerickx et al., 1976). The solid line ABCDEF represents the ship track along which seismic reflection profiling data were taken (profile from Lamont-Doherty Geological Observatory, R. V. Vema Cruise #28). The dashed line XY represents an anonymous seismic reflection data profile. Note the bathymetry shown, indicating the presence of the Cotabato Trench of depth 4700 m striking NNW in the vicinity of the mainshock rupture. The star represents the mainshock epicenter, the solid ellipse, the aftershock zone of the Philippine earthquake.

listed by the previous authors, are those which occurred on September 20 and 21, 1897. Their epicentral locations, given by Gutenberg (1956a) (6°N, 122°E), are shown in Figure 3-1. However, on closer examination Masó (1910) states that the tidal wave generated by the event on September 21, 1897 "claimed hundreds of victims on the western shores of Basilan", the large island south of Zamboanga, shown in Figure 3-1. It is quite possible, from this fact and the felt area, that the event occurred outside of the Celebes Sea and may be attributed to the southeast dipping subduction zone associated with the Sulu Trench (Figure 3-8), although this portion of the Sulu Trench has little evidence for seismic activity at present.

The earthquake of August 15, 1918, magnitude 8.25 (Gutenberg and Richter, 1965) listed by Geller and Kanamori (1976) as M_s = 8.0, m_b = 7.6, on the other hand, clearly lies in the N. Celebes Sea. Gutenberg and Richter (1965) relocated the epicenter at 5.5°N, 123.0°E. It is plotted in Figure 3-1 as one of the stars. In this study, the event was relocated by computer, using the International Seismological Summary (ISS) readings. All P-wave readings for stations in the distance range 0° to 90° and with residuals less than 3.5 sec were used in the relocation. The hypocenter was constrained at 10 km depth in order to obtain a solution. The resulting epicentral location (5.7°N, 123.5°E) is indicated by the solid square in Figure 3-1. This location, which has an associated error of 15 km, may then imply that the earthquake is located along the subduction zone, southeast of the mainshock. The maximum tsunami damage for this event, shown in Figure 3-1 as the

hatched coastal region (from Masó, 1918) is consistent with this location.

It is possible, then, that both the 1918 and 1976 earthquakes represent rupture of successive segments of the northeast dipping subduction zone in the N. Celebes Sea.

Although less prominent than the Philippine Trench (maximum depth ≈ 9500 m), the Cotabato Trench (maximum depth ≈ 5700 m) striking north-south in the region of the Philippine earthquake, curves west-northwest to east-southeast paralleling the southern Mindanao coastline and eventually trends north-south again in the region west of the W. Sangihe Ridge (Figure 3-8). The trench topography is seen also in the seismic reflection profile, ABCDEF (Figures 3-8 and 3-9). Note that the profile changes direction at each letter. In Figure 3-9, the Cotabato Trench (C.T.) can be seen at the three localities where the profile crosses it. The sense of motion of the subduction is shown at the bottom of Figure 3-9. Note the relatively undisturbed sediments in the Celebes Basin between D and E and their downwarping between E and F. Profile XY represents a seismic reflection profile (anonymous). From X to the midpoint of the profile, the sediments are again undisturbed, but from the midpoint to Y, i.e., on the eastern, or landward side of the trench, severe warping of the sediments can be seen.

One unusual aspect of the tectonic deformation of the Philippine earthquake sequence is the occurrence of the main aftershock (M_s = 6.8), twelve hours after the mainshock. It is unusual because the mechanism for this event appears to be pure strike-slip (Figures 3-1 and 3-3).

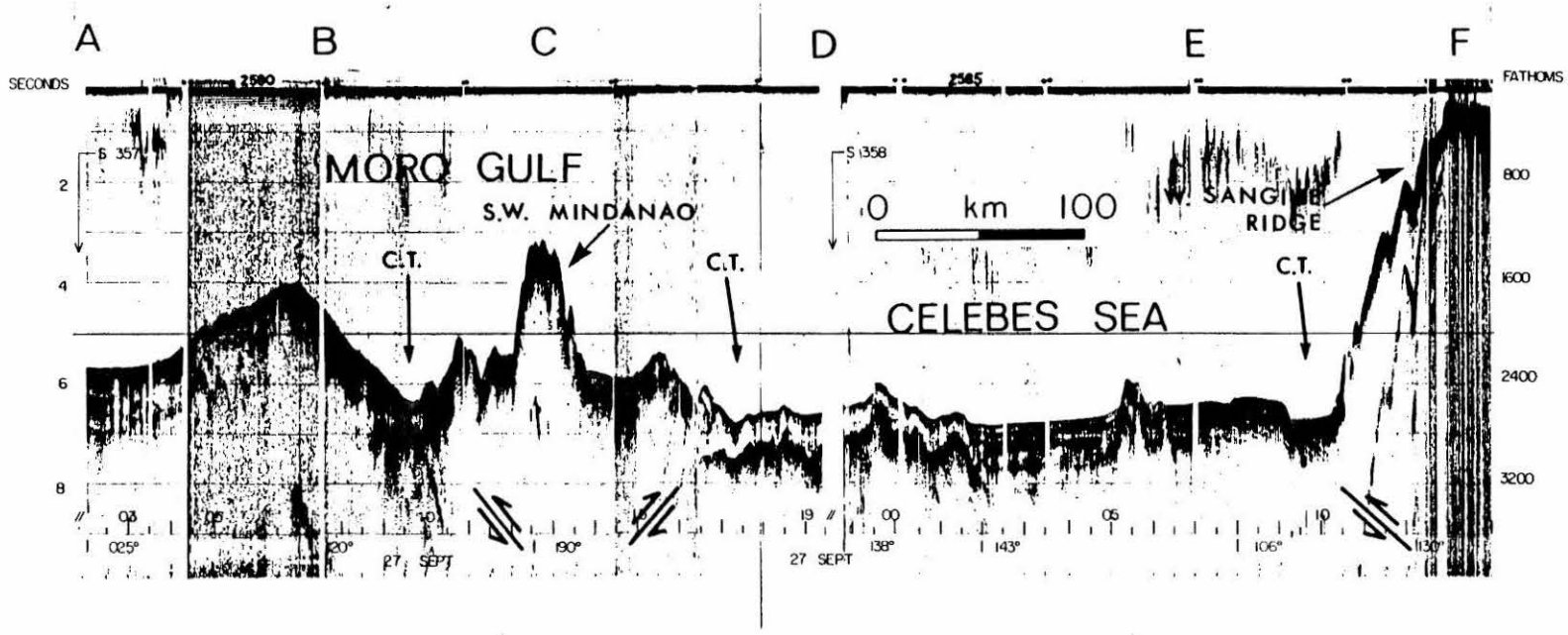

Figure 3-9. The seismic reflection profile data (see Figure 3-8 for location). C.T. represents the location of the Cotabato Trench. Note from Figure 3-8, that each letter represents a change in orientation of the profile. The relative motion vectors at the bottom of the figure represent the direction of subduction, i.e., to the northeast (Warren Hamilton, 1977, written communication).

The sense of motion, left-lateral displacement if the plane striking N 80°E is chosen, can be interpreted as tear faulting close to the northwest edge of the aftershock zone; the result of block movement to the northeast of the Moro Gulf relative to the western arm of Mindanao.

The dominant offshore features also influence the structural trends on land. For example, in eastern Mindanao they are dominated by the north-south strike of the Philippine Trench (Figure 3-10). Parallel to the trench in order east to west, lie the Pacific Cordillera, the Philippine Fault, the Agusan-Davao Trough and its seaward extension, the Sangihe Trough and the Central Cordillera with its widespread Tertiary volcanism (Krause, 1966; Ranneft et al., 1960). Deep and intermediate earthquakes, which are distributed along the west dipping Benioff zone, project to the surface along the trend of the Sangihe and Agusan-Davao Troughs, suggesting that subduction may have been concentrated in that region until subsequent development of the Philippine Trench, which now hosts most of the shallow seismicity (Caldwell and Isacks, 1978; Hamilton, 1974b).

West of the Central Cordillera, in southern Mindanao, the Mindanao Lineament, a depressed zone of high-angle reverse faults, deformation and volcanoes, strikes north-northwest, separating the northerly structural trends to the east and the northwesterly trends of folds and faults in Cotabato (Tiruray) Highlands (Gervasio, 1966). The Cotabato Highlands stand 22,000 feet above the adjacent floor of the Celebes Sea. They consist of discontinuous belts of Miocene sedimentary strata, intrusive andesite porphyry and basalt which have been tilted and block

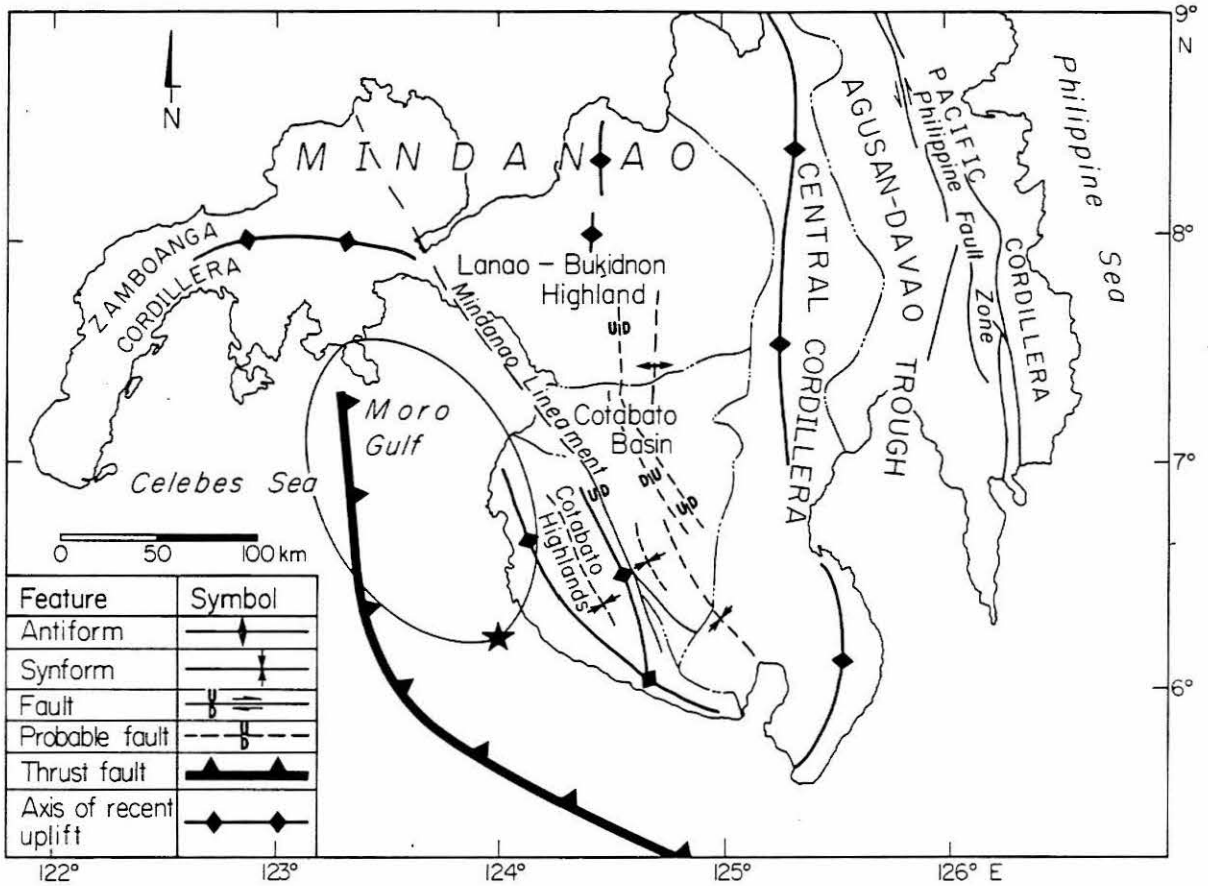

Figure 3-10. A schematic tectonic map of Mindanao, indicating the major features of the island. Note that the structures in the eastern part of Mindanao lie parallel to the Philippine Trench, i.e., in a north-south direction, while those in southern Mindanao, trend north-northwest, an influence of the northeast dipping subduction zone shown on the map. The star and ellipse represent the mainshock and aftershock pattern locations respectively, for the Philippine earthquake.

faulted along north-northwest trending faults. Terraced shorelines, steep mountain fronts, deeply dissected fluvial terrace deposits and hour-glass valleys imply recent uplifting of the Highlands region (Ranneft, et al., 1960).

The 1976 Philippine earthquake occurred in the Moro Gulf, directly west of the Cotabato Highlands, at the edge of the Celebes Sea. It is shown here that it represented thrust movement on a fault plane dipping, at a shallow angle, to the northeast, toward the Cotabato Highlands block. Thus the 1976 event may contribute to the Pleistocene and Recent pattern of uplift in the Cotabato Highlands and to the subduction of the Celebes Sea floor beneath the island of Mindanao.

CONCLUSIONS

The source mechanism of the August 16, 1976, Philippine earthquake is oblique thrust, with the fault plane dipping to the northeast (strike N 33°W, dip 22° and rake +68°, see Figure 3-2). The seismic moment, M_o = 1.9 x 10^{28} dyne-cm, is calculated from long-period multiple surface wave data, after accounting for the directivity of the source rupture by propagating the rupture unilaterally a distance of 160 km in an azimuth of 300° from the mainshock hypocenter, with a rupture velocity of 2.5 km/sec.

The occurrence of the largest aftershock (M_S = 6.8), a pure strike-slip event, at the northwest end of the aftershock zone, introduces additional complexity to the rupture process of the Philippine earthquake. This event, which occurred twelve hours after

the mainshock, had a pure strike-slip mechanism and most likely represents tear faulting along the northwest edge of the fault plane, as a result of the main event. The left-lateral sense of motion along its east-northeast trending nodal plane is consistent with this interpretation.

The source parameters cited above imply that significant tectonic deformation, predominantly thrusting to the northeast, occurred in this region at the time of the earthquake. Bathymetric data, as well as seismic reflection profile data, and the event's epicenter argue for the source of this event being along a relatively new (Oligocene or younger, Heezen and Fornari, 1975) and developing subduction zone boundary, located in the Moro Gulf region, between N. Celebes Basin and the island of Mindanao.

3.3 Aftershocks of the Great Chilean Earthquake of May 22, 1960.

ABSTRACT

Anomalous earthquakes such as creep events, tsunami earthquakes and silent earthquakes have been reported in the recent literature. In this section an anomalous "slow earthquake" that occurred on June 6, 1960 in southern Chile is discussed. Although the surface wave magnitude of this event is only 6.9, it excited anomalously large long-period multiple surface waves with a seismic moment of 5.6×10^{27} dyne-cm. The Benioff long-period seismogram of this earthquake recorded at Pasadena shows an extremely long, about 1.5 to 2 hour coda of Rayleigh waves, with a period of 10 to 25 sec. The coda length for other events with a comparable magnitude which occurred in the same region is about 10 minutes. This observation suggests that the long coda length is due to a long source rupture process which lasted at least 1 hour. Although at least 15 distinct events can be identified in the coda, no short-period body waves were recorded corresponding to these, except for the first one. These results suggest that a relatively small ($M_s \sim 6.9$) earthquake triggered a series of slow events; the duration of the whole sequence being longer than 1 hour. This aftershock appears to have a poorly constrained strike-slip mechanism, somewhat unusual considering that the Chile mainshock was a shallow dipping thrust event. This event probably occurred on a transform fault on the extension of the Chile Rise and provides important information regarding the nature of the transform fault.

INTRODUCTION

The duration of the energy release at an earthquake source is usually considered to be of the order of the source dimension (e.g., fault length) divided by the rupture velocity. Even for the largest earthquakes, this time constant is only several minutes. However, there are a number of exceptions. The creep events in central California (Tocher, 1960; Nason, 1971; King et al., 1973), often have time constants of several minutes or longer. For the 1960 Chilean earthquake, a slow precursory deformation with a time constant of 10 to 20 minutes was suggested (Kanamori and Cipar, 1974; Kanamori and Anderson, 1975a). Several earthquakes, called tsunami earthquakes, generate tsunamis with an amplitude disproportionately large for their earthquake magnitude, suggesting that the associated crustal deformation has a long time constant (Kanamori, 1972; Fukao and Furumoto, 1975; Shimazaki and Geller, 1977). Dziewonski and Gilbert (1974) suggested that the 1970 Colombian deep focus earthquake involved slow deformation. Nagamune (1977) reported evidence for slow crustal deformation associated with the May 29, 1976 Yunnan earthquake in China.

This section presents another example of an anomalous earthquake, the source process of which lasted for more than one hour. Because of the limited quality and quantity of the data, it was not possible to constrain the details of the mechanism of this earthquake, but the observed seismograms show extremely unusual characteristics so that the evidence for the anomalous nature of this event appears definitive.

ANALYSIS AND RESULTS

An earthquake with a magnitude M_s = 6.9 (Rothé, 1969; M_s at Pasadena is 6.75) occurred on June 6, 1960 near the southern end of the aftershock zone of the 1960 Great Chilean earthquake (Figure 3-11; origin time: $05^h\ 55^m\ 44^s$; latitude: 45.5°S; longitude: 73.5°W; and depth: normal). This earthquake is anomalous in two respects. First, long-period Rayleigh and Love waves recorded by the Press-Ewing (30-100) seismographs at Pasadena, California and Ruth, Nevada, were anomalously large (Figure 3-12). The amplitude of multiple surface waves was comparable to what is normally observed for an earthquake with $M_s \geq 8.0$. Second, short-period (10 to 20 sec) Rayleigh waves recorded by a broad-band seismograph (Benioff 1-90) at Pasadena showed an anomalously long duration, about 2 hours. Propagation effects, such as multi-pathing and lateral refractions and reflections can cause a prolonged wave train of short-period surface waves; however, as will be shown later, other events with a comparable M_s in the same area did not show such a long wave train, and so propagation effects are unlikely to be the cause of the long duration.

Unfortunately, the mechanism of this earthquake could not be constrained very well. Figure 3-13 shows the P-wave first-motion data taken from the ISC bulletin. Stations at the distance range $20^\circ < \Delta < 90^\circ$ are included. Although the data are incomplete, it is evident that, if all the readings are correct, the stations cannot be separated into four quadrants consistent with a double couple. However, the

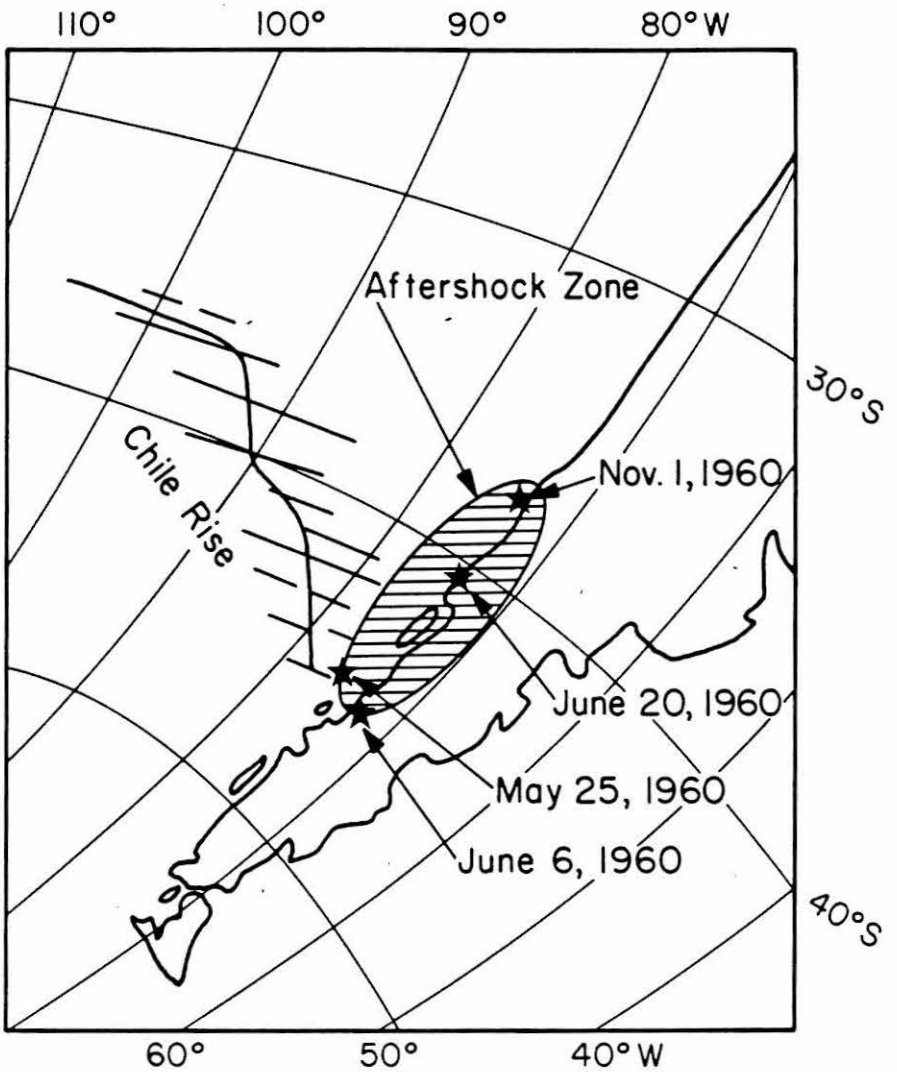

Figure 3-11. Map of southern tip of South America showing the aftershock zone of the May 22, 1960 Chilean earthquake. The stars indicate the locations of the events discussed in this section. Note the locations of the May 25 and June 6 events in relation to the geometry of the Chile Rise transform fault system.

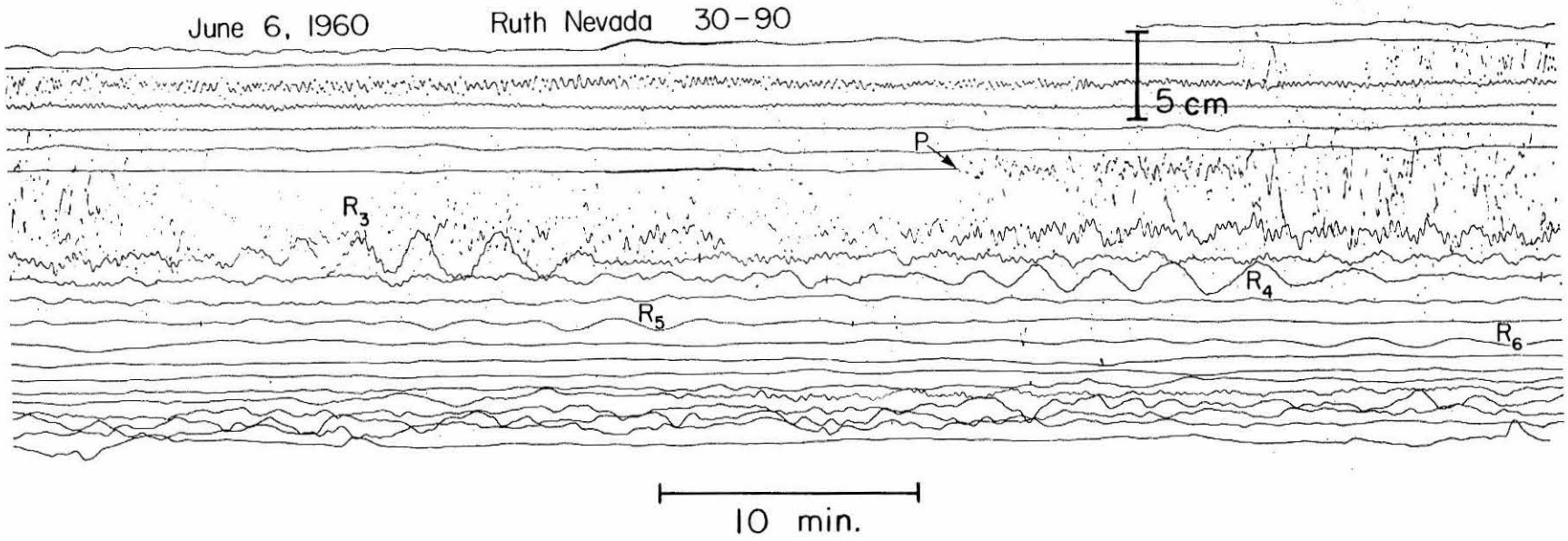

Figure 3-12. Vertical Press-Ewing seismograph recording of the June 6, 1960 Chilean aftershock recorded at Ruth, Nevada. Note the large amplitude of Rayleigh waves R_3 through R_6.

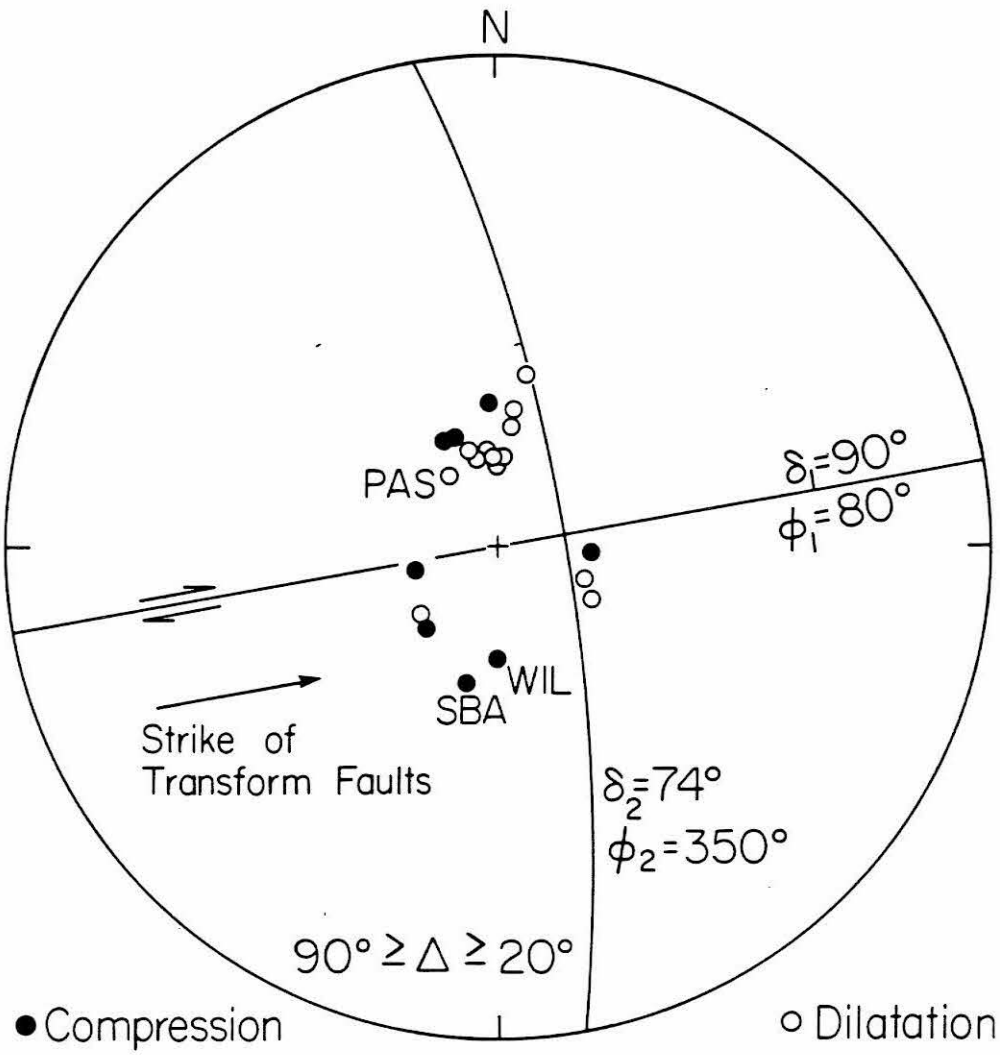

Figure 3-13. The P-wave first-motion data for the June 6, 1960 Chilean aftershock, indicating right-lateral strike-slip motion on the preferred fault striking N 80°E. A stereographic projection of the lower focal hemisphere is shown. Readings are taken from the International Seismological Summary (ISS) and are in the distance range of 20° to 90°.

first-motion data reported in the ISC bulletin usually include some unreliable readings. It is noted that most U. S. stations in the NW quadrant show dilatational first-motions. All the stations in the SW quadrant (Wilkes, Scott Base, Roxburgh and Afiamalu) except one station (Château) have compressional first-motions. These results suggest that the pattern shown in Figure 3-13 is not consistent with the east-dipping, low-angle thrust faulting of the mainshock of the 1960 Chilean earthquake (Ben-Menahem, 1971; Kanamori and Cipar, 1974). As shown in Figure 3-11, the location of this event is at the southern end of the aftershock zone of the 1960 event and on the eastern extension of one of the transform faults of the Chile Rise system. As shown in Figure 3-13, one fault plane can be drawn parallel to the local strike of the transform fault system, dividing the dilatational U. S. stations and the compressional stations in the SW quadrant. Then the other nodal line may be drawn as shown in Figure 3-13. Although this solution is poorly constrained and somewhat arbitrary, it is preferred because it matches the geometry of the ridge-transform fault system in the area. As will be shown later, this mechanism is also consistent with the observed amplitude ratio of Love to Rayleigh waves. However, this event is a complex multiple event with a relatively small emergent first event, and the mechanism determined from the P-wave first-motion data may not be particularly significant anyway.

The seismic moment of this earthquake was determined from multiple surface waves R_3, R_4 and G_4 recorded at Pasadena, California, and R_3 and R_4 recorded at Ruth, Nevada. Synthetic seismograms were computed for

the mechanism shown in Figure 3-13. The method is described in Kanamori (1970). A point source was assumed at the depth of 33 km and a step source time function was used. By matching the amplitude, the seismic moments were determined as shown in Table 3-1. An average of 5.6×10^{27} dyne-cm was obtained.

The good agreement of the results obtained from the Love and Rayleigh waves at Pasadena suggests that the mechanism shown in Figure 3-13 is reasonable. Figure 3-14 compares the observed R_3 and R_4 recorded at Ruth with the synthetic ones. It is interesting to note that the amplitude of the short-period (<100 sec) Rayleigh waves of the observed record is smaller than that of the synthetics. This discrepancy may reflect the slow source process of this earthquake, though quantitative analysis is not possible because of the uncertainty in the depth of this event. As shown in Figure 3-15, the seismic moment, M_o, of this earthquake is about one and a half orders of magnitude larger than that of other earthquakes with a comparable M_s, indicating that the source process of this event is anomalously slow.

Because of the uncertainty in the mechanism, the value of the seismic moment itself is somewhat uncertain. However, since the mechanism used here is the one that places Pasadena and Ruth in the direction of the maximum radiation of Rayleigh waves (note the azimuth of PAS in Figure 3-13), the present estimate of the seismic moment is probably the lower bound. Other mechanisms, with the constraint that they give rise to the correct Love to Rayleigh wave ratio at Pasadena, would give an even larger value of the seismic moment. Thus the

Table 3-1 Determination of Seismic Moment

$\phi_1 = 80^\circ$, $\delta_1 = 90^\circ$ $\lambda_1 = 196^\circ$

STATION	Δ (deg.)	ϕ_{ES} (deg.)	ϕ_{SE} (deg.)	Phase	Obs. PP	Syn. PP*	M_o^+
Pasadena	89.33	324.0	150.2	R_3	1.7 cm	0.41 cm	4.2
				R_4	1.1	0.21	5.3
				G_3	3.8	1.9	2.0
				G_4	2.8	0.7	4.0
Ruth	92.55	328.7	152.1	R_3	2.7	0.34	7.9
				R_4	1.8	0.18	10.0
						$\bar{M}_o^+$ =	(5.6 ± 2.9)

Δ is the epicentral distance.

ϕ_{ES} is the azimuth of the station from the epicenter.

ϕ_{SE} is the azimuth of the epicenter from the station.

* amplitude in cm. for $M_o = 10^{27}$ dyme-cm.

+ the units of M_o are x 10^{27} dyne-cm.

R_3, R_4 multiple Rayleigh wave used.

G_3, G_4 multiple Love waves used.

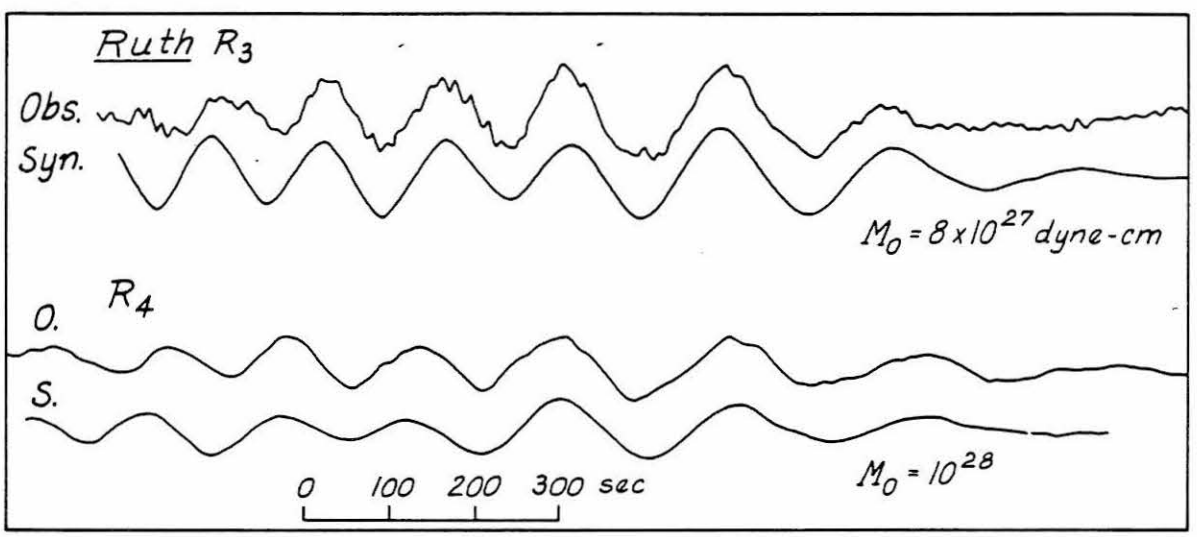

Figure 3-14. Comparison of observed and synthetic R_3 and R_4 Rayleigh waves at Ruth, Nevada. The seismic moment, M_o, is calculated by comparing the amplitude of the synthetic with the observed trace.

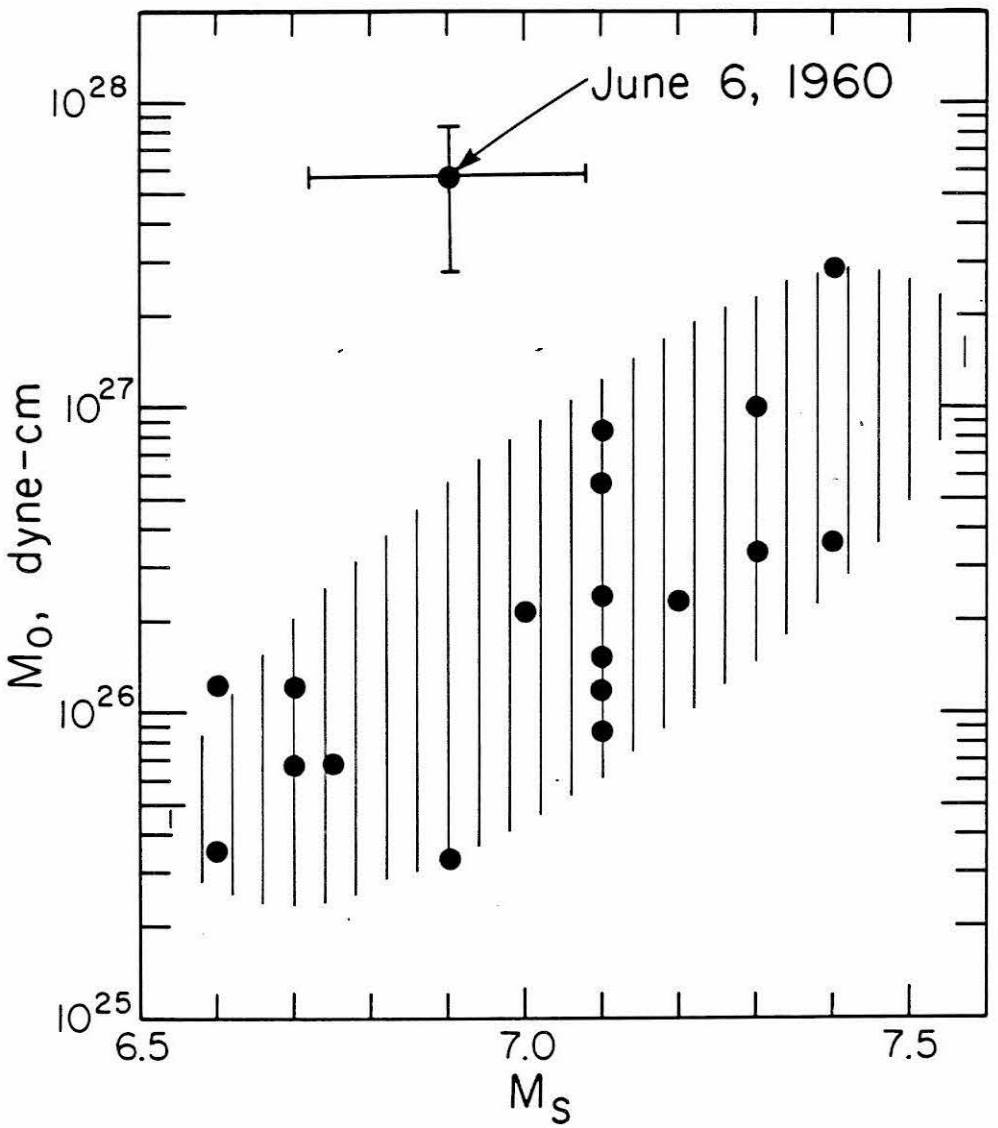

Figure 3-15. A plot of seismic moment, M_o, versus surface wave magnitude, M_s, for the June 6, 1960 Chilean aftershock. The plot shows that this event has much larger seismic moment than other events of similar surface wave magnitude (hatched area). Solid dots are data taken from Table 1 of Kanamori and Anderson (1975b).

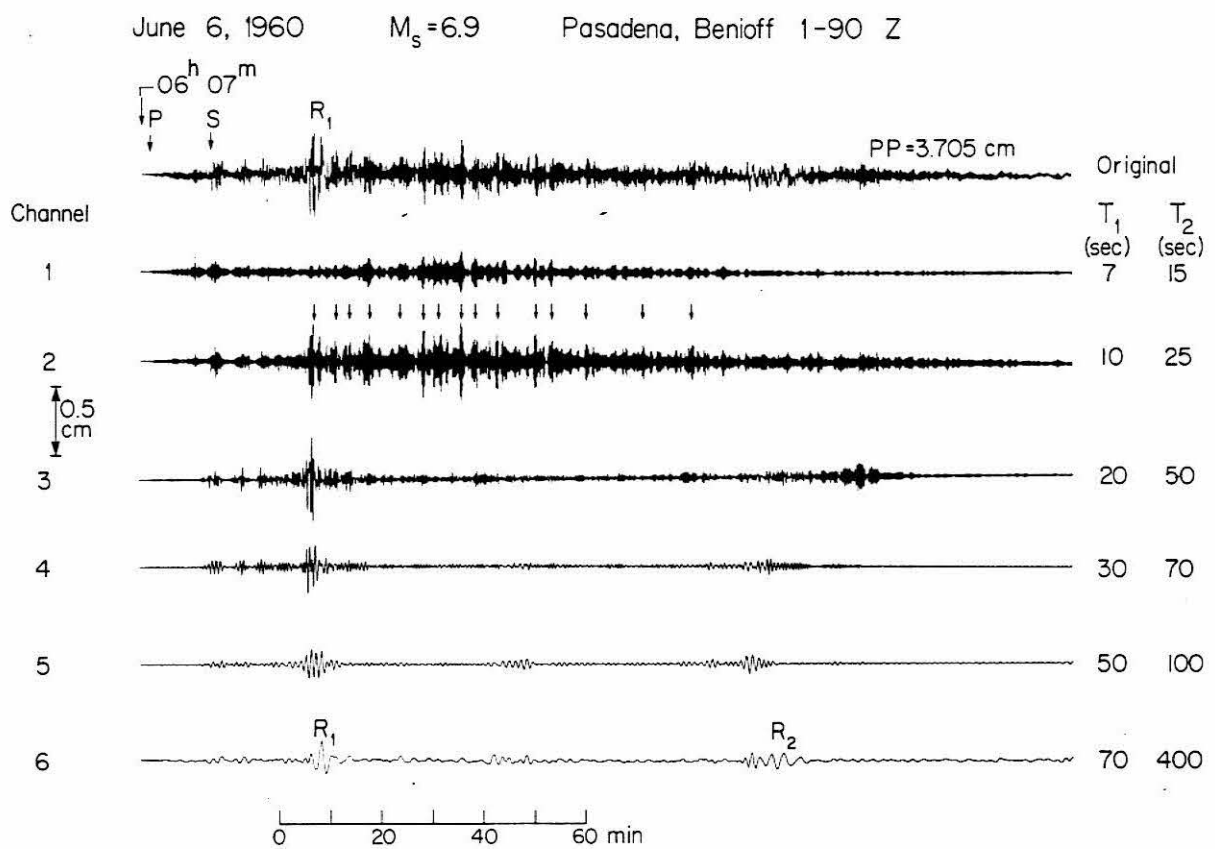

Figure 3-16. A plot of the original Pasadena long-period vertical Benioff seismograph recording of the June 6, 1960 Chilean aftershock (upper trace) and six band-pass filtered channel recordings of this record. The pass bands are given as T_1 and T_2 in seconds for each channel. Note the large amplitude long-period energy of R_1 and R_2 on channel 6. The arrows on channel 2 represent 15 multiple events with M_s ranging from 6.5 to 7.0.

disparity shown in Figure 3-15 would remain true despite the uncertainty in the mechanism.

The anomalous character of the June 6 event is further demonstrated by short-period Rayleigh waves recorded by the Benioff 1-90 seismograph at Pasadena. Figure 3-16 shows the unfiltered Benioff 1-90 seismogram together with band-pass filtered seismograms. A Gaussian band-pass filter given by:

$$F(\omega) = \exp\left[\frac{-4}{(\omega_1 - \omega_2)^2}\left(\omega - \frac{\omega_1 + \omega_2}{2}\right)^2\right]$$

is used, where ω is the angular frequency, and $(\omega_1 + \omega_2)/2$ is the central angular frequency. The two periods $T_1 = 2\pi/\omega_1$ and $T_2 = 2\pi/\omega_2$ determine the pass band. The trace on channel 2 which represents the energy at the period of about 20 sec (T_1 = 10 sec, T_2 = 25 sec) shows an extremely complex wave train. The coda length is at least 1.5 hours. It is also notable that this earthquake has a substantial amount of energy on channel 6 which has a pass band from 70 to 400 sec. The long-period Rayleigh waves R_1 and R_2 are clearly recorded.

The long coda length could be due to propagation effects such as multi-pathing, lateral refractions and reflections. However, this possibility can be eliminated by comparing this event with other events that have occurred in the same area. Figure 3-17 shows the seismograms of an event (M_s = 7.0) which occurred on June 20, 1960, at a location about 550 km to the north of the June 6 event (see Figure 3-11). The

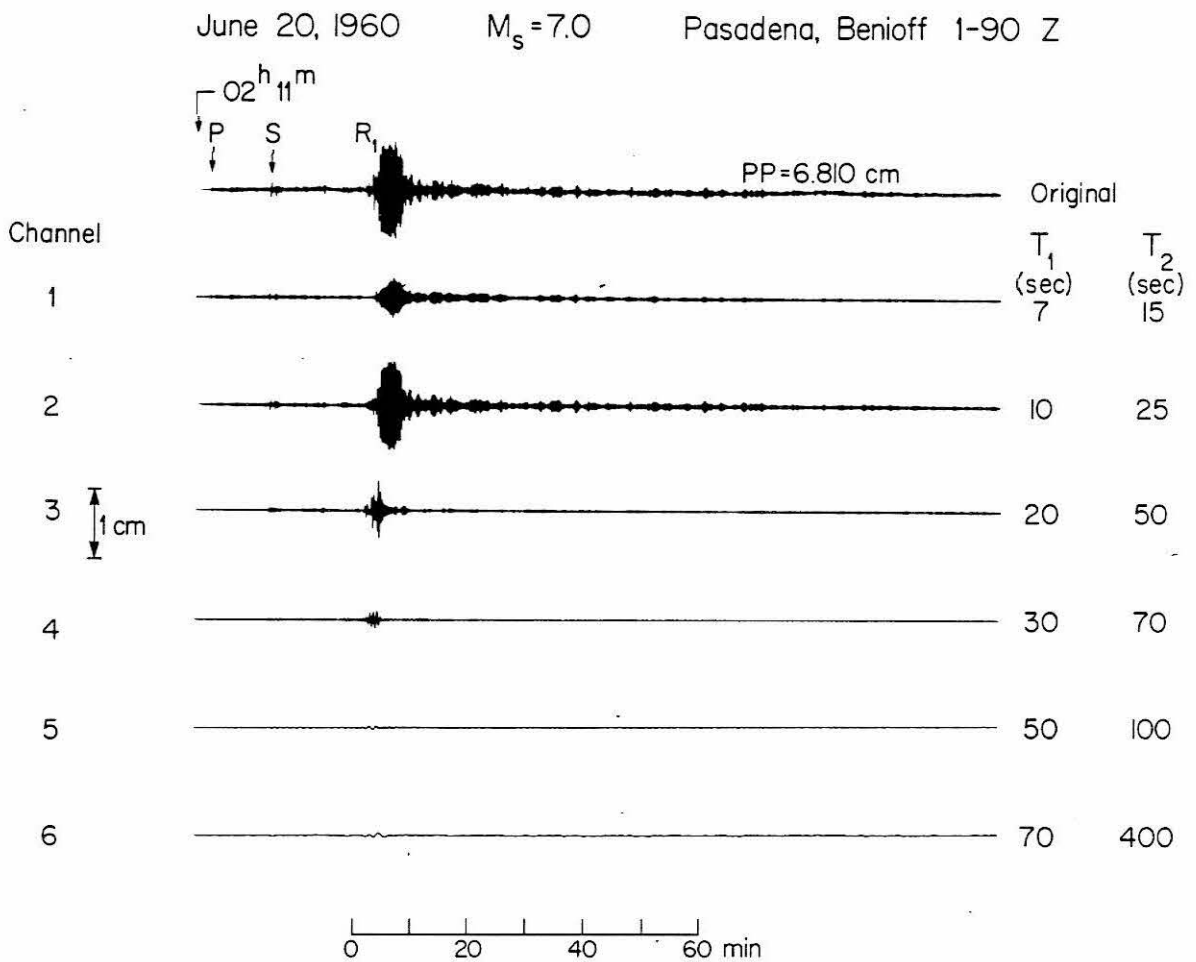

Figure 3-17. A plot of the original Pasadena long-period vertical Benioff seismograph recording of the June 20, 1960 Chilean aftershock (upper trace) and six band-pass filtered channel recordings of this record. The pass bands are given as T_1 and T_2 in seconds for each channel. Note the low amplitude of the long-period energy in channel 6.

same band-pass filter as that used for the June 6 event was applied to this event. The coda length of 20 sec Rayleigh waves (channel 2) is about 5 minutes and the energy contained in other channels is very small. Figure 3-18 shows another event (M_s = 7.2, November 1, 1960) which is very similar to the June 20 event. If the observed complexity of the June 6 event is due to the path effect, a similar complexity should be observed for other events in the same region which have approximately the same path. Thus, it is concluded that the complexity is due to the source. This earthquake is probably a complex multiple event and the short-period (about 20 sec) Rayleigh waves originating from the individual events appear as a distinct wave train as marked by arrows in Figure 3-16, channel 2. Because of the very complex waveform, the identification of the individual events cannot be made unambiguously. The assignment of arrows in Figure 3-16 is therefore only qualitative, but it is evident that there are at least 15 events with M_s ranging from 6.5 to 7. It is important to note that this event is different from ordinary multiple shocks in the following respect. The individual events of this multiple shock sequence, except the first one, do not show body-wave signals such as P and S-waves on short-period seismograms recorded at Pasadena, indicating that the source process of these events was rather slow. The first event has pronounced long-period (200 to 300 sec) energy indicating that it is a larger slow event. The total duration of the source process is at least 1.5 hours which is much longer than that of ordinary multiple shocks. The seismograms of this event recorded at De Bilt ($\Delta = 118.3^{\circ}$, $\phi_{ES} = 43.4^{\circ}$)

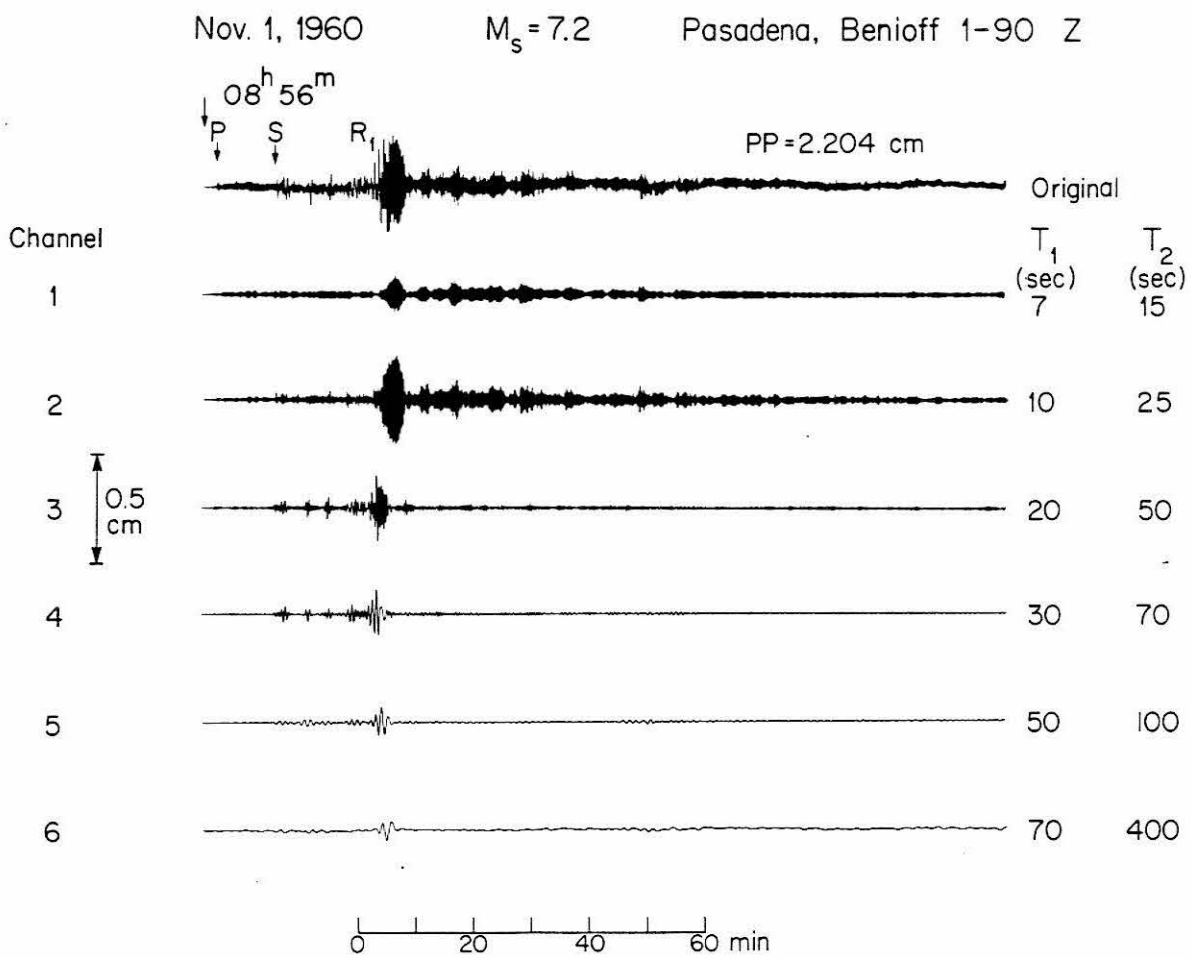

Figure 3-18. A plot of the original Pasadena long-period vertical Benioff seismograph recording of the November 1, 1960 Chilean aftershock (upper trace) and six band-pass filtered channel recordings of this record. The pass bands are given as T_1 and T_2 in seconds for each channel. Note the low amplitude of the long-period energy on channel 6.

and Tsukuba (Δ = 153.1°, ϕ_{ES} = 261.7°) also indicate the very complex nature of this event.

Another earthquake which occurred on May 25, 1960 in the immediate vicinity of the June 6 event shows complexity somewhat similar to that of the June 6 event, though to a much lesser extent (Figure 3-19). It is possible that this event has source characteristics intermediate between the slow event and the ordinary events.

Figure 3-20 compares the band-pass filtered records at 20 sec period (channel 2) for the four events studied in this paper. Although the above discussion is somewhat qualitative, the difference is so remarkable that the evidence for an anomalous slow event appears to be definitive.

CONCLUSIONS AND DISCUSSION

On the basis of the large amplitude of long-period surface waves and the complexity of the short-period Rayleigh wave coda, it is concluded that this earthquake consists of about 15 slow events with M_s ranging from 6.5 to 7, triggered by an event with $M_s \simeq 6.9$ which itself involved very slow motion. The spatial distribution of these slow events could not be determined, but the overall time history of the displacement at the source is schematically shown in Figure 3-21. The body waves were generated at the very beginning of the sequence. This relatively sharp onset was followed by a slow displacement with a time constant of at least 200 to 300 sec which gave rise to the long-period surface waves. This slow motion was then followed by a sequence of slow

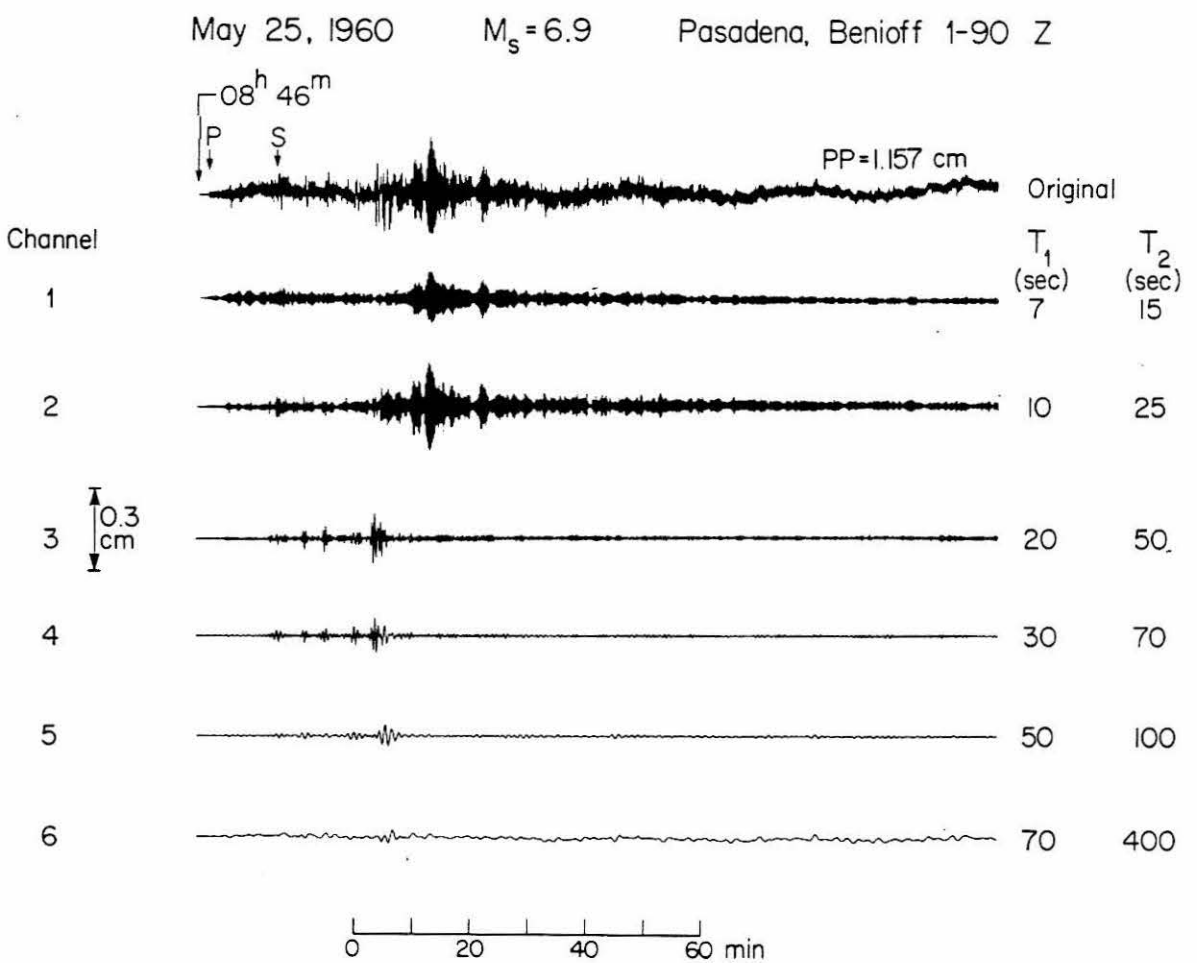

Figure 3-19. A plot of the original Pasadena long-period vertical Benioff seismograph recording of the May 25, 1960 Chilean aftershock (upper trace) and six band-pass filtered channel recordings of this record. The pass bands are given as T_1 and T_2 in seconds for each channel. Note the low amplitude of the long-period energy on channel 6.

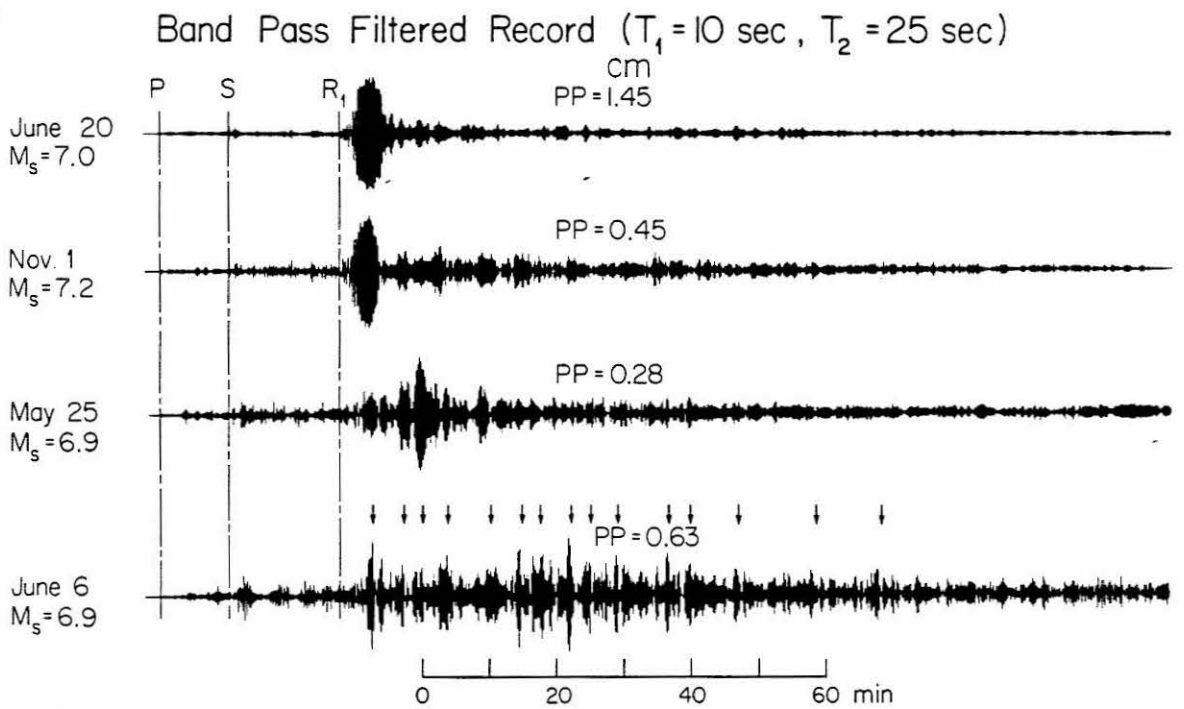

Figure 3-20. A comparison of the Chilean aftershocks discussed in this study. Band-pass filtered records (channel 2 of Figures 3-16 to 3-19) are shown for each event. Note the greater complexity shown in the traces of the June 6 event and to a lesser extent the May 25 event, compared with the others.

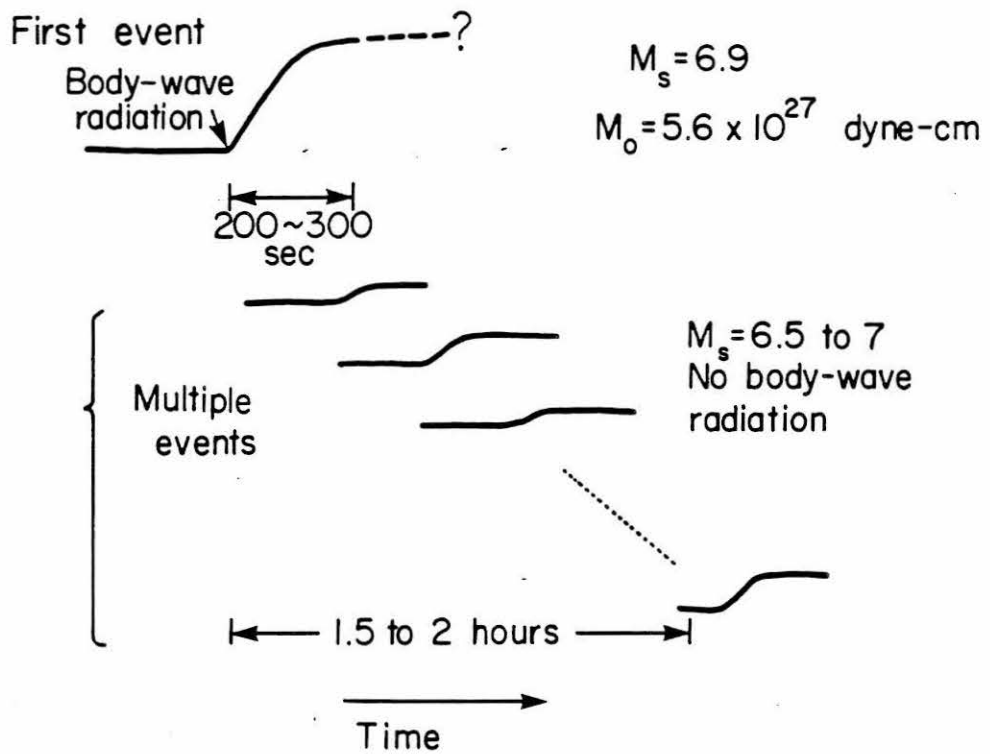

Figure 3-21. A schematic figure illustrating the time history of the displacement at the source for the June 6, 1960 Chilean aftershock.

events which spread out over a time period of 1.5 to 2 hours.

If the mechanism shown by Figure 3-13 is representative of the entire sequence, this earthquake may represent a relative motion between the subducted Nazca plate and the Antarctic plate, as schematically shown in Figure 3-22. Chung and Kanamori (1978) reported a very complex strike-slip event, which is similar to the June 6, 1960 event, along the subducted part of the D'Entre Casteaux Fracture Zone in the New Hebrides arc.

Detailed studies of this kind of anomalous events are important for understanding the constitutive relation of the material in the fault zone and the triggering mechanism of earthquakes under crustal pressure-temperature conditions.

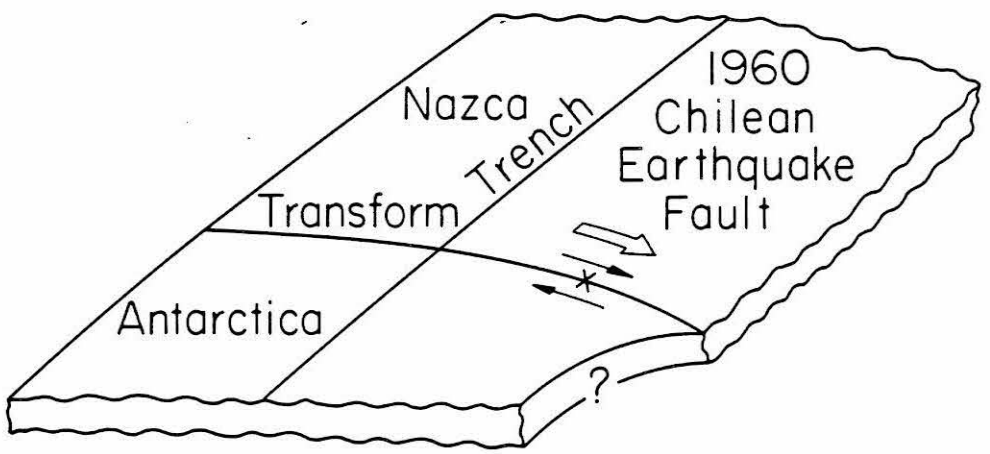

Figure 3-22. A schematic figure showing the location of the June 6, 1960 Chilean aftershock (X) in relation to the plate geometry and subduction beneath South America. The event lies on the easterly extension of the Chile Rise transform fault system.

3.4 The July 27, 1976 Tangshan, China Earthquake: A Complex Sequence of Intraplate Events.

ABSTRACT

The Tangshan earthquake (M_S = 7.7), of July 27, 1976 and its principal aftershock (M_S = 7.2), which occurred fifteen hours following the main event, resulted in the loss of life of over 650,000 persons in northeast China. This is the second greatest earthquake disaster in recorded history, following the 1556 Shensi Province, Chinese earthquake in which at least 830,000 persons lost their lives. Detailed analyses of the teleseismic surface waves and body waves are made for the Tangshan event. The major conclusions are: (1) The Tangshan earthquake sequence is a complex one, including strike-slip, thrust, and normal-fault events. (2) The mainshock, as determined from surface waves, occurred on a near vertical right-lateral strike-slip fault, striking N 40°E. (3) A seismic moment of 1.8 x 10^{27} dyne-cm is obtained. From the extent of the aftershock zone and relative location of the mainshock epicenter, symmetric (1:1) bilateral faulting with a total length of 140 km may be inferred. If a fault width of 15 km is assumed, the average offset is estimated to be 2.7 meters with an average stress drop of about 30 bars. (4) The mainshock was initiated by an event with a relatively slow onset and a seismic moment of 4 x 10^{26} dyne-cm. The preferred fault plane solution, determined from surface wave analyses, indicates a strike 220°, dip 80°, and rake -175°. (5) Two thrust events follow the strike-slip event by 11 and 19 seconds respectively. They

are located south-southwest of the initial event and have a total moment of 8 x 10^{25} dyne-cm. This sequence is followed by several more events. (6) The principal aftershock was a normal fault double event with the fault planes unconstrained by the P-wave first-motions. Surface waves provide additional constraints to the mechanism to yield an oblique slip solution with strike N 120°E, dip 45°SW, and rake -30°. A total moment of 8 x 10^{26} dyne-cm is obtained. (7) The triggering of lesser thrust and normal faults by a large strike-slip event in the Tangshan sequence has important consequences in the assessment of earthquake hazard in other complex strike-slip systems like the San Andreas.

INTRODUCTION

The Tangshan earthquake which occurred in northeast China on July 27, 1976 -- origin time $19^h\ 42^m\ 54.6^s$ U.T.; location 39.6°N, 118.0°E (U.S.G.S.); M_s = 7.7; m_b = 6.3 (U.S.G.S.) -- stands in terms of loss of life as the greatest earthquake disaster of modern times. The Times (London) reported on January 6, 1977 an estimate from the People's Republic of China of over 650,000 killed. The city of Tangshan with a population of 1.6 million was virtually destroyed and extensive damage was suffered throughout the densely populated surrounding region. Indeed, Chairman Hua Kuo-Feng has said that the earthquake caused death and destruction on a scale "rarely seen in history" (The Times, January 6, 1977). Without diminishing the significance of this event in human terms, the Tangshan earthquake stands uniquely as the largest continental intraplate earthquake since the establishment of the

World-Wide Standardized Station Network (WWSSN). The availability of these data affords us a special opportunity to gain insight into the tectonic processes of this class of earthquake. This varied importance of the Tangshan earthquake sequence merits a detailed seismological study of its faulting mechanism. Some local and regional studies of this event have been published in the Chinese literature: Qiu Qun, 1976; Zhu Chuan-zhen et al., 1977; Guo Shunmin et al., 1977; Ding Wenjing, 1978; Chen Pei-shan et al., 1978. This section shall be primarily concerned with the following: (1) the analysis of available teleseismic data to obtain source parameters for the main event and principal aftershock; (2) the complexity of the earthquake sequence and its implications for intraplate earthquake processes; (3) reasons for the enormously high casualties and destruction.

In this study long-period surface waves are analyzed to constrain the overall faulting parameters and seismic moments of the mainshock and its principal aftershock. Teleseismic body waves are used to detail the faulting process. Japanese P-wave first-motions (Katsumata, personal communication, 1976), are incorporated to provide additional regional control.

SEISMOLOGICAL DATA

The location of the mainshock and the distribution of aftershocks are plotted in Figure 3-23. The open and closed circles indicate aftershocks occurring before and after, respectively, the principal aftershock. The main aftershock, an M_S = 7.2 event, occurred fifteen

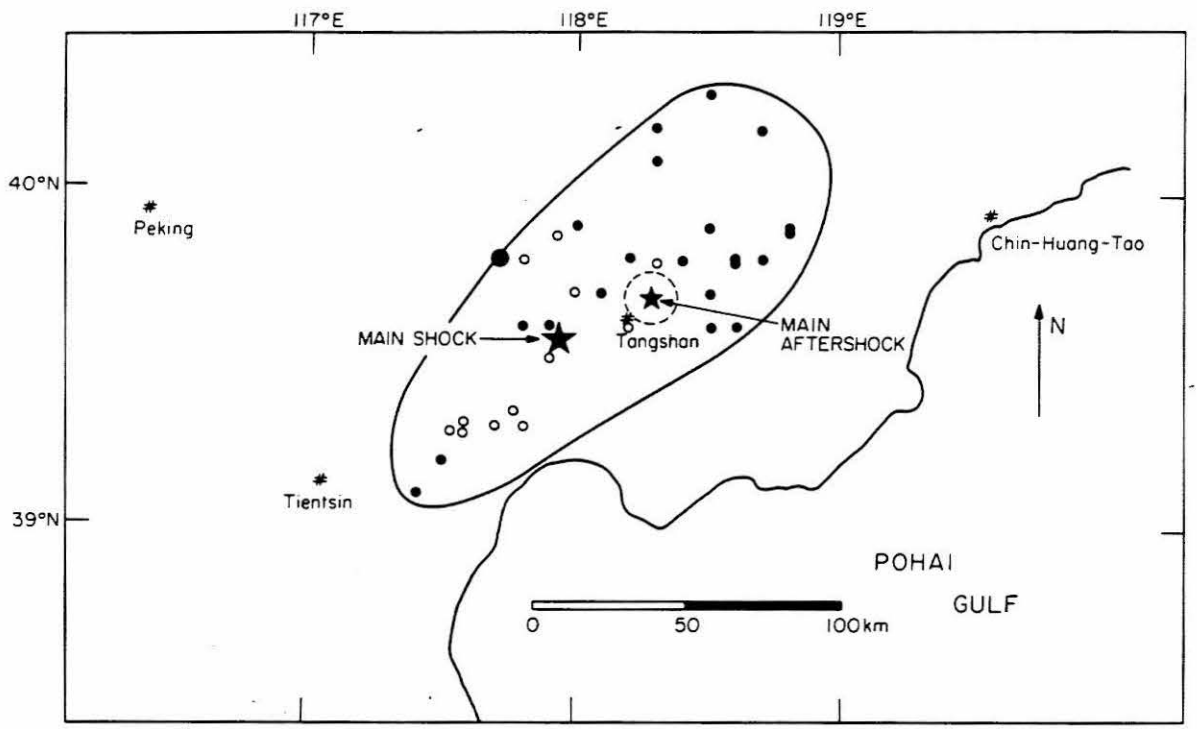

Figure 3-23. A map of the mainshock, main aftershock and other aftershock locations (U.S.G.S.). The open and closed circles are aftershocks which occurred before and after the principal aftershock, respectively.

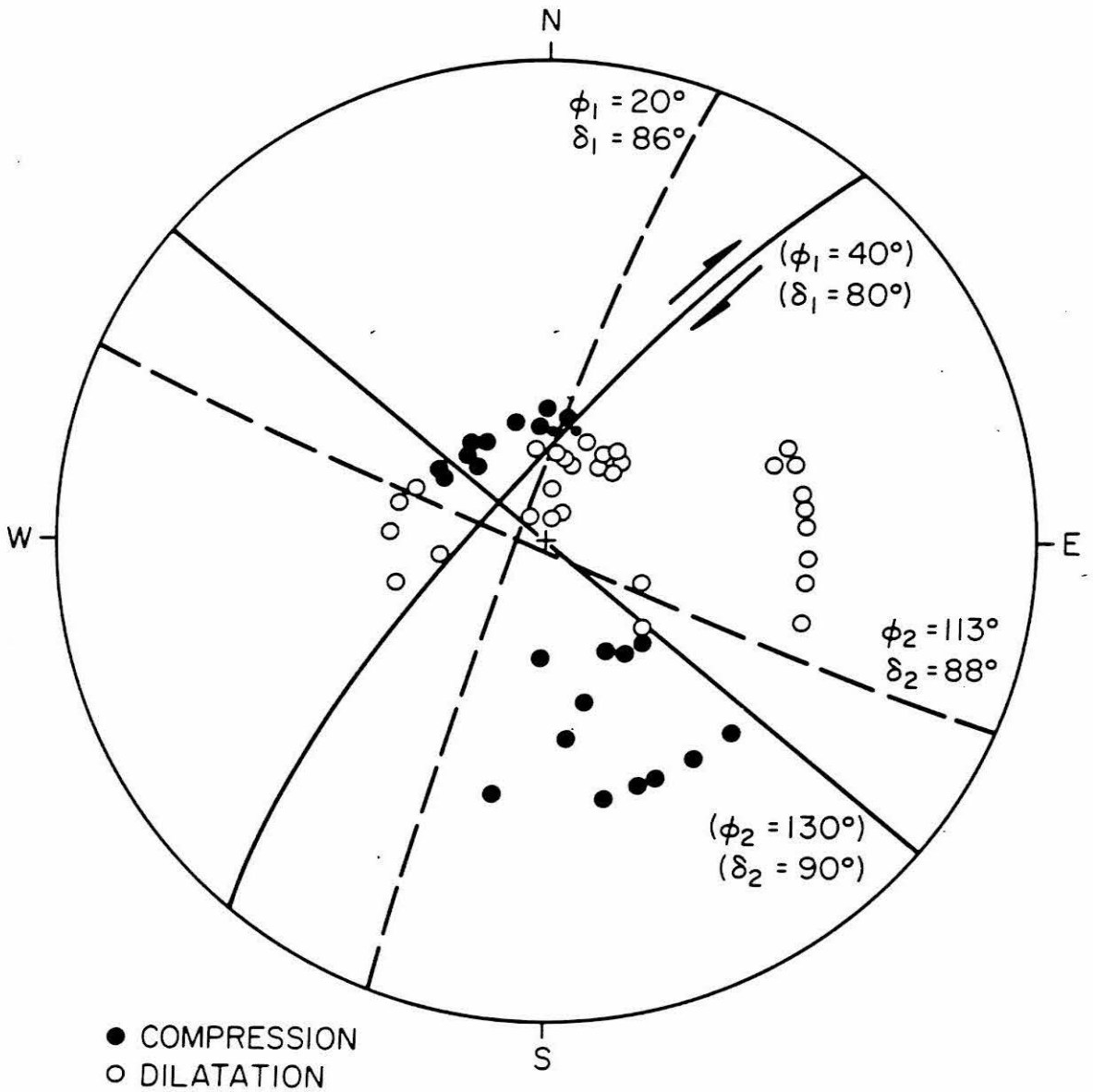

Figure 3-24. The P-wave first-motion data for the mainshock of the Tangshan earthquake sequence. The dashed lines indicate the preferred first-motion solution. The solid lines represent the best solution to the surface wave data. An equal-area projection of the lower focal hemisphere is shown. The arrows indicate right-lateral strike-slip motion of the preferred fault plane of N 40°E.

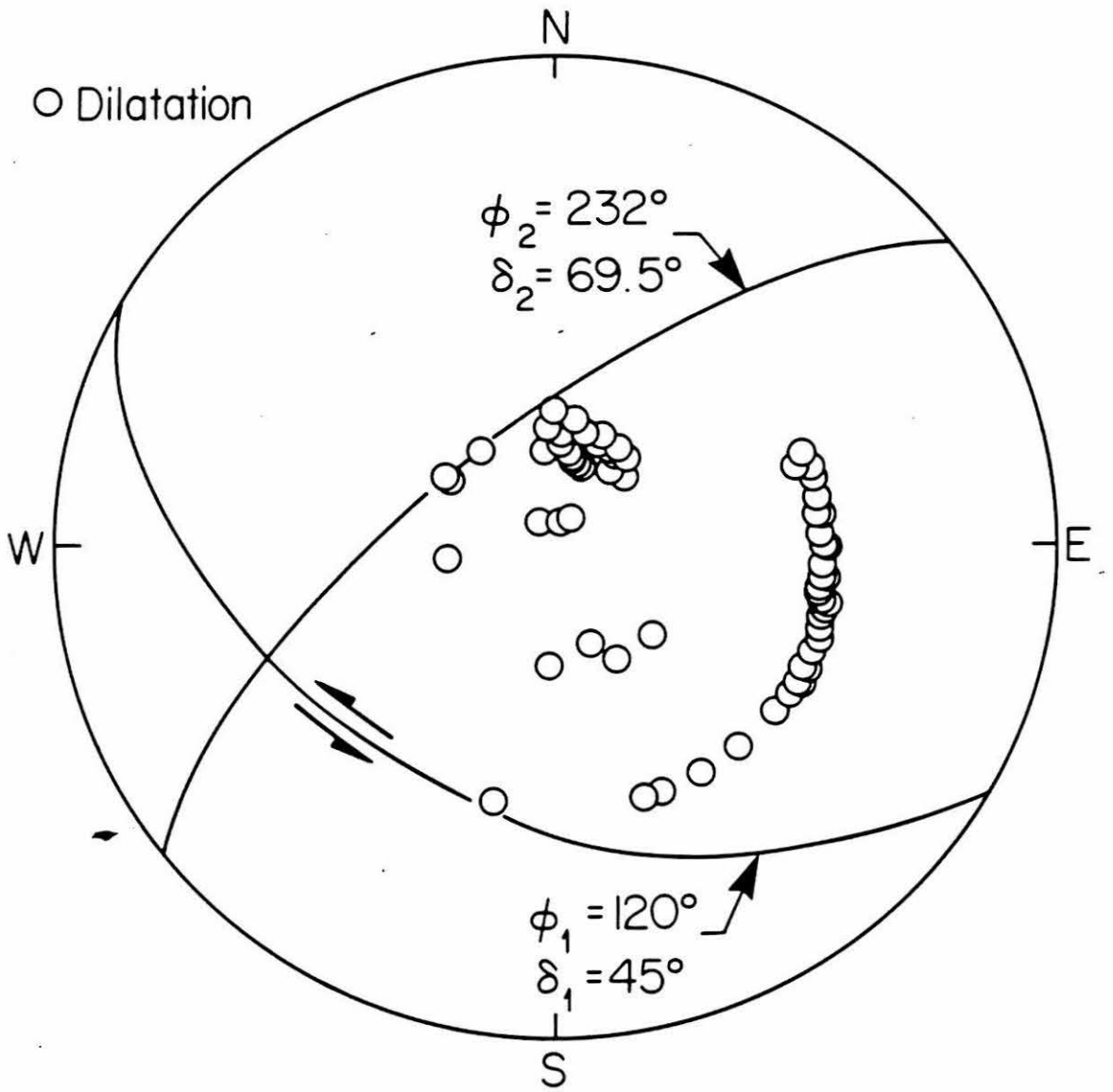

Figure 3-25. The P-wave first-motion data for the principal aftershock of the Tangshan sequence. All stations registered a dilatational arrival. The solution shown, constrained by the surface wave data, indicates oblique normal faulting.

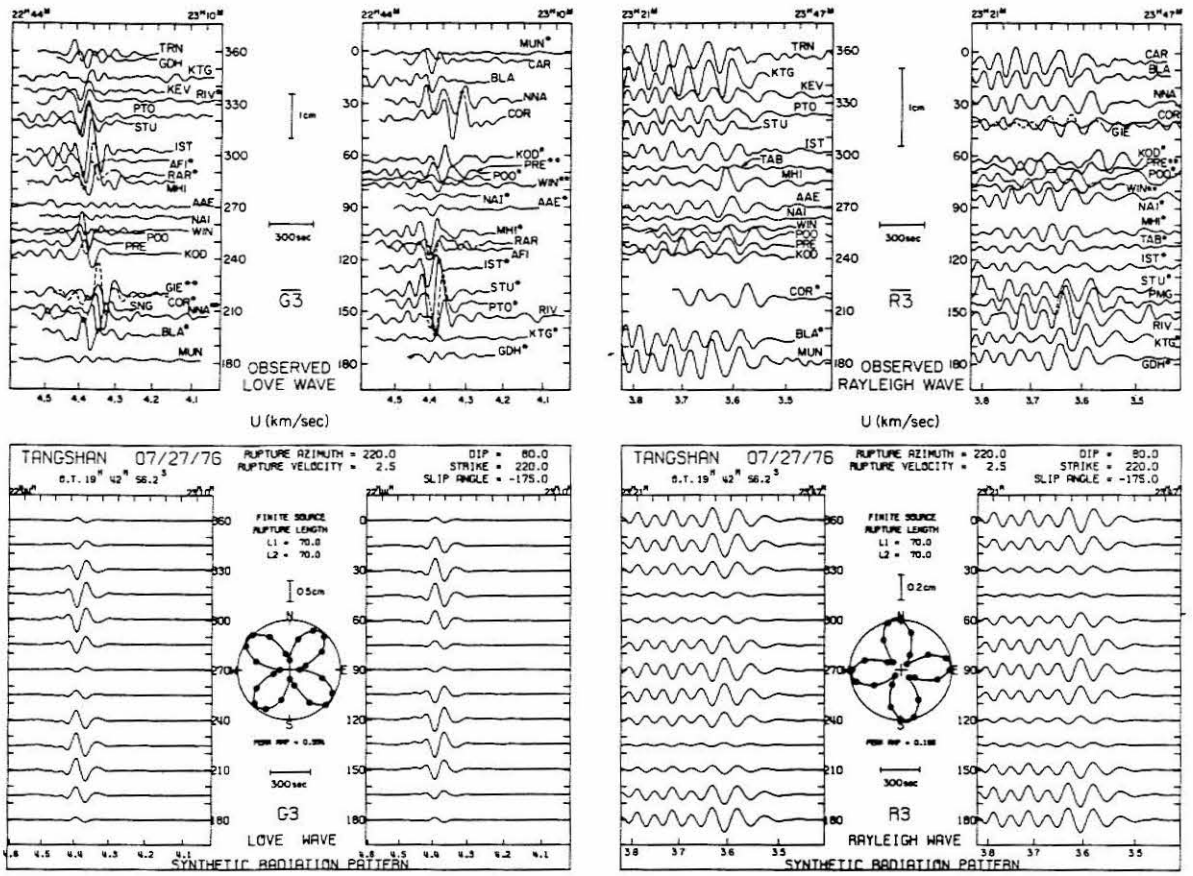

Figure 3-26. Azimuthal plots of equalized seismograms for $\bar{R}_3$ and $\bar{G}_3$ and synthetic seismograms computed for the mainshock of the Tangshan sequence. A seismic moment of 10^{27} dyne-cm is used in the synthesis. In the observed patterns one asterisk indicates that R_2 or G_2 data were equalized to R_3 or G_3 distances. Two asterisks indicate that R_4 or G_4 were equalized to R_3 or G_3 distances. The amplitude scale is for the trace amplitude on the WWSSN long-period instrument (15-100) with a magnification of 1500.

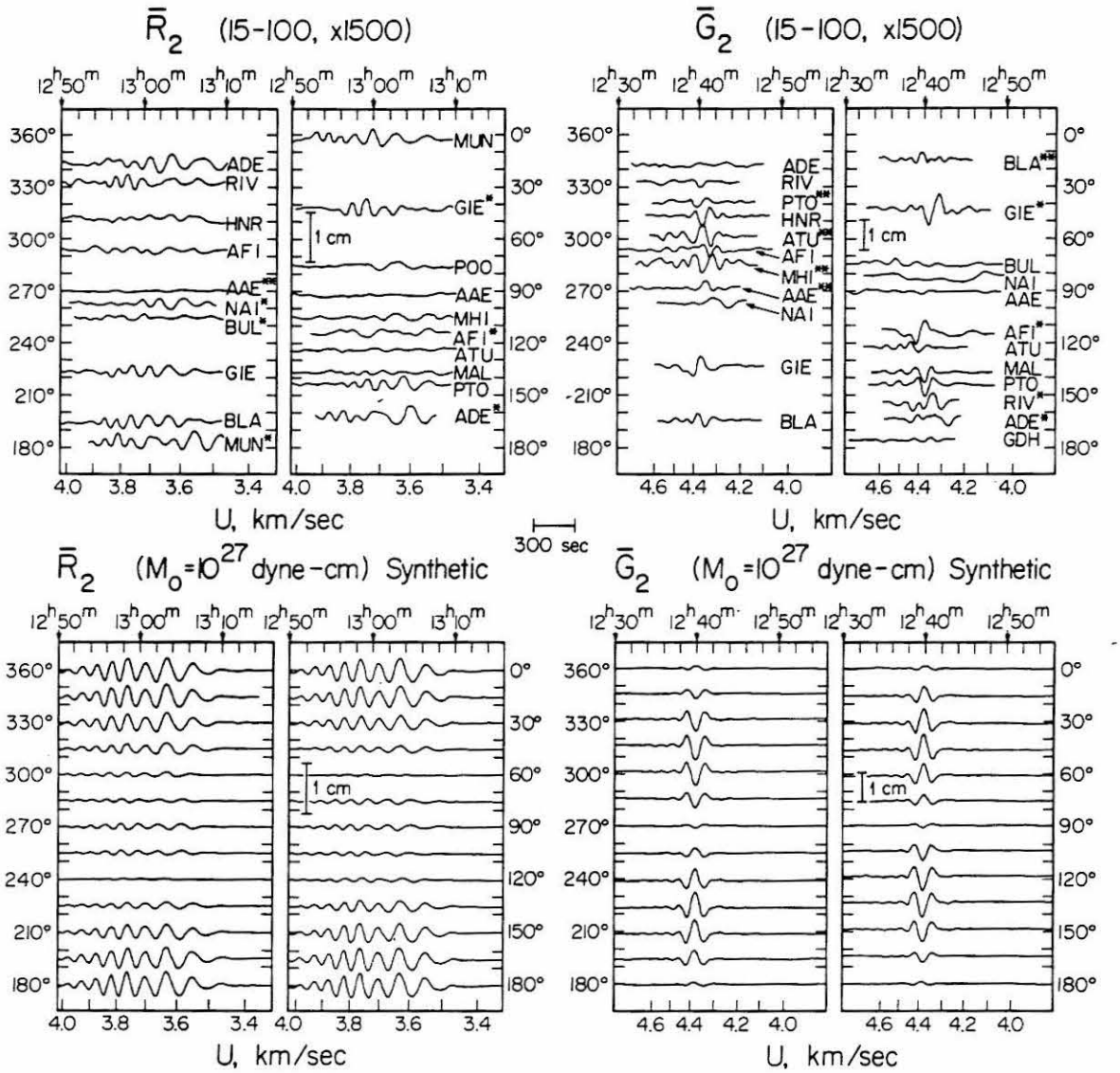

Figure 3-27. Azimuthal plots of equalized seismograms for $\bar{R}_2$ and $\bar{G}_2$ and synthetic seismograms computed for the principal aftershock of the Tangshan sequence. A seismic moment of 10^{27} dyne-cm is used in the synthesis. In the observed patterns one asterisk indicates that R_1 or G_1 data were equalized to R_2 or G_2 distances. Two asterisks indicate that R_3 or G_3 were equalized to R_2 or G_2 distances. The amplitude scale is for the trace amplitude on the WWSSN long-period instrument (15-100) with a magnification of 1500.

hours following the mainshock. Locations are taken from the U.S.G.S.

P-wave first-motion data for the main event are plotted in Figure 3-24. The dashed line solution is chosen to best constrain the first-motion data. The solid line solution represents the best solution to the surface wave data. The surface wave solution is more nearly consistent with the solution obtained by the local Chinese stations (Qiu Qun, 1976). First-motion data for the principal aftershock are plotted in Figure 3-25. As all stations are dilatational, there is no constraint to the normal fault solution from the P-wave first-motion data alone. The solution indicated is constrained by the surface wave analysis.

Figure 3-26 shows surface waves G_3 (Love waves) and R_3 (Rayleigh waves) for the mainshock recorded by WWSSN long-period seismographs and equalized to a propagation distance of $360^\circ + 90^\circ$. Surface waves G_2 and R_2 for the principal aftershock, equalized to a propagation distance of 270°, are shown in Figure 3-27. The equalization procedure is described by Kanamori (1970). As short-period ($T < 40$ seconds) surface waves are severely affected by structural heterogeneities during propagation, these waves are removed by using a filter described in Kanamori and Stewart (1976) with a short-period cut-off at 40 seconds and a long-period roll-off at 300 seconds. The Love and Rayleigh waves for the main event indicate a four-lobed radiation pattern which is consistent with a shallow strike-slip mechanism. However, from the nodal directions, a faulting orientation with a strike of N 40°E is preferred, slightly rotated with respect to the preferred P-wave

first-motion solution. This will be discussed in the body wave analysis section. For the major aftershock the surface wave radiation is consistent with a dip-slip faulting solution: a four-lobed Love wave and two-lobed Rayleigh wave pattern (see Kanamori, 1970). A strike of N 120°E may be inferred from the nodal directions of the surface waves. The location and strike of this event with respect to a local northwest-southeast trending structural boundary observed on the Tectonic Map of China (Geological Science Research Institute of China, 1975) is suggestive of a causal association.

SURFACE WAVE ANALYSIS

The general pattern of the surface wave radiation for the main event, as seen in Figure 3-26 is consistent with the strike-slip solution determined from P-wave first-motions, with the addition of a small rotation in strike. The geometry of the aftershock zone and the location of the epicenter suggest a northeast trending bilateral fault. Synthetic surface waves were computed for a double-couple at 16 km depth for a fault geometry with a strike 220°, dip 80°, and slip angle -175° (sign conventions are given in Kanamori and Stewart, 1976). The method of synthesis, the velocity and Q structure are described in Kanamori (1970) and Kanamori and Cipar (1974). To be consistent with the aftershock distribution, a small correction for fault finiteness is included assuming a symmetric bilateral rupture 140 km in length striking 220° with a rupture velocity of 2.5 km/sec (Ben-Menahem, 1961). The filter used on the observed data is also applied to the synthetics

to allow direct comparison. The computed synthetics are shown in Figure 3-26 beneath the observations. In Figure 3-28 the maximum trace amplitudes of the observed and synthetic records are compared. Using a seismic moment of 1.8×10^{27} dyne-cm, a quite satisfactory fit to the observations is obtained.

To model the surface waves for the principal aftershock, a double-couple is assumed at a depth of 16 km, striking N 120°E with a 45° dip. The slip angle is varied to find the best fit to the observed amplitude ratio between the Rayleigh and Love waves. A slip angle $\lambda = -30^{\circ}$ provides a satisfactory match. Although the effect is minor and probably not observable in the data, source finiteness is included for the sake of completeness to fit the relation of the principal aftershock's epicenter to the overall width of the Tangshan aftershock zone. A bilateral fault (35 km: 15 km) striking at 120° with a rupture velocity of 2.5 km/sec is assumed. Synthetic Rayleigh and Love waves are shown beneath the observations in Figure 3-27. The maximum trace amplitudes of the observations are compared in Figure 3-29 to the synthetics. Assuming a seismic moment of 8×10^{26} dyne-cm, a reasonably good fit is obtained.

Although details of the extent of faulting have not been released by the Chinese government, rough estimates of the average dislocation $\bar{D}$ and stress drop $\Delta\sigma$ may be made. A fault length L = 140 km for the main event can be assumed from the aftershock zone. The vertical extent w is unknown, but for illustrative purposes w = 15 km may be assumed. Under these assumptions we have $\bar{D} = M_o/\mu Lw = 2.7$ meters and $\Delta\sigma = 2\mu\bar{D}/\pi w = 30$

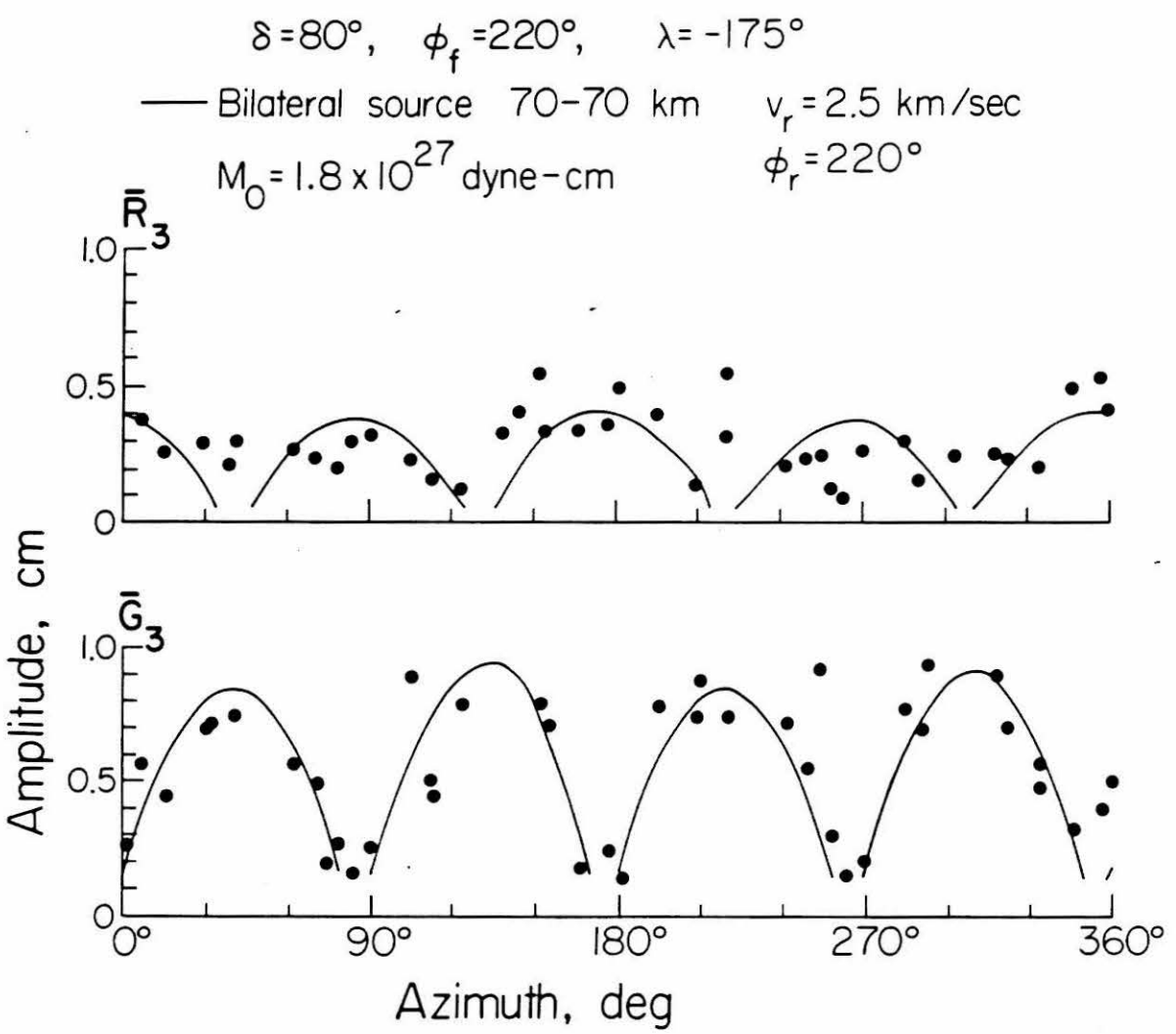

Figure 3-28. Equalized station peak-to-peak amplitudes for observed $\bar{R}_3$ and $\bar{G}_3$ data from the main event in the Tangshan sequence. The data (solid circles) are plotted as a function of azimuth. The curve represents the fault model used in this study.

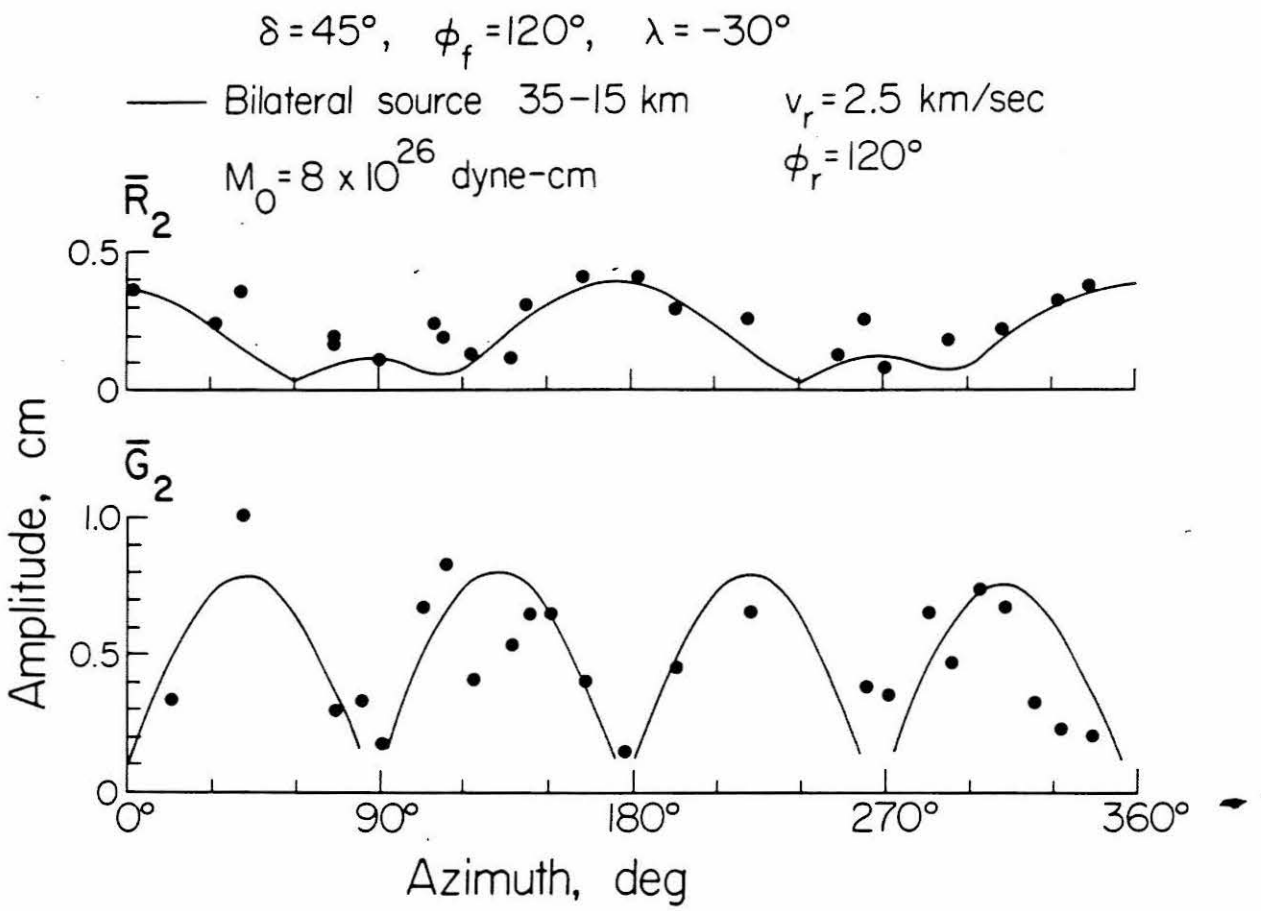

Figure 3-29. Equalized station peak-to-peak amplitudes for observed $\bar{R}_2$ and $\bar{G}_2$ data for the principal aftershock of the Tangshan sequence. The data (solid circles) are plotted as a function of azimuth. The curve represents the fault model used in this study.

bars, where a rigidity $\mu = 3.5 \times 10^{11}$ dyne/cm^2 is used and the fault is assumed to have broken at the free surface.

BODY WAVE ANALYSIS

The analyses of long-period surface waves for the main event and the principal aftershock yield gross fault parameters, but provide no resolution of details concerning the nature and complexity of the faulting process. To obtain this information, an analysis is made of the teleseismic body waves for these events. Figure 3-30 shows P-wave observations for the mainshock. The waveforms are quite complex, but a qualitative description can be made. At the distance range of most of these stations, the only later phase which might interfere with the P-wave train is PcP. However, for a vertical strike-slip fault PcP is always nodal, so that the observed complexity may be ascribed to the source. The initial motion is emergent in nature and reflects the strike-slip solution of the P-wave first-motion data. The difference between the teleseismic and local first-motion solutions is probably not significant, as strike-slip mechanisms can be quite sensitive to local non-planar structure (see Langston, 1977). A later arrival of much larger amplitude is consistently observed (most dramatically at stations RIV, TAU and ADE). There are two significant peculiarities associated with this arrival; its amplitude does not change sign in the four-lobed manner of vertical strike-slip radiation, and the relative timing of the phase varies with azimuth. These observations suggest that part of the faulting in the main Tangshan sequence was not of a strike-slip nature

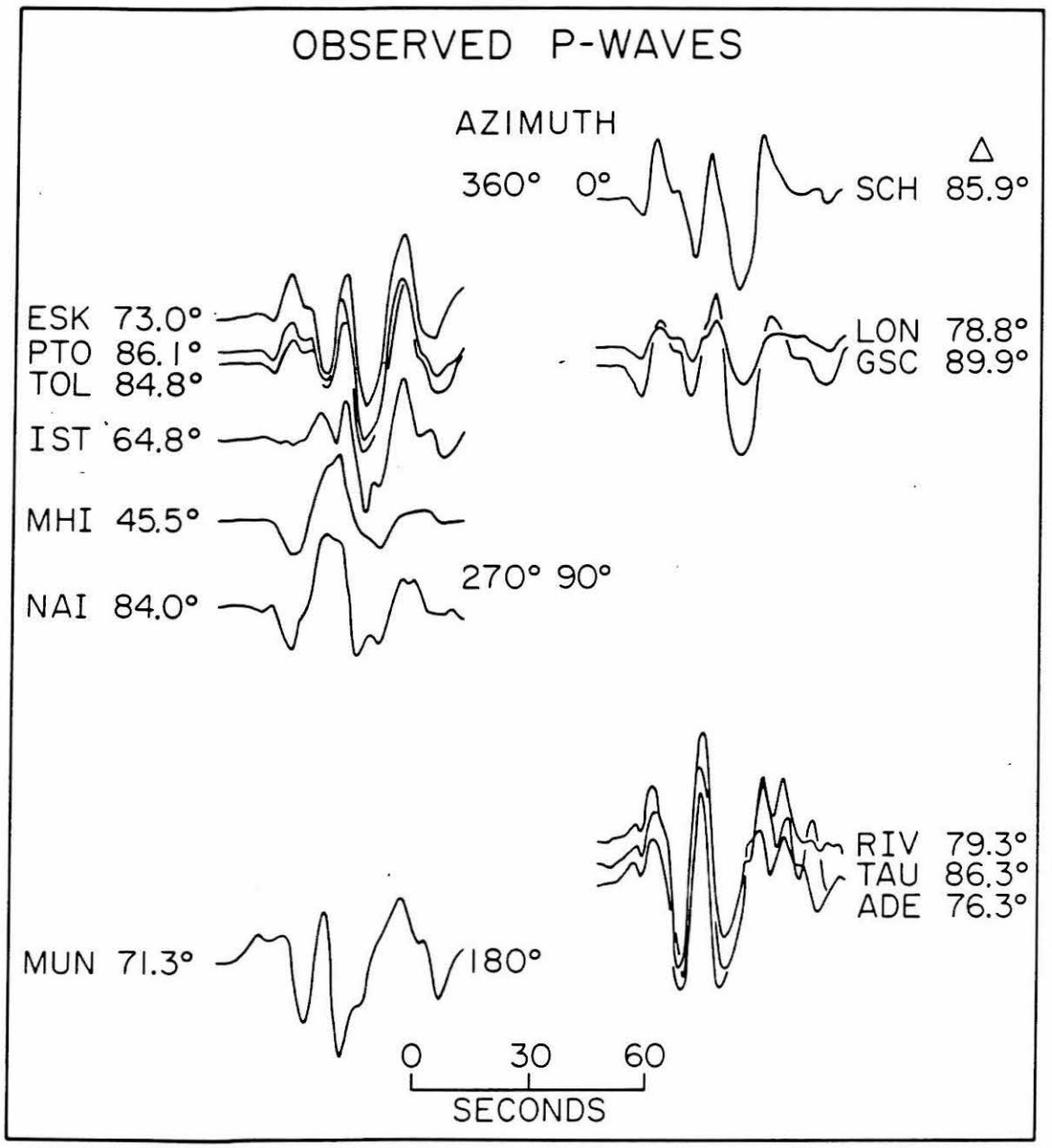

Figure 3-30. Observed long-period P-waves for the mainshock of the Tangshan sequence. The data are plotted as a function of azimuth. The distance in degrees is indicated beside the station name. The amplitudes are corrected for geometric spreading.

and occurred away from the mainshock epicenter.

A more quantitative description of the source is obtained by attempting to match the observed records by synthetic waveforms. This technique has been successfully applied to other complex events (Burdick and Mellman, 1976; Kanamori and Stewart, 1978; Rial, 1978; Stewart and Kanamori, 1978). To fit the first portion of the records, synthetics were generated for a point double couple with the mechanism of the P-wave first-motion solution at a depth of 10 km in a homogeneous half-space. The surface reflections pP and sP were included in the synthetics. The faulting solution obtained by first-motions provided a qualitatively good match to the observations. However, stations situated near the nodes (see IST) show significant complexities within the first few seconds that are not observed for stations away from the nodes. This is consistent with the hypothesis suggested above of some lateral heterogeneity within the source region. A triangular source time function with a rise time of 5.5 sec and fall-off time of 3.25 sec was used to provide an adequate fit to the pulse shape for the non-nodal stations. The seismic moment of this first event is estimated from the average of stations SCH, LON, GSC, RIV, TAU, ADE, and MUN to be 4×10^{26} dyne-cm with 25% uncertainty. This solution is fixed and the next arrivals are modeled. Kanamori and Stewart (1978) successfully fit P-wave seismograms of the 1976 Guatemalan earthquake, a major strike-slip event, by several sources lagged in time and all having identical mechanisms. An attempt to fit the later portion of the P-waves of the Tangshan event with a strike-slip solution was attempted

but a satisfactory fit was not found. The azimuthal variation of the relative timing between the first event and the later arrivals may be accounted for by locating the source of these phases roughly 45 km south to south-southwest of the epicenter of the main event. By body wave inversion (see Burdick and Mellman, 1976; Langston, 1976), and trial and error, a satisfactory fit to the observation was achieved by including two thrust events following the initial strike-slip event. The location of these events with respect to the main event is uncertain to approximately 15 km distance and 30^{o} azimuth. The first thrust event appears to have occurred roughly 11 seconds after the initial strike-slip source and had a relative seismic moment 5% of the initial event. The second thrust source was three times larger and followed the first thrust event by 8 seconds, or 19 seconds from the initial onset of the earthquake. The resolution of the thrust solutions is poor, but a mechanism with a north-northwest strike and a steep dip to the west helped to fit the somewhat different character of the waveforms in the western azimuths. The sum of the moments of these two events, 8×10^{25} dyne-cm, is a factor of five smaller than the initial strike-slip solution, but the arrivals from these events dominate the P-wave train. This happens because teleseismic P-waves for strike-slip events have take-off angles near the nodes of the radiation pattern, whereas for thrust events the P-waves leave near the maximum of the radiation pattern.

Figure 3-31 shows synthetics and observations for two representative, non-nodal stations. The fits are satisfactory

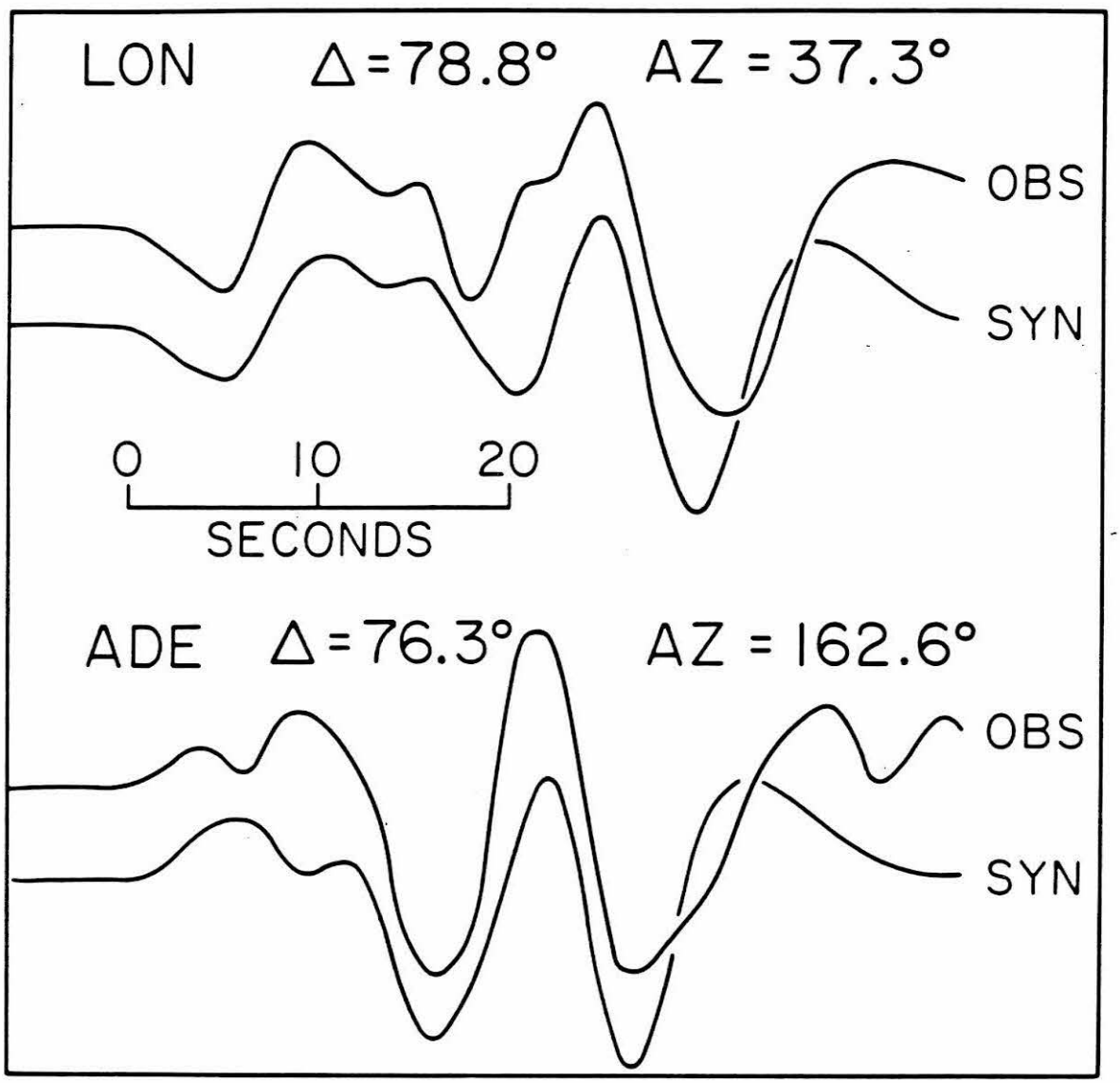

Figure 3-31. Observed and synthetic long-period P-waves for stations LON and ADE for the mainshock of the Tangshan sequence.

considering the complications in the problem. Further resolution is not worth pursuing for several reasons. Details of the local crustal structure, particularly the sediment cover, are not documented. The surface wave analysis has shown that the overall faulting was basically strike-slip, but due to radiation pattern effects, small, presumably triggered, thrust events mask the strike-slip radiation. Finally, there is some evidence from first-motions and nodal stations that lateral heterogeneity may affect the waveforms. Figure 3-32 shows short- and long-period vertical component records for Goldstone, California (GSC). The arrival times of the three modeled events are indicated on the short-period record. The emergent nature of the initial strike-slip solution is clearly seen. The long-period record shows a number of arrivals several minutes after the initial rupture. Presumably a number of these later events are strike-slip, such that the total moment sum of the body waves approaches that of the surface waves, which are sufficiently long-period (100-200 seconds) to average over the source complexity. Multiple event rupture in strike-slip earthquakes has been previously observed for the 1967 Caracas earthquake (Rial, 1978), the 1976 Guatemalan earthquake (Kanamori and Stewart, 1978) and the 1967 and 1976 Turkish earthquakes (Stewart and Kanamori, 1978).

Figure 3-33 shows several P-waves for the principal aftershock. The waveforms indicate that the earthquake was a normal faulting double event (see Figure 4 in Langston and Helmberger, 1975). Synthetics were generated for the aftershock to better resolve its faulting process. The strike and slip angle are not resolvable, but the amplitude ratio of

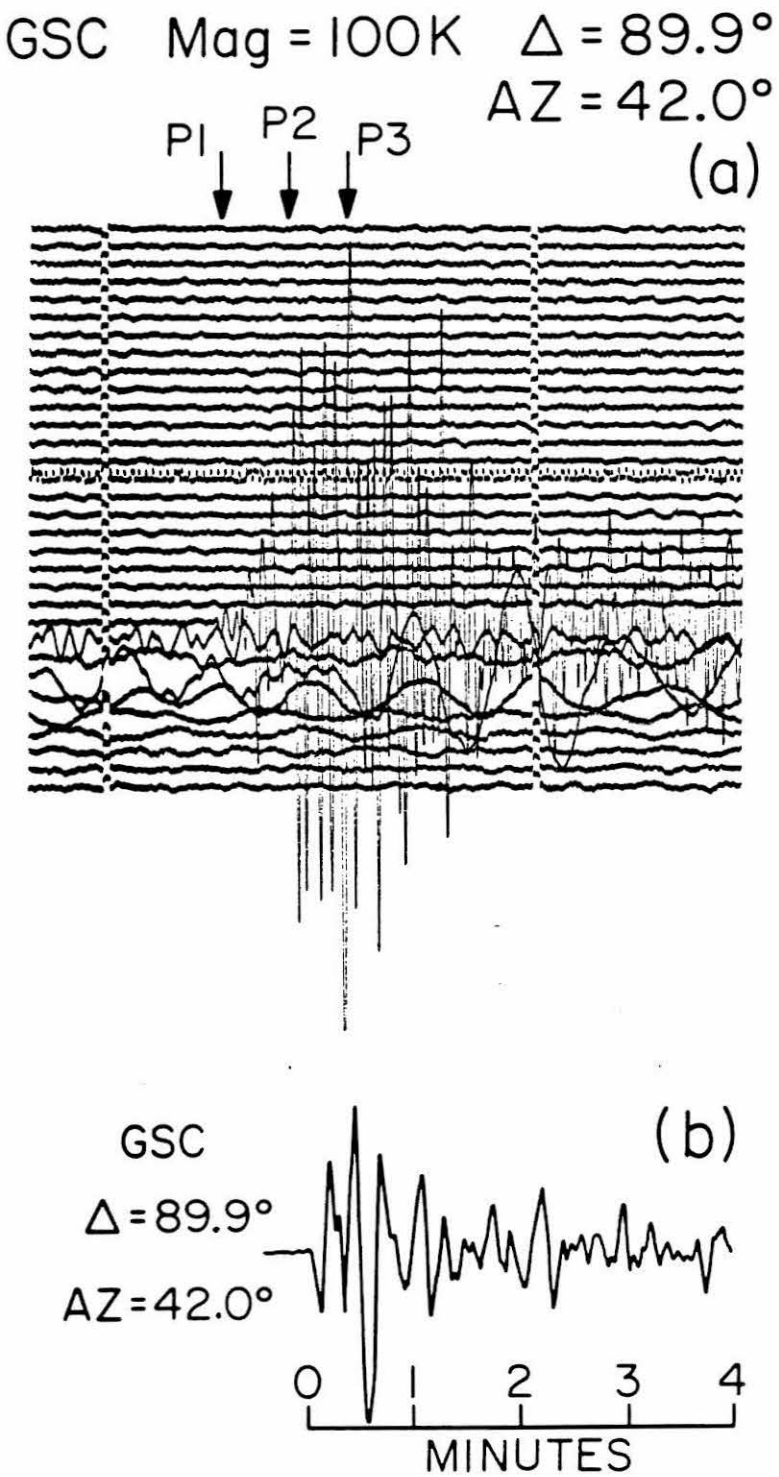

Figure 3-32. Observed P-waves from the short-period (a) and long-period (b) vertical component seismograms for station GSC at Goldstone, California. The arrows on the short-period record indicate the approximate arrival times of the initial strike-slip shock and the two thrust co-shocks from the main event.

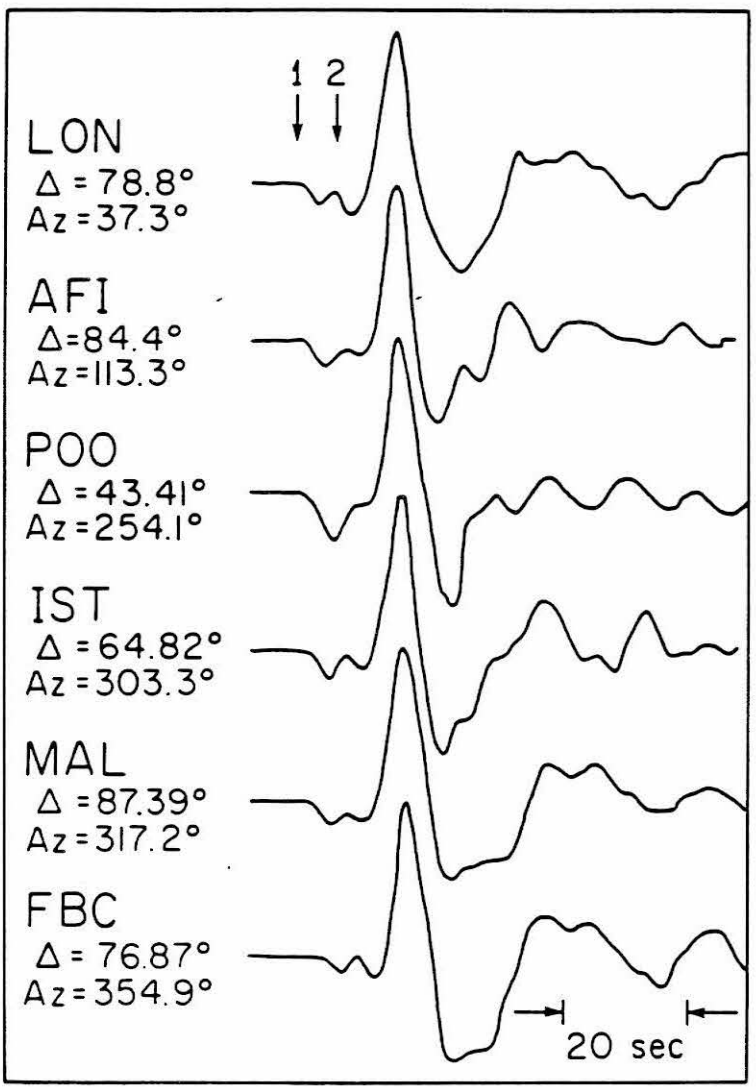

Figure 3-33. Observed long-period P-waves from the principal aftershock of the Tangshan sequence. The arrows indicate the two shocks of this double event.

pP to direct P suggests a dip near 45° and a depth of approximately 7 km. These constraints assume that the dip of the two mechanisms is similar. There is some azimuthal variation in the amplitude relationship of the two events, but uncertainties in the radiation pattern and in the effect of crustal structure preclude any judgment as to possible differences between the source mechanisms.

DISCUSSION

Incorporating the aftershock data and the surface and body wave analyses, a faulting scenario of the Tangshan sequence is illustrated in Figure 3-34. The initial rupture begins rather slowly and has a near vertical strike-slip mechanism, striking N 40°E. The rupture propagates in a bilateral fashion northeast and southwest. After roughly ten seconds the readjustment of the local stress system triggers thrusting 45 km south of the epicenter. These events, though small with respect to the overall radiation, are roughly of magnitude M_w = 6.5 (see Kanamori, 1977). Fifteen hours after the main event sequence a large oblique normal event occurs on a northwest-southeast trending structural boundary. In a simplified view, the system is one of block translation -- motion of the southeastern block produces compression at the southern boundary and extension at the northern boundary.

As the Tangshan event is the largest continental intraplate earthquake since the establishment of the WWSSN, it is pedagogically useful to make a comparison with the 1976 Guatemalan earthquake -- one of the largest continental strike-slip interplate events -- which was

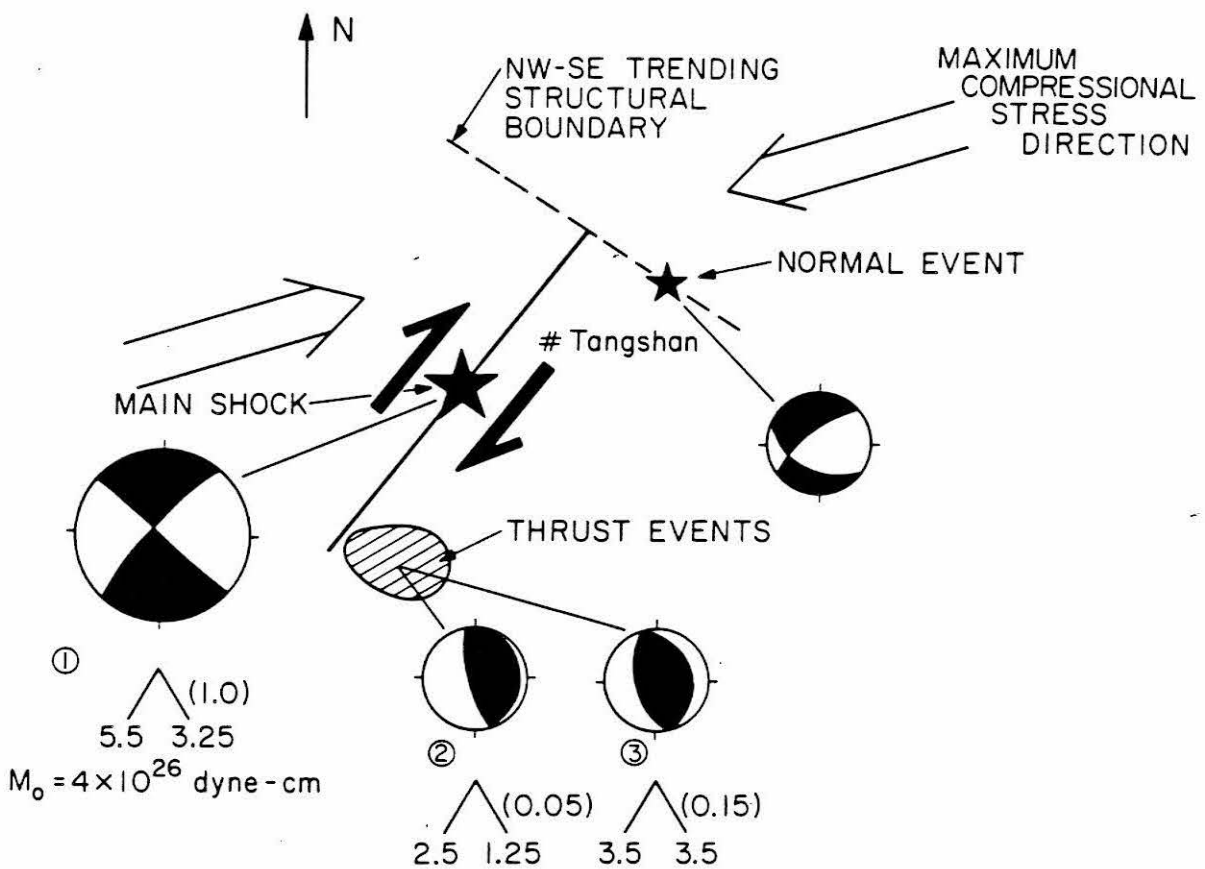

Figure 3-34. Seismotectonic illustration of the Tangshan earthquake sequence. Rise times and fall-off times for the triangular source time functions used in the body-wave synthetics of the initial strike-slip shock and thrust co-shocks are indicated. The relative moments are shown in parentheses. No body-wave moment or time function was determined for the normal aftershock.

studied in detail by Kanamori and Stewart, 1978. The Tangshan event is smaller both in fault length and moment. Assuming shallow faulting ($w \sim 15$ km) for both events, the average dislocation and stress drop for both events are similar: $\bar{D} \sim 2$ meters and $\Delta\sigma \sim 30$ bars. Both events had associated normal faulting. The normal aftershocks of the Guatemala earthquake were minor in size, whereas the large normal aftershock of the Tangshan earthquake was nearly half the size of the mainshock. No thrusting was observed to be associated with the Guatemalan earthquake. Both events consist of a number of smaller independent events. Overall, the Tangshan intraplate earthquake sequence with its variety and size of co-shocks and aftershocks is considerably more complicated in nature than the Guatemalan interplate earthquake.

Several factors undoubtedly contributed to the enormous loss of life and destruction caused by the Tangshan earthquake. Although the nature of the construction practices in the epicentral region are of primary importance and cannot be discussed within the scope of this thesis, three seismological factors are considered to have significantly increased the damage potential. The first relates to the overall nature and complexity of the earthquake. Vertical strike-slip earthquakes radiate most of their energy horizontally into the local source region. Small thrust co-shocks enlarged the region of high local intensities. The principal aftershock fifteen hours following the main event was exceptionally large and probably destroyed most structures which were weakened but survived the mainshock.

A second seismological factor contributing to the destructiveness

of the Tangshan sequence is the effect of the local geology on seismic energy release. The epicentral region of the Tangshan event is an area of sedimentary cover. The thickness of these sediments is not known; however, studies have shown that even moderate thicknesses of sediments effectively amplify seismic intensities relative to nearby bedrock (Gutenburg, 1956b, 1957; Borcherdt, 1970). Sedimentary basin structures can also trap and focus the seismic energy (Hong and Helmberger, 1978). The effects of sedimentary cover, though man-made land fill, were dramatically observed in the 1906 San Francisco earthquake. In the "Report of the State Earthquake Investigation Commission" on the 1906 event, H. O. Wood (1908) concluded in his discussion of the damage in San Francisco that "... the amount of damage produced by the earthquake... depended chiefly upon the geological character of the ground. Where the surface was solid rock, the shock produced little damage; whereas upon made land great violence was manifested..."

A third seismological consideration is with respect to the characteristic fall-off of intensity of shaking with distance in the region. This characteristic fall-off varies significantly, specifically exemplified in the United States. In the older eastern United States small earthquakes are felt over a much larger area than in the tectonic, younger west. Consequently, earthquakes of a given magnitude tend to be more damaging in the east than the west. The reasons for this phenomenon are not clearly understood, but are probably related to the attenuative properties of the crust and mantle. It is likely that the

intensity fall-off characteristics of northeast China are more akin to those of the stable continental eastern United States than the Basin and Range, tectonic environment of the west. Thus, the region of severe damage for the Tangshan event was probably much larger than would have been true for a similar event on the San Andreas system in California.

CONCLUSIONS

The Tangshan earthquake and its principal aftershock represent a complex intraplate event sequence with strike-slip, normal, and thrust faulting. The mainshock was a bilateral strike-slip event, striking N 40°E. Associated thrusting events occurred south of the mainshock epicenter concurrently with the main rupture. The principal aftershock was an oblique normal double event, striking approximately perpendicular to the mainshock. The seismic moment of the main event was 1.8×10^{27} dyne-cm; the moment for the principal aftershock was 8×10^{26} dyne-cm. The complexity of the sequence contrasts the intraplate Tangshan event with the large interplate Guatemala earthquake.

CHAPTER 4.

CONCLUDING REMARKS ON THE NATURE OF GREAT EARTHQUAKES ON THE SAN ANDREAS FAULT

4.1 Introduction.

Since a large earthquake has not taken place recently along the San Andreas fault, it is necessary to speculate on what such an event might look like, rather than be able to make direct observations. In this concluding chapter an attempt is made to bring together what has been learned from the preceding studies to focus on this important question.

Only since early this century has attention been given to understanding and mapping the San Andreas fault. The principal interest in the problem undoubtedly resulted from the occurrence of the April 18, 1906, San Francisco earthquake (Lawson et al., 1908). In fact, only since the 1950's have large cumulative displacements (~ 300 km) been recognized for the fault (Hill and Dibblee, 1953) and only since the 1960's (Wilson, 1965) has the transform fault interpretation for the San Andreas been established. During most of the 20th century less was known about the San Andreas in S. California compared with N. California. However, recently, the detailed investigations of Sieh (1978a and 1978b) have shed light on our understanding of the faulting process and recurrence times of great earthquakes in S. California. Hill (1981) has summarized the historical development of some of the

ideas concerning the San Andreas fault.

4.2 Implications for Faulting Associated with a Great Earthquake on the San Andreas Fault.

Simple v's Complex Rupture

From the discussions of simple earthquakes made in Chapter 1 and the detailed studies of large strike-slip events in Guatemala and Turkey, discussed in Chapter 2, it seems likely that a great earthquake having a rupture length of several hundred kilometers on the San Andreas will generate seismograms that have many similarities to those associated with faulting along the Motagua and Anatolian faults. Indeed, some of the old 1906 seismograms show such complexity; however, the quality of the records is generally poor, making any detailed study of them difficult.

In one of the first detailed studies made of the source characteristics of earthquakes along a transform fault, Kanamori and Stewart (1976) concluded that events along the Gibbs Fracture Zone (an oceanic transform fault) in 1967 and 1974 were characterized by a slow, simple rupture process. This is to be contrasted with the results for the Guatemalan and Anatolian events, both of which occurred in environments of continental strike-slip faulting. The differences in the mode of failure between the Gibbs Fracture Zone ("oceanic") and "continental" events are most likely the result of their respective environments.

On the one hand, the oceanic transform fault is in an environment of high heat flow and a plastic rheology, while on the other, the

continental fault region is more likely to have lower heat flow and be a more brittle environment. One explanation for the complexity -- the occurrence of asperities -- is more likely for the continental region.

One would expect, as a result, the next great earthquake on the San Andreas fault to exhibit characteristics similar to those observed for the Guatemala and Mudurnu Valley events, viz., a multiple-source character of individual events of approximately two minutes duration. If the faulting extends over greater distances than occurred in the Guatemala event (~ 250 km) (1906 event, ~ 450 km; 1857 event, ~ 350 km) then the multiple source character may last longer (especially if the rupture is unilateral) and may consist of more than the 10 events found in the Guatemala study. However, regardless of the size, the moment of each individual event is expected to be bounded at around 5×10^{26} dyne-cm. There is no reason to expect the fault width, and hence the size of an individual event, in a San Andreas earthquake to be significantly different from the Guatemala or Mudurnu Valley events. However, the complexity could be greater, perhaps as complex as that observed for the 1976 E. Turkey event. Butler and Kanamori (1980) and Kanamori (1979) have modeled the long-period ground motion from such a hypothetical event on the San Andreas fault.

Multiple Fault Complexity

In a faulting scenario of the next great earthquake on the San Andreas fault many possibilities could occur. In Chapters 2 and 3 large earthquakes occurring on an associated fault feature and not on the

mainshock rupture surface have been discussed. Their relative rupture planes are schematically shown in Figure 4.1. The mainshock is interpreted as triggering the later events in each case. The time constant, ΔT, is different in each case. Such a large event could occur within seconds or minutes, as perhaps happened for the thrust events associated with the Tangshan earthquake, in the E. Turkey event, the normal event of the Guatemala earthquake or for the strike-slip event associated with the St. Elias earthquake sequence reported by Dziewonski and Woodhouse (1981) and Dziewonski (personal communication, 1981). It could also occur within hours as with the normal later event of the Tangshan sequence or the strike-slip later event of the Philippine earthquake. For the great Chilean earthquake the later event occurred approximately 15 days after the mainshock. Nonetheless, for the events studied all except one had a large event occur within 24 hours. It is also possible that a large earthquake on a major boundary could be triggered by a small event on a less significant structure.

Obviously, a large number of events occur without any later event. Therefore, several constraints have to be met before such an event can occur. Probably most important are the presence of a significant tectonic feature in the vicinity of the impending event and a local pre-earthquake stress condition that allows rupture to take place following the mainshock. Indeed, repeated events occurring in the same location over time are unlikely to have a large later event associated with them on each occasion since the local stress condition will be

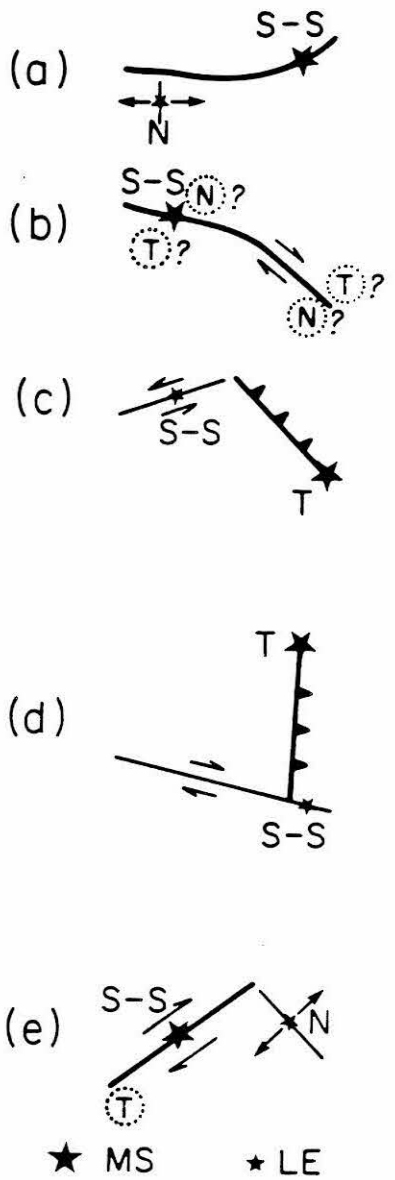

Guatemala MS February 4, 1976, M_s = 7.5
LE February 4, 1976, m_b = 5.8

ΔT < 1 hr.

E. Turkey MS November 24, 1976, M_s = 7.3
LE ?

ΔT = ?

Philippine MS August 16, 1976, M_s = 7.8
LE August 16, 1976, M_s = 6.8

ΔT = 12 hrs.

Chile MS May 22, 1960, M_w = 9.5
LE June 6, 1960, M_w = 7.8

ΔT = 15 days.

Tangshan MS July 27, 1976, M_s = 7.7
LE July 28, 1976, M_s = 7.2

ΔT = 15 hrs.

Figure 4.1. A schematic figure showing the rupture patterns for the mainshocks (MS) and later events (LE) discussed in Chapters 2 and 3. ΔT is the time difference between the mainshock and the later event; N represents normal faulting; T, thrust faulting; S-S, strike-slip faulting. A question mark denotes that the mode of faulting is presumed and not observed. Diagrams are not to scale.

different each time.

As regards the San Andreas fault, the major structural boundary close to it is the Transverse Ranges in S. California. It would not be surprising to have a large event occur somewhere in the Transverse Ranges following a great earthquake on the San Andreas fault. Most likely, from the studies performed so far, it would occur within a day or so of the mainshock, if it is to occur. The mainshock could also be triggered by a small event in the Transverse Ranges.

Several large earthquakes, in different regions of the world, have been studied in an attempt to understand the simplicity or complexity of their rupture process with respect to their local tectonic environment.

The contribution of this thesis has been to demonstrate that many earthquakes exhibit complexity and that this complexity occurs on different scales. To understand it requires a complete analysis of the seismic records and sometimes even then the records are too complex to arrive at a reasonable explanation. However, in many cases, it is possible to learn much from such studies, not only about the earthquake source but also about the tectonic environment in which it is located.

One should not, however, expect the process to be easy; Nature does not give up her secrets readily.

REFERENCES

Abe, K., (1972). Mechanisms and tectonic implications of the 1966 and 1970 Peru earthquakes, Phys. Earth Planet. Int., 5, 367-379.

Agnew, D., J. Berger, R. Buland, W. Farrell and F. Gilbert, (1976). International deployment of accelerometers: A network for very long-period seismology, EOS, Trans. Amer. Geophy. Un., 57, 180-188.

Aki, K., (1966). Generation and propagation of G-waves from the Niigata earthquake of June 16, 1964. Part 2. Estimation of earthquake moment, released energy, and stress-strain drop from the G-wave spectrum, Bull. Earthquake Res. Inst., 44, 73-88.

Aki, K., (1967). Scaling law of seismic spectrum, J. Geophys. Res., 72, 1217-1231.

Allen, C. R., (1981). Comparisons between the North Anatolian fault of Turkey and the San Andreas fault of California, Progress in Earthquake Prediction Research, 2, Verlag Vieweg Braunschweig, Wiesbaden, in press.

Ambraseys, N. N., (1970). Some characteristic features of the Anatolian fault zone, Tectonophysics, 9, 143-165.

Ambraseys, N. N., (1971). Value of historical records of earthquakes, Nature, 232, 375-379.

Ambraseys, N. N. and A. Zátopek, (1968). The Varto-Ustükran (Anatolia) earthquake of 19 August 1966; summary of a field report, Bull. Seism. Soc. Am., 58, 47-102.

Ambraseys, N. N. and A. Zátopek, (1969). The Mudurnu Valley, West Anatolia, Turkey earthquake of 22 July 1967, Bull. Seism. Soc. Am., 59, 521-590.

Ben-Menaham, A., (1961). Radiation of seismic surface waves from finite moving sources, Bull. Seism. Soc. Am., 51, 401-435.

Ben-Menahem, A., (1971). The force system of the Chilean earthquake of 1960 May 22, Geophys. J. R. Astr. Soc., 25, 407-417.

Borcherdt, R. D., (1970). Effects of local geology on ground motion near San Francisco Bay, Bull. Seismol. Soc. Am., 60, 29-61.

Bucknam, R. C., G. Plafker, R. V. Sharp and S. B. Bonis, (1976). Surface displacement in the Motagua fault zone during the 4 February 1976 Guatemala earthquake, (abstract), EOS, Trans. Am. Geophys. Un., 57, 949.

Burdick, L. J. and G. R. Mellman, (1976). Inversion of the body waves from the Borrego Mountain earthquake to the source mechanism, Bull. Seism. Soc. Am., 66, 1485-1500.

Butler, R., G. S. Stewart and H. Kanamori, (1978). The July 27, 1976 Tangshan, China earthquake -- a complex sequence of intra-plate events, Bull. Seism. Soc. Am., 69, 207-220.

Butler, R. and H. Kanamori, (1980). Long-period ground motion from a great earthquake, Bull. Seism. Soc. Am, 70, 943-961.

Cardwell, R. K. and B. L. Isacks, (1978). Geometry of subducted lithospheric plates beneath the southern Philippine, Sangihe and Halmahera island arcs, (abstract), EOS, Trans. Amer. Geophys. Un., 58, 381.

Chael, E. P., G. S. Stewart, K. Singh and K. McNally, (1980). Recent large earthquakes along the Middle America Trench and their implications for the subduction process (abstract), EOS, Trans. Am. Geophys. Un., 61, 297.

Chase, T. E., (1975). Topography of the oceans, Scripps Inst. of Oceanography, IMR Technical report series TR57, 1975.

Chen Pei-shan et al., (1978). The stress field of the Peking - Tientsin - Tangshan - Zhangjiakon area before and after the Tangshan earthquake of July 28,1976. Acta Geophysica Sinica, 21, No. 1, p. 57.

Chung, W.-Y. and H. Kanamori, (1978). Subduction process of a fracture-zone and aseismic ridges - focal mechanism and source characteristics of the New Hebrides earthquake of January 19, 1969 and some related events, Geophys. J. R. Astr. Soc., 54, 221-240.

Dean, B. W. and C. L. Drake, (1978). Focal mechanism solutions and tectonics of the Middle America Arc, Jour. of Geology, 86, 111-128.

Dewey, J. W., and B. R. Julian, (1976). The Guatemalan earthquake of February 4, 1976, A Preliminary Report: Main event source parameters from teleseismic data, U.S. Geol. Surv. Prof. Paper 1002, edited by A. F. Espinosa, 19-23.

Ding Wenjing (1978). Distribution characteristics and migration regularity of strong aftershock of Tangshan earthquake. Scientia Geologica Sinica, No. 1,p. 72.

Douglas, A., J. B. Young and J. A. Hudson, (1974). Complex P-wave seismograms from simple earthquake sources, Geophy. J. R. Astr. Soc., 37, 141-150.

Dziewonski, A., and F. Gilbert, (1974). Temporal variation of the seismic moment tensor and the evidence of precursive compression for two deep earthquakes, Nature, 247, 185-188.

Dziewonski, A. and J. H. Woodhouse, (1981). Analysis of complex earthquakes, (abstract), EOS, Trans. Am. Geophys. Un., 62, 330.

Ewing, M., G. H. Sutton and C. B. Officer, Jr., (1954). Seismic refraction measurements in the Atlantic Ocean, Part VI: Typical deep stations, North America basin, Bull. Seism. Soc. Am., 44, 21-38.

Fletcher, J. B., M. L. Sbar and L. R. Sykes, (1978). Seismic trends and travel-time residuals in eastern North America and their tectonic implications, Bull. Geol. Soc. of Amer., 89, 1656-1676.

Fukao, Y., and M. Furumoto, (1975). Mechanism of large earthquakes along the eastern margin of the Japan sea, Tectonophysics, 24, 247-266.

Geller, R. J. and H. Kanamori, (1977). Magnitude of great shallow earthquakes from 1904 to 1952, Bull. Seism. Soc. Am., 67, 587-598.

Geological Science Research Institute of China (1975). Tectonic Map of China, printed by Map Publication Service, China (available from New China Book Store, Beijing, China).

Gervasio, F. C., (1966). A study of the tectonics of the Philippine archipelago, Philippine Geologist, 20, 51-75.

Given, J. W., G. S. Stewart and D. V. Helmberger, (1981). Upper mantle structure of eastern North America, in preparation.

González, J., (1979). Some characteristics of the foreshocks ($M < 4.0$) to the Oaxaca earthquake ($M_s = 7.8$) of 29 November 1978, Professional thesis, Faculty of Science, UNAM, Mexico (in Spanish).

Guo Shunmin, et al., (1977). Discussion of the regional structural background and the seismogenic model of the Tangshan earthquake. Scientia Geologica Sinica, 1977, No. 4, 321.

Gutenberg, B., (1956a). Great earthquakes 1896-1903, (abstract), EOS Trans. Am. Geophys. Un., 37, 608-614.

Gutenburg, B. (1956b). Effects of ground on shaking in earthquakes, Trans. Am. Geophys. Un., 37, 757-760.

Gutenburg, B. (1957). Effects of ground on earthquake motion, Bull. Seismol. Soc. Am., 47, 221-250.

Gutenburg, B. and C. F. Richter, (1965). Seismicity of the Earth and Associated Phenomena, Hafner, New York, 310 pp.

Hamilton, W., (1974a). Sedimentary basins of the Indonesian region, U. S. Geol. Survey Map I-875-B.

Hamilton, W., (1974b). Earthquake map of the Indonesian region, U. S. Geol. Survey Map I-875-C.

Hamilton, W., (1977). Subduction in the Indonesian region; in Island Arcs, Deep Sea Trenches and Back-Arc Basins, M. Talwani and W. C. Pitman, III, eds., Am. Geophys. Un., 15-31.

Hanks, T. C. and M. Wyss, (1972). The use of body-wave spectra in the determination of seismic source parameters, Bull. Seism. Soc. Am., 62, 561-589.

Harkrider, D. G., (1964). Surface waves in multilayered elastic media. I. Rayleigh and Love waves from buried sources in a multilayered elastic half-space, Bull. Seism. Soc. Am., 54, 627-679.

Haskell, N., (1966). Total energy and energy spectral density of elastic wave radiation from propagating faults, 2, Bull. Seismol. Soc. Am., 56, 125-140.

Heaton, T. H., (1981). The 1971 San Fernando earthquake: A double event?, in preparation.

Heaton, T. H. and D. V. Helmberger, (1979). Generalized ray models of the San Fernando earthquake, Bull. Seism. Soc. Am., 69, 1311-1342.

Heezen, B. C. and D. J. Fornari, (1975). Geological map of the Pacific Ocean, Initial Reports of the Deep Sea Drilling Project, 30.

Helmberger, D. V., G. R. Engen, (1974). Upper mantle shear structure, J. Geophys. Res., 79, 4017-4028.

Helmberger, D. V. and L. R. Johnson, (1977). Source parameters of moderate size earthquakes and the importance of receiver crustal structure in interpreting observations of local earthquakes, Bull. Seism. Soc. Am., 67, 301-313.

Hill, M. L., (1981). San Andreas fault: History of concepts, Bull. Geol. Soc. Am., 92, 112-131.

Hill, M. L. and T. W. Dibblee Jr., (1953). San Andreas, Garlock and Big Pine faults, California, Bull. Geol. Soc. Am., 64, 443-458.

Hong, T.-L. and D. V. Helmberger, (1978). Glorified optics and wave propagation in non-planar structure, Bull. Seismol. Soc. Am., 68, 1313-1330.

Hudson, D. E., (1972). Local distribution of strong earthquake ground motions, Bull. Seism. Soc. Am., 62, 1765-1786.

Imamura, A., (1937). Theoretical and Applied Seismology, Maruzen Co., Tokyo, 358 pp.

Jordan, T. H., (1975). The present-day motions of the Caribbean plate, J. Geophys. Res., 80, 4433-4439.

Kanamori, H., (1970). Synthesis of long-period surface waves and its application to earthquake source studies, Kurile Islands earthquake of October 13, 1963, J. Geophys. Res., 75, 5011-5027.

Kanamori, H., (1972). Mechanism of tsunami earthquakes, Phys. Earth Planet. Int., 6, 346-357.

Kanamori, H., (1977). The energy release in great earthquakes, J. Geophys. Res., 82, 2981-2987.

Kanamori, H., (1978). Quantification of earthquakes, Nature, 271,

411-414.

Kanamori, H., (1979). A semi-empirical approach to prediction of long-period ground motion from great earthquakes, Bull. Seism. Soc. Am., 69, 1645-1670.

Kanamori, H. and D. L. Anderson, (1975a). Amplitude of the earth's free oscillations and long-period characteristics of the earthquake source, J. Geophys. Res., 80, 1075-1078.

Kanamori, H. and D. L. Anderson, (1975b). Theoretical basis of some empirical relations in seismology, Bull. Seism. Soc. Am., 65, 1073-1095.

Kanamori, H. and J. J. Cipar, (1974). Focal process of the great Chilean earthquake May 22, 1960, Phys. Earth Planet. Int., 9, 128-136.

Kanamori, H. and J. W. Given, (1981). Use of long-period surface waves for fast determination of earthquake source parameters, Phys. Earth Planet. Int., submitted, 1981.

Kanamori, H. and G. S. Stewart, (1976). Mode of the strain release along the Gibbs fracture zone, mid-Atlantic Ridge, Phys. Earth Planet. Int., 11, 312-332.

Kanamori, H. and G. S. Stewart, (1978). Seismological aspects of the Guatemala earthquake of February 4, 1976, J. Geophys. Res., 83, 3427-3434.

Kelleher, J., J. Savino, H. Rowlett and W. McCann, (1974). Why and where great thrust earthquakes occur along island arcs, J. Geophys. Res., 79, 4889-4899.

Kelleher, J., L. R. Sykes and J. Oliver, (1973). Possible criteria for predicting earthquake locations and their application to major plate boundaries of the Pacific and the Caribbean, J. Geophys. Res., 78, 2547-2585.

Kikuchi, M. and H. Kanamori, (1981). Inversion of complex body waves, Bull. Seism. Soc. Am., in press.

King, C.-Y., R. D. Nason, and D. Tocher, (1973). Kinematics of fault creep, Phil. Trans. Roy. Soc., London. Ser. A., 274, 355-360.

Krause, D. C., (1966). Tectonics, marine geology and bathymetry of the Celebes Sea - Sulu Sea region, Bull. Geol. Soc. Am.,

77, 813-832.

Langer, C. J., J. P. Whitcomb and A. Aburto Q., (1976). The Guatemalan earthquake of February 4, 1976, A Preliminary Report: Aftershocks from local data, U. S. Geol. Surv. Prof. Paper 1002, edited by A. F. Espinosa, 30-38.

Langston, C. A., (1976). A body wave inversion of the Koyna India, earthquake of December 10, 1967, and some implications for body wave focal mechanisms, J. Geophys. Res., 81, 2517-2529.

Langston, C. A., (1976). Body wave synthesis for shallow earthquake sources: inversion for source and earth structure parameters, Ph.D. Thesis, Califoria Institute of Technology.

Langston, C. A., (1977). The effect of planar dipping structure on source and receiver for constant ray parameter, Bull. Seismol. Soc. Am., 67, 1029-1050.

Langston, C. A., (1978). The February 9, 1971 San Fernando earthquake, Bull. Seism. Soc. Am., 68, 1-30.

Langston, C. A. and R. Butler, (1976). Focal mechanism of the August 1, 1975 Oroville earthquake, Bull. Seism. Soc. Am., 66, 1111-1120.

Langston, C. A., and D. V. Helmberger, (1975). A procedure for modeling shallow dislocation sources, Geophys. J. R. Astr. Soc., 42, 117-130.

Lawson, A. C., et al., (1908). The California Earthquake of April 18, 1906: Report of the State Earthquake Investigation Commission, Carnegie Inst. of Wash., Publ. 87, 1, 451pp.

Lay, T. and H. Kanamori, (1980). Earthquake doublets in the Solomon Islands, Phys. Earth and Planet. Int., 21, 283-304.

Lisowski, M. and W. Thatcher, (1981). Geodetic determination of horizontal deformation associated with the Guatemala earthquake, Bull. Seism. Soc. Am., 71, 845-856.

Mammerickx, J., R. L. Fisher, F. J. Emmel and S. M. Smith, (1976). Bathymetry of the East and Southeast Asian Seas, Geol. Soc. of Amer., Map and Chart 17.

Masó, M. S., (1910). Catalogue of Violent and Destructive Earthquakes in the Philippines, 1599-1909, Weather Bureau, Manila Central

Observatory, 1-25.

Masó, M. S., (1918). Great earthquake and tidal wave in southern Mindanao, P. I., Bull. Seism. Soc. Am., 8, 125-126.

Masters, T. G., J. Berger and F. Gilbert, (1980). Observations from the IDA network of the moment tensor of the Oaxaca earthquake November 29, 1978, Geofísica Internacional, 17, 281-286.

Matumoto, T., and G. V. Latham, (1976). Aftershocks of the Guatemalan earthquake of February 4, 1976, Geophys. Res. Lett., 3, 599-602.

McCann, W., S. Nishenko, L. R. Sykes and J. Krause, (1978). Seismic gaps and plate tectonics: Seismic potential for major plate boundaries, U. S. Geol. Survey Open-file Report #78-943, 441-584.

McKenzie, D. P., (1969). The relation between fault plane solutions for earthquakes and the directions of the principal stress, Bull. Seism. Soc. Am., 59, 591-601.

McKenzie, D. P., (1978). Active tectonics of the Alpine-Himalayan belt: the Aegean Sea and surrounding regions, Geophys. J. R. Astr. Soc., 55, 217-254.

McNally, K. C., L. Ponce, E. P. Chael and J. González, (1980). The 1978 November 29, Oaxaca, Mexico earthquake -- foreshock, mainshock, aftershock sequence, manuscript in preparation.

McNally, K. C. and J. B. Minster, (1981). Non-uniform seismic slip rates along the Middle-America trench, J. Geophys. Res., 86, 4949-4959.

Meyer, R. P., W. D. Pennington, L. A. Powell, W. L. Unger, M. Guzmán, J. Havskov, S. K. Singh, C. Valdés, J. Yamamoto, (1980). A first report on the Petatlán, Guerrero, Mexico earthquake of 14 March 1979, Geophys. Res. Lett., 7, 97-100.

Minster, J. B. and T. H. Jordan, (1978). Present-day plate motions, J. Geophys. Res., 83, 5331-5354.

Minster, J. B. and T. H. Jordan, (1980). Present-day plate motions: A summary, Éditions du Centre National de la Recherche Scientifique, Paris, ed. C. J. Allegre, 109-124.

Miyamura, S., S. Omote, R. Teisseyre and E. Vesanen,

(1964). Multiple shocks and earthquake series pattern, Int. Inst. Seismol. Earthquake Eng. Bull., 2, 71-92.

Molnar, P. and L. R. Sykes, (1969). Tectonics of the Caribbean and Middle America regions from focal mechanisms and seismicity, Bull. Geol. Soc. of Amer., 80, 1639-1684.

Nagamune, T., (1977). Time characteristics of crustal deformation of the Yunnan earthquake of May 29, 1976, as inferred from tilt recording, Jour. of Phys. of the Earth, 25, No. 2, 209-218.

Nason, R. D., (1971). Measurements and theory of fault creep slippage in central California, Roy. Soc. of New Zealand Bull., 9, 181-187.

Nishenko, S. P., H. Rowlett, G. M. Purdy and J. Ewing, (1978). 1978 Bermuda earthquake -- main shock and aftershock studies (abstract), Seismol. Soc. of Amer., eastern section meeting.

Nowroozi, A. A., (1972). Focal mechanism of earthquakes in Persia, Turkey, West Pakistan, and Afghanistan and plate tectonics of the Middle East, Bull. Seism. Soc. Am., 62, 823-850.

Officer, C. B., M. Ewing and P. C. Wuenschel, (1952). Seismic refraction measurements in the Atlantic Ocean. Part IV: Bermuda, Bermuda Rise and Nares Basin, Bull. Geol. Soc. Am., 63, 777-808.

Ohtake, M., T. Matumoto, G. V. Latham, (1977a). Seismicity gap near Oaxaca, southern Mexico as a probable precursor to a large earthquake, Pure and Appl. Geophys., 115, 375-385.

Ohtake, M., T. Matumoto, G. V. Latham, (1977b). Temporal changes in seismicity preceding some shallow earthquakes in Mexico and Central America, Bull. Int. Inst. Seis. and Earthquake Eng., 15, 105-123.

Person, W., W. Spence, and J. W. Dewey, (1976). The Guatemalan earthquake of February 4, 1976, A Preliminary Report: Main event and principal aftershocks from teleseismic data, U. S. Geol. Survey Prof. Paper 1002, ed. by A. F. Espinosa, 17-18.

Plafker, G., (1976). Tectonic aspects of the Guatemala earthquake of 4 February 1976, Science, 193, 1201-1208.

Plafker, G., M. G. Bonilla and S. B. Bonis, (1976). The Guatemalan

earthquake of February 4, 1976, A Preliminary Report: Geologic effects, U. S. Geol. Surv. Prof. Paper 1002, edited by A. F. Espinosa, 38-51.

Ponce, L., K. C. McNally, V. Sumin de Pontilla, J. González, A. del Castillo, L. González, E. P. Chael and M. French, (1980). Oaxaca, Mexico earthquake of 29 November 1978: A preliminary report on spatio-temporal pattern of preceeding seismic activity and mainshock relocation, Geofisica Internacional, 17, no. 2, 109-126.

Qui Qun, (1976). On the background and seismic activity of the M = 7.8 Tangshan earthquake, Hopei Province, of July 28, 1976. Acta Geophysica Sinica , 19, No. 4, p. 269.

Ranneft, T. S. M., R. M. Hopkins, Jr., A. J. Froelich and J. W. Gwinn, (1960). Reconnaissance geology and oil possibilities in Mindanao, Bull. Am. Assoc. Pet. Geol., 44, 529-568.

Reichle, M. S., K. Priestley, J. Brune and J. A. Orcutt, (1980). The 1978 Oaxaca earthquake source mechanism analysis from digital data, Geofísica Internacional, 17, 295-302.

Repetti, W. C., (1946). Catalogue of Philippine earthquakes 1589-1899, Bull. Seism. Soc. Am., 36, 133-322.

Reyes, A., J. N. Brune and C. Lomnitz, (1979). Source mechanism and aftershock study of the Colima, Mexico earthquake of January 10, 1973, Bull. Seismol. Soc. Amer., 69, 1819-1840.

Rial, J. A., (1978). The Caracas, Venezuela earthquake of July, 1967: A multiple source event, J. Geophys. Res., 83, 5405-5414.

Richter, C., (1958). Elementary Seismology, W. H. Freeman, San Francisco, 768 pp.

Rothé, J. P., (1969). The Seismicity of the Earth 1953-1965, Unesco, Paris, 336 pp.

Scholz, C. H., M. Wyss and S. W. Smith, (1969). Seismic and aseismic slip on the San Andreas fault, J. Geophys. Res., 74, 2049-2069.

Schouten, H. and K. D. Klitgord, (1981). Magnetic evidence for the persistence of minor offsets in the central north Atlantic mesozoic lineations, J. Geophys. Res., submitted.

Shimazaki, K., and R. J. Geller, (1977). Source process of the

Kurile Islands tsunami earthquake of June 10, 1975, (abstract), EOS, Trans. Amer. Geophys. Un., 58, p. 446.

Shuran, E. M. (Editor), (1971). World bathymetric map, published by the Chief Administration for Geodesy and Cartography of the USSR, Moscow.

Sieh, K. E., (1978a). Prehistoric large earthquakes produced by slip on the San Andreas fault at Pallett Creek, California, J. Geophys. Res., 83, 3907-3939.

Sieh, K. E., (1978b). Slip along the San Andreas fault associated with the great 1857 earthquake, Bull. Seism. Soc. Am., 68, 1421-1448.

Singh, S. K., J. Havskov, K. C. McNally, L. Ponce, T. Hearn and M. Vassiliou, (1980). The Oaxaca, Mexico earthquake of 29 November 1978: A preliminary report on aftershocks, Science, 207, 1211-1213.

Soufleris, C. and G. S. Stewart, (1981). A source study of the Thessaloniki (N. Greece) 1978 earthquake sequence, Geophys. J. R. Astr. Soc., in press.

Spence, W. and W. Person, (1976). The Guatemalan earthquake of February 4, 1976, A Preliminary Report: Tectonic setting and seismicity, U. S. Geol. Surv. Prof. Paper 1002, edited by A. F. Espinosa, 4-11.

Stewart, G. S., (1979). The Grand Banks earthquake of November 18, 1929 and the Bermuda earthquake of March 24, 1978 -- a comparative study in relation to their intraplate location, (abstract), EOS, Trans. Am. Geophys. Un., 60, 312.

Stewart, G. S., E. P. Chael and K. C. McNally, (1981). The 1978 November 29, Oaxaca, Mexico earthquake: A large simple event, J. Geophys. Res., 86, 5053-5060.

Stewart, G. S. and S. N. Cohn, (1979). The 1976 August 16, Mindanao, Philippine earthquake (M_s = 7.8) -- evidence for a subduction zone south of Mindanao, Geophys. J. R. Astr. Soc., 57, 51-65.

Stewart, G. S. and D. V. Helmberger, (1979). Lateral variation in upper mantle structure suggested by waveform data from the Bermuda earthquake, (abstract), EOS, Trans. Am. Geophys. Un., 60, 318.

Stewart, G. S. and H. Kanamori, (1978). Complexity of rupture propagation in large earthquakes, (abstract), EOS, Trans. Am. Geophys. Un., 59, 1127.

Stoiber, R. E. and M. J. Carr, (1973). Quaternary volcanic and tectonic segmentation of Central America, Bull. Volc., 37, 304-325.

Sykes, L. R., (1971). Aftershock zones of great earthquakes, seismicity gaps and earthquake prediction for Alaska and the Aleutians, J. Geophys. Res., 76, 8021-8041.

Sykes, L. R., (1978). Intraplate seismicity, reactivation of preexisting zones of weakness, alkaline magmatism and other tectonism postdating continental fragmentation, Rev. of Geophys. and Space Phys., 16, 621-688.

Sykes, L. R. and W. R. McCann, (1981). Relative motion of the Caribbean and North American plates, (abstract), EOS, Trans. Am. Geophys. Un., 62, 323.

Tajima, F. and K. C. McNally, (1981). Seismic rupture pattern in Oaxaca, Mexico, in preparation.

Tarr, A. C., (1974). World Seismicity Map, prepared by the U. S. Geological Survey.

The Times (London), January 6, 1977, page 1.

Tocher, D., (1960). Creep on the San Andreas Fault, Bull. Seismol. Soc. Am., 50, 396-403.

Toksöz, M. N., E. Arpat and F. Saroğlu, (1977). East Anatolian earthquake of 24 November 1976, Nature, 270, 423-425.

Trifunac, M. D., and J. N. Brune, (1970). Complexity of energy release during the Imperial Valley, California, earthquake of 1940, Bull. Seismol. Soc. Am., 60, 137-160.

U. S. Geological Survey, (1976). The Guatemalan earthquake of February 4, 1976, A Preliminary Report, edited by A. F. Espinosa, U. S. Geol. Surv. Prof. Paper 1002, 90 pp.

Vogt, P. R., A. Lowrie, D. Bracey and R. Hey, (1976). Subduction of aseismic oceanic ridges: effects on shape, seismicity and other characteristics of consuming plate boundaries, Geol. Soc. Am. Spec. Paper, 172, 59pp.

Wallace, R. E., (1968). Earthquake of August 19, 1966, Varto area, Eastern Turkey, Bull. Seism. Soc. Am., 58, 11-45.

Wallace, R. E., G. Pararas-Carayannis, R. Valenzuela, and J. N. Taggert, (1977). Earthquake and tsunamis of August 16 1976, Mindanao, Philippines, (abstract), Abstracts with programs, Geological Society of America, 9, No. 4, 523.

Wallace, T. C. and D. V. Helmberger, (1981). An analysis of the strong-ground motion of the August 13, 1978 Santa Barbara earthquake, Bull. Seism. Soc. Am., submitted.

Ward, S. N., (1979). Ringing P waves and submarine faulting, J. Geophys. Res., 84, 3057-3062.

Ward, S. N., (1980). A technique for the recovery of the seismic moment tensor applied to the Oaxaca, Mexico earthquake of November 1978, Bull. Seism. Soc. Amer., 70, 717-734.

Wilson, J. T., (1965). A new class of faults and their bearing on continental drift, Nature, 207, 343-347.

Wood, H. O., (1908). Distribution of apparent intensity in San Francisco, The California Earthquake of April 18, 1906, Report of the State Earthquake Investigation Commission, Carnegie Inst. of Wash., Publ. 87, Washington, D. C., 220-245.

Wyss, M., and J. N. Brune, (1967). The Alaska earthquake of 28 March 1964: A complex multiple rupture, Bull. Seismol. Soc. Am., 57, 1017-1023.

Yamamoto, J., (1978). Rupture processes of some complex earthquakes in southern Mexico, Ph.D. Thesis, Saint Louis University.

Zhu Chuan-zhen et al., (1977). Source parameters for small earthquakes before and after the M = 7.8 Tangshan earthquake. Acta Geophysica Sinica, 20, No. 4, p. 269.

Zuniga, F. R., C. M. Valdes, R. P. Meyer, J. Havskov and S. K. Singh, (1980). Aftershocks of the Petatlán, Mexico, earthquake of 14 March, 1979 (M_s = 7.6), (abstract), EOS, Trans. Am, Geophys. Un., 61, 289.